

**HEAT TRANSFER AND FRICTIONAL PRESSURE DROP
OF CROP FIBER SUSPENSIONS IN CLOSED CONDUIT
FLOW AND NANOFLUID FLOW IN BACKWARD-
FACING STEP**

SYED MUZAMIL AHMED

**DISSERTATION SUBMITTED IN FULFILMENT OF
THE REQUIREMENTS FOR THE DEGREE OF
MASTER OF ENGINEERING SCIENCE**

**FACULTY OF ENGINEERING
UNIVERSITY OF MALAYA
KUALA LUMPUR
2017**

UNIVERSITI MALAYA

ORIGINAL LITERARY WORK DECLARATION

Name of Candidate: **SYED MUZAMIL AHMED**

Registration/Matric No: **KGA150006**

Name of Degree: **MASTER OF ENGINEERING SCIENCE**

Title of Project Paper/Research Report/Dissertation/Thesis:

**HEAT TRANSFER AND FRICTIONAL PRESSURE DROP OF CROP FIBER
SUSPENSIONS IN CLOSED CONDUIT FLOW AND NANOFUID FLOW IN
BACKWARD-FACING STEP**

Field of Study: **Heat transfer**

I do solemnly and sincerely declare that:

- (1) I am the sole author/writer of this Work;
- (2) This Work is original;
- (3) Any use of any work in which copyright exists was done by way of fair dealing and for permitted purposes and any excerpt or extract from, or reference to or reproduction of any copyright work has been disclosed expressly and sufficiently and the title of the Work and its authorship have been acknowledged in this Work;
- (4) I do not have any actual knowledge nor do I ought reasonably to know that the making of this work constitutes an infringement of any copyright work;
- (5) I hereby assign all and every rights in the copyright to this Work to the University of Malaya ("UM"), who henceforth shall be owner of the copyright in this Work and that any reproduction or use in any form or by any means whatsoever is prohibited without the written consent of UM having been first had and obtained;
- (6) I am fully aware that if in the course of making this Work I have infringed any copyright whether intentionally or otherwise, I may be subject to legal action or any other action as may be determined by UM.

Candidate's Signature

Date

Subscribed and solemnly declared before,

Witness's Signature

Date

Name:

Designation:

ABSTRACT

Study of heat transfer and frictional pressure losses in fiber suspension a non-Newtonian fluid flow is one of the significant scientific interests as the characteristics of fiber suspension flow considerably changes with the addition of little amounts of fiber. The characteristics of the fiber suspension flow depends on the shear stress, consistency, fiber source, fiber properties, the treatments done on the fibers and the fluid velocity.

The non-Brownian motion of fibers in suspension flow are found in many applications, such as fiber composites, pulp and paper, textile, long-chain polymer etc. There are noticeable investigations conducted on properties of fiber suspensions but they are mainly wood pulp and family of pine groups. Study of the hydrodynamic behavior of non-wood fiber suspensions has become imminent due to increasing demand for non-wood fibrous materials. The nescience of non-wood fiber suspensions flowing in pipe elevated concerns regarding handling of non-wood fiber suspensions in papermaking process. As there are no significant reporting regarding non-wood pulp fibers flowing in pipes. So, it has become essential to investigate heat transfer and pressure drop of non-wood fiber suspensions in pipeline flow.

A set up was built with a straight pipe test section to evaluate the heat transfer and frictional pressure drop characteristics of turbulent flowing pulp fiber suspensions, where the data were taken at different velocities and consistencies at constant heat flux. Several experiments were conducted for different types of non- wood pulp fibers (Kenaf core, Kenaf bast, blend of non-wood and blend of wood pulp fibers) at different consistencies and flow rates. The measured heat transfer coefficient (h_c) and frictional pressure drop ($\Delta P/L$) data were correlated with the fiber and paper properties.

The results revealed that most of the fiber and paper properties could be correlated with both h_c and $\Delta P/L$ data. A specific range of h_c or $\Delta P/L$ can be used to monitor quality variations of fibers in suspension long before the paper is made, so that corrective action can be taken and the amount of rejected paper production could be minimized. The magnitude of h_c and $\Delta P/L$ were found depending on flow velocity, consistency, fiber population, fiber length, flexibility, and fiber surface topography.

Nanofluid flow and heat transfer to fully developed turbulent forced convection flow in a uniformly heated tubular horizontal backward-facing step were studied experimentally. Five different types of water based (Al_2O_3 , SiO_2 and MWNT) nanofluids have experimentally investigated. The experiments were conducted for concentration range of 0 to 0.1 wt.% and Reynolds number of 4000 to 16000 at uniform and constant heat flux.

Heat transfer coefficient increases nonlinearly with the increase of both the concentration and Reynolds number. The peak of the heat transfer coefficient has occurred after the sudden expansion and it moved far from the step height with the increase of Reynolds number for both the cases of pure water and nanofluids. The pressure drop variation increases with the increase of Reynolds number and nanoparticles concentration but the changes observed are insignificant in the present range of investigation.

ABSTRAK

Kajian pemindahan haba dan kehilangan tekanan geseran dalam penggantungan serat aliran cecair bukan Newton adalah salah satu kepentingan saintifik yang penting kerana ciri-ciri aliran suspensi serat berubah dengan penambahan sedikit serat. Ciri-ciri aliran suspensi gentian bergantung kepada tegasan ricih, konsistensi, sumber serat, sifat serat, rawatan yang dilakukan pada gentian dan halaju cecair.

Gerakan gentian non-Brownian dalam aliran penggantungan terdapat dalam banyak aplikasi, seperti komposit serat, pulpa dan kertas, tekstil, polimer rantaian panjang dan lain-lain. Terdapat penyiasatan yang ketara yang dilakukan terhadap sifat-sifat suspensi serat tetapi mereka terutamanya pulpa kayu dan Keluarga kumpulan pain. Kajian terhadap tingkah laku hidrodinamik penggantungan serat bukan kayu telah menjadi semakin dekat disebabkan peningkatan permintaan untuk bahan berserat bukan kayu. Unsur-unsur penggantungan serat bukan kayu yang mengalir di dalam kebimbangan paip yang tinggi mengenai penanganan suspensi serat bukan kayu dalam proses pembuatan kertas. Oleh kerana tidak ada laporan penting mengenai serat pulpa bukan kayu yang mengalir di dalam paip. Oleh itu, ia menjadi penting untuk menyiasat pemindahan haba dan penurunan tekanan penggantungan serat bukan kayu dalam aliran saluran paip.

Satu set dibina dengan seksyen ujian paip lurus untuk menilai pemindahan haba dan ciri penurunan tekanan geseran penggantungan serat pulpa yang mengalir bergelora, di mana data diambil pada halaju dan konsisten yang berlainan pada fluks haba tetap. Beberapa eksperimen dijalankan untuk pelbagai jenis serat pulpa bukan kayu (Kenaf core, Kenaf bast, campuran bukan kayu dan campuran serat pulpa kayu) pada pelbagai konsisten dan kadar aliran. Pekali pemindahan haba yang diukur (hc) dan penurunan tekanan geseran ($\Delta P / L$) dikaitkan dengan sifat serat dan kertas.

Keputusan menunjukkan bahawa kebanyakan sifat serat dan kertas boleh dikaitkan dengan data h_c dan $\Delta P / L$. Julat tertentu h_c atau $\Delta P / L$ boleh digunakan untuk memantau variasi variasi gentian dalam penggantungan jauh sebelum kertas dibuat, supaya tindakan pembetulan dapat diambil dan jumlah pengeluaran kertas yang ditolak dapat dikurangkan. Besarnya h_c dan $\Delta P / L$ didapati berdasarkan halaju aliran, konsistensi, populasi serat, panjang serat, fleksibiliti, dan topografi permukaan serat.

Aliran Nanofluid dan pemindahan haba ke aliran perolakan terpaksa bergelora yang telah dibangunkan sepenuhnya dalam langkah ke belakang yang menghadap ke belakang bersudut tubular seragam telah dikaji secara eksperimen. Lima jenis nanofluid berasaskan air (Al_2O_3 , SiO_2 , dan MWNT) telah disiasat secara percubaan. Eksperimen dilakukan untuk julat kepekatan 0 hingga 0.1 wt% dan Reynolds nombor 4000 hingga 16000 pada fluks haba seragam dan tetap.

Pekali pemindahan haba meningkat secara tak linear dengan peningkatan kedua-dua kepekatan dan nombor Reynolds. Puncak pekali pemindahan haba telah berlaku selepas pengembangan mendadak dan ia bergerak jauh dari ketinggian langkah dengan peningkatan bilangan Reynolds untuk kedua-dua kes air tulen dan nanofluid. Perubahan tekanan penurunan meningkat dengan peningkatan bilangan Reynolds dan kepekatan nanopartikel tetapi perubahan yang diperhatikan adalah tidak penting dalam pelbagai siasatan semasa.

Table of Contents

ABSTRACT	iii
ABSTRAK	v
Table of Contents	vii
List of Symbols and Abbreviations	xxii
List of Appendices	xxiv
CHAPTER 1: Introduction	1
1.1 Background and motivation	1
1.2 Objectives of present Study	3
CHAPTER 2: Literature Review	5
2.1 Study of flowing fiber suspensions in Pipe line	5
2.1.1 Study of Fiber and Paper Properties	5
2.1.2 Physical properties of fibers and papers	8
2.1.3 Derived values	9
2.1.4 Pulping	10
2.1.4.1 Mechanical pulping	10
2.1.4.2 Thermo-mechanical pulping	10
2.1.4.3 Chemical pulping	10
2.1.4.4 Kraft pulping	11
2.1.4.5 Hybrid pulping	11
2.1.5 Pulp suspension	11
2.1.6 Rheology of Pulp suspension	13
2.1.7 Pressure drop study of fiber suspension flow	14
2.1.7.1 Drag reduction	16
2.1.7.2 Fiber-induced Drag reduction	17
2.1.8 Heat transfer and pressure drop correlations	18
2.1.9 Heat transfer and pressure drop of fiber suspension flow	20
2.2 Study of nanofluid flow in backward-facing step	25
2.2.1 Fluid flow through sudden expansion	26
2.2.1.1 Nanofluid flow through sudden expansion	32
2.2.1.2 Fluid flow through a backward and forward-facing step	32
(a) Laminar fluid flow	33

(b)	Turbulent fluid flow	34
2.2.1.3	Laminar Nanofluid flow	37
2.2.1.4	Turbulent nanofluid flow	39
2.2.2	Nanofluids	41
2.2.3	Stability of Nanofluid	41
2.2.4	Mechanism of heat transfer using nanofluid	42
2.2.4.1	Brownian motion	42
2.2.4.2	Liquid layering on the nanoparticle-liquid interface	44
2.2.4.3	Nature of heat transport in nanoparticles	45
2.2.4.4	Effects of nanoparticles clustering	45
2.2.4.5	Thermophoresis	46
2.2.4.6	Reduction in thermal boundary layer thickness	46
2.2.5	Temperature effect	46
2.2.6	Viscosity	48
2.2.7	Heat Capacity	49
2.2.8	Pressure drop and nanofluid	50
2.3	Summery	51
CHAPTER 3:	METHODOLOGY	53
3.1.	Study of flowing fiber suspensions in Pipe line	53
3.1.1	Pipe line flow Experimental Setup	53
3.1.2	Data acquisition	55
3.1.3	Material	55
3.1.4	Experimental procedures	56
3.1.5	Data reduction and Calibration of Experiments	56
3.1.6	Preparation and Characterization of samples	58
3.1.6.1	Preparation of pulp fiber suspension	58
3.1.6.2	Preparation of hand sheets	58
3.1.6.3	Characterization of fibers and hand sheets	58
3.2	Study of nanofluid flow in backward-facing step	59
3.2.1	Analysis methods	59
3.2.1.1	FE-SEM	60

3.2.1.2	TEM.....	61
3.2.1.3	FT-IR.....	61
3.2.1.4	Raman.....	62
3.2.1.5	DSC.....	62
3.2.1.6	Rheometer.....	63
3.2.1.7	Stability.....	63
3.2.1.8	Electrical conductivity.....	64
3.2.1.9	Thermal conductivity.....	64
3.2.2	Experimental apparatus.....	66
3.2.3	Experimental data reduction.....	67
3.2.4	Design and Construction of step flow rig.....	68
3.2.4.1	Reservoir Tank.....	68
3.2.4.2	Gear Pump.....	68
3.2.4.3	Inverter.....	68
3.2.4.4	Electromagnetic Flow Meter.....	69
3.2.4.5	Differential Pressure Transducer.....	71
3.2.4.6	Cooling unit.....	73
3.2.4.7	Power Supply.....	73
3.2.4.8	Thermocouples.....	74
3.2.4.9	Data logging system.....	75
3.2.4.10	Test section.....	76
CHAPTER 4:	Results and Discussion.....	78
4.1	Pipe line flow.....	78
4.1.1	Data Reproducibility.....	78
4.1.2	Heat transfer to fiber suspension.....	80
4.1.2.1	Different concentration effect of fiber on heat transfer coefficient.....	80
4.1.2.2	Effect of bleaching.....	87
4.1.2.3	Effect of processing.....	89

4.1.2.4	Effect of Fibers blending	92
4.1.2.5	Fiber physical properties and Heat Transfer	93
4.1.2.6	Paper properties and Heat Transfer	98
4.1.3	Pressure drop of fiber suspensions.....	101
4.1.3.1	Different concentration effect of fiber on pressure drop.....	101
4.1.3.2	Effect of bleaching	105
4.1.3.3	Effect of processing.....	108
4.1.3.4	Effect of fiber blending	111
4.1.3.5	Fiber properties and frictional pressure drop	113
4.1.3.6	Paper properties and frictional pressure drop.....	115
4.2	Nanofluids and Step Flow study	118
4.2.1	Preparation of Nanofluid	118
4.2.1.1	Preparation of Aluminum oxide and Silicon dioxide nanofluids	118
4.2.1.2	Synthesis of MWCNT-Aspartic Acids.....	119
4.2.2	Characterization of Aluminum oxide and Silicon dioxide nanofluids	119
4.2.2.1	Alumina-water nanofluid	119
4.2.2.2	Silicon dioxide-water nanofluid	122
4.2.3	Functionalization Analysis	122
4.2.4	Stability.....	126
4.2.4.1	Alumina-water nanofluid	126
4.2.4.2	Silica-water nanofluid	128
4.2.5	Thermo-physical properties	130
4.2.5.1	Viscosity.....	130
4.2.5.2	Thermal conductivity	133
4.2.6	Heat transfer to nanofluid flow in a Backward-facing step.....	137
4.2.6.1	Alumina-water nanofluid	137
4.2.6.2	Silica-water nanofluid	144
4.2.6.3	MWNT-asp-water nanofluid	149
CHAPTER 5:	Conclusion And Further works	154

5.1	Conclusion.....	154
5.2	Suggestion for further works.....	155
	References.....	156
	List of Publications.....	168
	Appendix A.....	169
	Appendix B.....	173
	Appendix C.....	177
	Appendix D.....	180

University of Malaya

List of Figures

Figure 2. 1 Stratified structure of wood (Zhu et al., 2013)	6
Figure 2. 2 Frictional pressure drop as a function of velocity of a pulp suspension (G. G. Duffy, 1972).....	14
Figure 2. 3 The flow regimes of fiber suspension. (I) Plug flow regime with direct fiber-wall contact, (II) Plug flow regime with lubrication layer, (III) Plug flow with a smearing annulus, (IV) Mixed flow and (V) fully turbulent flow (Jäsberg, 2007).	16
Figure 2. 4 Measurement of velocity flow field at $Re = 100$. Goharzadeh and Rodgers (2009).....	27
Figure 2. 5 Measurement of velocity flow field at $Re = 300$. Goharzadeh and Rodgers (2009).....	27
Figure 2. 6 Measurement of velocity flow field at $Re = 500$. Goharzadeh and Rodgers (2009).....	28
Figure 2. 7 comparison of Nusselt number for SiO_2 at $Re = 100$, Santosh Christopher et al. (2012)	32
Figure 2. 8 Figure 2. 9 Local Nusselt number variation downstream of the step, H. I. Abu-Mulaweh (2005).....	36
Figure 2.10 Thermal conductivity enhancement of alumina-water nanofluids versus temperature (Putra et al., 2003). λ/λ_{water} denotes the ratio of thermal conductivities of the nanofluids to that of the base fluid.	47
Figure 2.11 Thermal conductivity enhancement of Copper oxid-water nanofluid versus temperature (Putra et al., 2003). λ/λ_{water} denotes the ratio of thermal conductivities of the nanofluids to that of the base fluid.	48
Figure 3. 1 . (a) Schematic diagram of the experimental flow loop. (b) Schematic view of the experimental test section.....	54

Figure 3. 2 photograph of the experimental setup of suspensions flow.....	55
Figure 3. 3 Flowchart of sheet making process.....	58
Figure 3. 4 Schematic setup of KD2 thermal properties analyzer	65
Figure 3. 5 Comparison between distilled water and previous data	65
Figure 3. 6 Schematic of BFSF rig	66
Figure 3. 7 Photographs of equipment's (a) Stock tank, (b) Magnetic gear pump, (c) Magnetic Flow meter, (d) Hoffman Muller inverter, (e) Differential Pressure Transducer, (f) Cooling unit, (g) Power supply.	70
Figure 3. 8 Thermocouple testing	75
Figure 3. 9 Photograph of experimental setup and test section.....	76
Figure 3. 10 Schematic view of the test section.....	77
Figure 3. 11 Thermocouples positions	77
Figure 4. 1 Heat transfer coefficient as a function of velocity for two runs of water.	78
Figure 4. 2 Pressure drop per unit length as a function of velocity for two runs of water.	79
Figure 4. 3 Comparison of Nusselt number as a function of velocity obtained from the experimental data and the standard correlations	80
Figure 4. 4 Comparison of measured experimental friction factor with Petukhov (1970) and Blasius (1908)	80
Figure 4. 5 h_c as a function of flow velocity for water and different concentrations of Kenaf Core Mechanical (kcm) fiber suspensions.	81
Figure 4. 6 h_c as a function of flow velocity for water and different concentrations of Kenaf Bast Mechanical (KBM) fiber suspensions.....	81
Figure 4. 7 h_c as a function of flow velocity for water and different concentrations of mixture of kenaf core and bast (kckb3) fiber suspensions.....	82
Figure 4. 8 h_c as a function of flow velocity for water and different concentrations of	

mixture of acacia mangun and kenaf bast (amkb) fiber suspensions.....	83
Figure 4. 9 h_c ratio as a function of flow velocity for water and different concentrations of kcm fiber suspensions.....	85
Figure 4. 10 Heat transfer coefficient ratio as a function of flow velocity for water and different concentrations of kenaf Bast Mechanical (KBM) fiber suspensions.	85
Figure 4. 11 h_c ratio as a function of flow velocity for water and different concentrations of blend of Kenaf Core and Kenaf Bast Mechanical (kckb3) fiber suspensions. ...	86
Figure 4. 12 h_c ratio as a function of flow velocity for water and different concentrations of blend of Acacia Mangun and Kenaf Bast (amkb) fiber suspensions.....	86
Figure 4. 13 h_c as a function of flow velocity for water and kccu and kccb fiber suspensions of concertation 0.6 wt.%.....	88
Figure 4. 14 Heat transfer coefficient as a function of flow velocity for water and kbcu and kccb fiber suspensions of concertation 0.6 wt.%.....	88
Figure 4. 15 h_c as a function of flow velocity for water and different processed Kenaf Core fiber (kccu and kcm) of concentration 0.6 wt.%.....	90
Figure 4. 16 h_c as a function of flow velocity for water and different processed Kenaf Core fiber (kccu and kcm) of concentration 0.6 wt.%.....	90
Figure 4. 17 h_c ratio versus flow velocity for water and different processed Kenaf Core fiber (kccu and kcm) of concentration 0.6 wt.%.....	91
Figure 4. 18 h_c ratio versus flow velocity for water and different processed Kenaf Core fiber (kccu and kcm) of concentration 0.6 wt.%.....	91
Figure 4. 19 h_c as a function of flow velocity for water and different blend of kenaf core and bast (kckb3, kckb4 and kckb5) fiber suspensions.	93
Figure 4. 20 fiber properties as a function of heat transfer coefficient for kcm, kccu and kccb (a) fiber length, (b) flexibility coefficient (c) Slenderness ratio.....	96
Figure 4. 21 fiber properties as a function of heat transfer coefficient for kbm, kbcu and	

kbc (a) fiber length, (b) flexibility coefficient (c) Slenderness ratio	97
Figure 4. 22 Paper properties of kcm, kccu, kccb, kbm, kbcu, and kbc as a function of Heat transfer coefficient.....	100
Figure 4. 23 Drag ratio of Kenaf core mechanical pulp suspensions as a function of velocity at different concentrations.....	102
Figure 4. 24 Drag ratio of Kenaf bast mechanical pulp suspensions as a function of velocity at different concentrations.....	102
Figure 4. 25 Drag ratio of blend of Kenaf core and bast mechanical pulp suspensions as a function of velocity at different concentrations	103
Figure 4. 26 Drag ratio of blend of Acacia mangun and Kenaf bast pulp suspensions as a function of velocity at different concentrations	104
Figure 4. 27 Pressure drop of kenaf bast bleached and unbleached pulp fiber suspensions as a function of velocity.....	106
Figure 4. 28 Drag ratio of kenaf bast bleached and unbleached pulp fiber suspensions as a function of velocity	106
Figure 4. 29 Pressure drop of kenaf core bleached and unbleached pulp fiber suspensions as a function of velocity.....	107
Figure 4. 30 Drag ratio of kenaf core bleached and unbleached pulp fiber suspensions as a function of velocity	107
Figure 4. 31 Pressure drop of kenaf bast mechanical and kenaf bast chemical unbleached pulp fiber suspensions as a function of velocity.....	108
Figure 4. 32 Drag ratio of kenaf bast mechanical and kenaf bast chemical unbleached pulp fiber suspensions as a function of velocity	109
Figure 4. 33 Pressure drop of kenaf core mechanical and kenaf core chemical unbleached pulp fiber suspensions as a function of velocity.....	110
Figure 4. 34 Drag ratio of kenaf core mechanical and kenaf core chemical unbleached	

pulp fiber suspensions as a function of velocity	110
Figure 4. 35 Drag ratio as a function of flow velocity for water and different pulp suspensions kbm, kcm and kckb3 at concentration of 0.6 wt.%.....	111
Figure 4. 36 Drag ratio as a function of velocity for water and different pulp suspensions kckb3, kckb4, and kckb5 at concentration of 0.6 wt.%.....	112
Figure 4. 37 Correlation of frictional pressure drop of kckb3, kcm and kbm pulp suspensions at consistency of 0.6 wt.% with (a) fiber length, (b) fiber lumen, and (c) fiber width.....	114
Figure 4. 38 Tear index as a function of pressure drop for Kenaf core mechanical (kcm), Kenaf bast mechanical (kbm) and blend of kcm and kbm (kckb3).	115
Figure 4. 39 Burst index as a function of pressure drop for Kenaf core mechanical (kcm), Kenaf bast mechanical (kbm) and blend of kcm and kbm (kckb3).....	116
Figure 4. 40 Tensile index as a function of pressure drop for Kenaf core mechanical (kcm), Kenaf bast mechanical (kbm) and blend of kcm and kbm (kckb3).....	116
Figure 4. 41 Folding endurance as a function of pressure drop for Kenaf core mechanical (kcm), Kenaf bast mechanical (kbm) and blend of kcm and kbm (kckb3).	117
Figure 4. 42 TEM images of Al ₂ O ₃ -water nanofluid at weight concentration of 0.1%.	121
Figure 4. 43 TEM images of SiO ₂ -water nanofluid at weight concentration of 0.1%..	121
Figure 4. 44 FTIR Spectra of pristine MWNT and Asp-treated MWNT.....	123
Figure 4. 45 Raman Spectra of pristine MWNT and Asp-treated MWNT.....	124
Figure 4. 46 TGA curves of pristine MWNT and Asp-treated MWNT.....	125
Figure 4. 47 TEM images of MWNT-Asp.....	125
Figure 4. 48 (a) Absorbance as a function of wavelength for Al ₂ O ₃ -water nanofluid at weight concentration of 0.1% and (b) Colloidal Stability of Al ₂ O ₃ -water nanofluid.	

.....	127
Figure 4. 49 (a) Absorbance as a function of wavelength for SiO ₂ -water nanofluid at weight concentration of 0.1% and (b) Colloidal Stability of Silica-water nanofluid.	
.....	127
Figure 4. 50 Viscosity as a function of shear rate for Silica-water nanofluid at different concentration and temperature.	132
Figure 4. 51 Viscosity as a function of shear rate for Alumina-water nanofluid at different concentration and temperature.	132
Figure 4. 52 Thermal conductivity as a function of concentration and temperature (a) Al ₂ O ₃ -water nanofluid, and (b) SiO ₂ -water nanofluid	134
Figure 4. 53 Experimental Nusselt number of distilled water and Al ₂ O ₃ -water nanofluids at different weight concentrations of 0.025%, 0.05%, 0.075% and 0.1% for different Reynolds numbers	138
Figure 4. 54 (a) Average heat transfer coefficient of distilled water and Alumina-water nanofluids over a backward-facing step and (b) Average (percent) heat transfer coefficient enhancement versus Reynolds number at different weight concentrations.	140
Figure 4. 55 The effect of Reynolds numbers and weight concentrations of Al ₂ O ₃ -water nanofluids on the local heat transfer coefficient at different axial ratios.....	142
Figure 4. 56 Performance index (ϵ) for the backward-facing step in the presence of distilled water and Al ₂ O ₃ -water nanofluids with different weight concentration .	143
Figure 4. 57 Experimental Pressure drop of distilled water and Al ₂ O ₃ -water nanofluids at weight concentrations of 0.025%, 0.05%, 0.075% and 0.1% for different Re number.	144
Figure 4. 58 Experimental Nusselt number of distilled water and SiO ₂ -water nanofluids at different weight concentrations of 0.05% and 0.1% for different Reynolds	

numbers	145
Figure 4. 59 (a) Average heat transfer coefficient of distilled water and SiO ₂ -water nanofluids over a backward-facing step and (b) Average (percent) heat transfer coefficient enhancement versus Reynolds number at different weight concentrations	146
Figure 4. 60 The effect of Reynolds numbers and weight concentrations of SiO ₂ -water nanofluids on the local heat transfer coefficient at different axial ratios.....	147
Figure 4. 61 Experimental Pressure drop of distilled water and SiO ₂ -water nanofluids at weight concentrations of 0.05% and 0.1% for different Re number.....	149
Figure 4. 62 Experimental Nusselt number of distilled water and MWNT-water nanofluids at different weight concentrations of 0.05% and 0.1% and at different Reynolds numbers.....	150
Figure 4. 63 (a) Average heat transfer coefficient of distilled water and MWNT-Asp--water nanofluids over a backward-facing step and (b) Average (percent) heat transfer coefficient enhancement versus Reynolds number at different weight concentrations	151
Figure 4. 64 The effect of Reynolds numbers and weight concentrations of MWNT-Asp-water nanofluids on the local heat transfer coefficient at different axial ratios.	152
Figure 4. 65 Experimental Pressure drop of distilled water and MWNT-Asp-water nanofluids at weight concentrations of 0.05% and 0.1% for different Re number.	153
Figure A. 1 SEM micrographs of the paper made from A. mangium fibers.....	169
Figure A. 2 SEM micrographs of the paper made from Kenaf bast pulp fibers	169
Figure A. 3 SEM micrographs of the paper made from un-bleached Kenaf bast pulp fibers.....	170

Figure B. 1 Temperature drop through heated wall (Kazi S. N., Ph.D. Thesis, 2002) .	173
Figure B. 2 $1/U$ as a function of u^n for thermocouple (a) T1, (b) T2 and (c) T3	175
Figure D. 1 Fiber property versus heat transfer coefficient	180
Figure D. 2 Fiber property versus heat transfer coefficient	180
Figure D. 3 Tensile index as a function of heat transfer coefficient.....	181
Figure D. 4 Tear index as a function of heat transfer coefficient.	181
Figure D. 5 Burst index as a function of heat transfer coefficient.	181
Figure D. 6 Folding endurance as a function of heat transfer coefficient.....	182
Figure D. 7 Fiber property versus pressure drop.....	182
Figure D. 8 Correlation of frictional pressure drop of kenaf bast pulp suspensions at consistency of 0.6 wt.% with Slenderness ratio.....	182
Figure D. 9 Correlation of frictional pressure drop of kenaf bast pulp suspensions at consistency of 0.6 wt.% with Flexibility coefficient	183
Figure D. 10 Correlation of frictional pressure drop of kenaf bast pulp suspensions at consistency of 0.6 wt.% with Runkel ratio.	183
Figure D. 11 Tensile index as a function of heat transfer coefficient.....	183
Figure D. 12 Folding endurance index as a function of heat transfer coefficient.....	184
Figure D. 13 Burst index as a function of heat transfer coefficient.	184
Figure D. 14 Tear index as a function of heat transfer coefficient.	184

List of Tables

Table 3. 1 Dimensions of test section	53
Table 3. 2 λ/x values in different locations at the test section for each thermocouple ...	57
Table 3. 3 Technical specifications for V8 series inverters	69
Table 3. 4 Technical specifications of Electromagnetic flow meter	71
Table 3. 5 Flow meter calibration data.....	71
Table 3. 6 Standard specifications of the Differential Pressure Transducers	72
Table 3. 7 Calibration conditions	72
Table 3. 8 Static pressure test.....	72
Table 3. 9 Differential pressure test	73
Table 3. 10 Specifications of the Cooling unit.....	74
Table 4. 1 Percent h_c enhancement	84
Table 4. 2 Heat transfer coefficient ratio at three different range of velocity.....	87
Table 4. 3 Properties of pulp fibers used in the experimental investigation.....	94
Table 4. 4 Paper properties of the pulp used in the experimental investigation.	98
Table 4. 5 Fourier transform infrared interpretation of the pristine and functionalized MWNT.....	123
Table 4. 6 Zeta potential, particle size distribution, polydispersity Index (PDI and mobility of oxides nanofluids.	129
Table 4. 7 Viscosity of different nanofluids in the various temperatures (mPa.s).....	131
Table 4. 8 Thermal conductivity (W/m.K) of MWNT-Asp-water nanofluid at different concentrations and temperatures.....	135
Table 4. 9 Density and Specific heat capacity of the MWNT-Asp-water at the bulk temperature of 30°C.	136
Table 4. 10 Density and Specific heat capacity of the Al ₂ O ₃ -water at the bulk temperature of 30°C.	136

Table 4. 11 Density and Specific heat capacity of the SiO ₂ -water at the bulk temperature of 30°C.	137
Table C. 1 Range of uncertainty for instrument and material used within the present Investigation.....	177

University of Malaya

List of Symbols and Abbreviations

A	Area, m ²
C _p	Specific heat, J/kg K
D	Diameter
<i>f</i>	Friction factor
H	Head loss (m)
h _c	Heat transfer coefficient, kW/m ² K
<i>I</i>	Current, Amp
k	Thermal conductivity, W/m K
<i>l</i>	Length of the tube, m
<i>m</i>	Mass flow rate, kg/s
Nu	Nusselt number
P	Power, Watts
Pr	Prandtl number
Q	Heat flow, Watts
<i>q</i>	Heat flux, W/m ²
Re	Reynolds number
T	Temperature, °C
u	Velocity, m/s
x	Distance of thermocouple from the inner surface of pipe

Greek symbols

ΔP	Differential Pressure drop
ε	Surface roughness
λ	Wall thermal conductivity

μ	Viscosity, kg/m ² s
ρ	Density

Subscripts

b	Bulk
<i>i</i>	Inlet
m	Mass
o	Outlet
t	Thermocouple
w	Wall

University of Malaya

List of Appendices

<u>Appendix A</u>	169
<u>Appendix B</u>	173
<u>Appendix C</u>	177
<u>Appendix D</u>	180

University of Malaya

CHAPTER 1: INTRODUCTION

1.1 Background and motivation

Fibers are transported in suspension forms in the industries. There are noticeable investigations conducted on suspension and rheological properties of fiber suspensions but they are mainly on wood pulp and family of pine groups. Study of suspension properties of non-wood fibers has become imminent as the paper demand has the needs to meet partially by the non-wood fibers. The main source of cellulose fibers for pulp and paper manufacturing are softwoods and hardwoods. Due to environmental concern and the rising global demand of fibers, shortage of trees worldwide and the slow growth rate of trees, non-wood fiber has become one of the important and economical alternative source of fibers. Non-wood cellulose fibers such as grasses, crops, agriculture residues and byproducts of certain industries handling non-wood fiber materials have been proposed as economical and potential sources of fiber for the pulp and paper industries.

The natural pulp fiber suspension flow is different from conventional suspension flow. In fiber suspension flow, the characteristics of the flow depends on the fiber source, fiber processing, fiber concentration and flow rate. Also, in fiber suspension flow, fiber interact the neighboring fibers and entangle even at low populations and can form bundles or entities that behave differently from the individual fibers. Natural fibers forms flocs and fiber network at curtain bulk velocities and with the increase of concentration that produces plug occupying the entire pipeline where the suspension pressure drop is lower than that of water flowing alone, this phenomenon is known as drag reduction. On the other hand, at high velocities and concentrations pressure losses are lower than that of water due to formation of a fiber-water annulus that damp turbulence. Later, it would be expected that fiber suspensions, their composite structures and typical flow characteristics would also modify heat transfer in a heat exchanger.

Due to distinct characteristics of natural fiber and variation of fiber properties sometimes the prepared paper is rejected. As natural non-wood fibers are the alternative of natural wood fibers and is used at a certain ratio with natural fibers in pulp and paper industry so study of non-wood pulp fiber suspensions flow and mixture of non-wood and wood pulp fiber suspensions flow is important for the design and development of equipment and piping system handling these kind of pulp fibers. To curb the production of reject paper it is important to monitor the variations in fiber properties, so that changes can be made during the fiber processing before the end product of pulp fiber suspension. The variation in fiber properties could be monitored by measuring heat transfer coefficient and pressure drop of flowing fiber suspension, once the heat transfer coefficient and pressure drop of a certain fiber suspension is correlated to the acceptable paper product qualities from those fibers.

Separation, recirculation regions, and consequent reattachment due to sudden expansion in flow geometry, such as a backward-facing step (BFS), play an important role in fluid mechanics and many engineering applications, where heat transfer occurs. This sudden expansion is present in heating or cooling applications such as high-performance heat exchangers, chemical processes, combustion chambers, cooling of nuclear reactors, cooling turbines blades, cooling electronic equipment and wide angle diffusers etc. In many circumstances, sudden expansion is undesirable and could be the source of enhanced pressure drop along with energy losses that require additional power supply. However, in many instances sudden expansions are encouraged, these leads to the enhanced heat and mass transfer rates due to higher mixing in separation and reattachment flow regions (Mohammed, Al-aswadi, et al., 2011). Because of this reality, the problem of laminar and turbulent flows over backward-facing and forward-facing steps test loop in natural, mixed and forced convection have been extensively investigated, both numerically and experimentally (H. Abu-Mulaweh, 2003).

Conventional heat transfer fluids such as water, oil, and ethylene glycol have characteristically low thermal conductivity than metal oxides and metals. Consequently, heat transfer characteristics of fluids are expected to be better than traditional heat transfer fluids due to suspending solid particles (Masuda et al., 1993). But fluids with suspended particles of millimeter or micrometer size in the practical application used as a cooling source has some problems, such as erosion, instability of particles and clogging of flow channels, and additional pressure loss (Kebinski et al., 2002; Wang et al., 2003; H.-q. Xie et al., 2002). In contrast, many researchers have reported that convective heat transfer coefficient and the effective thermal conductivity of base fluid can be enhanced by dispersing solid nanoparticles of a high thermal conductivity in the conventional base fluids (Beck et al., 2009; H. Chen et al., 2009; Murugesan & Sivan, 2010; Özerinç et al., 2010; Solangi et al., 2015). Dispersing solid nanoparticles in a base fluid such as water, oil or ethylene glycol are recognized as nanofluids. Solid particles can be metallic such as Al_2O_3 , SiO_2 , CuO , Cu , ZnO and TiO_2 , and nonmetallic e.g. carbon and graphene nanoparticles etc. (Mohammed, Al-Aswadi, et al., 2011). As nanofluids improves the heat transfer characteristics of base fluids so using nanofluids in an engineering flow geometries such as backward-facing step would enhance heat transfer.

1.2 Objectives of present Study

This project aims to study Malaysian non-wood and wood pulp fiber suspension flow in a circular pipe heat exchanger and nanofluids flow over a backward-facing step.

The objectives of the present study are:

1. To investigate the effect of Malaysian non-wood pulp fiber suspensions on both heat transfer and pressure loss in a circular pipe heat exchanger.

2. To investigate the effect of various mixtures of Malaysian non-wood and mixtures of non-wood and wood pulp fiber suspensions on both heat transfer and pressure losses in a circular pipe heat exchanger.
3. To correlate, heat transfer and pressure loss data with fiber and paper properties.
4. To investigate the effects of various nanofluids, nanoparticle concentrations and Reynolds numbers on the heat transfer enhancement over a tubular, horizontal backward-facing step.

University of Malaya

CHAPTER 2: LITERATURE REVIEW

2.1 Study of flowing fiber suspensions in Pipe line

2.1.1 Study of Fiber and Paper Properties

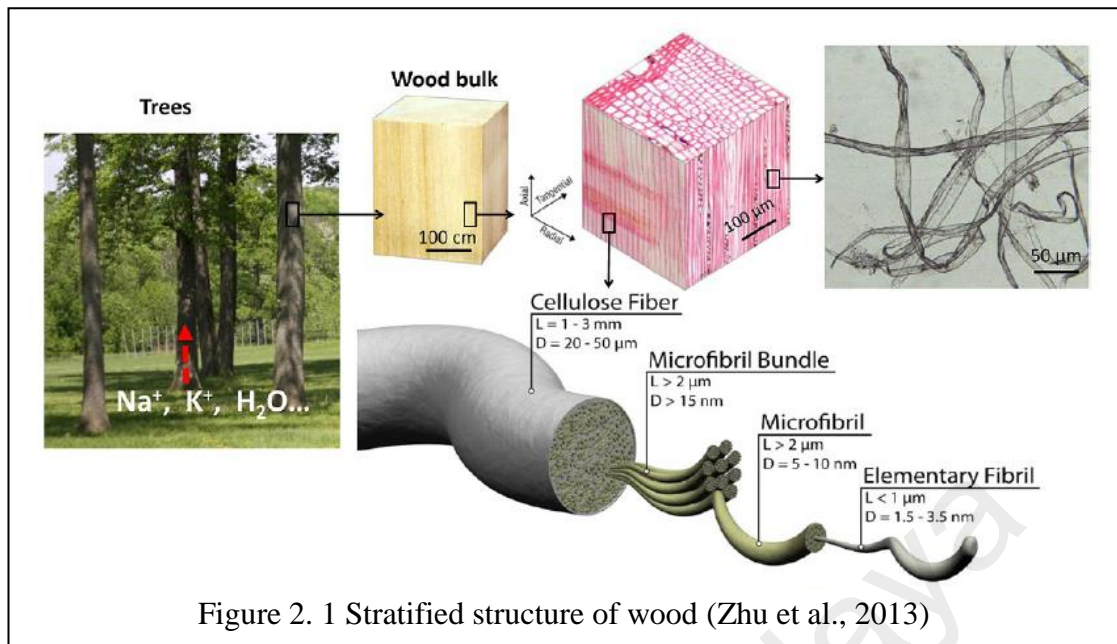
Paper properties are dependent on the pulp and source of fiber and the pulping method (Smook, 1992). Hereafter, different fiber source and pulping methods are necessary to study and characterize fiber and paper quality accordingly.

Fibers for pulp and paper industry can be characterized in three major categories, Wood, Non-wood and polymeric.

Trees are the leading source of cellulose fibers for pulp and paper industry. Wood further can be characterized in two groups; softwood and hardwood. Wood and cell structures vary with the source of wood, properties of pulp are highly affected by the wood groups and source. Currently softwoods are dominant source of fiber for pulp and paper production. Common species are spruce, fir and various types of pine for the production of fiber used in pulp and paper industry (Sjöström, 1993).

In spring, wood grows rapidly due to which tricheds (fibers when liberated from the wood) have a large diameter and thin walled and contrasting in dry months or in winter growth rate of trees are slow, which results in smaller diameter and thicker walled tracheids. Properties of wood depend on climate, species and age of the tree.

Structure of hardwood is quite different from softwood, due to diversity in cell types. Hard wood fibers are generally shorter than those of softwoods (1mm average length) and are present in two different forms, libriform cells and fiber tracheids. Hardwoods reveal similar seasonal growth patterns to softwoods, with early wood and latewood fibers present. Hardwoods consist of about 45 percent cellulose, 30 percent hemicellulose, 20 percent lignin and 5 percent extractives (Smook, 1992). Hardwoods are usually used for papermaking due to good formation properties.



Wood fibers are of tubular shape, tapered and sealed off at both ends. Having rectangular cross sectional shape with a wall thickness of about 10 percent of the fiber diameter. Fibers are composed of cellulose, hemicellulose and lignin. Cellulose is a polysaccharide with base units of glucose that exists in smaller units known as microfibrils. These microfibrils are bundles of 36 parallel cellulose molecules held together by hydrogen bonds. Fibre wall consists of several layers, each layer having different orientation of their microfibrils. The thin primary wall from outer to inner consists of cellulose, hemicellulose, protein and pectin. Microfibrils of cellulose are usually 900 to the cell axis. The second layer is thinner and a microfibril angle of 50-70. The next layer is the thickest and forms the major part of the cell, and is thus of the most interest to the papermaker. Here the microfibrils are 10-300 to the cell axis, with considerable variation both within the tree and between the trees.

Properties of fiber are greatly influenced by oriented angle of micro-fibrils. The innermost layer, and the final layer, acts as partition between the inner pithy core of the cell and the previous layer and does not play much part in the paper making process.

The zone between neighboring tracheids is the middle lamella. The region of the middle lamellar zone and between each cell contains a high percentage of lignin and serves to bind the cells together. It needs to be destroyed or broken down to release the fibers. Within the cell wall, cellulose, hemicellulose and lignin are considered to be arranged in order.

Due to increasing demand of fibrous material, limitation of wood source compare to demand, and environmental concern, plant-based fibers have become as an alternative source of wood fiber (Kaldor et al., 1990; Mossello et al., 2010).

The average ratio of non-wood fiber length ranges from 1 mm to 30 mm which depends on plant species and the plant part from which the fiber is derived. Non-woods have lower lignin content (compared to wood), so it can be pulped in less time compared to woods. With regards to non-wood fibers for example, kenaf bast and jute fiber provides long fiber furnish, where kenaf core, cotton stalks, corn stalks and straw provide short fiber furnish. Yet, fiber length is only one of many criteria that need to be considered when assessing the suitability for papermaking. Furthermore, the chemical and morphological characteristics of non-wood fibers vary by geographical location.

Kenaf is of the Hibiscus family that have more than 50 species among those species kenaf (*H. cannabinus* L.) have economic importance particularly for the pulp and paper production (Han & Rowell, 1997). Furthermore, Kenaf has two distinctive stem regions, the outer portion or bast is about 34 wt.% of the stem and inner, woody core, that is about 66 wt.% (Ashori, 2006). Kenaf bast fiber is long fiber resemble softwood fibers, could be used to manufacture products such as high-grade pulps for the pulp and paper industry, filters, textile and composite etc. (Dutt et al., 2009; Mossello et al., 2010; Villar et al., 2009).

2.1.2 Physical properties of fibers and papers

Physical properties and dimensional constraints of fiber effect the sheet properties formed by them. Generally, fiber length is expressed as average length calculated from percent by mass or weight. Fiber length affects sheet formation or uniformity of fiber distribution. The shorter the fiber the closer and more uniform will be the sheet formation. Fiber length also affects the physical properties of the sheet such as the strength and rigidity and especially the tearing strength, which decreases with a decrease in fiber length. The numerical average length of the fibers only has very little practical meaning unless they all are uniform. In pulp fibers, the length distribution makes more sense to use a weighted-average fiber length, either length-weighted or weight-weighted to reduce the influence of fines. Fines are defined as fibers or fragments of less than 0.2 mm length, should be treated separately when considering fiber lengths. Longer fibers can produce higher tear and tensile strength of papers and decrease sheet density (Paavilainen, 1990).

The effect of fiber diameter, wall thickness and coarseness on sheet properties is rather complex and not clearly established. These qualities primarily affect fiber flexibility. Fiber diameter may be expressed as mean cross section or ratio of wall thickness to diameter, sometimes termed fiber density. Fiber strength is the intrinsic strength of a single fiber, which is usually measured by the zero span tensile tests and sometimes by the viscosity of the dissolved fiber. It was found that the sheet strength depends on the surface available for bonding. All papers are bonded to some extent and the sheet properties are likely to be affected more by the relatively bonded to unbounded area than by the specific surface of the fibers from which the sheet is made. A very important effect of specific surface is its effect on drainage rate in the papermaking process. The higher the specific surface the slower the water will be drained from the sheet during its formation.

Most workers seem to agree that the sheet density is a good indication of fiber flexibility. If the fibers are flexible, the sheet will be compacted with relatively little pore space. If the fibers are relatively rigid, the sheet will be porous, open and not well bonded. The solid fraction of the sheet controls a wide range of physical properties of the sheet including light scattering, opacity, grease and oil penetration and air permeability. It is postulated by most workers that the fiber surface properties control the bonding.

2.1.3 Derived values

To assess the suitability of the plant raw materials for pulp and paper production, three derived values are commonly used for the comparison among softwoods, hardwoods and non-wood fibers and those are: slenderness ratio, flexibility coefficient, and Runkel ratio presented in equations 2.1, 2.2, 2.3 (Ogbonnaya et al., 1997; Saikia et al., 1997) respectively are given by:

$$\text{Slenderness ratio} = \frac{\text{length of fiber}}{\text{fiber diameter}} \quad (2.1)$$

$$\text{Flexibility coefficient} = \frac{\text{fiber lumen diameter}}{\text{fiber diameter}} \times 100 \quad (2.2)$$

$$\text{Runkel ratio} = \frac{(2 \times \text{fiber cell wall thickness})}{\text{Lumen diameter}} \quad (2.3)$$

Some derived values for Kenaf core, Kenaf bast, Kenaf whole etc. compared with softwood and hard wood are shown in table 2.1:

Table 2. 1 Derived values of various fibers

Material	Slenderness ratio	Flexibility coefficient	Runkel ratio	References
Kenaf core	33.3	59.5	0.5	(Ververis et al., 2004)
Kenaf bast	105.9	54.3	0.7	
Kenaf whole	58.3	57.5	0.67	
Cotton	42.3	65.3	0.5	
Softwoods	95-120	75	0.35	
Hardwoods	55-75	55-70	0.4-0.7	

2.1.4 Pulping

The process of converting lignocellulosic material into a fiber material is known as pulping and the product is known as pulp that is used for papermaking. The common commercial processes are generally categorized in three processes those are mechanical, chemical and hybrid pulping.

2.1.4.1 Mechanical pulping

Mechanical pulping is one of the oldest pulping process that debark and mechanically ground wood into pulp by refiners or disk refiner or grindstone. The common mechanical pulping process are Pressure Ground Wood (PGW), Stone Ground Wood (SGW), Pressurized Refiner Mechanical Pulping (PRMP), Thermo Mechanical Pulping (TMP) and Refiner Mechanical Pulp (RMP) (Biermann, 1996).

2.1.4.2 Thermo-mechanical pulping

In thermo-mechanical pulping, the wood chips are pre-treated with steam at 130 °C in order to soften them and refine at 2-4 bar in a pressurized disc refiner. Thermo-mechanical pulp (TMP) is stronger than RMP, contains little screen reject material and preserves much of its original fiber length due to good separation of the fibers. Its opacity and printing quality are lower than that of SGW.

2.1.4.3 Chemical pulping

Chemical pulping is one of a common pulping process during which wood chips are cooked at elevated temperature (140-190°C) and pressure (0.6-1.0 MPa) in either alkaline or acid medium. Chemical pulping process usually removes the lignin about 90% (Sjöström, 1993), that is binding material which holds fibers together and also other non-cellulose materials that includes hemicellulose. The product yield of chemical pulping is usually between 40-50% depending on the pulping process applied and the fiber source. Cooking has the great effect on the yield beyond a certain cooking time and it limits the large yield loss which is due to the degradation of carbohydrates. Later,

the chemical reaction must be stopped at an optimum point where the acceptable and maximum yield can be achieved (James P, 1981; Sixta, 2006).

2.1.4.4 Kraft pulping

The Kraft or sulphate process is the major chemical process used in the pulp and paper industry. It involves cooking of the wood chips at elevated temperatures in sodium hydroxide and sodium sulphide to soften and dissolve the lignin.

In the sulphite process, an acidic mixture of sulfur dioxide, water and limestone are used to dissolve the lignin. The yield is 45 to 55 percent and the pulp is light in color and has a lower tear strength than Kraft pulp. Bisulphite pulping is carried out using sodium or magnesium as a base, produces pulps of light color than that are used for tissues and printing grades.

2.1.4.5 Hybrid pulping

For the preparation of hybrid pulp both chemical and mechanical treatment are utilized and hence the prepared pulp has intermediate properties. Low chemical dosing for this process as compared with the full chemical pulping process. Chemical treatment for hybrid pulping is to pre-soften the wood chips for mechanical process so the prepared fibers are more refined. The energy consumption is indirectly reducing during this process. This is further categorized into chemical pulping and semi-chemical pulping. The chemical pulping has better strength and yield range of 85-95% than those of mechanical pulping (Mossello et al., 2010).

2.1.5 Pulp suspension

Fiber suspensions are the only non-Newtonian fluid which is pumped in such large volumes, but yet fibers suspensions flow is the least understood and the most complex industrial flow phenomenon. For the fibers suspensions flow pulp concentration is the most important parameter and is categorized in three ranges, low

consistency, medium consistency, high consistency and ultrahigh consistency. Low consistency pulp suspension is water-fiber suspension where the concentrations are less than 0-8%, medium consistency pulp suspensions are prepared by mechanical means and that is the suspensions with the concentration ranges from 8-20%, high consistency 20-40% pulp suspensions are formed by pressing water mechanically from a medium consistency suspensions and ultra-high consistency pulp suspensions are those with the concentration range of higher than 40% (Kerekes et al., 1985). Pulp suspension flow is further categorized by proposed particle existence that is individual particles, floccettes, floc, and Network by (G. G. Duffy, 2006). Fiber individual particles behavior exists in pulp suspensions at low concentrations where it can bend and absorb turbulent energy, whereas an increase in suspension concentration source in the fiber movements' limitation and existence of floccettes as the new particles. Floccettes can entangle together at high range of consistency to form entities known as "floc". When each fiber becomes impeded by several other fibers, and permanently locked in position take place and the permanently locked in position is known as network formation.

To predict the state of fiber interactions (Kerekes & Schell, 1992), suggested by the crowding number N based on volumetric and mass concentrations, as presented below

$$N = \frac{2}{3} C_v \left(\frac{L}{d}\right)^2 \cong 5 C_m \frac{L^2}{\omega} \quad (2.4)$$

where, C_v is the volumetric concentration (%), L is the length-weighted average length of the pulp fibers, d is the fiber diameter, C_m is the mass concentration (%) and ω is the fiber coarseness (mass per unit length, Kg/m).

Concentration of Pulp suspensions based on crowding number N are categorized for $N=1$, which is critical concentration suspensions having crowding number less than 1 are considered as dilute suspensions. Suspensions having crowding number ranges from 1-60 are known as semi-concentrated and concentrated suspensions are having

crowding Number value higher than 60. Another critical crowding number $N \sim 16$ known as “gel crowding number” is introduced by Martinez et al. (2003).

At low consistency, pulp suspensions exist in a two-phase slurry, while it changes into three phase heterogeneous mixture of water at medium and higher consistencies. At the higher gas contents, instead of mass consistency the use of volumetric concentration is useful. Volumetric consistency is defined by (Derakhshandeh et al., 2011).

$$C_v = C_m \left(\frac{1}{\rho_f} + \frac{X_w}{\rho_w} + V_L \right) \rho_b, \quad (2.5)$$

where, C_m is the fiber mass fraction, ρ_f is the fiber density (kg/m^3), ρ_w is the water density (Kg/m^3), ρ_b is the bulk density (kg/m^3), X_w is the water adsorbed within the fiber wall (kg water/kg fiber) and V_L is the volume per unit mass of the hollow channel in the middle of the fiber referred to as lumen ($\text{m}^3/\text{kg fiber}$).

2.1.6 Rheology of Pulp suspension

Fiber suspensions are known as non-Newtonian fluids. The characteristics of fiber suspensions are similar to those of solutions and polymer melts, such as the Weissenberg effect (i.e., rod-climbing) (Mewis & Metzner, 1974; Nawab & Mason, 1958), viscoelasticity (Thalen & Wahren, 1964; Wahren, 1964) and shear thinning (Goto et al., 1986; Kitano & Kataoka, 1981). Rheological properties of fiber suspensions depend on the suspension structure. The structure of fiber suspension is affected by such parameters, such as fiber interaction, fiber properties, the flow field imposed and suspending fluid properties.

The fluid flow properties can significantly change with the addition of fibers to a fluid. Kitano and Kataoka (1981) reported shear thinning of long fiber suspensions (aspect ratio $r_p \equiv L/d \geq 100$, where L and d are the fiber length and diameter, respectively) for vinylon fibers in silicone oil and glass, nylon, and vinylon fibers in glycerin are reported by Goto et al. (1986). Shear thinning became more Evident as the

fiber aspect ratio increased or the flexibility increased (flexibility $\propto 1/(E_Y I)$, where E_Y is the fiber's Young's modulus and I is the area moment of inertia) observed by Goto et al. (1986).

2.1.7 Pressure drop study of fiber suspension flow

Fiber suspensions flowing in pipelines usually found in papermaking processes. Due to the simple axi-symmetric geometry of a pipe flow, most experimental research has focused on this type of flow (Moayed, 1999). The earliest studies on flow mechanisms of pulp suspensions in pipelines were conducted by some researchers (Daily and Bugliarello (1958); Forgacs (1957)). They distributed the flow behavior in three different regimes that is Plug, mixed and turbulent flow regimes. Further developments into hydrodynamic behavior of suspensions were reported by the researchers (G. Duffy & Titchener, 1975; Geoffrey G Duffy et al., 1976).

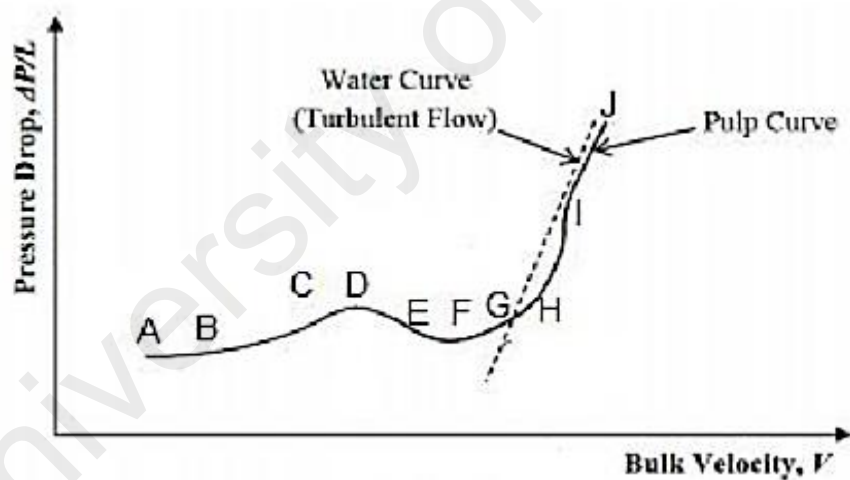


Figure 2. 2 Frictional pressure drop as a function of velocity of a pulp suspension (G. G. Duffy, 1972)

G. G. Duffy (1972), proposed different regimes of chemically cooked pulp suspensions in terms of head-loss velocity curve presented in Figure 2. 2. The letters used in frictional pressure drop curve (Figure 2. 2) refer to different regimes. The region A to H, containing several sub- regimes attributed to the plug flow, where AB zone present a fiber network region with no shearing motion. The weak shear stress due to low flow rate could not interrupts the fiber network, and hence the suspension has plug

structure (G. G. Duffy, 1972). In this process, the turbulent energy of fibers is partly absorbed by the elastic energy of the network. This elastic energy establishes itself as an elastic force that pushes fibers towards the pipe wall. In this regime of low flow velocity, elastic force exists, large enough to keep the fiber plug in a contact with the wall. In the zone BC, where velocity increasing, a water layer would have developed near the pipe wall. Furthermore, increase in velocity results in an increase in frictional pressure drop. The laminar water annulus is formed at point C.

DF regime resembles to the plug flow with water annulus in laminar shear. In this region the pressure drop curve decreases. Slightly before F regime, the point E is the onset of turbulence annulus.

FG regime resembles to the plug regime with water annulus in turbulent shear where pressure drop increasing. G zone is a critical point where the frictional pressure drop of the suspension is same as water and corresponds to the onset of drag reduction. This phenomenon is more in section 2.1.7.1.

The region H to I is known as mixed or transition regime. The plug flow disruption begins at point H. The shear stress is higher than yield stress and the fiber plug is only formed at the core and a turbulent annulus remains in proximity of the pipe wall. Moayed (1999) showed that the thickness of plug in this region is proportional to the yield stress to shear stress times the pipe diameter.

I to J regime resembles to the fully developed turbulence where the fibers are homogeneously dispersed in the suspension. In this region, the frictional pressure drop curves are still below water curve. The transition from mixed flow regime into fully turbulent regime is gradual.

Jäsberg (2007) proposed an schematic of flow behavior of pulp suspensions in a straight pipe according to the proposed mechanisms of G. G. Duffy (1972). He conducted experiments to obtain detailed hydrodynamic behavior of chemically prepared pine or birch pulps with consistency of 0.52 wt.% in a pipe flow loop with diameter of 40 mm. He presented more features of the plug flow by measuring the

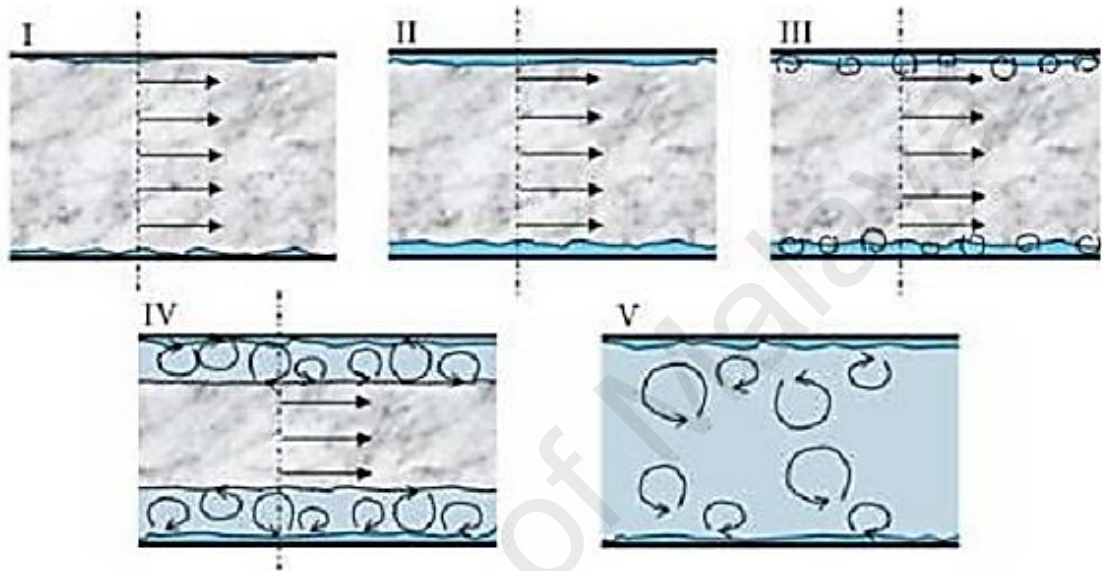


Figure 2. 3 The flow regimes of fiber suspension. (I) Plug flow regime with direct fiber-wall contact, (II) Plug flow regime with lubrication layer, (III) Plug flow with a smearing annulus, (IV) Mixed flow and (V) fully turbulent flow (Jäsberg, 2007).

thickness of a lubricating layer based on the intensity of laser light reflected by fibers and showed that the thickness of the layer reduces with the increase of the pulp concentration.

Based on the results, it is proposed that the flow may be divided into five different regimes according to flow rate, namely plug flow with wall contact, plug flow with a lubrication layer, plug flow with a smearing annulus, mixed flow, and fully turbulent flow.

2.1.7.1 Drag reduction

A fluid exhibit less pressure drop upon the addition of any additive at a similar flow rate, the phenomenon termed as drag reduction (G. G. Duffy, 1972). Phenomena of Drag reduction can be further described as reduction in the normal rate of frictional

energy loss due to any modification to a turbulent fluid flow system. The strength and nature of the vortices formed due to effect of Drag reduction, resulting structural modification of the turbulent boundary layer near wall (MacKenzie et al., 2014). The ratio of frictional loss of solvent-additive and frictional loss of solvent (Drag ratio, D_R) which could only be termed as Drag reduction when a fluid has a value of D_R less than 1 at the constant velocity is defined as (G. G. Duffy et al., 2000).

$$D_R = \left(\frac{\left(\frac{\Delta P}{L}\right)_{solvent-additive}}{\left(\frac{\Delta P}{L}\right)_{solvent}} \right) \quad (2.6)$$

2.1.7.2 Fiber-induced Drag reduction

Drag reduction phenomena has been observed in one of the most consistent solid-liquid suspensions that is pulp slurries (M. S. N. Kazi et al., 1999). To get insight into pulp suspension turbulence, it is important to investigate the drag reduction in the fiber slurry. Many researchers reported that pulp suspensions damping turbulence due to existence of fiber, flocs and Drag reduction behavior(Higgins & Wahren, 1982; M. S. N. Kazi et al., 1999).

Asbestos fibers are injected into the center of a turbulently flowing water suspension and into the boundary layer for drag reduction study by Sharma (1980). Their study reveal that the drag reduction in case of fibers injection into boundary layer was greater than that of fibers injection into the center, however in both cases the region of influence of the fibers was the turbulent core. Variations between the drag reductions for different fibers occur due to the strength variation of the fiber networks formed, that is owing to the individual fiber properties and dimensions.

Usually Drag reduction phenomenon based on the two mechanisms, momentum transfer and fiber damping. Pseudo-viscosity of slurry increases with the addition of fiber to the suspension, consequently momentum transport increases resulting more drag

without Reynolds stresses. Fiber interlocking and network formation during plug flow transition to fully developed turbulent flow enhances momentum transfer. Additionally, fiber and flocs formation have damping effect on turbulence, resulting decrease rate of momentum transfer. Usually momentum transfer is dominant at low flow rates, although at high flow rates fiber damping is dominant (Fällman, 2009). Geoffrey G Duffy et al. (1978) found that the maximum level of drag reduction at intermediate flow rates resulted by the two mechanism. Fibers must reduce turbulent momentum transfer without increasing other forms of momentum transfer to acquire exclusive drag reduction (MacKenzie et al., 2014).

2.1.8 Heat transfer and pressure drop correlations

Heat transfer and pressure drop correlations have long felt needed by heat transfer equipment's engineers which would give identical formulas for cooling and heating as well as evaluate the effect of temperature difference at the same time. Additionally, the empirical correlations would consider only satisfactory correlations, which use the same dimensionless groups computed in the same way throughout all phases of flow. Many researchers reported correlations for heat transfer and pressure drop (in terms of friction factor) for the design, development and simplicity of engineering equipment in which heat transfer and pressure drop phenomenon take place.

The Nusselt number for fully developed turbulent flow is defined as (Petukhov, 1970).

$$\text{Nu} = \frac{\left(\frac{f}{8}\right) \text{RePr}}{1.07 + 12.7\left(\sqrt{\frac{f}{8}}\right) (\text{Pr}^{\frac{2}{3}} - 1)} \quad (2.7)$$

Equation 2.6 is applicable for the range of $0.5 < \text{Pr} < 2000$ and Reynolds number $4000 \leq \text{Re} \leq 5 \times 10^6$, Where f is the Petukhove (Petukhov, 1970) friction factor presented by equation (2.7) for evaluation of friction factor for water flow.

$$f = (0.79 \ln Re - 1.64)^{-2} \quad (2.8)$$

The Nusselt number for fully developed turbulent flow is defined as (Dittus & Boelter, 1930) :

$$Nu = 0.023Re^{0.8}Pr^{0.4} \quad (2.9)$$

Martinelli (1947) obtained correlation for fully developed turbulent flow in a circular duct of a rough surface in the form:

$$Nu = \frac{\left(\frac{f}{8}\right) (Re - 1000)Pr}{5(Pr + \ln(1 + 5Pr) + 0.5\ln(Re\sqrt{\frac{f}{8}}/60))} \quad (2.10)$$

Then, the Nusselt number for fully developed turbulent flow in a circular duct is defined as (Gnielinski, 1975)

$$Nu = \frac{\left(\frac{f}{8}\right) (Re - 1000)Pr}{1. + 12.7\left(\sqrt{\frac{f}{8}}\right) (Pr^{\frac{2}{3}} - 1)} \quad \left\{ \begin{array}{l} 0.5 \leq Pr \leq 2000 \\ 2300 \leq Re \leq 5 \times 10^6 \end{array} \right. \quad (2.11)$$

For Newtonian liquid flowing in a pipe, Darcy-Weisbach proposed the energy loss due to friction as:

$$H = f \frac{L u^2}{D 2g} \quad (2.12)$$

where, f is the Moody friction factor (f_M), presented in equation 2.12.

$$f_M = \frac{D g \cdot H}{L \frac{1}{2} u^2} = \frac{D \Delta P}{L \frac{1}{2} \rho u^2} \quad (2.13)$$

Instead of Moody fraction factor, the Fanning friction factor (f_f) can also be used and given by:

$$f_f = \frac{\tau_w}{\frac{1}{2} \rho u^2} = \frac{1}{4} \frac{D \Delta P}{L \frac{1}{2} \rho u^2} \quad (2.14)$$

Prandtl's universal law of friction for smooth pipes which has been verified by Nikuradse (1932) for fully developed turbulent flow in smooth pipe with $3000 < Re <$

3.4×10^6 is taken in the form:

$$\frac{1}{\sqrt{f_D}} = 2.0 \log(\text{Re}\sqrt{f_D})^{-0.8}, \quad (2.15)$$

where, f_D is Darcy friction factor which is four times the Fanning friction factor (f_f) i.e. $f_D = 4f_f$. For fully developed turbulent flow in rough pipes with $(D/\epsilon)/(\text{Re}\sqrt{f_f}) > 0.01$ Von Karman (1930) proposed:

$$\frac{1}{\sqrt{f_D}} = 2.0 \log\left(\frac{D}{\epsilon}\right) + 1.74, \quad (2.16)$$

Where ϵ is the roughness of the pipe. Colebrook et al. (1939) developed the transition and fully developed turbulent flow region with both (ϵ/D) and Reynolds number for smooth and rough pipes and given by:

$$\frac{1}{\sqrt{f_D}} = -2.0 \log\left(\frac{\epsilon}{3.7065D} + \frac{2.5226}{\text{Re}\sqrt{f_D}}\right), \quad (2.17)$$

Colebrook et al. (1939) shown that the equation on 2017 is valid up to a value of $(D/\epsilon)/(\text{Re}\sqrt{f_f}) = 0.01$.

2.1.9 Heat transfer and pressure drop of fiber suspension flow

One of the primitive investigation for heat transfer to fiber suspensions have been reported by Middis et al. (1994). They studied the fiber stiffness, aspect ratio, fiber properties and experimental parameters (bulk temperature, particle concentration and bulk velocity) effect on wood pulp fiber and model Nylon fibers suspensions flowing through a 25.3mm ID horizontal brass pipe with constant ΔT . The effect of short fibers was similar to that of the pressure drop on the heat transfer coefficient. The heat transfer ratio (heat transfer coefficient of fiber/ heat transfer coefficient of water) increases up to velocity of 3.5m/s and then remains constant at higher velocities. The heat transfer ratio tends towards unity at low velocities. At high concentrations and low velocities, suspensions of long fiber showed some heat transfer enhancement. The magnitude of the heat transfer ratio for Nylon fibers was generally slightly less, although the pressure drop and heat transfer ratios exhibits similar trends. Heat transfer reduction of up to

40% was observed at low velocities. The crossover from heat transfer enhancement to reduction appeared to correspond to the point at which a water annulus formed around the fiber plug. This can be seen from the wood pulp fiber data as a local maximum in the pressure drop ratio results. They observed that the wood pulp fiber data showed regions of both heat transfer reduction and enhancement. The heat transfer ratio for Nylon fibers almost always lay below unity over the range of velocities, 2-10 m/s.

For velocities greater than 1m/s the heat transfer reduction for the pulp was much greater than those of nylon fibers (Middis et al., 1994). They concluded that the wood pulp fibers have thermal conductivity about two/three times less than that of Nylon fibers. The higher conductivity may offset some of the heat transfer reduction because of the increased thermal conduction within the fibers themselves. They stated that at high bulk velocities (3-10m/s) and fiber concentration (0.03%) some heat transfer enhancement for suspensions that had the similar pressure drop as water. They reported that for Nylon fibers at low aspect ratios $r < 60$ the heat transfer coefficients and the pressure drop of the suspensions were similar to those for water. The differences are due to the turbulence damping effect of the fibers. They stated that the heat transfer coefficient ratios curves (suspension/water) and frictional pressure drop ratios (suspension/water) were shifted to higher values at higher concentrations with the increase of velocities. This effect shows similar trends both in wood and nylon pulp fibers.

M. S. N. Kazi et al. (1999), investigated frictional pressure drop and heat transfer characteristics of different grades of wood pulp fibers suspensions at different concentrations. They observed that at low flow rates, the heat transfer coefficient ratio is less than unity. At higher flow rates they observed similar trends with minima in the curves at intermediate flow rates and the curves approaching unity at low flow rates. They reported that the initial decrease in heat transfer coefficient ratio occurs at much

lower velocities than at onset of drag reduction and the subsequent initial decrease in drag reduction ratio. For heat transfer and drag reduction study with different types of fibers, they observed that the more flexible fibers (ultralow coarseness Pinus Radiata) reduce the heat transfer coefficient largely. They also observed that the drag reduction increases with the increase of fiber flexibility. M. S. N. Kazi et al. (1999), observed the suspensions at low fiber concentrations augmenting heat transfer coefficient.

The extensive experimental study (M. S. N. Kazi et al., 1999) of pulp slurries at low concentration (<0.4%) for heat transfer and pressure drop in both annular pipes and pipe has been extended by G. Duffy et al. (2011). They studied heat transfer and pressure drop characteristics of wood and synthetic pulp fibers in annular flow. They conducted a series of experiments for several suspensions of an eucalypt pulp, Kraft pine pulps and a spruce pulp, as well as five synthetic fibers (Nylon 6,6, Nylon 6,6-different dimensions, Polyester, Polypropylene and Acrylic). They studied effect of fiber concentrations, fiber flexibility and length, heat transfer to synthetic fiber etc. They investigated concentrations (0.1, 0.2, 0.3 and 0.4 wt. %) effect in the velocity range of 0.1 to 2 m/s. Their results revealed that with the increase of fiber concentration heat transfer is attenuated owing to enhanced damping of turbulent eddies, the data trend spread at velocities greater than 0.5 m/s, the similar results obtained by (M. S. N. Kazi, 2001). They concluded that the increase in heat transfer coefficient than that of water at lower velocities (<0.5 m/s) is due to some fiber-fiber interaction and partial network build-up at lower shear rates, similarly in synthetic fiber suspensions the heat transfer enhancement at low velocities is due to conduction-dominated heat transfer. The fiber flexibility and length effect of different pine fibers (ULo, Lo, Med and Hi), eucalyptus Eu, and Kraft spruce Sp, at a weight concentration of 0.4 percent had correlated with heat transfer coefficient. They observed that at velocities below 0.3 m/s heat transfer coefficient of pulp suspensions were higher than that of water and

observed a lowering of heat transfer coefficient at higher velocities. Heat transfer coefficient decreases as both fiber length and fiber coarseness decrease. The obvious increase in heat transfer coefficient at low velocities was due to the high tendency for fiber to collide and entangle. G. Duffy et al. (2011), highlighted fiber variables that contributed to the modification of heat transfer, those were longitudinal flexibility, interactive and fiber aspect ratio, fiber stiffness, population, and coarseness. They also reported the effect of concentration, fiber flexibility and length, and fiber properties on frictional pressure loss. The highest concentration had the highest-pressure drop at low velocities while with the increase of velocity pressure drop moves towards the water value. Whereas with increase of fiber flexibility and length or with decrease of coarseness the pressure drop decreases.

S. Kazi et al. (2012), validated the previous heat transfer data obtained in a small pipe heat exchanger using a larger annular-area test unit with longer axial entry flow and calming section. They adopted water and two suspensions of long-fiber softwood Kraft pulps with fibers having different coarseness over a range of flow rates with fiber concentration of 0.4% and compared with the data obtained from previous heat transfer study. They reported that with the increase of annular gap size for both water and fiber suspensions flow, heat transfer coefficient decreases at the same velocities. Also, the heat transfer coefficient varies systematically with the various fiber dimensions and fiber characteristics. To study the effect of fibers and range of fiber concentrations (0.1-0.4%) on heat transfer, they used bleached kraft pine fiber of mean length 2.53 mm and coarseness 0.246 mg/m. The study revealed that the data trends for the larger test section is similar to that obtained previously for pipe flow (G. Duffy et al., 2002). They stated that the increase of heat transfer coefficient at low velocities < 0.5 m/s owing to fiber-fiber interactions and formation of some network fragment structures. Whereas the thermal conductivity of fiber suspensions are less than that of water however the higher

overall heat transfer coefficient at low velocities owing to fiber characteristics that provide a solid path for heat conduction through the fibers themselves.

S. Kazi et al. (2014a), studied the effect of entry length in turbulent flow on heat transfer to fiber suspensions in annular passage. They used Kraft pine high and ultra-low coarseness at concentrations of 0.2 and 0.4% respectively and water for comparison at a range of velocities. They observed that change in entry length have insignificant effect on heat transfer coefficient in case of Kraft pine high with fiber concentration of 0.2%. While considering Kraft pine ultra-low pulp suspension with concentration of 0.4%, they observed that the smaller entry length has 13.9% higher heat transfer coefficient than that of longer entry length at a higher velocity of 1.5 m/s but the heat transfer coefficient remain lower than that of water.

To validate friction loss and heat transfer data of fiber suspensions in circular pipe heat exchanger, S. Kazi et al. (2014b) conducted comparative study of heat transfer and friction loss of fiber suspensions in a circular and coaxial pipe heat exchanger. They used water and two suspensions of long-fiber Kraft pulp of soft wood with fibers having different coarseness. They accumulated and compared data with fiber concentrations up to 0.4% over a range of flow rates. The results showed that with increase of velocity for both water and fiber suspensions, heat transfer coefficient increases. Whereas heat transfer coefficient varies systematically with various fiber dimensions and fiber characteristics at the same experimental conditions for both circular and coaxial pipe heat exchangers. They reported that the data obtained from both pipe and annular coaxial pipe heat exchanger for fiber suspensions showed that the relationships among momentum and heat transfer and specific properties and characteristics of paper could be obtained from either type of heat exchanger.

G. Duffy et al. (2000), hypothesized that the correlation of the heat transfer coefficient, fiber and paper properties could be a new way to monitor wood

pulp quality for the characterization of the papermaking pulps. Once an acceptable range of paper qualities and heat transfer coefficient has been set, later that range of heat transfer coefficient could be used as pulp quality indicator or parameter. However, yet it is a question that to what extent the diversity in the properties of fibers used in industries resulted from different pulp sources and pulping processes, could affect the characterizations and correlations.

2.2 Study of nanofluid flow in backward-facing step

The demand for Energy is increasing day to day. The primary energy demands are covered by fossil fuels and that is decreasing due to continuous extraction. Furthermore, due to environmental concern, environmental agencies are putting pressure on companies to reduce emissions and become more energy efficient. The large portion of Energy is consumed in wide range of fields and industries e.g. oil and gas, automotive industries, food, electrical, etc. where thermal energy exchange takes place in heating or cooling applications such as heat exchangers, chemical processes, cooling of nuclear reactors, cooling of turbines blades, cooling electronic equipment and wide angle diffusers etc. In thermal energy transportation, huge energy is being lost due to lack of efficient heat exchanging equipment and use of ineffective fluids. Therefore currently, researchers are more involved in exploration of better heat exchanging fluids where Nanofluids are getting importance as heat exchanging fluid than that of conventional liquids.

Separation, recirculation regions, and consequent reattachment flow occurs due to sudden expansion in flow geometry, such as a backward-facing step (BFS), forward-facing step (FFS), corners, sharp turns and high angles of attack all represent sharply decelerating flow situations where energy and pressure losses are maximum. In many circumstances, sudden expansion is undesirable and could be the source of enhanced pressure drop along with energy losses that require additional power supply. However,

in many instances sudden expansions are encouraged, these lead to the enhanced heat and mass transfer rates due to higher mixing in separation and reattachment flow regions (Mohammed, Al-aswadi, et al., 2011). Because of this reality, the problem of laminar and turbulent flows over backward-facing and forward-facing steps test loop in natural, mixed and forced convection have been extensively investigated, both numerically and experimentally (H. Abu-Mulaweh, 2003).

2.2.1 Fluid flow through sudden expansion

Many researchers have investigated flow separation in the past decades. The pioneer researchers Boelter et al. (1948), Ede et al. (1956), Abbott and Kline (1962), Filetti and Kays (1967), Macagno and Hung (1967), Goldstein et al. (1970) and Seban (2012) established theoretical and experimental methods of studying separation flow that take place due to changes in the cross section of the passage.

Durst et al. (1974) reported flow visualization and laser-anemometry measurements over a sudden expansion with symmetric expansion ratio 3:1 in a duct with an aspect ratio of 9.2:1 downstream of the expansion. It was observed that flow is highly depending on Reynolds number, strongly three dimensional even well away from the duct corners at lowest measurable velocities. The results obtained for Reynolds number 56 shown that the separation regions behind each step were of equal length. From the expansion to a fully developed parabolic profile, symmetric velocity profiles exist for downstream, while considerable three-dimensional effects in the vicinity of the separation regions were exists. The obtained velocity profiles were with good agreement to that of obtained from the two-dimensional momentum equation. The observed two separation regions at a Reynolds number of 114 were of different lengths leading to asymmetric velocity profiles and a third separation zone observed on one wall at Reynolds number 252, downstream of the smaller of the two separation zones adjacent to the steps. Goharzadeh and Rodgers (2009) experimentally studied water flow in a

confined annular channel through sudden expansion. Refractive index matching (RIM) and particle image velocimetry (PIV) were used to measure reattachment length and velocity. Their results revealed that with the increase of Reynolds number separation length increases as illustrated in Figure 2. 4 to Figure 2. 6. Furthermore, their obtained results were with a good agreement to that of numerical results reported by Nag and Datta (2007).

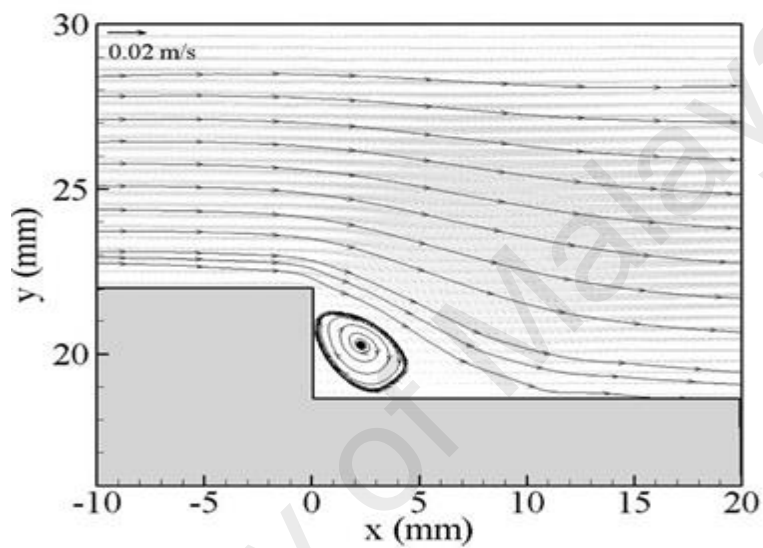


Figure 2. 4 Measurement of velocity flow field at $Re = 100$. Goharzadeh and Rodgers (2009).

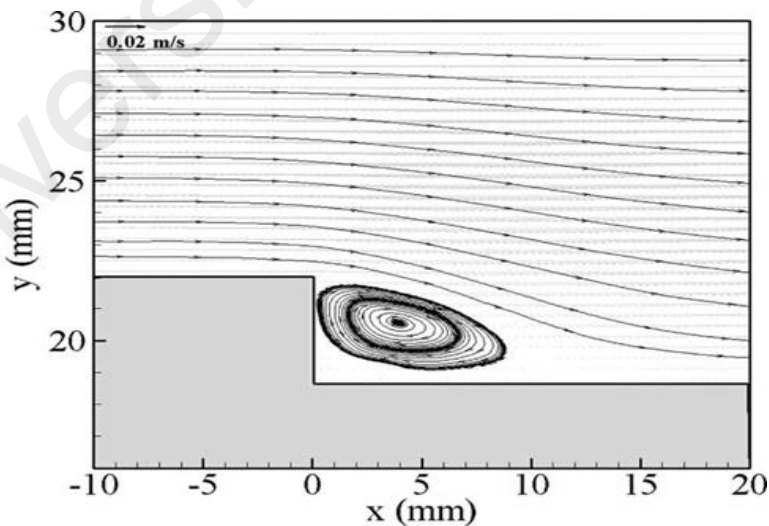


Figure 2. 5 Measurement of velocity flow field at $Re = 300$. Goharzadeh and Rodgers (2009)

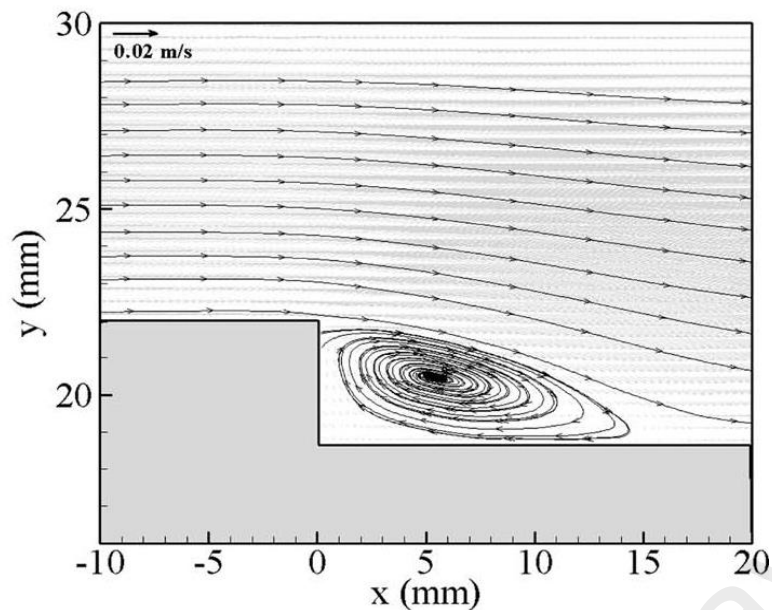


Figure 2. 6 Measurement of velocity flow field at $Re = 500$. Goharzadeh and Rodgers (2009).

Sudden expansion gas flow has been investigated numerically by Guo et al. (1996) to study the heating effect on the corner recirculation zone (CRZ). They observed that with the increase of heat length of corner recirculation zone decreases and at sufficiently high heating intensity, CRZ could even disappear. Chiang et al. (2000) conducted computational investigation to study the sidewall effect on the structure of laminar fluid flow over a plane symmetric sudden expansion. In their investigation 3 expansion ratio and 14 aspect ratios has been used. They reported symmetric nature of the flow up to the aspect ratio of 3.5, while flow symmetry can no longer remain beyond this critical aspect ratio owing to the Coanda effect. Hence, dimensions are an important variable for characterization of flow.

Boughamoura et al. (2003) numerically investigated laminar fluid flow and heat transfer of a position-driven in a cylinder containing a sudden expansion. Control-volume-based finite element method used with a moving grid and staggerd, and SIMPLER algorithm for pressure-velocity coupling. They reported that splitting, stretch, and vortexes emergence depend on the Reynolds number, expansion ratio and the initial clearance. Furthermore, pressure gradient effect is important as the initial clearance and the expansion ratio decrease or the Reynolds number increase. Pinho et

al. (2003) investigated pressure losses of laminar non-Newtonian fluid flow through a sudden expansion with diameter ratio 1 to 2.6. The obtained numerical results revealed that with decrease of shear thinning recirculation length decreases and the eddy strength weakened.

Thiruvengadam et al. (2009) investigated three dimensional mixed convections in vertical duct having sudden expansion to study the effect of heat flux, buoyancy force and aspect ratio on the laminar flow. They observed a sharp peak in recirculation regions with increase of Nusselt number and aspect ratio and linear increasing of stream wise distribution and independent aspect ratio after recirculation region.

Yang and Tsai (1996) performed an experimental study of heat transfer from a hot stream flowing during a sudden expansion where cold air injected from its porous base. The combustor entrance had 30 mm high and 200 mm wide and the aspect ratio (channel width to step height) for the step height (15mm) was 13.3. The results revealed, the heat transfer coefficient increases with increase of Reynolds number and inlet fluid temperature, whereas it decreases with increase of injection rate of the cooling air. Further, they observed that increase in the length of recirculation zone about 7.8 times of the step height when the Reynolds number increase over 6300 so that the length of recirculation zone was in the same diversity in comparison with Tsou et al. (1991) and Soong and Hsueh (1993). They have also reported that by decreasing the temperatures in the recirculation zone obtain from cooling effects of the injected fluid were considerable in the recirculation zone than other regions due much smaller velocity in the recirculation zone than that of free stream and the redeveloped boundary layer. Further, they observed that the maximum and average Nusselt numbers were larger in a higher Reynolds number.

Park and Ota (2010) experimentally studied turbulent separation flow and heat transfer in a symmetric expansion plane channel. The step used was 200 mm wide, 20

mm high, and the range of Reynolds number 5,000 to 35,000 has been manipulated. From the experimental measurements of the mean and turbulent fluctuation of temperatures and velocities, they resulted that local Nusselt number profile was remarkably different at the lower and upper walls owing to the Coanda effect that was sourced by instability between the lower and upper separated shear layers. Additionally, they (Park & Ota, 2010) used the empirical formulas and obtained the difference between heat transfer from the lower and upper walls that increased with an increase in Reynolds number and reached up to about 45% and they are chosen:

$$Nu_{max} = 0.079(U_{ref} \frac{H}{\nu})^{0.071} \text{ (Upper wall)} \quad (2.18)$$

$$Nu_{max} = 0.053(U_{ref} \frac{H}{\nu})^{0.0712} \text{ (Lower wall)} \quad (2.19)$$

D. H. Lee et al. (2011) investigated heat transfer at axisymmetric sudden expansion followed by sudden contraction called cavity in a circular channel with uniform wall temperature. The results revealed that the maximum Nusselt numbers appeared between 9 and 12 step heights from expansion step. They also obtained a good agreement with numerical results evaluated by using equation (2.21) for local Nusselt numbers is given by:

$$Nu_x = \frac{h_x D}{k_a} = \frac{v_s^2 D}{[A_s(T_{s,x} - T_{b,x})K_a R_s]} \quad (2.20)$$

Various studies have been conducted for analysis of heat transfer in separated flow with sudden expansion using different models and compared the obtained numerical results with experimental data or with other numerical data.

Recent Numerical studies in turbulent fluid flow through sudden expansions are: Sugawara et al. (2004, 2005) applied LES method to analyze three dimensional turbulent heat transfers and separated flow numerically in a symmetric expansion plane channel. They used Smagorinsky model and the analysis and fundamental equations based on the finite difference method. Their obtained numerical results agree with

previous experimental data. Several researches are concerned, to the numerical simulation for three dimensional heat transfer and separated flow in sudden expansion rectangular channel. Yoshikawa et al. (2002) investigated heat transfer in unsteady separated and reattached flow around a symmetric sudden expansion channel, similarly steady separated flow reported by Yoshikawa et al. (2004), both studies are based on Navier-Stokes equations and energy one based on finite difference method. Their results revealed that the recirculation region and separated shear layer becomes unstable with increase of Reynolds number and they also reported that the created vortices are important by greater influence on the heat transfer rate. Whereas, (Ota et al., 2000) presented numerical study of two and three dimensional heat transfer and separated flow in enlarged channel by using Navier-Stokes equations and energy one based on finite difference method. They showed that the effect aspect ratio in both results of two and three dimensional on local heat transfer rate and the transitions from symmetric to asymmetric flow due to increase of the aspect ratio.

Terekhov and Bogatko (2008) investigated the effect of boundary layer thickness before the flow separation on heat transfer and aerodynamic characteristic behind an abrupt expansion in a round tube. They used fluent program for calculation that based on menter turbulence model of shear stress transfer and found decrease of maximum heat transfer coefficient owing to increase of boundary layer thickness. Whereas, Terekhov and Pakhomov (2009) reported predictions of turbulent flow and heat transfer in gas droplets flow at a downstream of a sudden pipe expansion. Euler/Euler two-fluid model have used for the gaseous and dispersed phases. They observed heat transfer enhancement two-fold greater than that of single-phase flow upon addition of evaporating droplets at the mass concentration of droplets $ML \leq 0.05$ and also it was observed that reattachment length of dispersed phase increased in turbulent gas flow. Nusselt number decreases with increase in the diameter of initial

droplet due to reduction of interphase contact area at a fixed mass concentration of droplets.

2.2.1.1 Nanofluid flow through sudden expansion

Experimental studies of laminar and turbulent nanofluid flow through sudden expansion have not yet fully investigated. Whereas, numerical studies of laminar and turbulent nanofluid flow through sudden expansion is very limited. (Santosh Christopher et al., 2012) numerically investigated heat transfer to nanofluid in a two-dimensional sudden expansion. They used Ag, Al₂O₃, CuO, SiO₂ and Cu nanofluid and the same solving method (Kanna & Das, 2006) used for sudden expansion flow and backward facing flow with volume fraction of 0.5, 0.2, and 0.1 and Reynolds number from 30 to 150. They resulted about 1.3% decrease in reattachment length on comparison with Abu-Nada (2008) as presented in .

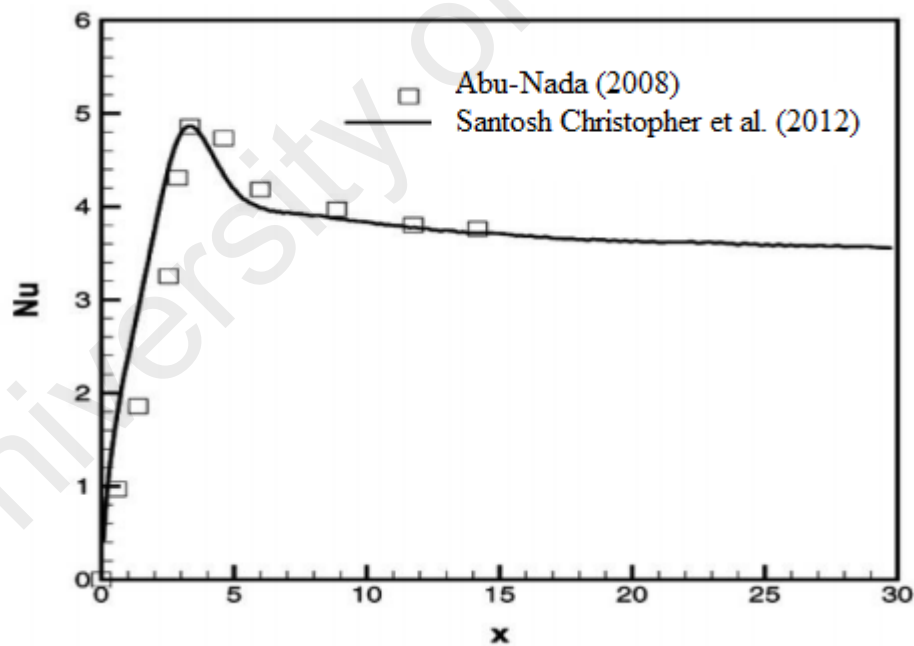


Figure 2. 7 comparison of Nusselt number for SiO₂ at Re = 100, Santosh Christopher et al. (2012)

2.2.1.2 Fluid flow through a backward and forward-facing step

Backward and forward-facing steps are important flow geometries in fluid mechanics and many engineering applications. Hereafter, fluid flow through a backward

and forward-facing step has been extensively investigated both experimentally and numerically.

(a) *Laminar fluid flow*

Stüer et al. (1999) investigated laminar flow through forward facing step experimentally using the hydrogen bubble technique to visualize and particle tracking velocimeter to get more information about separation phenomena. The experimental results revealed the increase of distance between the breakthrough in span at decreased Reynolds number and they also noticed the transverse direction of separation was slowly in comparison with short time scale.

Armaly et al. (2003) reported experimental measurements of velocity in three-dimensional laminar separated air flows on backward facing step using two components laser Doppler velocimeter with expansion ratio 2.02 and the range of Reynolds number 98.5 to 525. They observed that the size of recirculation regions was increased with the increase of Reynolds number and the maximum locations of stream wise velocity line component (u) was zero at the stepped wall with constant Reynolds number.

Saldana et al. (2005) numerically studied laminar mixed convective air flow over horizontal backward-facing step using finite volume method. They heated step from below at a constant temperature and the expansion ratio 2, aspect ratio 4 and range of Richardson number (Ri) varied between 0 to 3. The numerical results revealed that with the increase of Richardson number the primary size of recirculation region decreases and also moved the maximum value of average Nusselt number.

Barbosa-Saldaña and Anand (2007) studied laminar air flow over a three-dimensional horizontal forward-facing step numerically using a finite volume method. They considered the aspect ratio 4 and expansion ratio 2 and the inlet flow to be fully developed and three dimensional. Effect of range of Reynolds number 100, 200, 400, and 800 on the separation line, the reattachment line, velocity profiles at different planes

and span wise averaged Nusselt numbers are investigated. The numerical results indicated the formation of two recirculation regions and the size and location of these recirculation regions depend on Reynolds number. Furthermore, the size of these recirculation zones increases with the increase of Reynolds number.

Lima et al. (2008) numerically investigated two-dimensional laminar air flow over a backward facing step using two Computational Fluid Dynamics codes the first one based on finite element method (COMSOL MULTIPHYSICS) and the second finite volume method (FLUENT) and the range of Reynolds number. The obtained results were compared with the previous experimental data presenting a good agreement where the reattachment length increased non-linearly.

Velazquez et al. (2008) studied heat transfer enhancement in the laminar flow regime over a backward facing step using flow pulsation. Their results revealed augmentation of heat transfer, at Reynolds number 100 the maximum time average of Nusselt number was 55% higher in comparison with steady case.

Selimefendigil and Öztop (2013) numerically investigated the laminar air flow over a backward facing-step with a thin adiabatic fin mounted on upper wall. They studied the effects of different parameters such as Reynolds number, pulsating frequency and fin length on the fluid flow and heat transfer characteristics considering Reynolds numbers in the range of 10 and 200 with expansion ratio of 2. The numerical equations are solved using FLUENT, created on finite volume based solver. The results indicated that with the increase of Reynolds number and fin length heat transfer augmentation increases.

(b) Turbulent fluid flow

Terekhov et al. (2003) experimentally investigated characteristics of a turbulent gas flow and heat transfer behind a step and a rib and distributions of temperatures, heat transfer coefficients and pressures behind the obstacles. They analyzed the features of

heat transfer in recirculation and relaxation zones of separated gas flow and they determined the effect of separation on intensification and suppression of turbulent heat transfer. They also showed the results obtained agree with previous data for a downward step (Alemasov et al., 1989) where at the maximum recirculation velocity about 5-10% enhancement was obtained. They observed, decrease in the obstacle height which resulted in a significant augmentation of heat transfer and the maximum augmentation was obtained closer to the obstacle. For the flow with separation past a rib, the maximum heat transfer is shifted also in the downstream direction from the flow separation point compared to the case of a downward step.

H. I. Abu-Mulaweh (2005) experimentally studied turbulent fluid flow and heat transfer of mixed convection boundary-layer of air flow over an isothermal two-dimensional, vertical forward-facing step. They investigated the effect of step heights on local Nusselt number distribution as shown in

, and obtained that the local Nusselt number increases with the increasing of step height and it obtains the greatest value at the reattachment zone. Their results indicated that the increase of step height leads to increase of the reattachment length transvers velocity fluctuations, intensity of temperature fluctuations and the stream wise turbulence intensity.

For analysis of heat transfer in separated flow over backward facing step, large eddy simulation model applied by many researchers where the pioneer investigation was presented by Labbé et al. (2002), Avancha and Pletcher (2002), and Mehrez et al. (2009). They observed significant enhancement of heat transfer rate in the recirculation zone and obtained the trends of heat transfer coefficients which validates previous experimental data.

Three dimensional convective fluid flow and heat transfer over a backward facing step had been studied by many researchers (Kitoh et al., 2007; Nie & Armaly, 2002; Sakuraba et al., 2004; Saldana et al., 2005; Uruba et al., 2007). They focused on effect of Reynolds number, expansions ratio, and injection or suction on augmentations of heat transfer over backward-facing step.

Y. Chen et al. (2006) numerically investigated two dimensional turbulent forced convection flows adjacent to backward facing step. They focused the effects of step height on turbulent separated flow and heat transfer. In their study the Reynolds number and duct's height at downstream from the constant step used are Re 28,000 and H 0.19 m respectively. Constant and uniform heat flux having value of $q = 270 \text{ w/m}^2$ at the stepped wall downstream from the step while other walls were insulated. Bothe the velocity and the temperature fields were calculated using two equations at low Reynolds number turbulence models (Abe et al., 1994, 1995). Since recirculation flow took place after the step, the results showed that the peak values of the transverse velocity component had become smaller with the increase of the step height. The surface

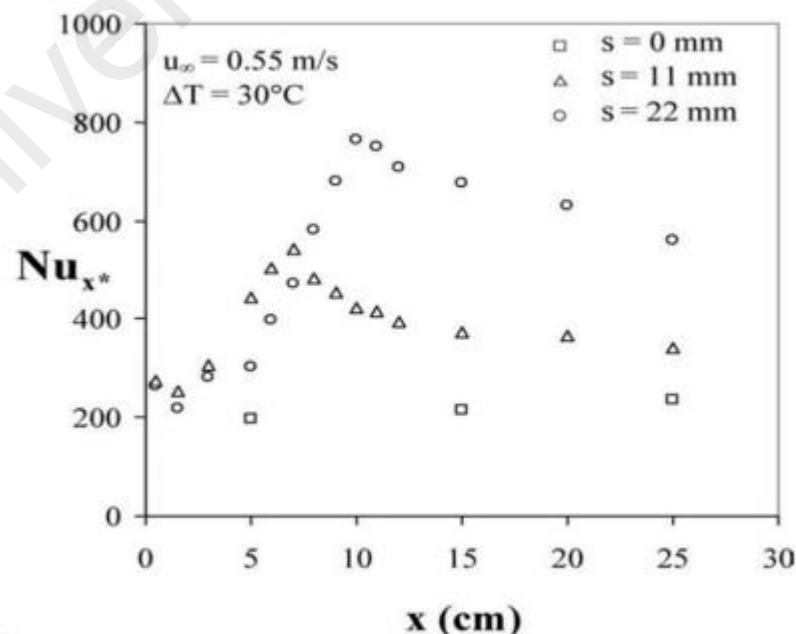


Figure 2. 8 Figure 2. 9 Local Nusselt number variation downstream of the step, H. I. Abu-Mulaweh (2005)

temperature increases with the increase of step height. Furthermore, with the increase of step height, the bulk temperature increases more rapidly.

Öztop (2006) numerically studied forced convection flow and heat transfer over a double forward-facing step. They used the standard K- ϵ model in simulations and the range of first step from 1 cm to 8 cm and second step from 2 to 8 cm and step length varied as well. The step was heated from the bottom and the rest of the test section were insulated. They observed that with the increase of Reynolds number both the turbulent intensity and heat transfer were increasing. Furthermore, step height ratio is a more effective parameter than the length ratio. Consequently, Oztop et al. (2012) numerically studied turbulent flow and heat transfer over double forward facing step with obstacle. The bottom wall of the step was heated and the rest of the test section were insulated. The range of Reynolds number varied between 30,000 to 100,000 and the height of first steps were 2, 4, and 6 cm and the heights of the second steps were 4, 6, and 8 cm. The aspect ratios of the obstacles were ranged from 0.5 to 1. They used finite volume method with K- ϵ model through FLUENT 6.2 software. They observed the enhancement of heat transfer with the increase of Reynolds number and step heights and also noticed the effect of obstacle aspect ratio on Nusselt number where the maximum Nusselt number occurred at aspect ratio of obstacle $Ar = 1$.

2.2.1.3 Laminar Nanofluid flow

Kherbeet et al. (2015) investigated heat transfer characteristics of laminar nanofluid flow over the microscale forward-facing step and backward-facing step experimentally. In their experimental investigation, the Reynolds number range of 280-480, concentration of SiO₂-water nanofluid 1% and 0.5 % with a nanoparticle diameter of 30 nm were used.

Abu-Nada (2008) is pioneer researcher reported laminar forced convective heat transfer over backward-facing step flow using Al₂O₃, TiO₂, Cu, CuO, and Ag

nanofluid, volume fractions between 0.05 and 0.2 and over the range of Reynolds numbers ranging from 200-600. He assumed two-dimensional laminar flow situation solving the backward-step flow problem numerically. An investigation of findings indicates that the Nusselt number increased with the Reynolds number and volume fraction. Al-aswadi et al. (2010) investigated the laminar forced convective flow over a 2D horizontal backward-facing step in a duct numerically using finite volume method with different nanofluids. They reported that the reattachment length and recirculation size showed an increase with increases the Reynolds number. Low dense nanoparticles such as SiO_2 exhibited the highest velocity than those with high dense nanoparticles such as Au. The effects of nanofluid on a mixed convective heat transfer over 2D microscale backward-facing step in the range of laminar flow are investigated numerically by A. Sh Kherbeet et al. (2012). They used four types of nanoparticles; CuO, Al_2O_3 , ZnO, and SiO_2 , with a volume fraction range of 1-4%. Their results revealed that SiO_2 nanofluid showed the highest Nusselt number among all the used nanofluids. Also, results indicated that with the increase of volume fraction of nanoparticles in the base fluid the Nusselt number increases.

combined convection flows in the range of laminar flow are investigated numerically over a two-dimensional forward-facing step with a blockage using different types of nanofluids (SiO_2 , Al_2O_3 , ZnO, and CuO), different diameters (25nm-80nm) of nanoparticles and different volume fractions (1-4%), were investigated numerically by A Sh Kherbeet et al. (2014). Additionally, effects of different shapes of blockage (Square, Circular, and triangular) were investigated. An investigation of findings showed that highest Nusselt number achieved in the circular blockage followed by square blockage and triangular blockage. They also reported that nanofluids with SiO_2 nanoparticles have the highest Nusselt number. Conversely, Nusselt number increases with the increase of volume fraction and Reynolds number and decreases as the

nanoparticles diameter increases A. Sh Kherbeet et al. (2014). In this study, the nanofluid EG-SiO₂ with a nanoparticle diameter of 25 nm and volume fraction of 0.04, was used. They reported that with the increase of the step height the Nusselt number and skin friction coefficient increases. Their findings also showed that the pressure drop and Reynolds number decreases with an increase in the step height.

2.2.1.4 Turbulent nanofluid flow

Togun et al. (2014) numerically studied heat transfer to turbulent and laminar Cu-water nanofluid over a backward-facing step using finite volume method and FORTRAN code was used for solving the momentum, continuity, energy and turbulence equations. The shear stress transport K- ω Model was used for turbulence modelling. They used two volume fractions of nanofluid (2% and 4%) along with water, Reynolds number range 50 to 200 for laminar range and 5000 to 20,000 for the turbulent range. The expansion ratio of 2 and constant heat flux of 4000 W/m² was considered. Their results indicated that nanofluid concentrations have significant effect on Nusselt number both in laminar and turbulent range. The recirculation flow at the downstream inlet region owing to expansion ratio that increase Nusselt number and enhanced heat transfer. Pressure drop increases with increase of Reynolds number and decrease of nanofluid volume fraction, whereas the maximum pressure drop was detected in the downstream. The highest heat transfer enhancement was 26% and 36% for turbulent and laminar range, respectively.

Safaei et al. (2014) investigated turbulent forced convective heat transfer of functionalized multi-walled carbon nanotube (FMWCNT) nanofluids through a forward-facing step. The shear stress transport K- ω Mod was used for turbulence modelling. They considered the range of Reynolds number 10,000 to 40,000, heat flux range of 1,000 to 10,000 W/m², and volume fractions of 0.00% to 0.25%. The two-dimensional equations were solved by finite volume method. They studied the effect of

shear force, heat flux, nanoparticle concentration, turbulence and contraction on fluid flow and heat transfer to nanofluid. The results showed that the concentration and Reynolds number have significant effect on the heat transfer coefficient. Enhancement of local heat transfer coefficient was marked with the increase of both Reynolds number and concentration. Furthermore, the channel passage contraction leads to the formation of two recirculation regions with augmented local heat transfer coefficient value.

Ahmad Amiri et al. (2016), conducted an experimental study on thermophysical properties of ethylene glycol-functionalized graphene nanoplatelets/water-ethylene glycol nanofluids (EGGNP-WEG) and a numerical study on the convective heat transfer through a backward-facing step. To achieve a stable colloidal suspension in water-ethylene mixture EGGNP was synthesized. They characterized EGGNP-flakes for the analysis of surface morphology and functionality. For convective heat transfer coefficient study in turbulent regime, a numerical study was conducted at different concentrations of EGGNP. They resulted that the higher weight concentration showed the highest heat transfer coefficient and thermal conductivity.

Ahmad Amiri et al. (2017), synthesized single layer graphene (SGr) with high specific surface area and functionalized with hydrophilic groups for highly stable colloidal suspensions. They characterized the synthesized single layer graphene for stability, thermal conductivity, surface morphology etc. furthermore, they studied heat transfer in transitional and turbulent flow regimes to the synthesized SGr nanofluid flowing through a duct with a backward-facing step. The investigation revealed that with the increase of Reynolds number the average heat transfer coefficient ratio $(h_{nf}/h_{bf})_{avg}$ decreases from 233.5% at Reynolds number of 2000 to 83.8% at Reynolds number of 16,000 at the same weight concentration of 0.01%.

2.2.2 Nanofluids

Conventional heat transfer fluids such as water, oil, and ethylene glycol have characteristically low thermal conductivity than metal oxides and metals. Consequently, heat transfer characteristics of fluids are expected to be better than traditional heat transfer fluids upon suspending solid particles (Masuda et al., 1993). But fluids with suspended particles of millimeter or micrometer size in the practical application used as a coolants source have some problems, such as corrosion, erosion, instability of particles, clogging of flow channels, and additional pressure drop (Kebllinski et al., 2002; B.-X. Wang et al., 2003; H.-q. Xie et al., 2002). In contrast, many researchers have reported that the convective heat transfer coefficient and the effective thermal conductivity of the base fluid can be enhanced via dispersing solid nanoparticles of a high thermal conductivity in conventional base fluids (Beck et al., 2009; H. Chen et al., 2009; Murugesan & Sivan, 2010; Özerinç et al., 2010; Solangi et al., 2015). Solid particles can be metallic such as Al_2O_3 , SiO_2 , CuO , Cu , ZnO and TiO_2 , and nonmetallic e.g. carbon and graphene nanoparticles etc. (Mohammed, Al-Aswadi, et al., 2011).

2.2.3 Stability of Nanofluid

Preparation of stable homogeneous suspension of nanoparticles, still a technical challenge as the nanoparticles always form aggregates due to strong van der Waals forces among nanoparticles. Stability of nanofluids is important in practical applications as the thermos-physical properties of unstable fluids change with time (Bianco et al., 2014; Haghghi et al., 2013). Although for the preparation of nanofluids various methods have been developed but the nanofluids prepared from these methods still unstable due to particle agglomeration. The stable nanofluid can be achieved by homogenous dispersion of nanoparticles in the base fluid. Stability of nanofluids increases its thermal and electrical properties (Philip & Shima, 2012; Ponmani et al., 2014). Nanoparticles agglomeration along with sedimentation and clogging of micro

channels also decreases the thermal conductivity of nanofluids (Beck et al., 2010).

For preparation of stable and homogeneous nanofluid, addition of surfactants is one of the common method. Surfactants such as sodium dodecyl sulfate (SDS) source electrostatic repulsion among surfactant-coated nanoparticles that significantly decreases particle agglomeration (Fendler, 2001; Tantra et al., 2010).

Fluids are either stationary or moving in heat transfer equipment in various industries such as petroleum, mineral, and mining. The probability of particles sedimentation on the tube in flowing nanofluids is low due to mixing. However, there exists higher sedimentation probability in natural convection and pool boiling environments owing to stationary condition of the bulk fluid. Consequently, the settled particles could clog fluid channels and add resistance to thermal wall where wall materials are highly thermal conductive. Eventually, these kinds of nanofluids could decrease heat transfer instead of enhancement (Witharana et al., 2013).

2.2.4 Mechanism of heat transfer using nanofluid

2.2.4.1 Brownian motion

Random motion of particles suspended in a fluid is known as Brownian motion. Due to Brownian motion particles move through liquid and probably collide, thereby heat transport from one to another directly due to solid-solid transport (Kebinski et al., 2002). Many researchers reported effect of Brownian motion on the thermal conductivity of nanofluids. Considering Brownian motion of the nanoparticles Bhattacharya et al. (2004) used Brownian dynamics simulation to determine the effective thermal conductivity of nanofluids. The effective thermal conductivity k_{eff} for nanofluid was defined as:

$$k_{\text{eff}} = \phi k_p + (1 - \phi) k_f, \quad (2.21)$$

where, k_p is bulk thermal conductivity of nanoparticles including the effect of Brownian motion of the nanoparticles on the thermal conductivity. Brownian dynamics

simulation method was developed to calculate k_p , then the effective thermal conductivity of Al_2O_3 /ethylene glycol and Cu/ethylene glycol nanofluids were calculated for different particle volume fractions. Their results were within agreement with previous experimental data (Eastman et al., 2001; H.-q. Xie et al., 2002) upon comparison. The effect of convection induced and translational Brownian motion by Brownian motion, compared by Prasher et al. (2005). They also considered the existence of an interparticle potential. From order-of magnitude analysis, they concluded that the anomalous thermal conductivity enhancement of nanofluids is mainly due to convection in the liquid induced by Brownian motion of nanoparticles.

In contrast, some studies proposed that thermal conductivity enhancement is not very effected by Brownian motion. The thermal conductivity enhancement owing to Brownian motion is a very small portion of the thermal conductivity of the base fluid, which has theoretically proved by Evans et al. (2006). Additionally, molecular dynamics simulations also prove it. The author concluded that anomalous thermal conductivity enhancement of nanofluids could not be mainly owing to Brownian motion of nanoparticles. C. Li and Peterson (2007) numerically investigated the effect of mixing due to the Brownian motion of nanoparticles on the effective thermal conductivity of nanofluids. For a single nanoparticle, pressure, velocity, and temperature distribution around the nanoparticles were investigated. It was observed that enhancement in thermal conduction capability of the nanofluid induced by a single nanoparticle was less than twice the improvement observed for the two nanoparticles that were close to each other. For the simulation of several nanoparticles, a similar behavior was observed. Hence, the author concluded that the mixing effect owing to Brownian motion of the nanoparticles is an important reason of the anomalous thermal conductivity enhancement of nanofluids.

2.2.4.2 Liquid layering on the nanoparticle-liquid interface

The liquid molecules form layered structures around solid surfaces (C.-J. Yu et al., 1999) and it is expected that those nanolayers have a higher effective thermal conductivity than the liquid matrix (W. Yu & Choi, 2003). Consequently, thermal conductivity enhancement of nanofluids owing to the formation of layered structures around nanoparticles (W. Yu & Choi, 2003).

Absence of experimental data regarding the thickness and thermal conductivity of these nanolayers is an important downside of the proposed mechanism. Some theoretical models have been developed, by few researchers considering liquid layering around nanoparticles and illustrate the predictions of their model by assuming thickness of the monolayer and thermal conductivity value (W. Yu & Choi, 2003). In addition, some researchers have modeled thermal conductivity of the nanolayer so that it linearly varies across the radial direction (H. Xie et al., 2005). Furthermore, thermal conductivity of these layers is considered temperature dependent (Sitprasert et al., 2009).

Thermal conductivity and thickness of the nanolayer calculation method has been proposed by D. Lee (2007) considering electric double layer formation around the nanoparticles. They reported that thickness of nanolayer depends on the ionic strength, dielectric constant and temperature of the nanofluid. The parameters of the thermal conductivity of the nanolayer are ion density in the electric double layer, thermal conductivity of base fluid and nanoparticles, total charged surface density and pH value of the nanofluid. Tillman and Hill (2007) proposed another theoretical method of calculating the thermal conductivity and thickness of the nanolayer. To obtain a relation between the radial distribution of thermal conductivity in the nanolayer thickness and nanolayer, classical heat conduction equation along with suitable boundary conditions has been utilized. The relation requires an initial guess about the function that defines

radial variation of thermal conductivity inside the nanolayer. As per the guess, checking the validity and determining the thickness of the nanolayer associated with assumption is possible. In contrast, some researchers reported that nanolayers are not the main source of the thermal conductivity enhancement with nanofluids, such as Xue et al. (2004) using molecular dynamics simulations determined the effect of nanolayer and showed that nanolayers do not affect the thermal transport. A simple monoatomic liquid was considered during simulations and in case of water authors noted that, the results might be different.

2.2.4.3 Nature of heat transport in nanoparticles

Heat is transferred through conduction signify that heat is transfer internally, via vibration of molecules and atoms. The vibrations of the atoms that are linked together, as it gives rise to the vibrations of the entire crystal, that is to lattice vibrations. The energy of the whole vibrating system is quantized, and the quantum of thermal energy emitted or absorbed via an atom is known a phonon. Consequently, a phonon is a quantized mode of vibration arising in rigid crystal lattice and plays a major role in material's thermal conduction. The phonon mean free path is much shorter in the liquid than in the particle demonstrated by Koblinski et al. (2002) and would be effective as the distance between the thickness of the liquid layer and particles are small. A lower phonon density exists in cooler regions of a crystal than in hot regions. Accordingly, heat conduction is important owing to the diffusion of phonons, and since the temperature gradient changes from hot to cold regions.

2.2.4.4 Effects of nanoparticles clustering

Effective thermal conductivity could be greatly affected due to clustering of particles by creating paths of low thermal resistance. It is well known, that as particles agglomeration increases, the size of cluster increases and becomes denser therefore they clustered down, this phenomenon results decrease in thermal conductivity

enhancement. To minimize or avoid the particle clustering, nanofluids should comprise of small particles size and low concentration. The effective volume of a cluster, which is the volume from which other clusters are excluded, can be much larger than the physical volume of the particles (Eastman et al., 2004; Koblinski et al., 2002). Furthermore, the thermal conductivity may increase significantly as the volume fraction of highly-conductive phase is larger than the volume of solids, subsequently heat can flow very rapidly within such cluster (Koblinski et al., 2002).

2.2.4.5 Thermophoresis

The Sorèt effect or thermophoresis is a phenomenon observed when a mixture of two or more than two types of motile particles is subjected to a temperature gradient force. This phenomenon is most substantial in a natural convection process, where the flow is driven via temperature and buoyancy. The particles travel in the direction of decreasing temperature and the process of heat transfer increases with a decrease in the bulk density.

2.2.4.6 Reduction in thermal boundary layer thickness

Thermal boundary layer study has been done by a few researchers (Ding & Wen, 2005). They reported that a decrease in the thermal boundary layer thickness may be a mechanism that causes heat transfer enhancements in nanofluids.

2.2.5 Temperature effect

Putra et al. (2003) discovered that nanofluid is a very strong temperature dependent, using the same nanofluids CuO and Al₂O₃ particles as those used by S. Li and Eastman (1999). They measured the thermal conductivity of oxide nanofluids using the temperature oscillation technique over temperature range of 21-50 °C. The author concluded that the thermal conductivity enhancement for alumina and copper oxide nanofluids, an almost threefold increase as shown in Figure 2.11 and Figure 2.10 respectively.

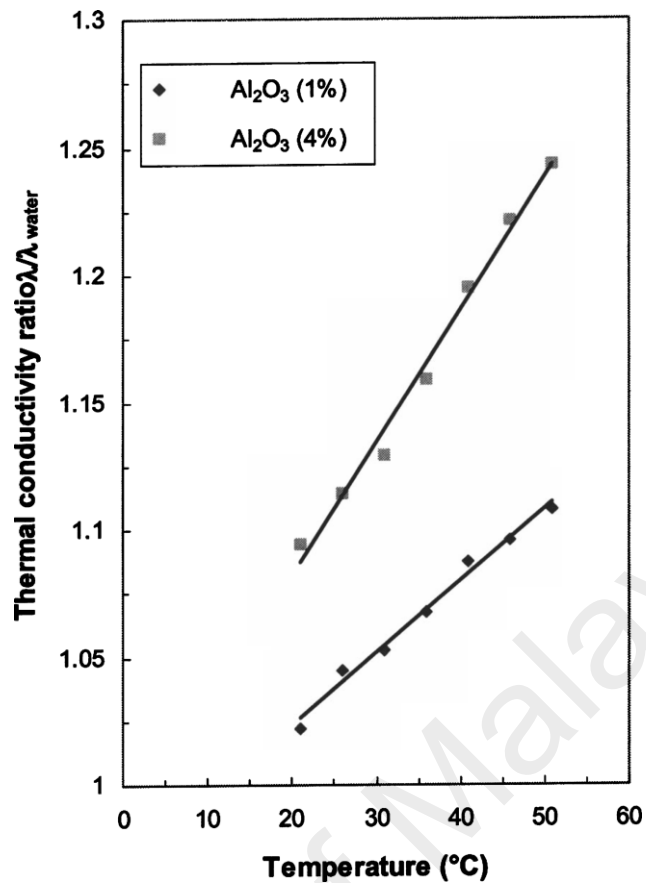


Figure 2.10 Thermal conductivity enhancement of alumina-water nanofluids versus temperature (Putra et al., 2003). $\lambda/\lambda_{\text{water}}$ denotes the ratio of thermal conductivities of the nanofluids to that of the base fluid.

Thermal conductivity results observed by Putra et al. (2003) is contrary to that of the results observed at room temperature by S. Lee et al. (1999). The obtained results for both CuO and Al₂O₃ are not within the agreement of Hamilton and Crosser (1962) model since over this temperature range the model is not sensitive to temperature. These obtained results revolutionized the concept of nanofluid due to anomalous increase of thermal conductivity in the heated state. They suggested that a certain particle movement within the fluid may exist that dramatically changes with temperature.

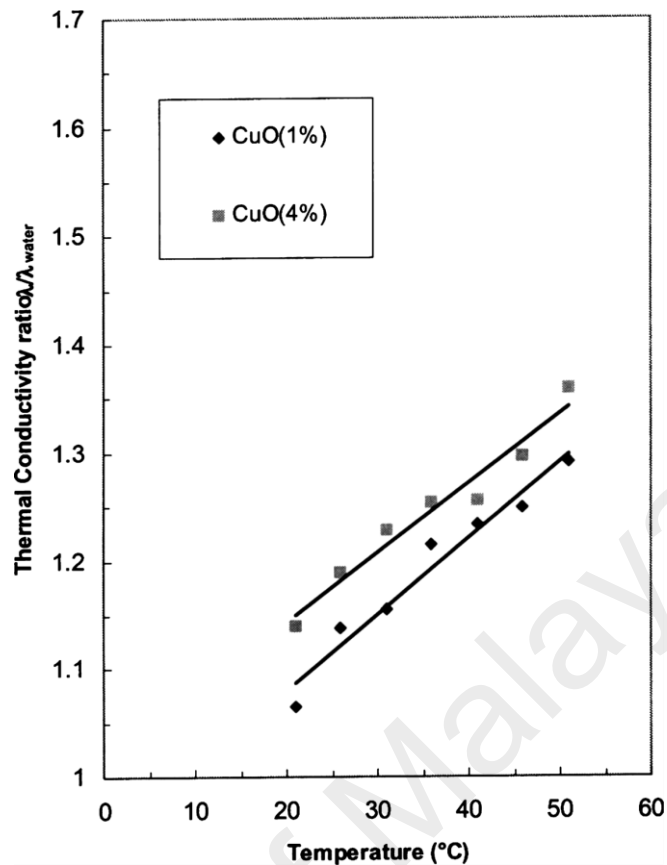


Figure 2.11 Thermal conductivity enhancement of Copper oxid-water nanofluid versus temperature (Putra et al., 2003). $\lambda/\lambda_{\text{water}}$ denotes the ratio of thermal conductivities of the nanofluids to that of the base fluid.

The findings of S. Lee et al. (1999) and Patel et al. (2003) have been reconfirmed by Chon et al. (2005) and also they confirmed the temperature effect obtained by Sarit Kumar Das et al. (2003). Furthermore, they (Chon et al., 2005) showed the inverse dependence of particle size on the thermal conductivity enhancement with three sizes of alumina nanoparticles suspended in water.

2.2.6 Viscosity

Viscosity of nanofluid is an important property for all fluids, used for thermal applications, also viscosity describes the internal resistance of a fluid to flow (Kole & Dey, 2010). The pumping power is associated with the Viscosity of a fluid. The pressure drop in laminar fluid flow is directly proportional to the viscosity. Additionally, viscosity effects the convective heat transfer coefficient. Viscosity of nanofluids has been studied by a very few researchers while for heat transfer

performance, study of a nanofluid viscosity is a significant property (Eastman et al., 2004; Maiga et al., 2005)

Jia-Fei et al. (2009) mentioned that viscosity of nanofluid is dependent on particle size and morphological structure for particular nanoparticle loading; small and high length-to-width ratio particles yield high value.

Primarily viscosity of nanofluids is dependent on nanoparticle size, concentration and temperature. Particle interaction is high for the nanofluids with large size nanoparticles and high concentration that may result in particles agglomeration and hence decrease the heat transfer enhancement and increase the flow resistance. Particles rotate as they move during the shear process therefore particle shape plays an important role. Spherical particles take up less volume when rotating than cube-shaped particles and hereafter more free volume is available for the liquid between the particles (H. Chen et al., 2007; Sarit K Das et al., 2003; Kole & Dey, 2010; Kwak & Kim, 2005; J.-H. Lee et al., 2008; J. Li et al., 2002; Nguyen et al., 2007; Prasher et al., 2006).

2.2.7 Heat Capacity

The amount of heat required to change temperature of a substance by one Kelvin is known as heat capacity, and has units of joule per Kelvin (J/K) in the SI system. The specific heat capacity is the heat capacity per unit mass, generally per gram of material (J/g K). While the specific heat capacities of nanofluids are different from that of the base fluid and it increase with the size and volume concentration of nanoparticles decrement. The enhancement of specific heat capacity of nanofluid is also due to the high specific interfacial area of the nanoparticles can absorb liquid molecules to their surfaces and form liquid layers that conversely compel nanoparticles and turns its free boundary surface atoms to be bound to inner atoms (He et al., 2007; B.-X. Wang et al., 2006; L.-P. Zhou et al., 2010; S. Zhou & Ni, 2008).

2.2.8 Pressure drop and nanofluid

Extensive study has been conducted both experimentally and numerically to improve the heat transfer performance and pressure drop of nanofluids at different concentrations in laminar and turbulent flow regimes (Sarkar, 2011; Youssef et al., 2012).

Nanofluids decrease friction and wear and operation of components such as pumps and compressor, consequently leading to more than 6% fuel savings, considerable energy saving could be obtained in the future (Bhogare & Kothawale, 2013; C. Choi et al., 2008). Sundar et al. (2012) obtained 30.96% and 10.01% heat transfer and friction factor enhancement with concentration of 0.6 vol.% of Fe_3O_4 nanofluid at a Reynolds number of 22,000. Duangthongsuk and Wongwises (2010), reported that the pressure drop of nanofluids were slightly higher than those of the base fluids and increases with the increase of concentration. Teng et al. (2011) studied pressure drop of Titanium dioxide (TiO_2) nanofluid in circular pipe. They reported that the pressure drop under turbulent flow conditions was lower than that of laminar flow conditions. Sajadi and Kazemi (2011) studied the turbulent heat transfer characteristics of TiO_2 nanofluids in circular pipes in the turbulent flow regime for various volumetric concentrations. They observed slightly higher pressure drop for nanofluids than that of base fluids and pressure drop increases with the increase of concentration. Vajjha et al. (2010), reported that the pressure drop of nanofluids increases with the increase of concentration, and the increase of pressure loss of 10% Al_2O_3 nanofluid was about 4.7 times the data from the base fluid. Duangthongsuk and Wongwises (2009) reported that the pressure drop data of the nanofluids were very close to those of the base fluids.

2.3 Summery

Study on the effect of heat transfer and friction loss of crop fiber suspensions such as Kenaf core and Kenaf bast and blend of crop short and long fibers such as Kenaf core and Kenaf bast at different ratios and blend of crop and wood pulp fiber suspensions are important as there is no significant work reported in the literature as in case of wood pulp fiber suspensions. The aim of present work is to generate experimental data for crop, blend of crop-crop and blend of crop-wood pulp fiber (non-wood fiber) for future development of valid models of turbulent fiber suspensions and introduce insight on the advancement of fiber processing and decrease of paper production loss by monitoring of heat transfer coefficient or frictional pressure loss of fiber suspensions.

Separation, recirculation regions, and consequent reattachment due to sudden expansion in flow geometry, such as a backward-facing step (BFS), play an important role in fluid mechanics and many engineering applications, where heat transfer occurs. This sudden expansion is present in heating or cooling applications. In many circumstances, sudden expansion is objectionable. However, in many instances sudden expansions are encouraged, these leads to the enhanced heat and mass transfer rates due to higher mixing in separation and reattachment flow regions. Because of this reality, the problem of laminar and turbulent flows over backward-facing and forward-facing steps test loop in natural, mixed and forced convection have been extensively investigated, both numerically and experimentally using conventional fluids. But, conventional heat transfer fluids such as water, oil, and ethylene glycol have characteristically low thermal conductivity than metal oxides, metals and carbon family. Consequently, heat transfer characteristics of fluids are expected to be better than traditional heat transfer fluids due to suspending solid nanoparticles. Solid particles can be metallic such as Al_2O_3 , SiO_2 , CuO , Cu , ZnO and TiO_2 , and nonmetallic e.g. carbon

and graphene nanoparticles etc. As nanofluids improves the heat transfer characteristics of base fluids so using nanofluids in an engineering flow geometry such as backward-facing step would enhance heat transfer, as Al_2O_3 -water, SiO_2 -water and MWCNT-asp-water nanofluids in backward-facing step for heat transfer study has been not reported in the literature.

University of Malaya

CHAPTER 3: METHODOLOGY

3.1. Study of flowing fiber suspensions in Pipe line

3.1.1 Pipe line flow Experimental Setup

The schematic and photograph of the flow loop of the test section and experimental setup is shown in **Figure 3. 1** and **Figure 3. 2** . The magnitudes of the dimensions of the test section are presented in *Table 3. 1* and **Figure 3. 1**.

Table 3. 1 Dimensions of test section

Parameters	Test Section
Heated length m	0.9
Heated area m ²	0.1422
Total thermocouple length m	0.79
Pipe cross sectional area m ²	0.001353

The flow loop of test section consists of stainless steel piping, jacketed stock tank connected with a chiller for cooling of pulp suspension up to the desired bulk temperature, a variable speed pump, a magnetic flow meter, differential pressure transducer, heated test section and recycle piping setup. The test section is made of Aluminum and is a 900 mm length of 41.5 mm internal diameter. The heat transfer test section was cut for three grooves along the flow direction from the discharge end up to 110 mm inside along the test section. The longitudinal grooves were used to house the thermocouples. The grooves were cut as deep as possible while ensuring that the inside surface of the pipe was not disturbed. A distance of 2.25 mm was maintained between groove surface and the inner surface of the tube and of a 1.5 mm diameter stainless steel

Ten flat coil heaters 900 W each were utilized for the heating of test section. The pulp suspension was pumped from the 100 L capacity mild steel tank by the LOWARA stock pump driven by a 2.71 KW AC motor which is controlled by a variable speed AC Controller.



Figure 3. 2 photograph of the experimental setup of suspensions flow.

3.1.2 Data acquisition

The inlet, outlet, and wall temperatures data were logged using a data logger (Graphtec, midi logger GL220). Flow rate was measured using Magnetic flow meter 8000 A SERIES (FOXBORO) and a Differential Pressure cell transmitter IDP10 (FOXBORO) was used to measure the pressure drop. Heater power was calculated from the current and voltage supplied to the heater, and the supplied current and voltage data were measured by 1000 A true RMS meter (Agilent). All the data were taken at steady-state conditions at an instantaneous velocity, bulk temperature, and heat flux.

3.1.3 Material

In the present investigation two non-wood Kenaf core and kenaf bast and softwood (*Acacia mangium*) are used as a pulp fiber source. All pulp source has been prepared in Forest Research Institute of Malaysia (FRIM).

Pulp samples produced by mechanical process from Kenaf core (short fiber) and Kenaf bast (long fiber) non-wood sources are Kenaf core mechanical pulp fiber (kcm) and Kenaf bast mechanical pulp fiber (kbm), which are prepared by mechanical process,

refining mechanical pulping (RMP).

Chemical processed pulp fiber samples produced from Kenaf core, kenaf bast and Acacia mangium non-wood and wood sources are kenaf core chemical unbleached (kccu), kenaf bast chemical unbleached (kbcu) and Acacia mangium chemical unbleached (amcu) respectively. Bleached pulp fiber samples kenaf core chemical bleached (kccb), Kenaf bast chemical bleached (kbcb) and Acacia mangium chemical bleached (amcb) pulp fiber samples are prepared by bleaching kccu, kbcu and amcu respectively.

Three samples of pulp fibers kckb3, kckb4 and kckb5 are prepared from mixing non-wood short (kenaf core) and long fiber (Kenaf bast) pulp fibers with the ratio of 9:1, 8:2 and 7:3 respectively. Amkb pulp fiber sample is prepared by mixing amcb and kbcb with the ratio of 9:1, respectively.

3.1.4 Experimental procedures

The pulp fibers were disintegrated in the disintegrator up to 35000 rpm before each experiment. The disintegration process was carried out per the TAPPI standard where the revolutions were not more than 50,000 (TAPPI, 2002). Then pulp suspensions were prepared in the stock tank, stirred for 1 hour then pumped through the loop for approximately two hours to ensure homogeneous fiber dispersion before any data was taken. The surface temperatures T_s is given by equation (3.1) and experimental corrections for the thermocouples λ/x values are given in Table 3.2.

$$T_s = T_{tc} - \dot{q}/(\lambda/x) \quad (3.1)$$

3.1.5 Data reduction and Calibration of Experiments

Data of inlet and outlet temperatures and wall temperatures were logged using a data logger (Graphtec, midi logger GL220) and the flow rate was logged with an I/A Series magnetic flow transmitter. The total energy input to the heater per unit surface area was calculated as heat flux \dot{q} , which is the total power input divided by the heated area A. The power inputs were calculated from measuring current and voltage supplied,

by 1000 A true RMS clamp meter (Agilent). The temperature of wall T_w of the test section was calculated using calibration corrections for the distance of the thermocouples above the pipe inner surface by the thermocouple reading T_{tc} in the test section. The actual surface temperature is therefore calculated from heat flux \dot{q} and wall resistance λ/x using equation (3.1) and presented in Appendix B.

Table 3. 2 λ/x values in different locations at the test section for each thermocouple

Location	λ/x	Values w/m ² °K
1	λ/x_1	2500
2	λ/x_2	2500
3	λ/x_3	5000

The local heat transfer coefficient h_c is calculated from the calculated wall temperature T_w , the bulk temperature T_b and the heat flux \dot{q} , is described by:

$$h_c = \frac{\dot{q}}{T_w - T_b}, \quad (3.2)$$

where the bulk temperature T_b is the position-weighted average value of the inlet and outlet temperatures (T_{in} and T_{out}). The temperature of bulk is based on the assumptions that the fluid temperature increases linearly over the heated section and remains constant in the unheated sections of the rig and is given by:

$$T_b = (TCL/HL) * (T_{out} - T_{in}) + T_{in} \quad (3.3)$$

Where, TCL and HL are distance of thermocouples tip along the flow direction and the heated length respectively. This is reasonable because the temperature rise between inlet and outlet thermocouples was normally less than 1 °C.

The Nusselt number is described by:

$$Nu = \frac{h_{avg} \times D}{k}, \quad (3.4)$$

where h_{avg} is average heat transfer coefficient of fluid, D is internal diameter of the pipe and k is thermal conductivity fluid.

3.1.6 Preparation and Characterization of samples

3.1.6.1 Preparation of pulp fiber suspension

The pulp fibers suspensions were prepared by disintegrating pulp in the disintegrator up to 35000 rpm before each experiment to make sure all fiber bundles are dispersed. For a known concentration the required amount of the pulp sample was disintegrated. The pulp sample was poured into 2L tap water (keeping 1.2 % consistency) at $23 \pm 2^\circ\text{C}$. The disintegration process was carried out according to the TAPPI standard where the revolutions were not more than 50,000 (TAPPI, 2002). Then pulp suspensions were prepared in the stock tank, stirred for 1 hour then pumped through the loop for approximately two hours to ensure homogeneous fiber dispersion before any data was taken



Figure 3. 3 Flowchart of sheet making process

3.1.6.2 Preparation of hand sheets

A flow chart of paper making process is presented in Figure 3.2. Hand sheets of all fiber samples are prepared according to the TAPPI Standard T-205 (TAPPI, 2002). A complete description of hand sheets preparation process has been presented in Appendix A.

3.1.6.3 Characterization of fibers and hand sheets

To measure different fibers properties of pulp fiber samples, the pulp fibers were boiled in water to remove air from the fibers and then placed in separate test tubes

containing an equal amount of glacial acetic acid and 35% hydrogen peroxide. Few drops of the prepared suspension were placed on microscopic slides at 105°C to vaporize water. Fiber properties measured during this study are, fiber length (L), fiber diameter (D), fiber cell wall thickness (T) and fiber lumen diameter (d) were measured at an average rate of 50 measurements using Quantimeter Image Analyzer equipped with a Lecia microscope and Hipad digitizer (from Quantimet 520, Cambridge Instruments). Three derived values: Flexibility ratio or Elastic coefficient ($d/D \times 100$), Slenderness ratio or Felting coefficient (L/D), Runkel ratio or Rigidity coefficient ($2 \times T/d$) were calculated using the measured values (Ogbonnaya et al., 1997; Saikia et al., 1997)

The microscopic images (Appendix A, Figures A.1-A.5) of fibers and hand sheets made of the same fiber were snapped using scanning electron microscope (SEM) and optical microscope. Hand sheets physical properties were examined using different devices according to TAPPI procedure (Appendix A, Table A.1). Tensile index (Tensile strength/grammage $\times 1000$) was calculated from the tensile strength, which were measured using horizontal tensile tester (BUHEL, VENDELIER 11-3905). Tear index (Tearing force/grammage) were calculated using L&W TEARING TESTER (Lorentzen & Wettre). Burst index (pressure/grammage) using burst tester (FRANK Prufgerate GmbH). Folding endurance were obtained by FODING TESTER (A B LORENTZEN & WETTRES). Brightness were determined using opacimeter (technidyne, Color Touch 2).

3.2 Study of nanofluid flow in backward-facing step

3.2.1 Analysis methods

Characterization of the nanoparticles and nanofluids are important before used for heat transfer study. Details of the methods are stated in the following sections.

3.2.1.1 FE-SEM

Field emission scanning electron microscopy (FE-SEM) is utilized for inspecting topographies of specimens at very high magnifications using a piece of equipment called the scanning electron microscope. In FE-SEM inspection, a beam of electrons is focused on a spot volume of the specimen, resulting in the transfer of energy to the spot. These bombarding electrons referred to as primary electrons, which dislodge electrons from the specimen itself. The dislodged electrons, also known as secondary electrons, are attracted and collected by a positively biased grid or detector, and then translated into a signal.

To produce the FE-SEM image, the electron beam is swept across the area being inspected, producing many such signals. These signals are then amplified, analyzed, and translated into images of the topography being inspected. Finally, the image is shown on a CRT screen. The energy of the primary electrons determines the quantity of secondary electrons collected during inspection. The emission of secondary electrons from the specimen increases as the energy of the primary electron beam increases, until a certain limit is reached. Beyond this limit, the collected secondary electrons diminish as the energy of the primary beam is increased, because the primary beam is activating electrons deep below the surface of the specimen. Electrons coming from such depths usually recombine before reaching the surface for emission.

Aside from secondary electrons, the primary electron beam results in the emission of backscattered (or reflected) electrons from the specimen. Backscattered electrons possess more energy than secondary electrons, and have a definite direction. As such, they cannot be collected by a secondary electron detector, unless the detector is directly in their path of travel. All emissions above 50 eV are considered to be backscattered electrons. Backscattered electron imaging is useful in distinguishing one material from another, since the yield of the collected backscattered electrons increases

monotonically with the specimen's atomic number. Backscatter imaging can distinguish elements with atomic number differences of at least 3, i.e., materials with atomic number differences of at least 3 would appear with good contrast on the image. Field emission scanning electron microscopy (FESEM- CARL ZEISS- AURIGA 60) was used to observe the microstructures of the nano-particles.

3.2.1.2 TEM

Transmission electron microscopy (TEM) is the primary technique to verify the dimensions of a single particle and to identify agglomerations of particles. The electron beam can be used to observe the features in the nanometer level. A major drawback to the use of TEM is that samples must be dried out of solution in order to be attached to the carbon matrix and place in the vacuum chamber of the TEM; therefore the particles are not exactly in the colloid state and agglomeration might occur during drying. However, TEM can be used in combination with dynamic light scattering to acquire exact sizing in nanofluid form. Another drawback of TEM is the cost and time investment needed to prepare and view the sample. It was decided to perform some initial imaging as a feasibility study. Transmission electron microscopy (TEM) measurements were conducted on a CARL ZEISS-LIBRA120 microscope.

3.2.1.3 FT-IR

For Fourier transform infrared spectroscopy (FTIR), samples were prepared by grinding a very low concentration of dry material with potassium bromide (KBr) to form a very fine powder. This powder is then compressed into a thin pellet which can be analyzed.

Functional groups on the multi-walled carbon nanotubes (MWCNT) surface were analyzed by Fourier Transformation Infrared Spectrometer (Perkin Elmer-spectrum100 model FT-IR) at the wave ranges of 4000-400 cm^{-1} .

3.2.1.4 Raman

Raman spectroscopy is a spectroscopic technique used to observe vibrational, rotational, and other low-frequency modes in a system. It relies on inelastic scattering, or Raman scattering, of monochromatic light, usually from a laser in the visible, near infrared, or near ultraviolet range. The laser light interacts with molecular vibrations, phonons or other excitations in the system, resulting in the energy of the laser photons being shifted up or down. The shift in energy gives information about the vibrational modes in the system. Infrared spectroscopy yields similar, but complementary, information. Typically, a sample is illuminated with a laser beam. Electromagnetic radiation from the illuminated spot is collected with a lens and sent through a monochromator. Elastic scattered radiation at the wavelength corresponding to the laser line due, called elastic Rayleigh scattering, which is filtered out while the rest of the collected light is dispersed onto a detector by either a notch filter or a band pass filter.

Thus, Raman spectroscopy is used to provide a fingerprint by which molecules can be identified. Raman spectra were collected by using a Renishaw Invia Raman Microscope with laser excitation at 514nm.

3.2.1.5 DSC

Differential scanning calorimetry (DSC) is a powerful tool to measure the heat capacity of nanofluids. The difference in the amount of heat flow required for heating up a sample pan and reference pan are measured as a function of temperature. During the whole process, the sample and reference pans are maintained at nearly the same temperature throughout the experiment. The heat capacity of the reference pan is already known. By measuring the difference in heat flow, the heat capacity of the sample is obtained. If there are phase transitions happened in the sample pan, heat will need to flow to it than the reference to maintain both at the same temperature, so endothermic or exothermic peaks are shown on the DSC curves, corresponding to

melting or freezing, respectively. The phase transition temperatures and latent heats are determined per the DSC curves. The heat capacities of nanofluids were obtained from a differential scanning calorimeter (METTLER TOLEDO 820C-Error $\pm 0.25-1^{\circ}\text{C}$) at a heating rate of $5^{\circ}\text{C}/\text{min}$ in purified nitrogen atmosphere.

3.2.1.6 Rheometer

The viscosity of nanofluids is one of the most critical parameters, which determines the quality of the heat transfer fluid. As with simple fluids, the viscosity of a nanofluid depends largely on the temperature. Besides, the viscosity of nanofluids is measured at different RPMs of the rotor to investigate whether the nanofluids are Newtonian or non-Newtonian fluids. The rheological behavior of nanofluids with a certain amount of nanoparticle was measured by an Anton Paar rheometer (Physica MCR 301). In order to verify the accuracy of viscometer as well as to assess the reliability of the experimental procedures, the obtained values from water tests is given by:

$$\mu = e^{(1.12646-0.039638*T)/(1-0.00729769*T)}/10000 \quad (3.5)$$

where T is the temperature in Kelvin and μ is the viscosity (mPa.s). which could be the correlation for the dynamic viscosity of distilled water (Hagen, 1999).

3.2.1.7 Stability

A UV-vis spectrum is a common procedure employed to study dispersibility of aqueous suspensions with sedimentation time. This procedure works based on various light wavelengths in which it could be absorbed or distributed by other substances in the nanofluids. The UV-vis spectra procedure follows the Beer-Lambert law, and shows the absorbance is directly proportional to the nanoparticle concentration in colloids. Although the stability of nanofluid is very important for practical application, the data is limited on estimating the stability of nanofluids. The zeta potentials of the nanofluids were measured by a zetasizer nano (Malvern instruments ltd., United Kingdom). The

light transmission of all samples was measured with a Shimadzu UV spectrometer (UV-1800) operating between 190 and 1100 nm. The nanofluid solution was diluted with distilled water to allow sufficient transmission while each measurement was repeated three times to achieve a better accuracy.

3.2.1.8 Electrical conductivity

Electrical conductivity of the nanofluids both as functions of loading and fluid temperature were measured using a AB200 pH/Conductivity Meter (Fisher Scientific). The conductivity meter has a measuring range between 0 to 500mS/cm and a resolution of 0.1%. Prior to the measurements, the meter was calibrated using the buffer solutions of known electrical conductivities. Measurements were taken by using ~40 ml of the nanofluid sample in a beaker which is placed in an isothermal bath, with the conductivity probe immersed in it. At each temperature, the measurements were repeated 5 times, and the average value was taken.

3.2.1.9 Thermal conductivity

To select the desired fluids to be fully characterized, enhanced thermal conductivity is possibly the most important element in this study, because it points to the nanofluid with high heat transfer potential. There is an inexpensive commercially available system for the measurement of the thermal conductivity. The Decagon Devices KD2 thermal properties analyzer (KD2 Pro, Decagon Devices, Inc., USA), after some initial testing, it is used for all nanofluids at room temperature as a first check. In the following sections, the transient hot wire method (THW), on which the KD2 operates, has been described in full along with the true thermal conductivity measurement apparatus. The accuracy of the KD2 is given as 5% by the manufacturer over a span of temperatures from 0 to 60°C. However, it is found that through trial and error, the KD2 operates very accurately if the probe is setup perfectly vertical and an isothermal bath is used to maintain the sample at 25°C. These techniques prevent

convection problems and the external boundary effect problems as well. A schematic of the KD2 setup with the isothermal bath is shown in **Figure 3.4**.

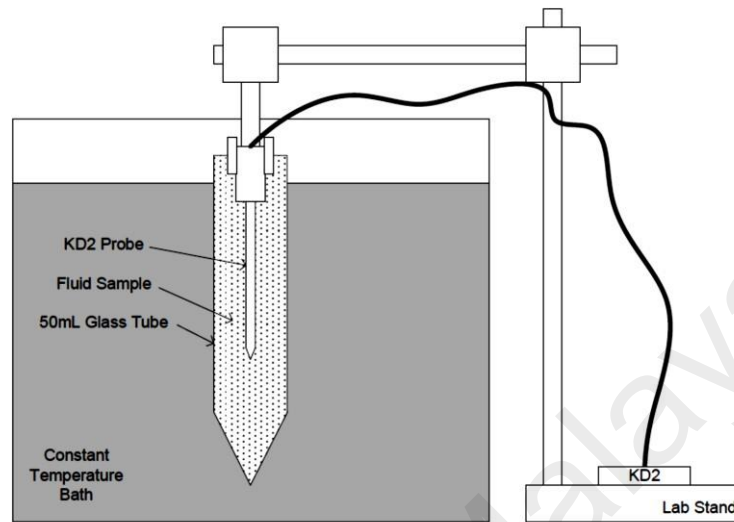


Figure 3. 4 Schematic setup of KD2 thermal properties analyzer

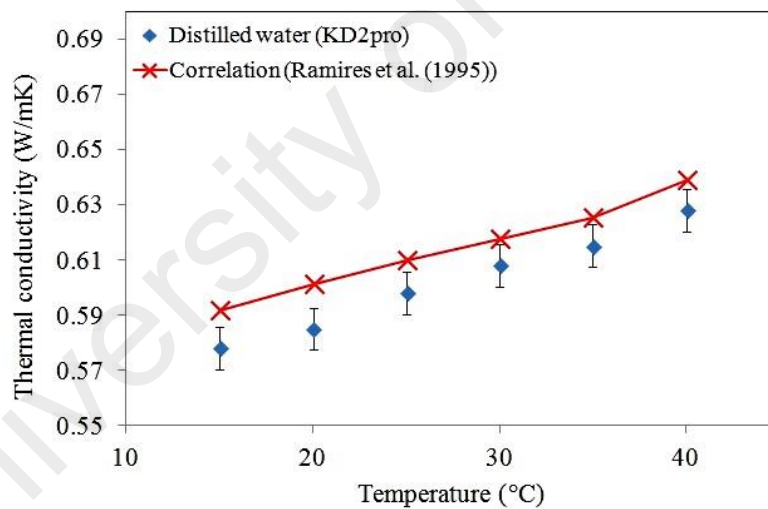


Figure 3. 5 Comparison between distilled water and previous data

Thermal conductivity measurements in this work were done based on THW method and the used analyzer device has 5% accuracy between 5°C and 50°C . The thermal conductivity measurement for distilled water are within 2-4% of previously reported data (Ramires et al., 1995) as shown in **Figure 3. 5**. The thermal conductivity measurements were repeated ten times and the average values were reported.

3.2.2 Experimental apparatus

Flow loop of the test section is presented in **Figure 3. 6**.

The flow loop of test section consists of stainless steel piping, jacketed stock tank connected with a chiller for cooling of the stock solution up to the desired bulk temperature, a variable speed pump, a magnetic flow meter, differential pressure transducer, heated test section and recycle piping setup. The Nanofluid were pumped from a 20 L capacity stainless steel jacketed tank by a Cole-Parmer™ magnetic drive pump, and the pump flow was controlled by a Hoffman Muller™ inverter. The flow rate and the pressure drop were measured using a N-FLO-25 Electromagnetic flow meter and a Foxboro™ differential pressure transmitter, respectively. The test section is made of Stainless steel and is an 800 mm length of 25.4 mm internal diameter with separation ratio 2. All the walls of the test section were fabricated using a thick glass wool to ensure a good isolation with ambient. Sixteen Omega Type-K thermocouples were mounted on upstream of the test section from a distance x1 to x16 presented in **Figure 3. 11**. The test section was heated by supplying a constant 600 W DC power

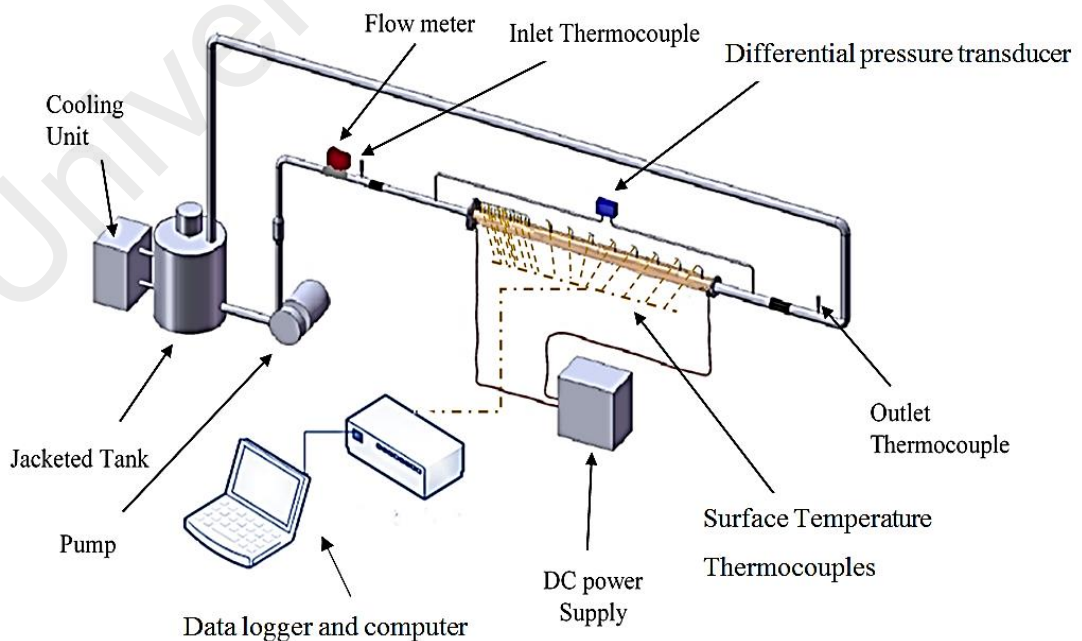


Figure 3. 6 Schematic of BFSF rig

supply using Agilent technologies N8731A (details are presented in 3.2.4.7). Two RTD (PT-100) sensors (Omega, Singapore) were inserted to obtain bulk temperature at the inlet and outlet of the test section. The thermocouples and RTDs were connected to the SCADA system for the continuous monitoring and recording of the temperature data by a WINCC software in the computer.

3.2.3 Experimental data reduction

The power supply added to the downstream channel wall are:

$$\Phi = V.I, \quad (3.6)$$

$$Q = \dot{m}C_p(T_{out} - T_{in}), \quad (3.7)$$

$$\dot{q} = Q/A_w), \quad (3.8)$$

The local heat transfer coefficient h_x , temperature of bulk T_b and temperature of wall T_w are given by:

$$h_x = \dot{q}/(T_{wx} - T_{bx}), \quad (3.9)$$

$$T_{b,x} = T_{in} + \frac{Lx}{mC_p} \dot{q}, \quad (3.10)$$

$$T_w = T_{TC} - \dot{q}/(\lambda/x), \quad (3.11)$$

Heat transfer enhancement is calculated by equation (3.12) to analyze heat transfer enhancement, by the addition of nanoparticles to the base fluid (water).

$$\eta = \frac{h_{c.nf} - h_{c.bf}}{h_{c.bf}} * 100 \quad (3.12)$$

To evaluate the adequacy of nanofluids, a performance index (ε) is chosen as a proper parameter to elucidate the scope of temperature and velocity that can be utilized by the nanofluids. ε is given by:

$$\varepsilon = \left(\frac{h_{c.nf}}{h_{c.bf}} \right) / \left(\frac{\Delta P_{nf}}{\Delta P_{bf}} \right) \quad (3.13)$$

3.2.4 Design and Construction of step flow rig

Some basic requirements are developed as design considerations for the convection loop. These requirements are generated to meet certain goals: some to mimic heat exchanger conditions, some to meet existing equipment and lab requirements, and finally some arbitrary conditions.

3.2.4.1 Reservoir Tank

The reservoir tank is a Jacketed Stainless steel made and in cylindrical shape with a capacity of 14 liters. The reservoir is kept 30 cm above the gear pump so that the gear pump will have adequate pressure avoiding it to run dry. At the bottom of the reservoir a piping connects to the gear pump while at the top a bypass line, return line and top stirrer to mixing fluid inside the tank are connected **Figure 3. 7 (a)**.

3.2.4.2 Gear Pump

The gear pump used for the experiment is a Liquid flow sealed gear pump (ColeParmer magnetic drive pump), (**Figure 3. 7 (b)**). It is rated for a maximum flow of 120 LPM and Max Head is 8 M. This pump can operate at variable speed with the maximum rated speed of 3200 RPM. The suction side of the pump is connected to the reservoir.

The pump can operate with water up to 80°C, due to the shaft seal limitations. After rough estimation of the total loop pressure losses, assuming maximum 15mm inner diameter tubing, and from knowledge of the pump characteristic curve, it is found that the pump should can produce around 52LPM. This will deliver a significantly turbulent flow rate for water at room temperature, up to Reynolds of 30,000. Therefore, the pump is deemed usable for the experiment.

3.2.4.3 Inverter

A Hoffman Muller inverter was used to control the speed of the pump as shown in **Figure 3. 7 (d)**.

The specifications of the inverter are presented in Table 3.3.

Table 3.3 Technical specifications for V8 series inverters

Items	Contents
Model	HM-V8A11P5B
Input	AC, 1PH, 230V, 50/60 HZ
Output	3PH, 1.5 KW, 7A, 0-650 HZ

3.2.4.4 Electromagnetic Flow Meter

N-FLO-25 Electromagnetic flow meter was used to measure fluid flow rate (see **Figure 3.7** (c)). A magnetic flow meter (mag flowmeter) is a volumetric flow meter which does not have any moving parts and is ideal for wastewater applications or any dirty liquid which is conductive or water based. Magnetic flowmeters will generally not work with hydrocarbons, distilled water and many non-aqueous solutions. Magnetic flowmeters are also ideal for applications where low pressure drop and low maintenance are required.

The operation of a magnetic flow meter or mag meter is based upon Faraday's Law, which states that the voltage induced across any conductor as it moves right angles through a magnetic field is proportional to velocity of that conductor. The technical specifications are presented in **Table 3.4**.



Figure 3. 7 Photographs of equipment's (a) Stock tank, (b) Magnetic gear pump, (c) Magnetic Flow meter, (d) Hoffman Muller inverter, (e) Differential Pressure Transducer, (f) Cooling unit, (g) Power supply.

Table 3. 4 Technical specifications of Electromagnetic flow meter

Items	Contents
Model	N-FLO-25 Electromagnetic flow meter
Sensor range	DN10-DN3000
Operational pressure	PN 10 (1.0 MPa) for DN 15 to 300, Tri Clover
Measurement flow range	8 m ³ /h
Measurement accuracy	±0.5%
Repeatability	0.1%
Environment temperature	-20 – 50°C
Minimum conductivity of measured liquid	5µs/cm
Lining	Teflon (PTFE)
Measuring electrodes	Hastelloy C4 standard

As stated above, the flow meters were supplied after calibration by the manufacturer, as shown in **Table 3. 5**. Fluid viscosity can become an issue if the viscosity is higher than that of water. The deviation of the flow meter reading becomes an issue when the meter is running in the lower 25% of its operating range for fluids of viscosity less than 30 times that of water. Nanofluids used in the experimental investigation were typically only 5 times more viscous than water, therefore the calibration had not been an issue.

Table 3. 5 Flow meter calibration data

Flow (m ³ /hr)	Volume (L)	Actual (L)	Error (%)	Repeatability (%)
0.3	5.201	5.214	0.24	0.062
0.8	12.374	12.368	-0.05	0.105
1.60	20.871	20.787	-0.40	0.019

3.2.4.5 Differential Pressure Transducer

The smart FoxboroTM differential pressure transmitter (Model: IDP10-T22D21DLIT) with accuracy of ±0.075% of span connected to the inlet and outlet of the test section was used in this test (**Figure 3. 7 (e)**).

The standard specifications of the Differential Pressure Transducers are presented in Table 3. 6 . The calibration condition, static pressure test and differential pressure test are presented in **Table 3. 7** to **Table 3. 9**.

Table 3. 6 Standard specifications of the Differential Pressure Transducers

Items	Contents
Model	IDP10-T22D21D-LIT
Process Fluid	Liquid, Gas or Vapor
Application	Differential Pressure, Gauge Pressure, Absolute Pressure
Measuring Range	0 - 0.125 Kpa ~ 0 - 1.5 Kpa (Minimum) 0 - 4.0 Mpa ~ 0 - 1500.0 Kpa (Maximum)
Accuracy	± 0.075% of span
Stability	± 0.15% of URL for 2 years
Working Temperature	-25 to 95°C
Max. Pressure	1500Kpa
Body material	SS 304
Diaphragm	SS316L

Table 3. 7 Calibration conditions

Ambient temperature	20C	Relative humidity	60%
Grounding resistance	> 200MH	Calibration range	0~50 KPa

Table 3. 8 Static pressure test

Differential pressure value	Static pressure 4.00 MPa			
	1 ATM	Error (%)	4 MPa	Error (%)
0.0 KPa	4.000 mA	0.000	4.012 mA	0.075
50.0 KPa	20.003 mA	0.019	20.000 mA	0.000

Table 3. 9 Differential pressure test

D/P Value	output	Zero to F.S.	Error (%)	F.S.to Zero	Error (%)
0.0	4.000 mA	3.998 mA	-0.012	4.009 mA	0.056
12.5	8.000 mA	7.991 mA	-0.056	7.997 mA	-0.019
25.0	12.000 mA	11.992 mA	-0.050	11.992 mA	-0.050
37.5	16.000 mA	15.990 mA	-0.062	15.999 mA	-0.006
50.0	20.000 mA	19.997 mA	-0.019	19.992 mA	-0.050

3.2.4.6 Cooling unit

A Refrigerated Bath Circulator (DAIHAN-brand, WCR- P30) was used to balance the heat input and it is inside the jacketed tank (**Figure 3. 7 (f)**). This refrigerated bath has:

1. RS232C Interface for Remote Monitoring and Controlling with PC
2. Stainless steel Bath (#304) for Superior Durability & High Thermal Efficiency.
3. Powerful Circulation Pump ensures temperature Uniformity: Internal and External Circulation.
4. Locking Mode Supported for Experimental Safety (Input to Jog-Shuttle can be Disabled)

The specifications of the Refrigerated Bath are listed in **Table 3. 10**.

3.2.4.7 Power Supply

The test section was heated by providing a constant DC power supply using Agilent technologies N8731A DC power supply units. That can supply up to 8 volts and 400 A (32000 W) as presented in **Figure 3. 7 (g)**.

Table 3. 10 Specifications of the Cooling unit

Items	Contents	
Capacity & Models	30 L, WCR- P30	
Temp. Range & Accuracy	-25°C~ +150C, ± 0.1 C	
Temp. Resolution	0.1 °C-Display, 0.1°C-Control	
Temp. Uniformity & Probe	± 0.2 °C at -10C, PT100	
Heating Power	2.2 kW	
Refrigerator	7/8 HP	
Cooling Capacity	at +20°C	631 W
	at 0°C	429 W
	at -20°C	284 W
Refrigerant	CFC -Free(R-404A) Refrigeration System	

3.2.4.8 Thermocouples

Two different types of thermocouples were used for the experiments. The thermocouples used for the bulk fluid inlet and outlet (bulk) temperatures in respect to the test section are thermocouples from Omega (Model: PR-12-2-100-1/8-6-E-RP) with temperature range of -50 to 250°C. It is a RTD sensor (PT-100) thermocouple with 3mm sheath diameter and 100mm length. The tip of the thermocouple was inserted into the middle of the flow path of the fluid. The thermocouple is then attached to the data acquisition unit where the bulk temperature was recorded and analyzed. Another type of thermocouples used for surface temperature are type-K from Omega (Model: TJ36-CASS-032U-6). The metal transition barrel provides a solid mounting surface and the PFA insulated lead wire is a cost-effective solution for environmental temperatures to 260°C. This type-K thermocouple has 1 mm sheath diameter and 150 mm length. The thermocouples come specified from the manufacturer to have ± 1 °C accuracy. All thermocouples are not calibrated in the technical sense and they are tested with standard temperatures to ensure no manufacturing or connection flaws are creating erroneous readings. The heat transfer results are directly affected by the temperature measurements. Thus, all the thermocouples (Type-K and RTD sensor) used in this experiment must be calibrated to determine their accuracy. The thermocouples are

calibrated by two ways:

1. 650SE - Reference Temperature Calibrator

The system gives significant improvement in the calibration accuracy up to $\pm 0.04^{\circ}\text{C}$ with use of the external reference sensor. Axial homogeneity in the calibration well is important, as the typical thermo-sensitive element of a sensor can vary from 5mm to 60mm. The actual temperature in the well could inherently deviate from the ideal temperature as a function of the proximity to the bottom of the well

2. The thermocouples were immersed in well mixed boiling-water bath which was at 100.16°C for the laboratory pressure and a well-mixed ice-water bath maintained was at 0°C (**Figure 3. 8**).

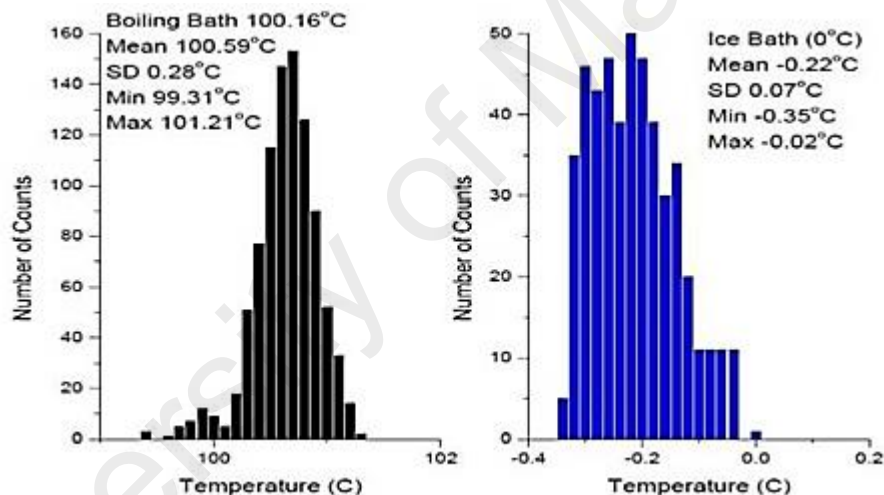


Figure 3. 8 Thermocouple testing

3.2.4.9 Data logging system

The several types of data acquisition system are used for this experiment including Graphtec (midi logger gl220), Scada system (TK4H) and Multi Power Monitor. All these systems were connected to a PC for continuous data logging and monitoring.

All the type-K thermocouples are connected to the channels of PLC system. The PLC system was connected to computer to allow data upload in real time as well as remote configuration and real time data acquisition. The RTD sensors, flow meter and

pressure transducer were attached to the PLC system. The PLC system was linked with computer where WINCC software were installed. The WINCC software was set to record the data at every minute interval.

3.2.4.10 Test section

The positioning of the thermocouples was done at outer surface of the cylindrical tube to avoid boundary layer interruption originating from the thermocouple probe protruding into the conduit inner surface. Photographs of the test section and thermocouples arrangement is presented in **Figure 3. 9**. schematic wive of test section and thermocouple positions are presented in **Figure 3. 10** and **Figure 3. 11** respectively.



Figure 3. 9 Photograph of experimental setup and test section

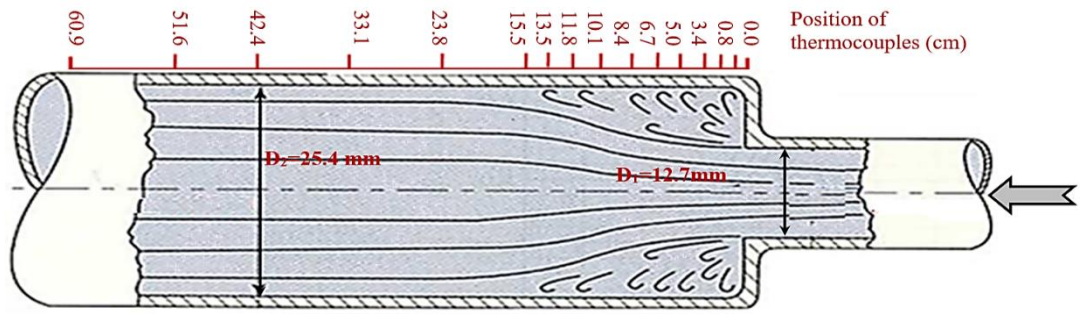


Figure 3. 10 Schematic view of the test section

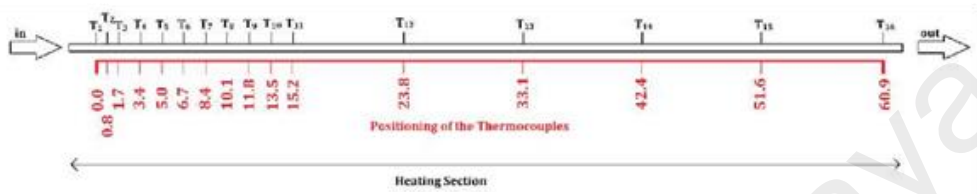


Figure 3. 11 Thermocouples positions

CHAPTER 4: RESULTS AND DISCUSSION

4.1 Pipe line flow

4.1.1 Data Reproducibility

Two water run was conducted for Data reproducibility studies. Heat transfer coefficient was compared as a function of velocity at a constant inlet temperature $32\text{ }^{\circ}\text{C}$ and constant heat flux 23203 W/m^2 presented in **Figure 4. 1**. It is observed that the results for the two identical runs are showing good agreement and remains within 5% difference.

Similarly, the frictional pressure drop of the two identical water runs presented in **Figure 4. 2** is showing data reproducibility. The data show good agreement and remain within 5% of deviation.

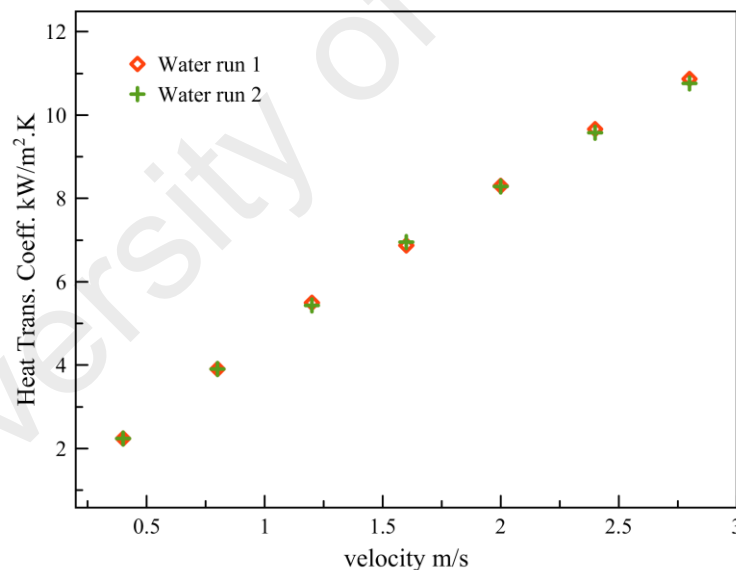


Figure 4. 1 Heat transfer coefficient as a function of velocity for two runs of water.

To validate the new experimental heat transfer data, a preliminary set of tests were conducted keeping water as a working fluid. The measured Nusselt numbers for the new experimental data were correlated with the Petukhov (1970) and Gnielinski (1975) correlations and presented in **Figure 4. 3**. It is revealed that the measured experimental data are in good agreement with the evaluated values from the empirical

correlations. In particular, Petukhov (1970) empirical correlation are within agreement of about 4% with the experimental data and Gnielinski (1975) are also in good agreement of about 5% within the experimental data, which validates the experimental methodology.

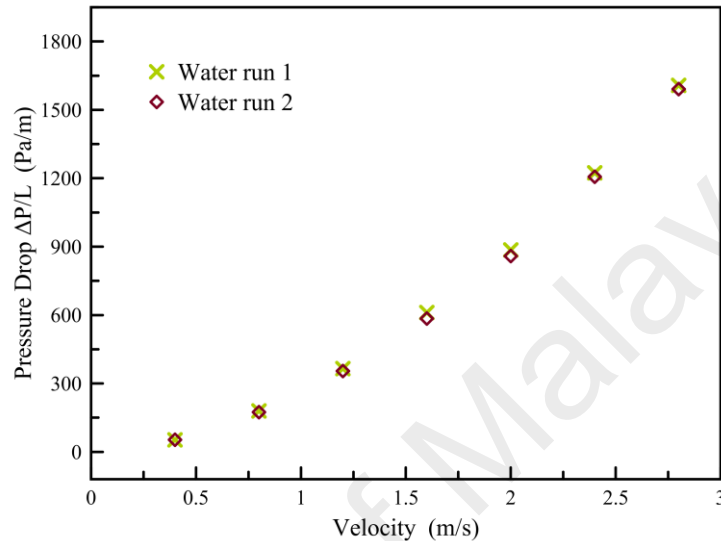


Figure 4. 2 Pressure drop per unit length as a function of velocity for two runs of water.

To validate the new experimental pressure drop data, a preliminary set of tests were conducted keeping the water as a working fluid. The measured Pressure drop for the new experimental data was correlated with the Petukhov (1970) and Blasius relation (Blasius, 1908) correlations and presented in **Figure 4. 4**. It is revealed that the measured experimental data are in good agreement with the evaluated values from the empirical correlations. Also, it is observed that with an increase of velocity the deviation between experimental and correlations decreases. In particular, Petukhov (Petukhov, 1970) empirical correlation are within the agreement of about 6.7% with the experimental data and Blasius relation (Blasius, 1908) are also in good agreement of about 7.2% within the experimental data, which validates the experimental methodology.

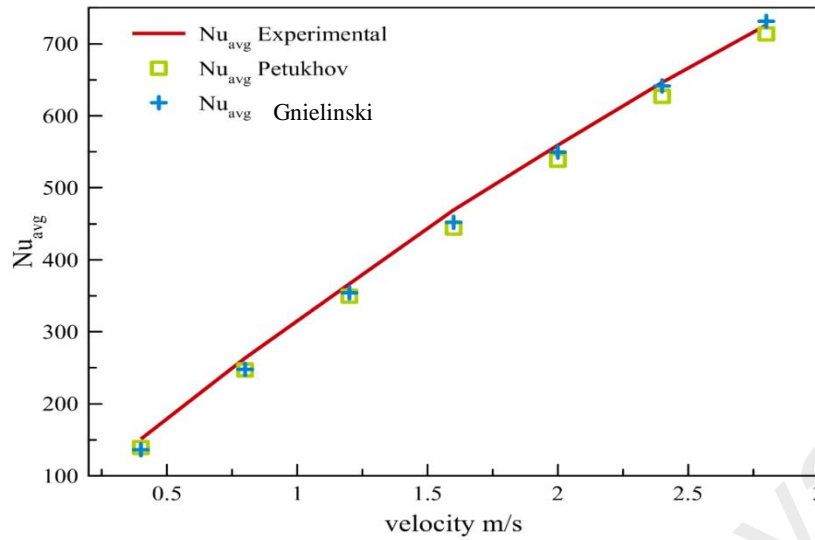


Figure 4.3 Comparison of Nusselt number as a function of velocity obtained from the experimental data and the standard correlations

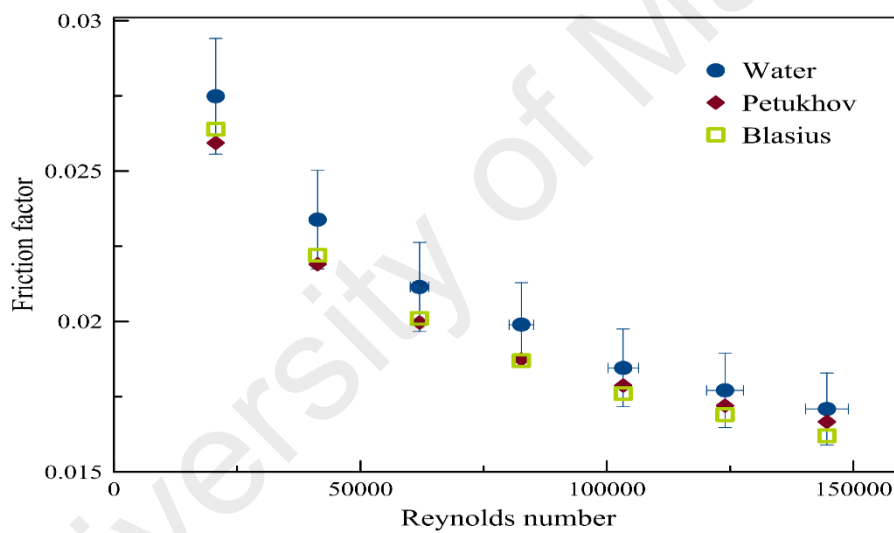


Figure 4.4 Comparison of measured experimental friction factor with Petukhov (1970) and Blasius (1908)

4.1.2 Heat transfer to fiber suspension

4.1.2.1 Different concentration effect of fiber on heat transfer coefficient

Effect of fiber and fiber concentration on heat transfer to suspensions of the fibers were studied using kenaf core mechanical (kcm), kenaf bast mechanical (kcm), mixture of kenaf core and bast (kckb3) and blend of Acacia mangun and kenaf bast (amkb) pulp fibers.

Heat transfer coefficient (h_c) data at three different concentrations (0.2, 0.4 and 0.6 wt.%) of fiber suspensions (kcm, kbm, kckb3 and amkb) along with water are presented in **Figure 4. 5** –**Figure 4. 8**.The data were taken at 32 °C inlet temperature and constant heat flux of 23.2 KW/m².

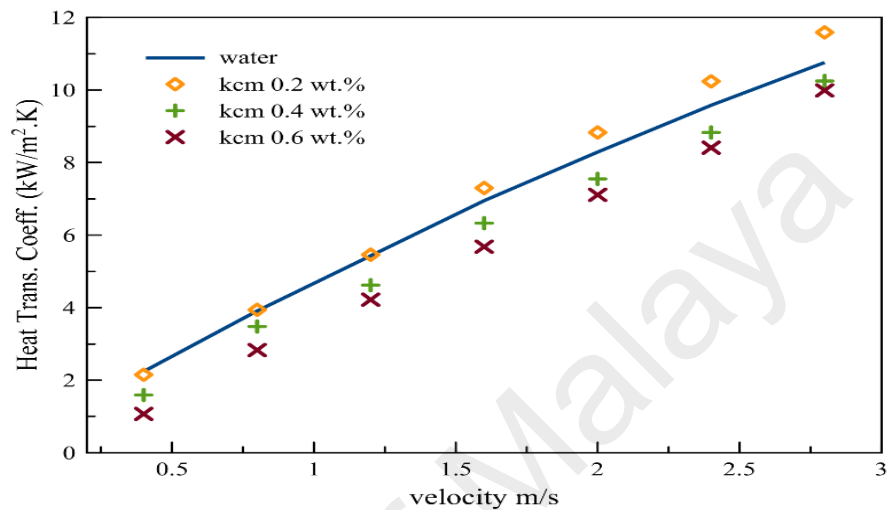


Figure 4. 5 h_c as a function of flow velocity for water and different concentrations of Kenaf Core Mechanical (kcm) fiber suspensions.

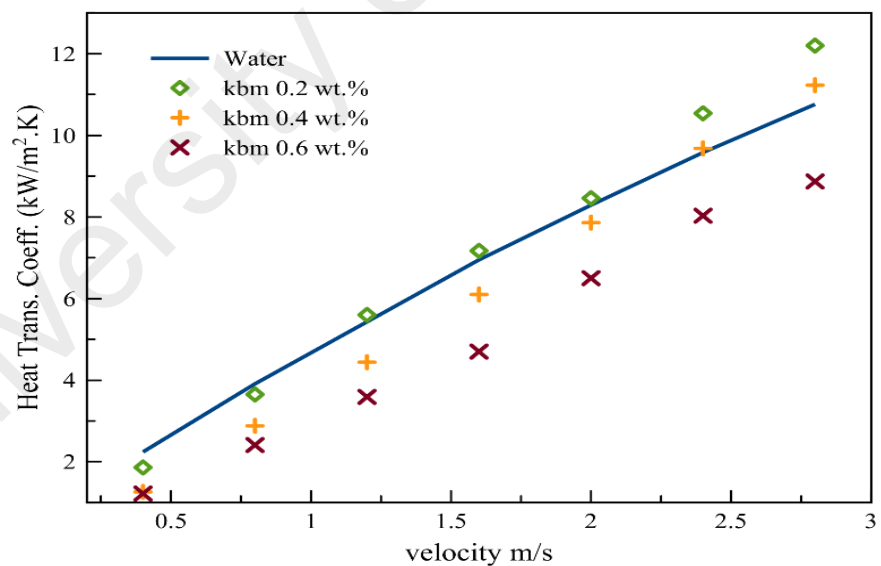


Figure 4. 6 h_c as a function of flow velocity for water and different concentrations of Kenaf Bast Mechanical (KBM) fiber suspensions.

Figure 4. 5 shows heat transfer coefficient h_c as a function of velocity for water and kcm pulp fiber suspension at three different concentrations (0.2, 0.4 and 0.6 wt.%). The data were obtained at 32°C inlet temperature and constant heat flux of 32.2 kW/m². The present study reveals that the kenaf core mechanical (kcm) at higher concentrations

of 0.4 wt.% and 0.6 wt.% have h_c values below the water values throughout the range of velocity. Whereas, at lower fiber concentration 0.2 wt.%, h_c is higher than water at the velocity greater than 0.4 m/s.

Figure 4. 6 represents heat transfer coefficient as a function of bulk velocity for the water and kenaf bast (kcm) pulp fiber suspensions at different concentrations (0.2, 0.4 and 0.6 wt.%). The results reveal that the kcm pulp fiber suspension at concentration 0.4 wt.% and 0.6 wt.% have h_c values below the water values at the range of velocity, while concentration of 0.4 wt.% have higher h_c at velocity higher than 2 m/s. whereas, at lower fiber concentration 0.2 wt.%, h_c is higher than water at the velocity greater than 0.8 m/s.

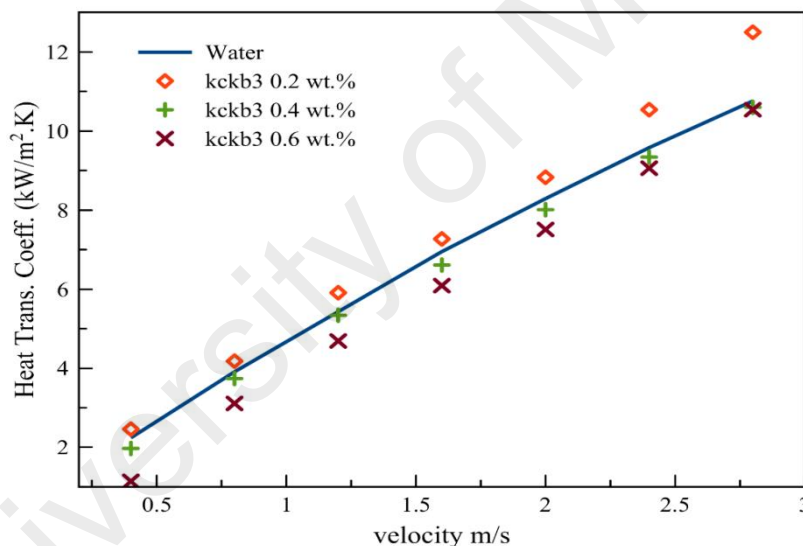


Figure 4. 7 h_c as a function of flow velocity for water and different concentrations of mixture of kenaf core and bast (kckb3) fiber suspensions.

Figure 4. 7 represents heat transfer coefficient as a function of velocity for blend of kenaf core and bast pulp fibers with ratio of 9:1 at three different concentrations (0.2, 0.4 and 0.6 wt.%). The data trends show that the kckb3 have h_c values higher than water throughout the range of velocity at fiber concentration of 0.2%. however, at higher concentrations 0.4% and 0.6% h_c values are lower than water at the range of velocity.

Figure 4. 8 shows heat transfer coefficient versus bulk velocity for blend of acacia mangun and kenaf bast with ratio of 9:1 at three different concentrations (0.2, 0.4 and 0.6 wt.%). In the present study, at concentration of 0.4 wt.% and 0.6 wt.% h_c values are below the water data throughout the velocity range of investigation, but 0.4 wt.% concentration at velocity greater than 2 m/s show higher h_c values than water. Although, at lower fiber concentration 0.2 wt.% h_c values are above the water values throughout the velocity range of investigation.

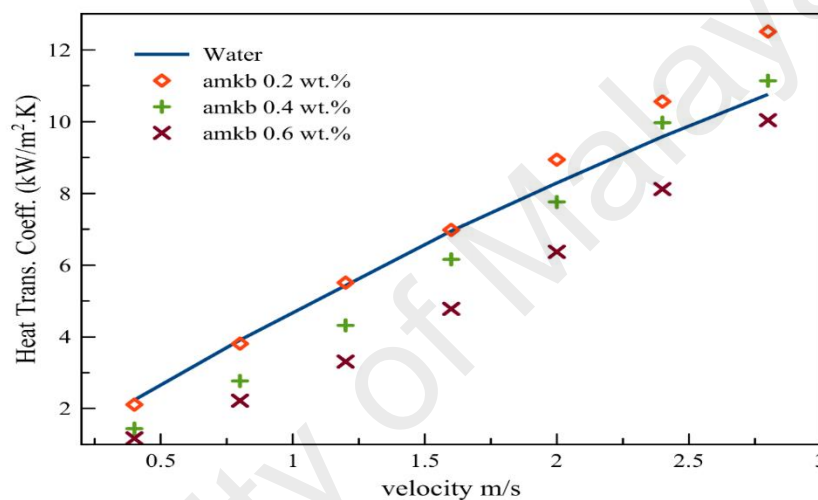


Figure 4. 8 h_c as a function of flow velocity for water and different concentrations of mixture of acacia mangun and kenaf bast (amkb) fiber suspensions.

The study (**Figure 4. 5-4. 8**) marked that all the non-wood kenaf pulp fiber samples and blend of wood and nonwood pulp fiber showing similar data trend. It is observed that fiber suspension at low concentrations enhancing heat transfer coefficient significantly and the h_c values gradually approaches the water values as the concentration of pulp fiber increases. The effect of fiber concentrations on heat transfer coefficient is more visible at higher velocities and fiber concentrations. The enhancement of heat transfer coefficient at low concentrations and with the increase of velocity while, thermal conductivity of fiber suspensions is lower than that of water, is due to contribution of fibers modifying the turbulent eddies. Whereas with the increase of fiber concentration fiber contribution of modifying the turbulent eddies is less than

the contribution of fiber thermal conductivity which decrease with the increase of fiber concentration. To magnify this phenomenon, h_c enhancement percentage for different pulp fiber suspensions at three different velocities at lower, middle and higher range are selected and is presented in Table 4.1.

Table 4. 1 Percent h_c enhancement

Sample	% h_c enhancement at velocity 0.4 m/s		
	0.2 wt.%	0.4 wt.%	0.6 wt.%
KCM	-4	-29	-52
KBM	-17	-44	-46
KCKB3	10	-12	-49
AMKB	-6	-36	-48
Sample	% h_c enhancement at velocity 1.6 m/s		
KCM	5	-9	-18
KBM	3	-12	-32
KCKB3	5	-5	-12
AMKB	0	-11	-31
Sample	% h_c enhancement at velocity 2.8 m/s		
KCM	8	-5	-7
KBM	13	4	-18
KCKB3	16	-1	-2
AMKB	16	4	-7

To highlight and make visible the effect of different pulp fiber concentrations on heat transfer, heat transfer coefficient ratio as a function of bulk fluid velocity for different pulp fibers are plotted keeping the water values on unity at constant heat flux 23203 W/m^2 and bulk inlet temperature 32°C . Heat transfer coefficient ratio was defined as ratio of h_c value of pulp sample to h_c value of water (h_{cf}/h_{cw}). **Figure 4. 9-** **Figure 4. 12** shows the heat transfer coefficient ratio of different pulp suspensions at the range of velocity 0.4-2.8 m/s. In the presented figures, the h_c difference between water and different concentrations of pulp are more distinguishable.

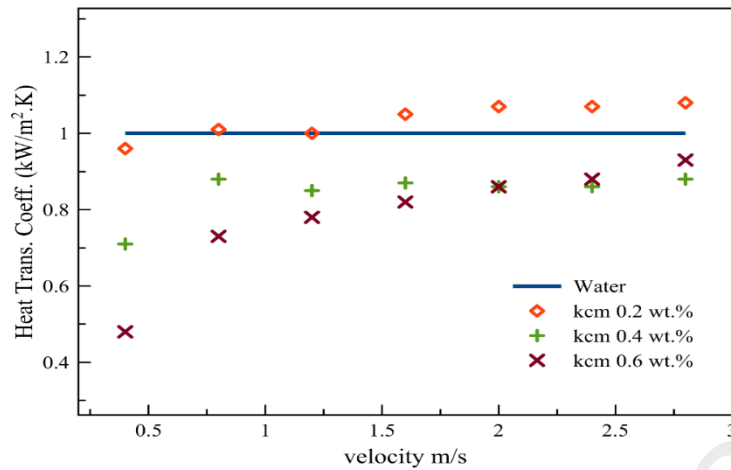


Figure 4. 9 h_c ratio as a function of flow velocity for water and different concentrations of kcm fiber suspensions.

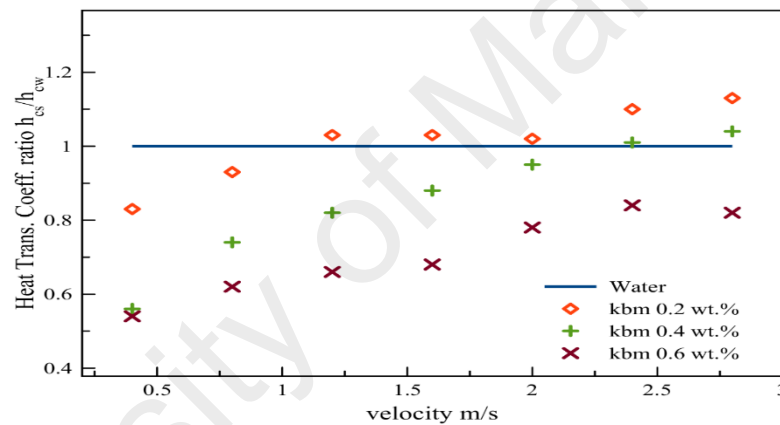


Figure 4. 10 Heat transfer coefficient ratio as a function of flow velocity for water and different concentrations of kenaf Bast Mechanical (KBM) fiber suspensions.

Pulp suspensions at low concentrations 0.2 wt.%, the heat transfer coefficient ratio (h_{cf}/h_{cw}) of Kenaf core, Kenaf bast, kckb3 and amkb approaches to unity at low range of velocity ($u < 1$ m/s), while at middle range ($1 \text{ m/s} \leq u \leq 2 \text{ m/s}$) and high range ($u > 2 \text{ m/s}$) h_{cf}/h_{cw} values are higher than unity.

Unlike pulp suspensions at low concentrations 0.2 wt.%, pulp suspensions of 0.4 wt.% are significantly lower than unity at low range of velocity ($u < 1$ m/s) and at middle range of velocity ($1 \text{ m/s} \leq u \leq 2 \text{ m/s}$) slightly lower than unity and approaches to unity at higher range of velocity ($u > 2 \text{ m/s}$). In contrast, kbm and amkb at 0.4 wt.% and velocity higher range of velocity ($u > 2 \text{ m/s}$) show h_c values higher than that of water.

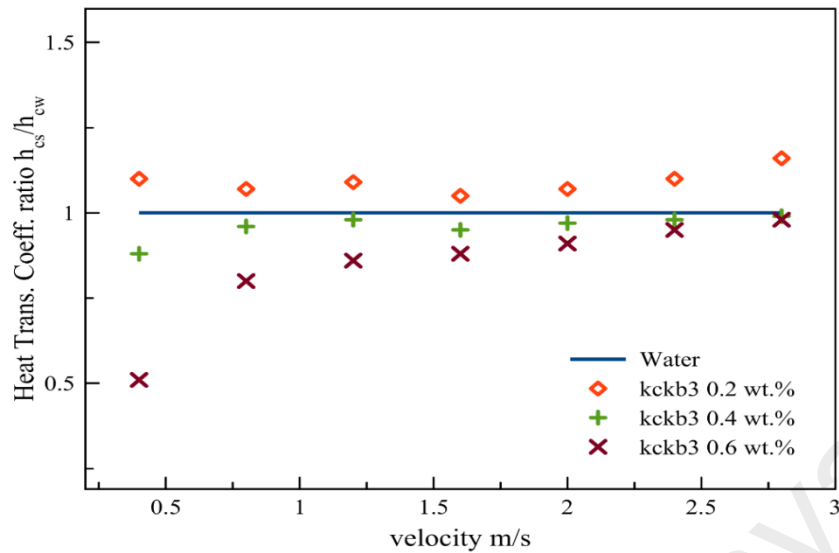


Figure 4.11 h_c ratio as a function of flow velocity for water and different concentrations of blend of Kenaf Core and Kenaf Bast Mechanical (kckb3) fiber suspensions.

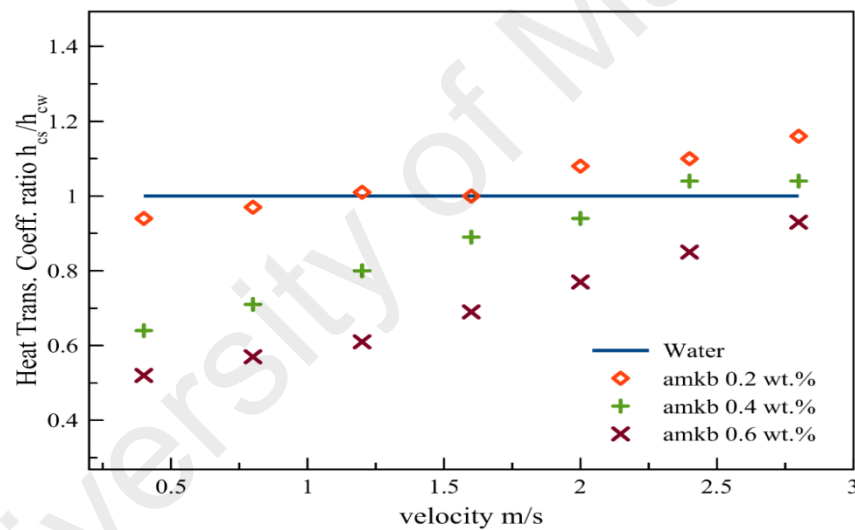


Figure 4.12 h_c ratio as a function of flow velocity for water and different concentrations of blend of Acacia Mangun and Kenaf Bast (amkb) fiber suspensions.

All pulp suspensions at 0.6 wt.% showed the minimum heat transfer coefficient ratio (h_{cf}/h_{cw}) at low range of velocity, while h_{cf}/h_{cw} ratio remain below than unity at both middle and higher range of velocity.

Table 4.2 represent h_{cf}/h_{cw} values for all samples at three different velocity range low, middle and high range (i.e 0.4, 1.6 and 2.8 m/s) generated form Figures.

Table 4. 2 Heat transfer coefficient ratio at three different range of velocity

Sample	Heat transfer coefficient ratio at velocity 0.4 m/s		
	0.2 wt.%	0.4 wt.%	0.6 wt.%
KCM	0.96	0.71	0.48
KBM	0.83	0.56	0.54
KCKB3	1.10	0.88	0.51
AMKB	0.94	0.64	0.52

Sample	Heat transfer coefficient ratio at velocity 1.6 m/s		
	0.2 wt.%	0.4 wt.%	0.6 wt.%
KCM	1.05	0.87	0.82
KBM	1.03	0.88	0.68
KCKB3	1.05	0.95	0.88
AMKB	1.00	0.89	0.69

Sample	Heat transfer coefficient ratio at velocity 2.8 m/s		
	0.2 wt.%	0.4 wt.%	0.6 wt.%
KCM	1.08	0.88	0.93
KBM	1.13	1.04	0.82
KCKB3	1.16	0.99	0.98
AMKB	1.16	1.04	0.93

4.1.2.2 Effect of bleaching

In the pulp and paper industries natural fibers are processed differently to meet different particular requirements of the intermediate and final products. Estimating the effect of a particular processing event on the fiber, heat transfer characteristic of processed fibers is a unique method of measurement. In chemical pulping, materials are detached both from the fiber wall and amid the fibers. Fibers swell in chemical pulping. Bleaching further remove lignin from the fiber wall. Detaching and modification of lignin as well as changing in the cell-wall microstructure and in cross-dimensional fiber properties affect fiber conformability. Fiber cell wall structure become loosen upon removal of lignin allowing water molecules to get between the micro fibrils and hence lesser young's modulus.

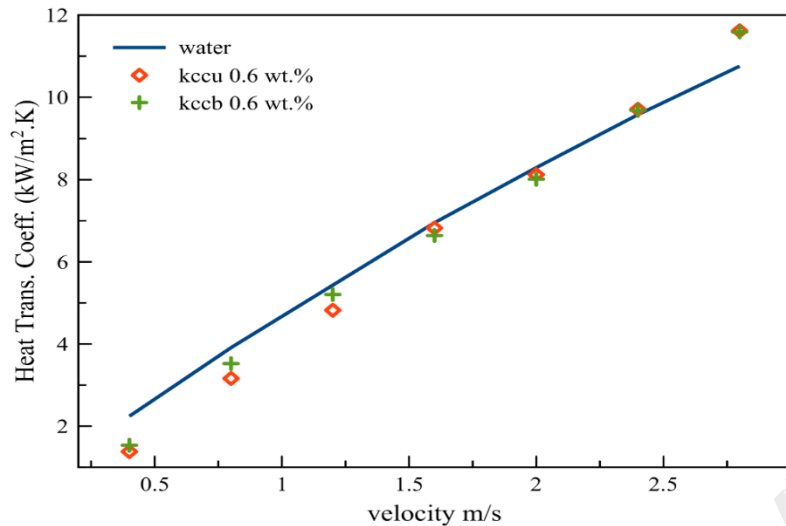


Figure 4. 13 h_c as a function of flow velocity for water and kccu and kccb fiber suspensions of concentration 0.6 wt.%.

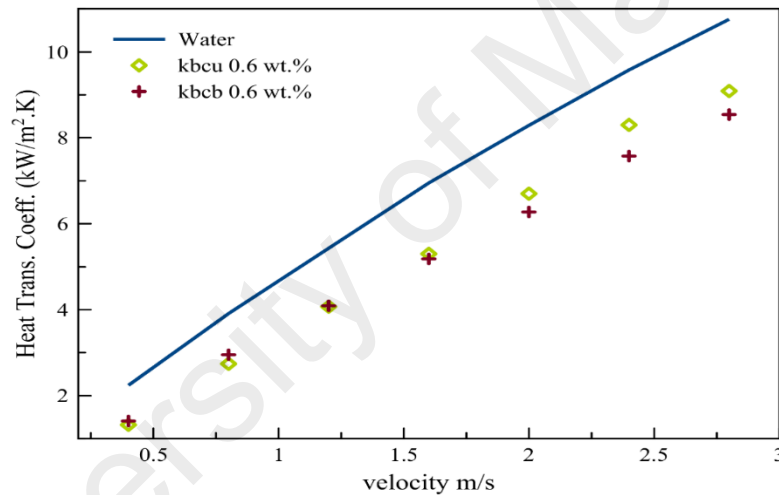


Figure 4. 14 Heat transfer coefficient as a function of flow velocity for water and kbcu and kbcb fiber suspensions of concentration 0.6 wt.%.

Bleaching effect on heat transfer coefficient is investigated, in **Figure 4. 13** is higher than water at velocity 2.8 m/s for both unbleached and bleached kenaf core pulp fiber whereas h_c values are lower than water for velocities below 2.8 m/s, there is a small difference between unbleached and bleached kenaf core pulp fiber suspensions.

Figure 4. 14 represents bleaching effect on heat transfer coefficient for kenaf bast pulp fiber suspensions at 0.6 wt.% concentration. h_c is found lower than water at the range of velocity for both unbleached and bleached kenaf Bast pulp fiber

suspensions. The significant difference between unbleached and bleached kenaf bast pulp fiber suspensions at higher velocities is observed, which is due to increase of fiber flexibility due to bleaching effect.

4.1.2.3 Effect of processing

The pulps are prepared by different methods in different industries. In the present study, the pulp is prepared by two common pulping methods mechanical pulping and soda pulping (chemical pulping). In **Figure 4. 15** heat transfer coefficient as a function of flow velocity for water and Kenaf Core mechanical (kcm) pulp and Kenaf Core chemical unbleached (kccu) pulp fiber suspensions at 0.6 wt.% concentration is presented at constant inlet temperature of 32 °C and constant power supply 3300W.

Heat transfer coefficient is found higher than water at velocity 2.8 m/s for Kenaf Core chemical unbleached pulp fiber suspension whereas h_c values are lower than water for velocities below 2.8 m/s kccu and kcm values are lower than water at the range of velocity investigated. the small difference between kccu and kcm pulp fiber suspensions is observed at velocity 0.4 m/s and 0.8 m/s while above 0.8 m/s the difference is more visible.

In **Figure 4. 16** heat transfer coefficient as a function of flow velocity for water and Kenaf Bast mechanical (kbm) pulp and Kenaf Bast chemical unbleached (kbcu) pulp fibers suspensions at 0.6 wt.% concentration is presented at constant inlet bulk temperature of 32 °C and constant power supply 3300W. Heat transfer coefficient is found lower than that of water at the range of velocity for both kenaf bast chemical unbleached and kenaf bast mechanical pulp fiber suspensions whereas h_c values of kbm are lower than kbcu throughout the experiment. The small difference of h_c between kbcu and kbm pulp fiber suspensions is observed at the range of velocity, which is due to fiber flexibility domination in fiber processing.

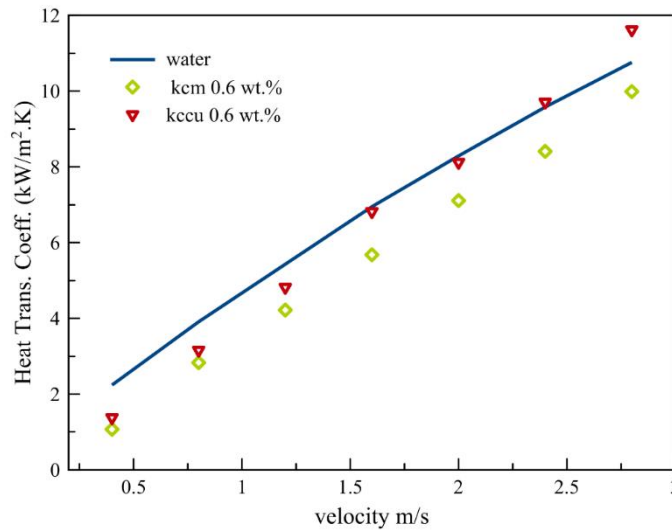


Figure 4.15 h_c as a function of flow velocity for water and different processed Kenaf Core fiber (kccu and kcm) of concentration 0.6 wt.%..

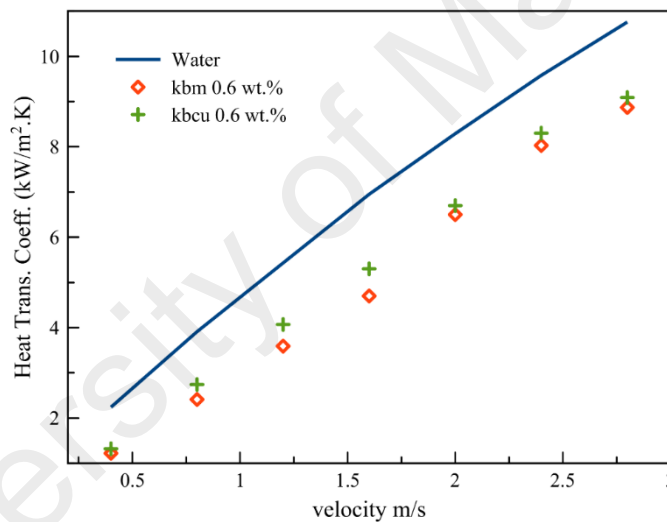


Figure 4.16 h_c as a function of flow velocity for water and different processed Kenaf Core fiber (kccu and kcm) of concentration 0.6 wt.%..

The pulp fiber (kbcu) prepared from soda pulping process exhibit higher h_c due to higher fiber wall thickness and width than that of kbm (RMP) fiber pulp. Pulp prepared from soda pulping process (kbcu) are more uniform in shape, width, thickness and length than that of pulp prepared from RMP pulping process (kbm).

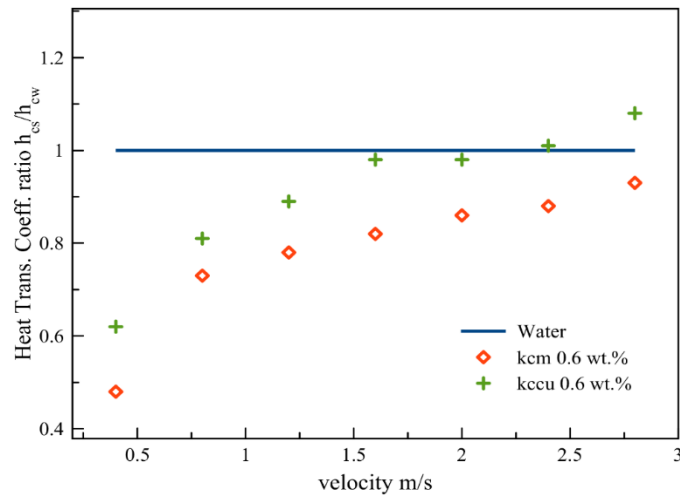


Figure 4. 17 h_c ratio versus flow velocity for water and different processed Kenaf Core fiber (kccu and kcm) of concentration 0.6 wt.%.

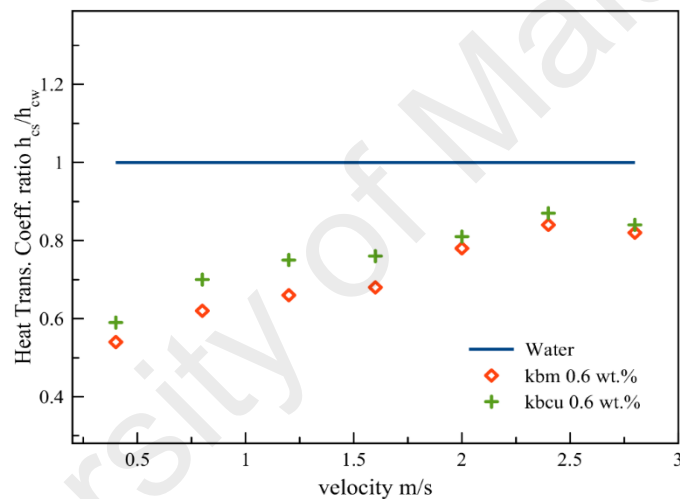


Figure 4. 18 h_c ratio versus flow velocity for water and different processed Kenaf Core fiber (kccu and kcm) of concentration 0.6 wt.%.

Figure 4. 17 shows heat transfer ratio of two pulps samples (kcm and kccu) liberated by two different pulping processes (RMP and Soda pulping respectively). The heat transfer coefficient ratio values for kcm and kccu are 0.93 and 1.08 at velocity of 2.8 m/s respectively. The decrease of heat transfer coefficient could be due to irregular shape of fiber and higher lignin content or a combination of these. M. S. N. Kazi (2001) reported that heat transfer behavior of individual fiber in suspension evidently dominated by flexibility, as fiber length of kbm (0.924 mm) is higher than that of kbcu (0.833 mm) pulp fiber hence fiber length could be a strong reason of decrease in heat transfer coefficient.

The heat transfer coefficient ratio values for kbm and kbcu pulp samples are 0.82 and 0.84 respectively for concentration of 0.6 wt.% at velocity of 2.8 m/s presented in **Figure 4. 18**. The decrease of heat transfer coefficient could be due to fiber length as in case of kcm. With the increase of fiber flexibility, the hc value decreases in suspension due to more energy absorption from fiber-eddy collision and, also from more interaction. To magnify the effect of fiber length on heat transfer, short and long fiber blends are prepared and heat transfer data are correlated with these blends details are in following section.

4.1.2.4 Effect of Fibers blending

The demand of non-wood pulps is increasing due to limitation of wood source and environmental concern. Hereafter, pulp and paper industries mix wood and non-wood fibers to meet the demand and decrease the use of wood pulp. Furthermore, short and long pulp fibers are also mixed together to improve paper properties. Therefore in this section, wood and non-wood pulps and short and long crop pulp fibers are blended and compared with their individual heat transfer coefficients.

Figure 4. 19 illustrates heat transfer coefficient as a function of velocity for water and different blend of crop pulp fibers suspensions. The heat transfer data were obtained at the constant inlet bulk temperature of 32°C and constant heat flux of 23203 W/m². The results reveal that with the increase of long fibers in suspensions heat transfer coefficient decreases. Throughout the experiments heat transfer coefficient of suspensions remain lower than that of water and the suspension having long fibers in low quantity shows higher heat transfer coefficient that is kckb3 followed by kckb4 and then kckb5.

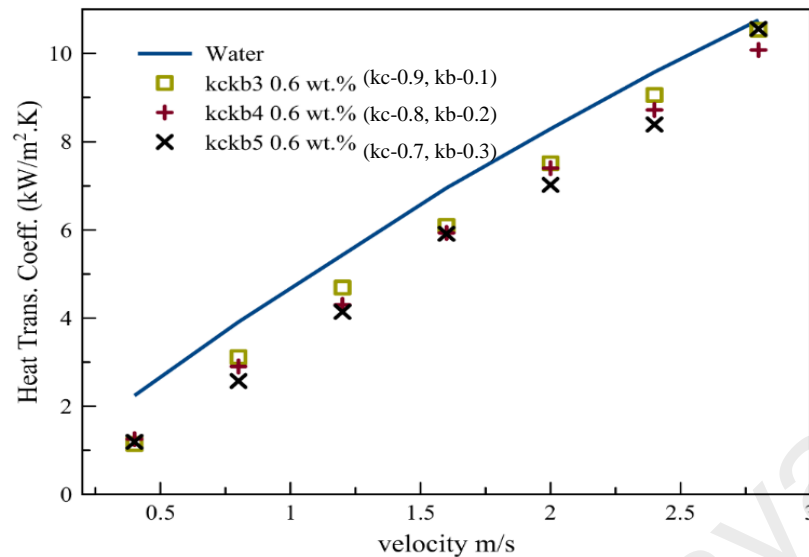


Figure 4.19 h_c as a function of flow velocity for water and different blend of kenaf core and bast (kckb3, kckb4 and kckb5) fiber suspensions.

4.1.2.5 Fiber physical properties and Heat Transfer

Fiber physical properties (length, flexibility, fines, coarseness, lumen diameter, cell wall thickness and the fiber surface roughness) could modify turbulent eddies that effect heat and momentum transfer. Among physical properties of fiber, fiber flexibility and length are the important physical properties that affect flocculation significantly. Due to practical and economic reasons, papermaking technologists are interested in flocculation (Hubbe, 2007). Flocculation effects paper strength, uniformity, appearance (MJ Korteoja et al., 1997; M Korteoja et al., 1998; Rojas & Hubbe, 2005) and adversely affects subsequent operations, such as coating (Hua et al., 1996). Hereafter, flocculation has a great importance in fiber suspension flow that takes place in many industries such as paper making, textile manufacturing, fiber composites etc. Any deviation in fiber properties particularly fiber length and flexibility would change the flocculation and consequently the heat and momentum transfer. Also, many researchers (S. Kazi et al., 2014b; Paavilainen, 1993) reported that fiber flexibility is dependent on cross-dimensional fiber properties and increases with the decrease of fiber cell wall thickness. Furthermore, fiber flexibility characteristics affect fiber bonding and fiber network

structure that affects paper properties as well (S. Kazi et al., 2015). Particular fiber characteristics and some paper characteristics could be analyzed by heat and momentum transfer (G. Duffy et al., 2002; G. Duffy et al., 2000, 2011; S. Kazi et al., 2015). Considering those previous studies which were based on wood and synthetic fibers, there was a need to evaluate heat and momentum transfer measurements over a range of flow conditions for crops fiber that is covered in the following sections.

Table 4. 3 Properties of pulp fibers used in the experimental investigation.

Pulp	Length weighted average length L (mm)	Width W (mm)	Thickness T (mm)	Lumen d (mm)	Slenderne ss ratio	Flexibility coefficient	Runkel ratio
kbm	2.208	0.0151	0.0049	0.0053	146.59	35.23	1.84
kbcu	2.248	0.0164	0.0063	0.0038	137.14	22.90	3.37
kccb	2.574	0.0125	0.0046	0.0034	205.31	26.83	2.73
kcm	0.924	0.0363	0.0038	0.0287	25.45	79.063	0.2662
kccu	0.833	0.0254	0.0054	0.0146	32.80	57.480	0.7397
kccb	0.897	0.0403	0.0030	0.0342	22.25	84.913	0.1777
kckb3	1.052	0.0342	0.0039	0.0264	30.79	77.132	0.2979
kckb4	1.181	0.0321	0.0040	0.0240	36.84	74.944	0.3357
kckb5	1.309	0.0299	0.0041	0.0217	43.74	72.446	0.3816
amcb	0.989	0.023	0.003	0.017	43.19	73.45	0.3615
amkb	1.148	0.0219	0.0032	0.0155	52.48	70.777	0.4129

Paper properties are strongly affected by fiber properties. The well-known physical properties of fibers are fiber length, fiber width and fiber lumen. There is diversity in fiber properties based on the source of the fibers. Physical characteristics of fiber used in this study are presented in **Table 4. 3**. The fiber length of Kenaf bast chemical bleached (kbc) pulp fiber is the longest and also holding the lowest width of lumen diameter among all the pulp fibers in this study. While, Kenaf core chemical unbleached (kccu) pulp fiber have the smallest fiber length among all the pulp samples.

To correlate heat transfer of different flowing pulp fiber suspensions with the fiber properties, the consistency of 0.6 wt.% and the velocity of 1.6 m/s (which is a critical point in most of the cases) were selected in this research as shown in the **Figure 4. 20** and **4.21**.

From **Figure 4. 20 (a)** and **Figure 4. 21 (a)** a clear trend is that, a decrease in fiber length causes an increase in heat transfer coefficient. Similar trend is obtained for fiber flexibility. Fiber flexibility versus heat transfer coefficient, plotted in **Figure 4. 20 (b)** and Error! Reference source not found. **(b)** show that with the increase of fiber flexibility heat transfer coefficient decreases

Slenderness ratio that is fiber length to fiber width ratio presented in **Figure 4. 20 (c)** and **Figure 4. 2 (c)** as a function of heat transfer coefficient. Results shows that with the increase of Slenderness ratio the heat transfer coefficient decreases in case of pulp liberated from the same pulping method such as kccu and kccb, while pulp liberated from different method (RMP and soda pulping) shows heat transfer increases with the increase of Slenderness ratio.

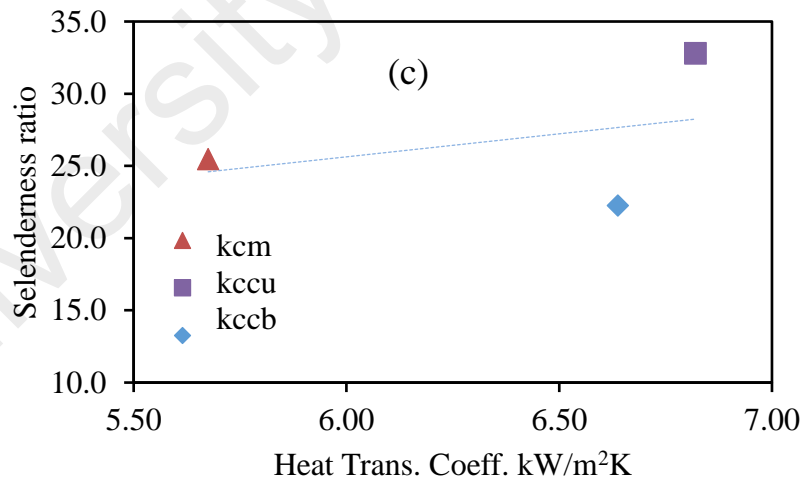
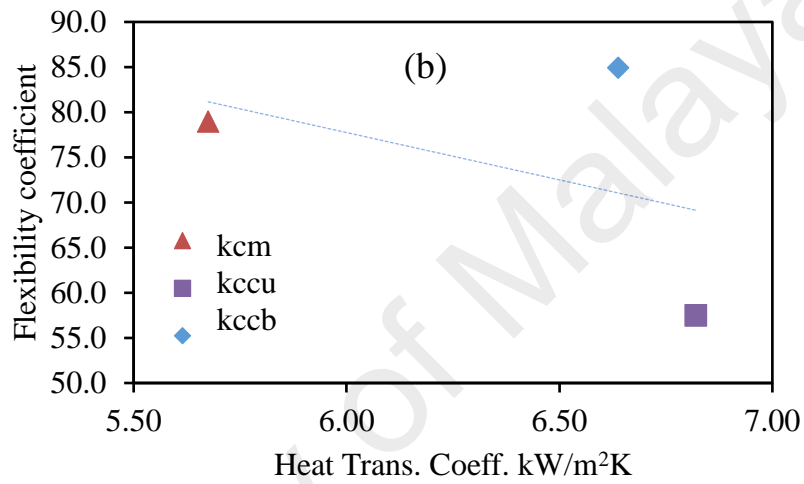
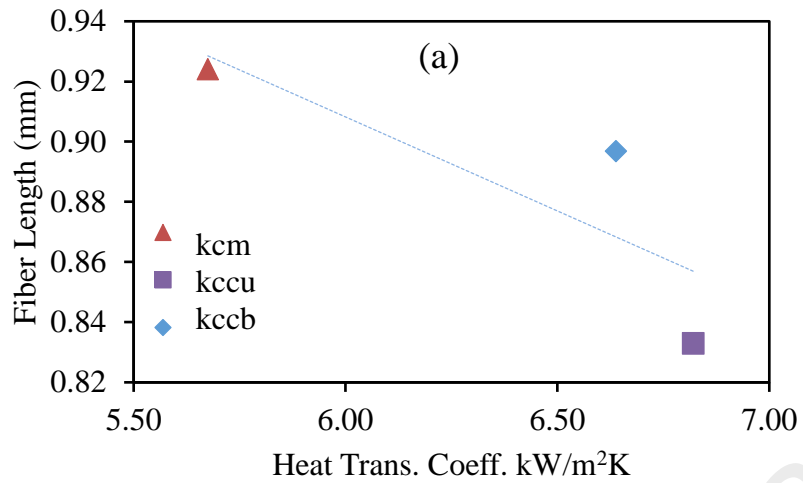


Figure 4. 20 fiber properties as a function of heat transfer coefficient for kcm, kccu and kccb (a) fiber length, (b) flexibility coefficient (c) Slenderness ratio

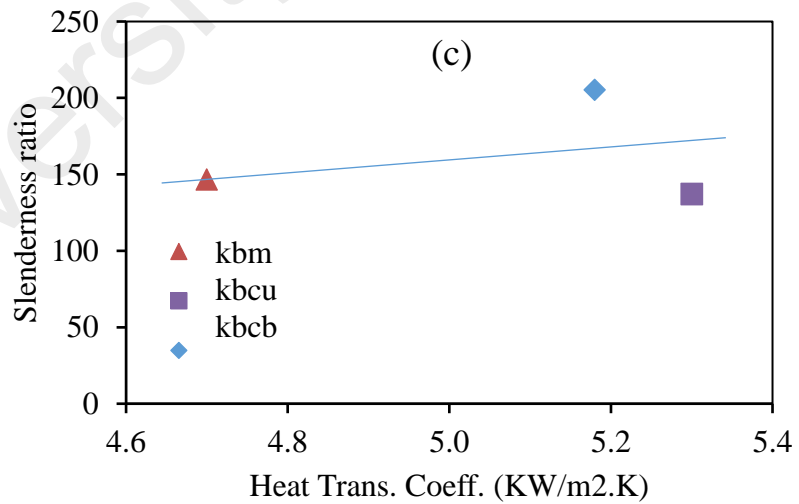
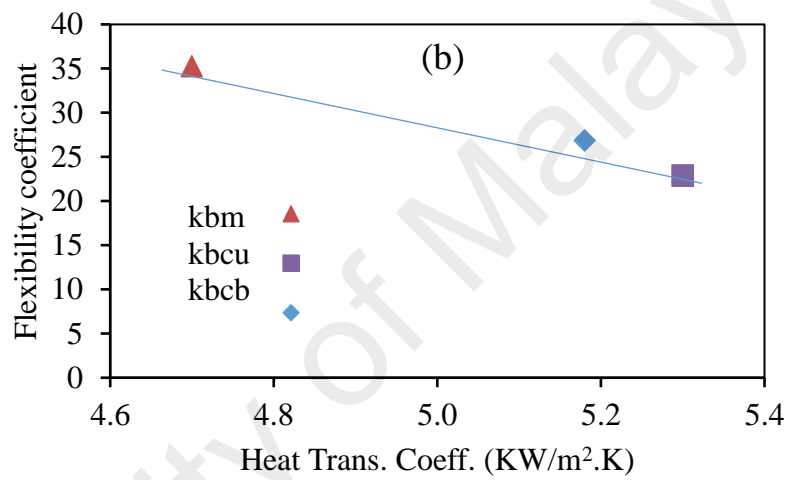
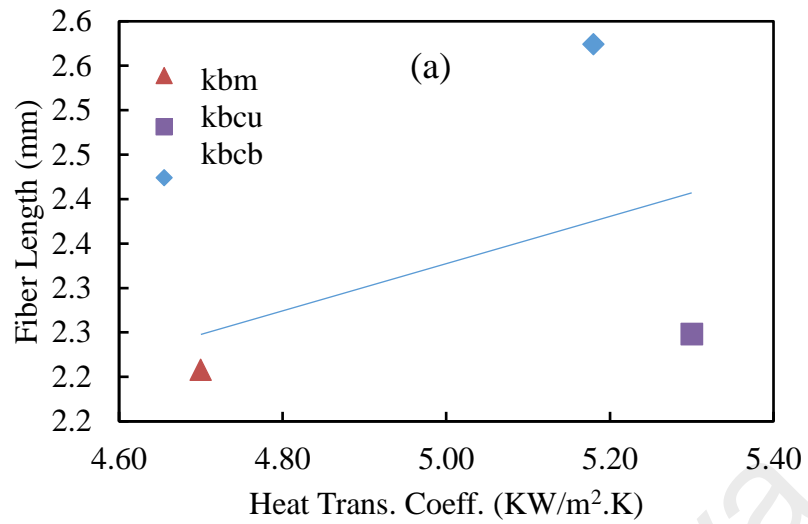


Figure 4. 21 fiber properties as a function of heat transfer coefficient for kbm, kbcu and kbcb (a) fiber length, (b) flexibility coefficient (c) Slenderness ratio

4.1.2.6 Paper properties and Heat Transfer

Paper properties such as tensile index, burst index and tear index are the most important parameters in paper making considerations. Some paper properties of the samples are presented in **Table 4. 4**.

Tensile index of kcm, kccu and kccb as a function of h_c is plotted as illustrated in **Figure 4. 22**. The h_c values increases with a decrease of tensile index which contradict to the results obtained for fiber length and fiber flexibility but similar to the results of previous researchers (G. Duffy et al., 2000). The distinct properties of kenaf core pulp could be due to the adoption of different pulping method, usually the mechanical pulping is not recommended as from this process fiber with uniform

Table 4. 4 Paper properties of the pulp used in the experimental investigation.

Pulp	Tensile index	Burst index	Tear index	Folding endurance	brightness
kbm	61.87	3.96	4.66	38.33	15.28
kbcu	36.72	2.41	9.42	27.00	31.41
kccb	30.91	1.95	14.62	21.33	82.84
kcm	25.08	1.20	2.14	1.66	41.29
kccu	70.59	4.00	2.60	48.50	33.16
kccb	57.65	3.58	4.08	35.66	82.45
kckb3	44.04	1.89	3.60	4.50	36.54
kckb4	44.41	2.14	3.42	9.16	33.62
kckb5	45.60	2.20	4.86	16.33	31.20
amkb	37.68	1.87	6.95	7.50	84.83

morphology cannot produce.

Tensile index of kbm, kbcu, and kbcb as a function of h_c is plotted as illustrated in **Figure 4. 22**. The h_c values increasing with the decrease of tensile index which corresponds to the results obtained for flexibility coefficient versus h_c as is shown in **Figure 4.21 (b)**.

Bursting strength measures the paper resistance to being burst when hydraulic pressure applies to the paper. **Figure 4. 22** shows heat transfer coefficient of the fiber suspensions as a function of paper sheet burst index for the kcm, kccu, kccb, kbm, kbcu, and kbcb pulp samples. The bulk inlet temperature of the fiber suspensions was maintained at 32°C. The relationship between paper sheet burst strength and heat transfer coefficient for kenaf core pulp samples shows upward trend. A clear data trend can be seen for kenaf core pulp fibers that indicates that the heat transfer coefficient increases with the increase of burst index. In contrast, heat transfer coefficient for kenaf bast pulp fibers increases with the decrease of burst index, however the h_c values of kenaf bast pulp fibers are lower than that h_c values of kenaf core pulp fibers.

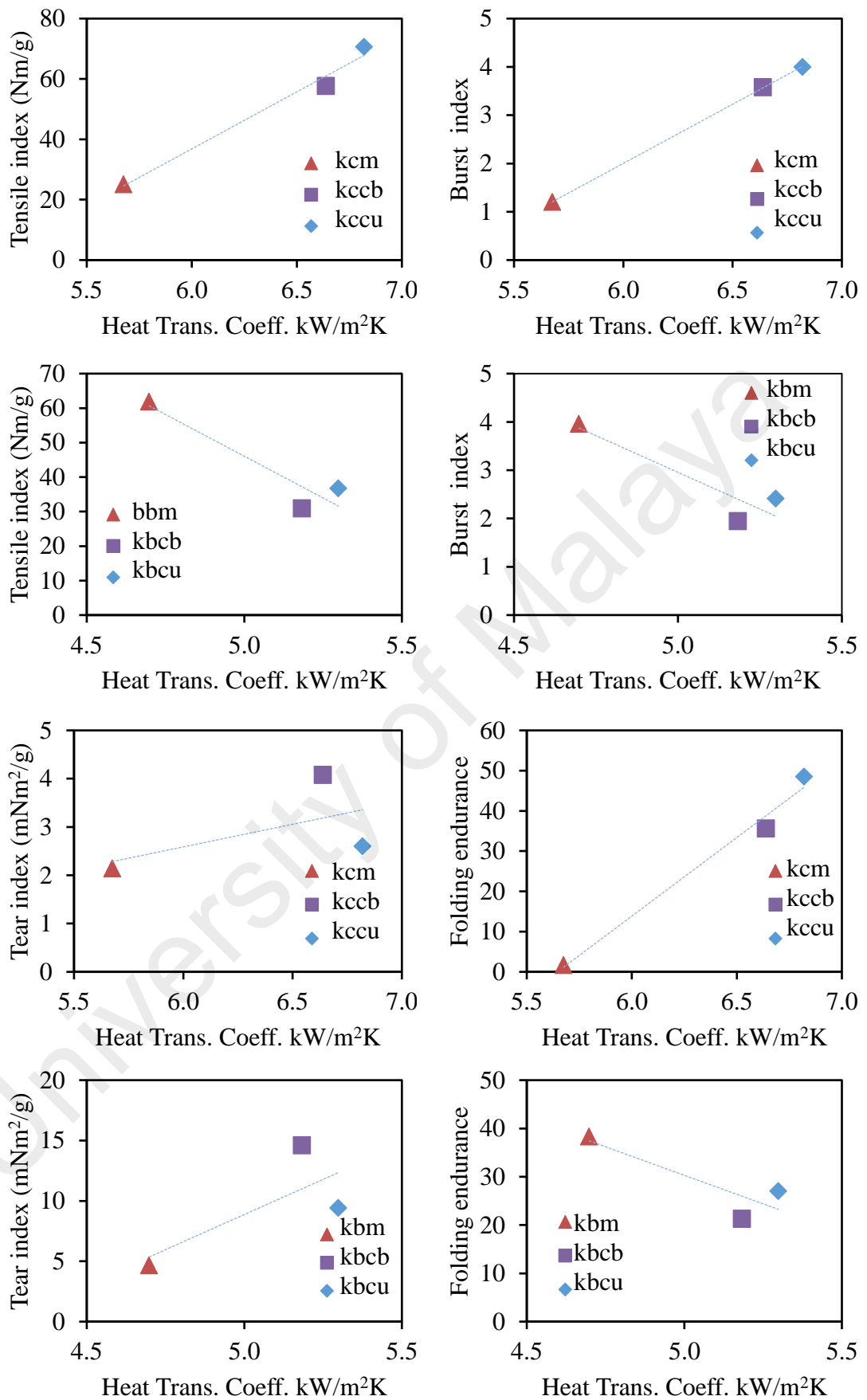


Figure 4. 22 Paper properties of kcm, kccu, kccb, kbm, kbcu, and kccb as a function of Heat transfer coefficient.

The relationship between tear index and h_c is presented in **Figure 4. 22** for kcm, kccu and kccb; and kbm, kbcu, and kccb pulps. This can be explained, since under the condition of tightly bonded fibers, more fibers are ruptured through the initial cut, and fiber rupture requires less energy than pulling fibers out from network, so tear strength is reduced (Mossello et al., 2010). Tear index for both kenaf core and bast pulp fibers showed a similar data trend different from tensile and burst index. Heat transfer coefficient for both kenaf core and kenaf bast pulp fibers decreases with the decrease of tear index. Kenaf core pulp fibers showed higher h_c values than that of kenaf bast but tear index of kenaf core samples is much lower than the tear index of kenaf bast pulp samples.

Folding endurance test have been used to estimate the ability of paper to withstand repeated bending, folding, and creasing (TAPPI, 2006). The paper was folded backwards and fronts repeatedly between tow roller that rolling at 120 double folds per minute (Hassan et al., 2014). Increase of folding endurance increases h_c in case of kenaf core pulp fiber while in case of kenaf bast pulp fibers h_c values decreases with the decrease of folding endurance as can be seen from the **Figure 4. 22**.

4.1.3 Pressure drop of fiber suspensions

4.1.3.1 Different concentration effect of fiber on pressure drop

Figure 4. 23 presents drag ratio versus bulk velocity at three different concentrations (0.2, 0.4 and 0.6 wt.%) and velocity range of (0.4-2.8 m/s). At low velocities, the higher the concentration the higher is the drag ratio due to floc formation. At 1.2 m/s, concentration of 0.4 wt.% and 0.6 wt.% suspensions showed equal and lower drag ratio than concentration of 0.2 wt.% suspension. At concentration of 0.6 wt.% suspension, drag ratio is closer to unity at velocity 2.8 m/s but no drag reduction is observed at the range of velocities and concentrations.

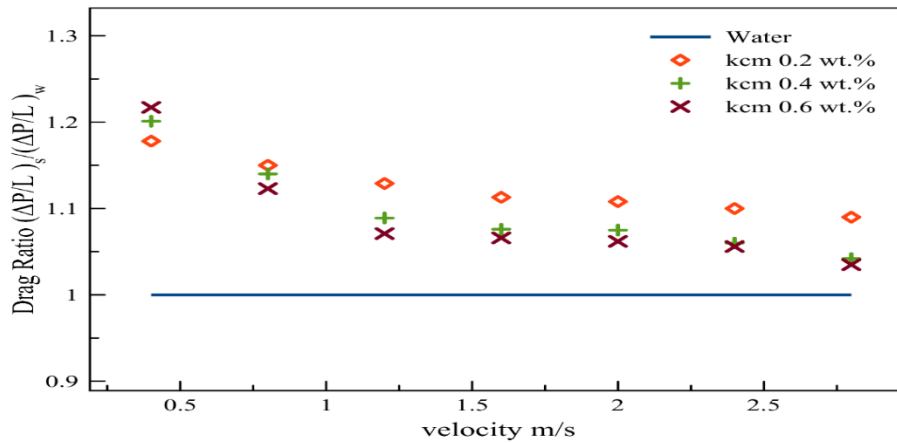


Figure 4. 23 Drag ratio of Kenaf core mechanical pulp suspensions as a function of velocity at different concentrations.

Figure 4. 24 presents the ratio of the pressure drop of suspensions and pressure drop of water as a function of velocity for water and Kenaf bast pulp suspension (when the magnitude of this ratio is less than unity is known as drag reduction) at different concentrations and at a constant inlet temperature of 32 °C.

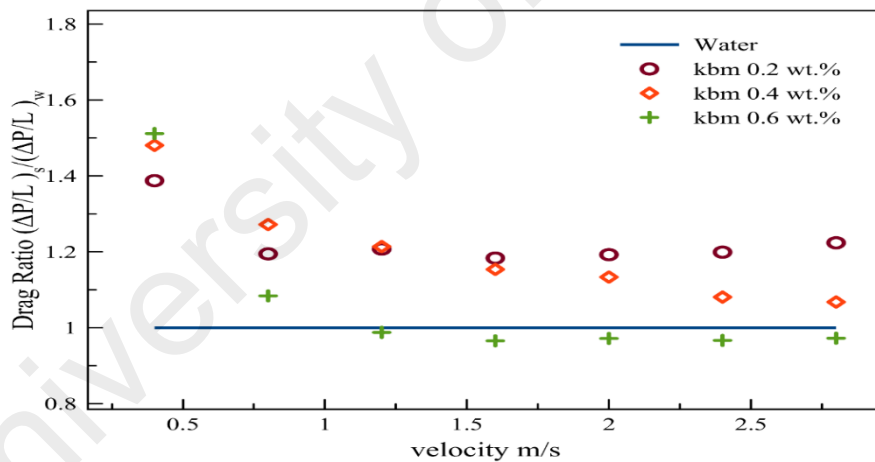


Figure 4. 24 Drag ratio of Kenaf bast mechanical pulp suspensions as a function of velocity at different concentrations

It is observed that at the lowest velocity 0.4 m/s the drag ratios of suspensions are sufficiently higher than water, whereas at the higher concentration (0.6 wt.%) showed the highest drag ratio followed by the concentrations of 0.4 wt.% and 0.2 wt.% respectively. Higher drag ratio at low velocity, substantially owing to the presence of a plug where the turbulent sheared layer between the plug and the pipe wall is very thin and the velocity profile is steep (M. S. N. Kazi et al., 1999). The pulp suspensions at

concentrations of 0.2 wt.% and 0.4 wt.% indicated no drag reduction throughout the investigated range of velocity (0.4 – 2.8 m/s). The subsequent decrease in drag ratio with an increase of flow is owing to the dominance of fiber damping the turbulence. Whereas at a velocity higher than 0.8 m/s and the concentration of 0.6 wt.% showed drag reduction. It is observed that the magnitude of drag ratio decreases with the increase of velocity. The maximum drag reduction is observed at 1.6 m/s and that is 3.5% less than the pressure drop of water.

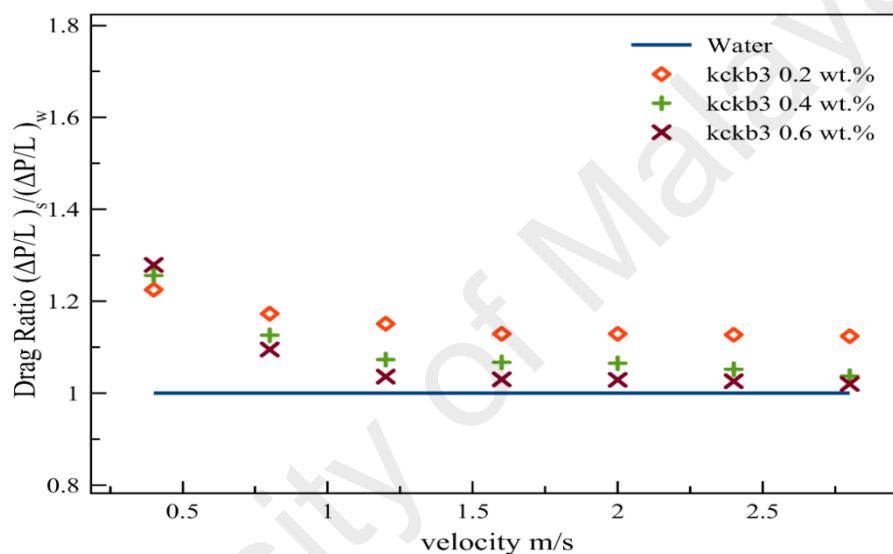


Figure 4. 25 Drag ratio of blend of Kenaf core and bast mechanical pulp suspensions as a function of velocity at different concentrations

Effect of fiber concentration on drag reduction was studied using kckb3 pulp.

Figure 4. 25 presents the ratio of the pressure drop of suspensions and pressure drop of water as the function of velocity for water and kckb3 at different concentrations (0.2, 0.4, and 0.6 wt.%) and a constant inlet temperature of 32 °C and constant heat flux of 23.2 KW/m². It is observed that at the lowest velocity 0.4 m/s the drag ratios of suspensions are sufficiently higher than that of water, whereas at the highest concentration of 0.6 wt.% have shown the highest drag ratio. Higher drag ratio at low velocity, substantially owing to the presence of a plug where the turbulent sheared layer between the plug and the pipe wall is very thin and the velocity profile is steep (M. S. N. Kazi et al., 1999). The drag reduction is not achieved throughout the range of

velocity (0.4 – 2.8 m/s) for all consistencies of pulp suspensions. The subsequent decrease in drag ratio with an increase of flow is owing to the dominance of fiber damping the turbulence. It is observed that the magnitude of drag ratio decreases with the increase of velocity and consistency. The minimum drag ratio is observed for highest concentration of 0.6 wt.% at 2.8 m/s and that is slightly higher than the pressure drop of water.

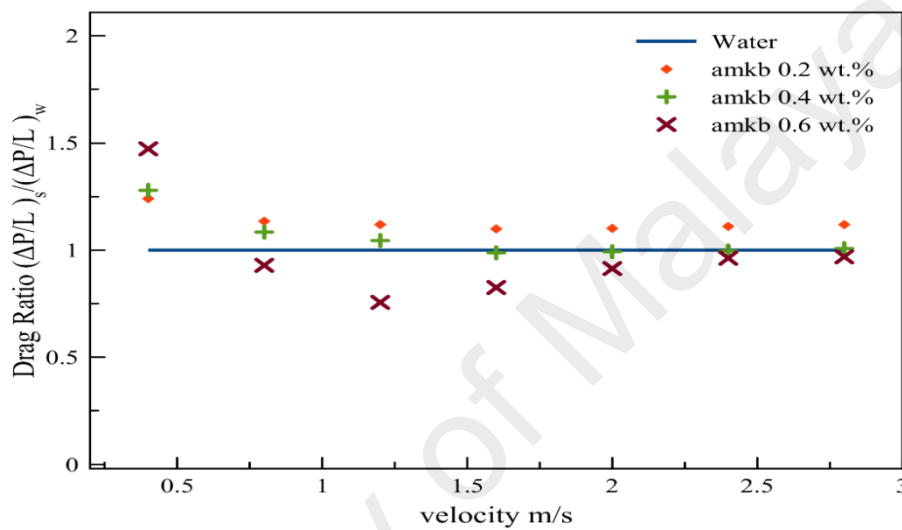


Figure 4. 26 Drag ratio of blend of Acacia mangum and Kenaf bast pulp suspensions as a function of velocity at different concentrations

Figure 4. 26 presents drag ratio of the blend of Acacia mangum and Kenaf bast pulp fibers suspensions as a function of velocity at three different weight concentrations 0.2, 0.4, and 0.6% at the constant inlet bulk temperature of 32°C. At a low velocity of 0.4 m/s, the adequate distinction is observed in the drag ratio of the concentration of 0.6 wt.% with the concentration of 0.2 and 0.4 wt.%, whereas the enormous difference between pulp suspensions and water values are revealed. Drag reduction is observed at a velocity higher than 0.4 m/s for the weight concentration of 0.6%, while for lower concentration the drag reduction is not observed throughout the experiment.

4.1.3.2 Effect of bleaching

Bleaching effect on pressure drop was investigated by bleached Kenaf Bast chemical (kbc) pulps, which were prepared by bleaching of the kenaf bast chemical unbleached (kbcu) pulp fiber. The pressure drop data were obtained for both kbc and kbcu for the concentration of 0.6 wt.% over a range of velocity (0.4 – 2.8 m/s) at a constant inlet bulk temperature of 32°C for the pulp suspensions and compared these data with water data as presented in **Figure 4. 27**. The results showed that pressure drop of both kbc and kbcu are lower than that of water at the range of investigated velocity. Except at velocity 0.4 m/s kbc indicated about 27.9 % higher pressure drop than that of water, whereas kbcu at velocity 0.4 and 0.8 m/s indicated 34.9% and 3% higher pressure drop than that of water, respectively.

Figure 4. 28 presents drag ratio of water, kbcu, and kbc versus velocity at the concentration of 0.6 wt.% and the constant inlet bulk temperature of 32 °C. At a low velocity of 0.4 m/s, the adequate distinction is observed in the drag ratio values of kbcu and kbc, whereas the enormous difference between pulp suspensions and water values are revealed. Drag reduction is observed at a velocity higher than 0.4 m/s, except at the velocity 0.8 m/s drag the reduction is not marked for kbcu. Furthermore, kbc exhibited low drag reduction than that of kbcu throughout the drag reduction regime.

The significant pressure drop and drag ratio at low velocity (0.4 m/s) is substantially owing to floc formation whereas the subsequent decrease in pressure drop and drag ratio with an increase of velocity is owing to fiber damping of turbulence. Furthermore, with an increment of flow rate the shear stress increases and that ultimately decreases fluid viscosity (Charani et al., 2013), hence with the reduction of viscosity the frictional losses reduces which develops drag reduction and low-pressure drop. The kbc pulp fiber indicates lower pressure drop and drag reduction than kbcu due to higher fiber flexibility. In chemical pulping, the materials are detached both from

the fiber wall and amid the fibers. Fibers swell in chemical pulping. Fiber cell wall structure becomes loose upon removal (Bleaching) of lignin allowing water molecules to get between the microfibrils and hence lessen the young's modulus, which increases flexibility as the young's modulus is inversely proportional to flexibility (Goto et al., 1986).

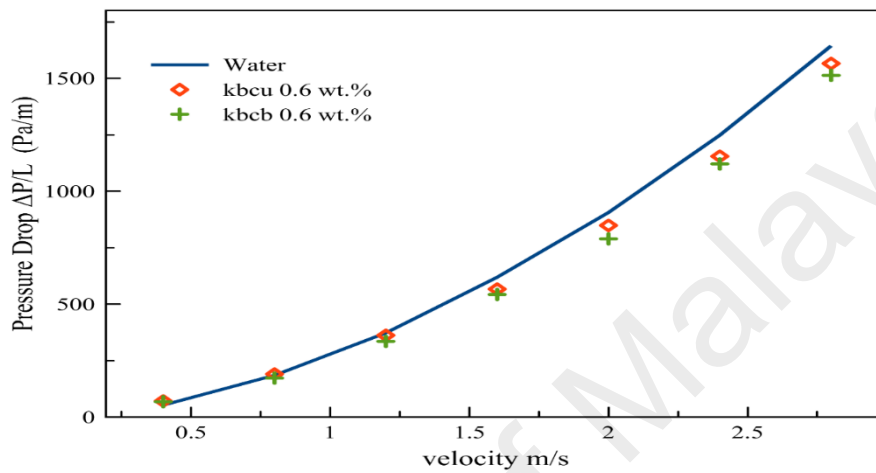


Figure 4.27 Pressure drop of kenaf bast bleached and unbleached pulp fiber suspensions as a function of velocity.

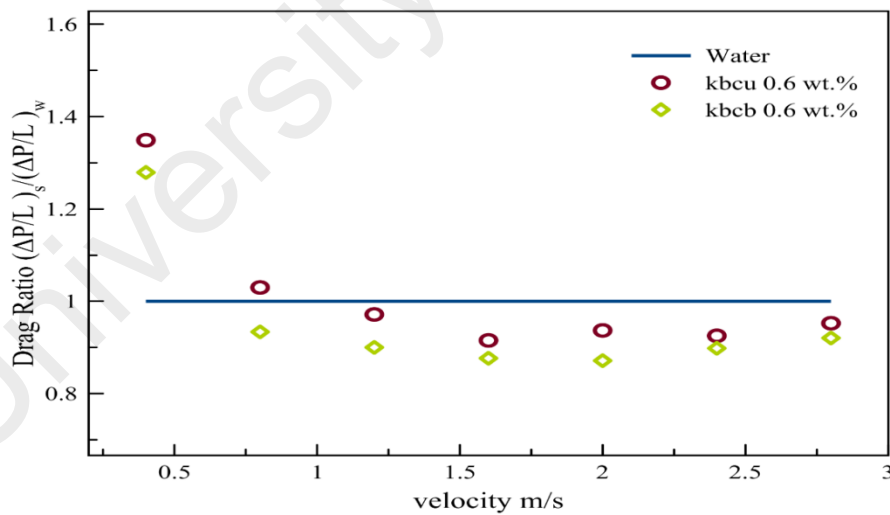


Figure 4.28 Drag ratio of kenaf bast bleached and unbleached pulp fiber suspensions as a function of velocity

Detaching lignin contents from a pulp fiber by means of bleaching makes fiber more flexible and hence pressure drop and drag reduction decrease with the increase of fiber flexibility. Similar results were revealed by the previous researcher (S. Kazi et al.,

2015).

Bleaching effect of kccu pulp fiber suspension on frictional pressure drop and drag ratio are studied and presented in **Figure 4. 29** and **Figure 4. 30** respectively. Frictional pressure drop and drag ratio as a function of velocity for kccu and kccb pulp fiber suspensions at a concentration of 0.6 wt.% and water as a reference are investigated. Alit could be seen that the data points of kccu and kccb are group together throughout the investigation and have higher frictional drop than water and no drag ratio is observed

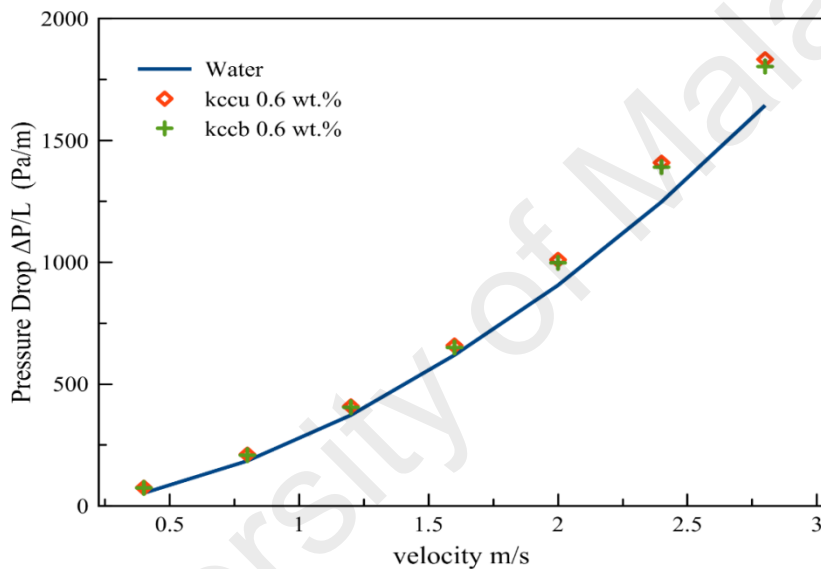


Figure 4. 29 Pressure drop of kenaf core bleached and unbleached pulp fiber suspensions as a function of velocity.

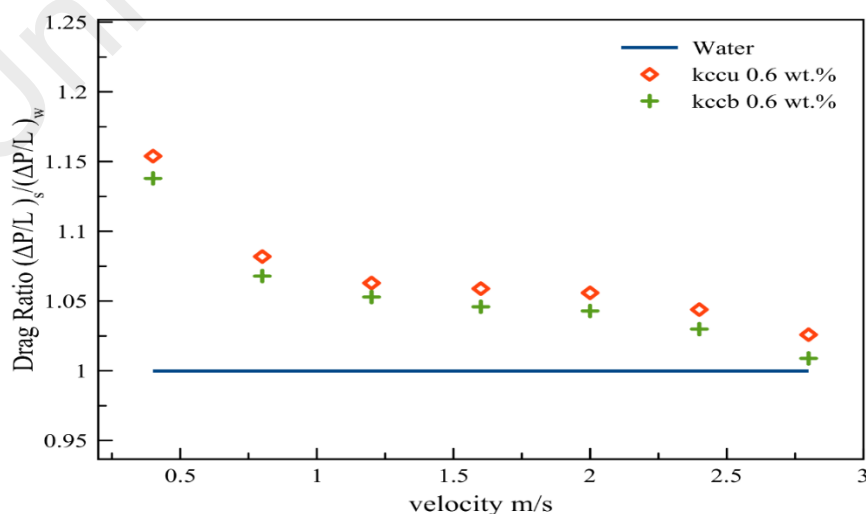


Figure 4. 30 Drag ratio of kenaf core bleached and unbleached pulp fiber suspensions as a function of velocity

4.1.3.3 Effect of processing

The pulps are prepared from the raw materials (wood chips, crops, and residue of fiber materials) by different pulping processes such as mechanical pulping, chemical pulping and thermomechanical pulping in different industries depending on the end product. In the present study, it is prepared by two common pulping methods such as RMP and soda pulping.

In **Figure 4. 31** pressure drop as a function of flow velocity for water and kbm and kbcu, pulp fiber suspensions at 0.6 wt.% concentration are presented at constant inlet bulk temperature of 32 °C and constant heat flux of 23.2 kW/m². Pressure drop is found lower than that of water at the range of velocity for both kenaf bast chemical unbleached (kbcu) and kenaf bast mechanical (kbm) pulp fiber suspensions except at low velocities of 0.4 and 0.8 m/s where the pressure drop values of kbcu and kbm are marked higher than water values. Whereas pressure drop values of kbcu are lower than kbm throughout the experiment. The small difference in pressure drop data between kbcu and kbm pulp fiber suspensions is observed at the range of velocities that is due to fiber flexibility domination in fiber processing.

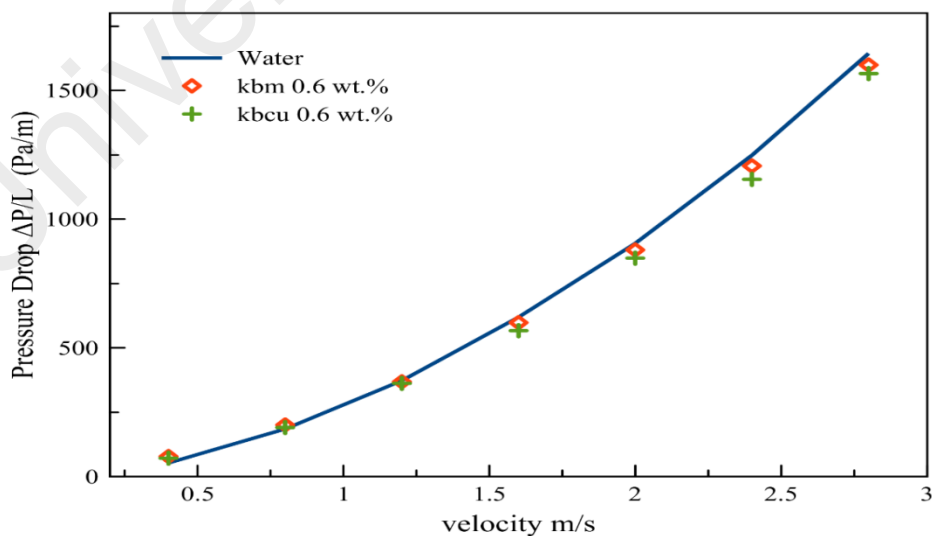


Figure 4. 31 Pressure drop of kenaf bast mechanical and kenaf bast chemical unbleached pulp fiber suspensions as a function of velocity

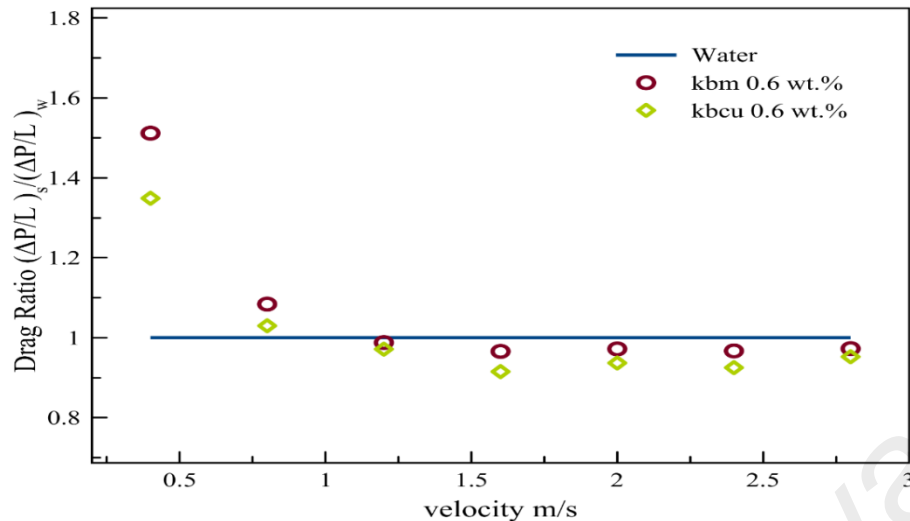


Figure 4.32 Drag ratio of kenaf bast mechanical and kenaf bast chemical unbleached pulp fiber suspensions as a function of velocity

Drag ratio calculated from water, kbm, and kbcu are presented in **Figure 4.32** for fiber concentration of 0.6 wt.%. The experiments were conducted in the velocity range of 0.4 to 2.8 m/s. At the very low velocity of 0.4 m/s drag ratio of kbm and kbcu marked significant deviation, while both kbm and kbcu drag ratios are enormously higher than water values owing to plug flow existence. Whereas at velocity 0.8 m/s drag ratio is near to water but drag reduction is not observed. Drag reduction is observed at velocity 1.2 m/s and above. The maximum drag reduction 8.5% and 3.5% are observed for kbcu and kbm pulp suspensions respectively at velocity 1.6 m/s, above this critical point drag reduction is decreasing, which is due to decrease of fiber interlocking and network formation tendency and hence disruption of fiber network initiated (Cui & Grace, 2007). As it is dependent on concentration and shear stress so after a critical point the tendency of fiber interlocking and network formation decreases. Similar data trends were observed by previous researchers (G. Duffy et al., 2002; G. Duffy et al., 2011; Gharekhani et al., 2017). The significant deviation between kbcu and kbm is owing to fiber flexibility, kbm is less flexible than kbcu since in mechanical pulping process lignin content cannot be fully removed. Additionally, pulp prepared from soda pulping process (kbcu) are more uniform in shape, width, thickness and length than that

of pulp prepared from RMP pulping process (kcm).

Figure 4. 33 and **Figure 4. 34** represent frictional pressure drop and drag ratio respectively of kenaf core pulp prepared by two different methods (soda pulping and mechanical pulping) plotted as a function of velocity at constant heat flux of 23.2 kW/m² and inlet temperature of 305 K. The data points of kccu and kcm are grouped together and have higher frictional pressure drop than that of the water throughout the investigation and there is no drag reduction observed.

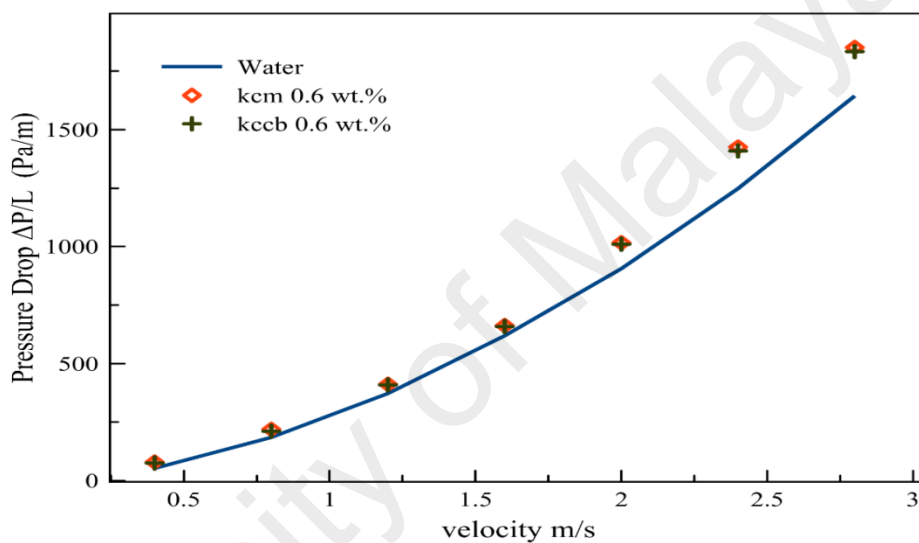


Figure 4. 33 Pressure drop of kenaf core mechanical and kenaf core chemical unbleached pulp fiber suspensions as a function of velocity

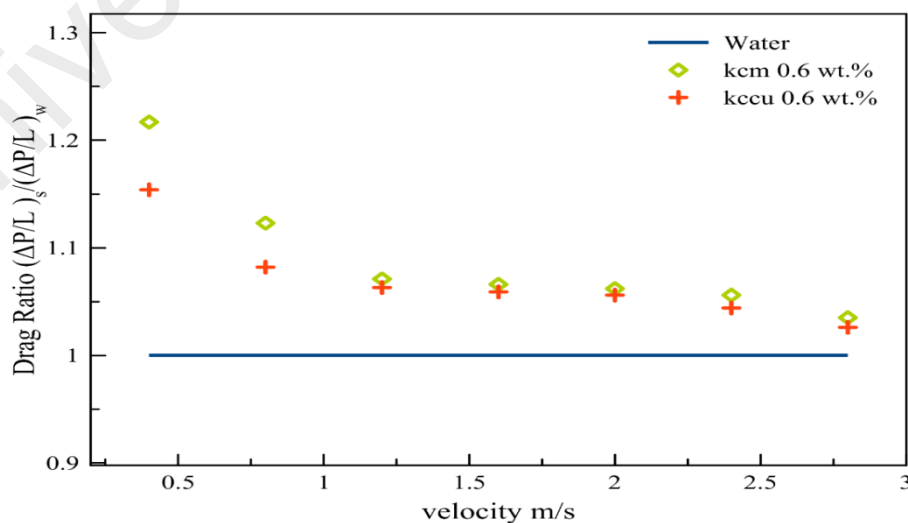


Figure 4. 34 Drag ratio of kenaf core mechanical and kenaf core chemical unbleached pulp fiber suspensions as a function of velocity

4.1.3.4 Effect of fiber blending

To study the effect fiber source on frictional pressure drop, the blend kckb3 (a mixture of kcm and kbm with mass ratio 9:1) pulp suspension were compared with primary pulp fibers kcm and kbm at a range of velocity 0.4-2.8 m/s and with a concentration of 0.6 wt.% and constant inlet bulk temperature of 32°C along with water presented in **Figure 4. 35** as a drag ratio. At low velocity of 0.4 m/s, adequate distinction is observed in the drag ratio values of kcm, kbm and kckb3 whereas the the enormous difference between pulp suspensions and water values is marked.

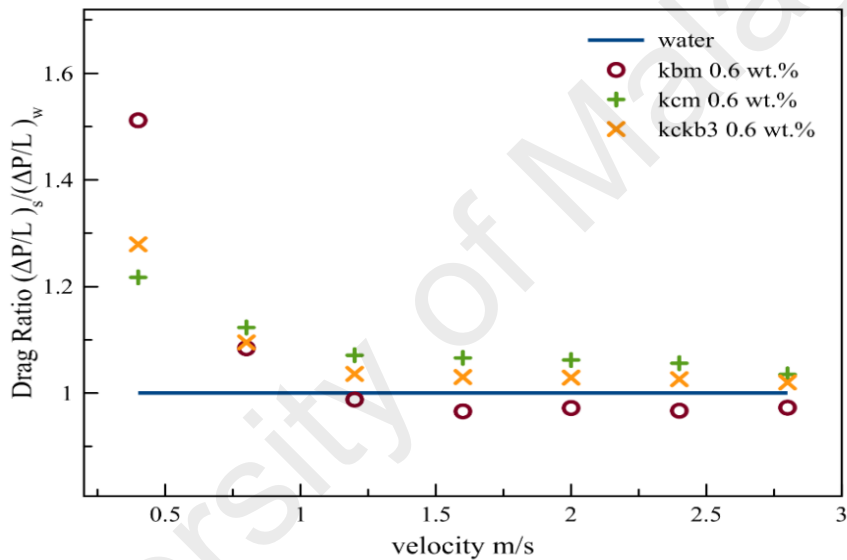


Figure 4. 35 Drag ratio as a function of flow velocity for water and different pulp suspensions kbm, kcm and kckb3 at concentration of 0.6 wt.%.

Furthermore, kbm showed the highest drag ratio 1.512 followed by kckb3 1.279 and kcm 1.217. The blend increased the drag ratio about 5.09% than that of kcm (the primary pulp in the blend) at a low velocity of 0.4 m/s. High drag ratio at low velocity, substantially due to the presence of a plug where the turbulent sheared layer between the plug and pipe wall is very thin and the velocity profile steep. The highest drag ratio marked by kbm at low velocity 0.4 m/s is due to heist aspect ratio that interacts with neighboring eddies, deflect, bend and absorb turbulent energy.

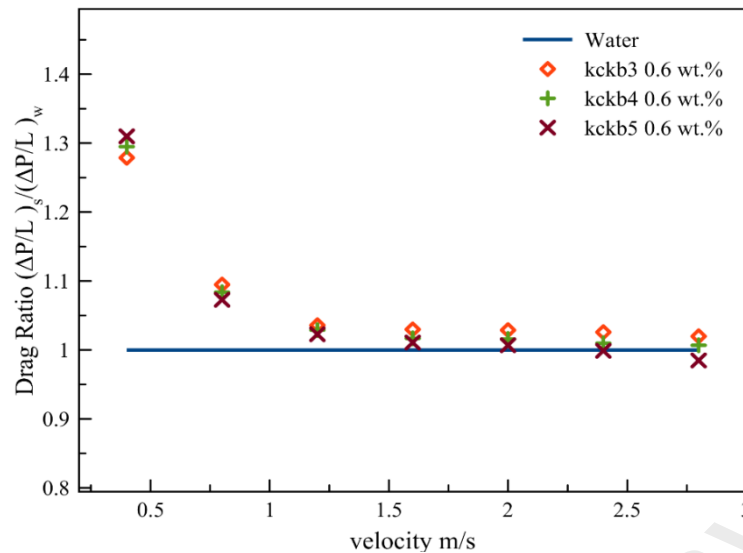


Figure 4.36 Drag ratio as a function of velocity for water and different pulp suspensions kckb3, kckb4, and kckb5 at concentration of 0.6 wt.%.

The minimum drag ratios 0.966, 1.02 and 1.035 are observed for kbm, kckb3 and kcm at velocity 1.6, 2.8 and 2.8 respectively. These results indicate that floc and network formation even at same concentration occur at different velocities and in the case of long fiber (kbm) the minimum drag ratio is observed in the mid-range of velocity 1.6 m/s over this point drag ratio successively increases slightly. While short fiber (kcm) and kckb3 showed a successive decrease in drag ratio until the maximum velocity 2.8 m/s investigated in the present study. Whereas, addition (blending) of 10 wt.% long fiber (kbm) in short fiber (kcm) decreased pressure drop about 1.45% than that of kcm.

To magnify the phenomenon of deflecting, bend and absorbing turbulent energy or aid in transmitting momentum with aspect ratio, the blend kckb3 were prepared by mixing pulp fibers with high aspect ratio 146.58 (kbm) with low aspect ratio 25.45 (kcm). The results reveal that with the increase of aspect ratio of fibers in suspension pressure drop decreases. Furthermore, consequent decrease in pressure drop with an increase of velocity is owing to the dominance of shear stress and formation of flocs and network that have special plastic-elastic characteristics.

Figure 4. 36 presents drag ratio as a function of flow velocity for water and three different blend of kcm and kbm i.e. kckb3, kckb4, and kckb4 pulp fiber suspensions at 0.6 wt.% concentration are presented at constant inlet bulk temperature of 32 °C and constant heat flux of 23.2 kW/m². Drag ratios are found higher than that of water at the range of velocity for all the samples except at high velocities of 2.4 and 0.8 m/s where the pressure drop values of kckb5 are marked lower than water values. The small difference in pressure drop data between the different pulp fiber suspensions is observed at the range of velocities that is due to fiber flexibility domination and fiber flexibility domination increases with the increase of addition of long fibers.

4.1.3.5 Fiber properties and frictional pressure drop

Fiber physical properties could modify turbulent eddies that affect frictional pressure drop. Due to practical and economic reasons, papermaking technologists are interested in flocculation (Hubbe, 2007). Flocculation effect paper strength, uniformity, appearance (MJ Korteoja et al., 1997; M Korteoja et al., 1998; Rojas & Hubbe, 2005) and adversely affect subsequent operations, such as coating (Hua et al., 1996). Flocculation and consequently the frictional pressured drop would be affect by any deviation in fiber properties particularly fiber length and flexibility. Also, many researchers (S. Kazi et al., 2014b; Paavilainen, 1993) reported that fiber flexibility is dependent on cross-dimensional fiber properties and increases with the decrease of fiber cell wall thickness. Some fiber characteristics could be analyzed by pressure drop measurements (G. Duffy et al., 2000; S. Kazi et al., 2015). Considering those previous studies which were based on wood and synthetic fibers, there was a need to evaluate pressure drop measurements over a range of flow conditions for crop pulp fibers. To correlate pressure drop of flowing crop pulp suspensions with the fiber length, fiber lumen, and fiber width (other properties are presented in appendix D), the consistency of 0.6 wt.% and the velocity of 1.6 m/s were selected in the present study as shown in

the **Figure 4. 37** (a – c).

The results reveal that the presser drop could be used for monitoring deviations in fiber characteristics and hence pulp and paper quality. The deviations in pressure drop between kcm, kbm and kckb3 pulp suspensions are due to fiber flexibility and lignin content and aspect ratios. The findings and data trends are similar with the previous researchers for wood pulp and synthetic fibers (G. Duffy et al., 2000, 2011; Gharekhani et al., 2017; M. S. N. Kazi et al., 1999; S. Kazi et al., 2012)

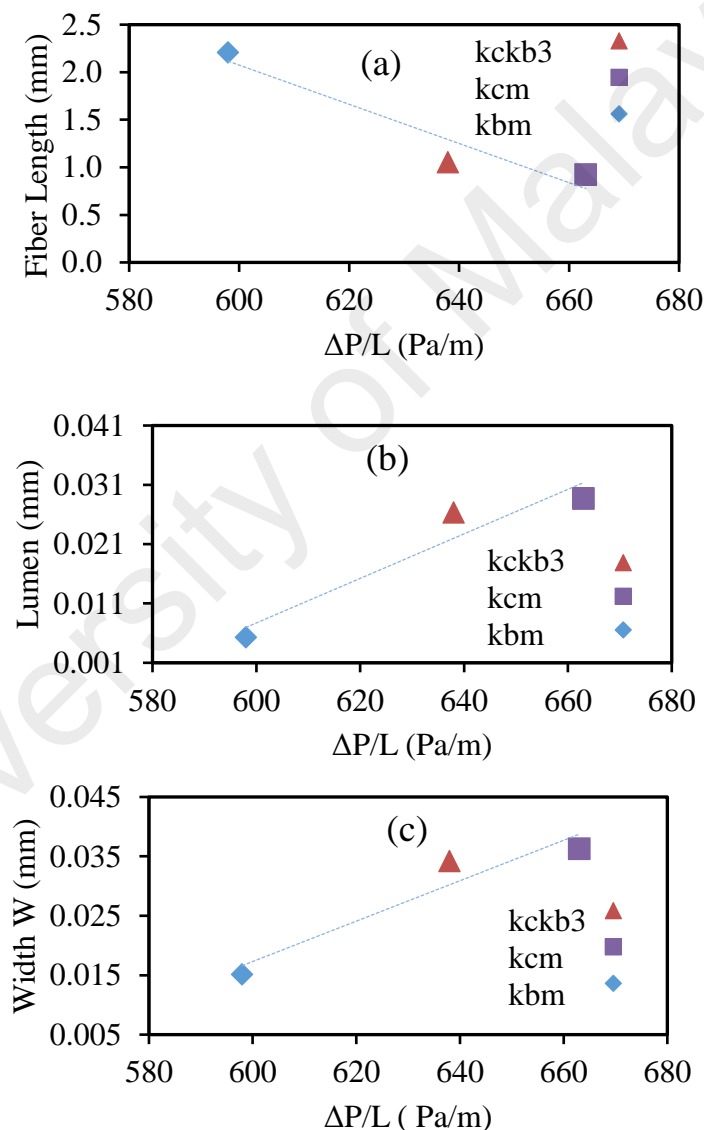


Figure 4. 37 Correlation of frictional pressure drop of kckb3, kcm and kbm pulp suspensions at consistency of 0.6 wt.% with (a) fiber length, (b) fiber lumen, and (c) fiber width.

4.1.3.6 Paper properties and frictional pressure drop

Frictional pressure drop measurement of fiber suspensions were used to correlate $\Delta P/L$ data with the properties of paper sheets made from the same type of fibers. Paper properties were obtained from laboratory-made hand sheets prepared from the same pulp fibers. Some of the data are presented in graphical form in **Figure 4. 38** to **Figure 4. 41**. Approximate linear relationship is found for paper tear index versus pressure drop at the velocity of 1.6 m/s and temperature of 32 °C (**Figure 4. 38**). The hand sheets used for tests were at the same grammage. The tear test is very sensitive to the physical properties of the fiber (Main et al., 2015). The decrement order of tensile index remains same as for the fiber length, such as kckb3, kcm and kbm respectively.

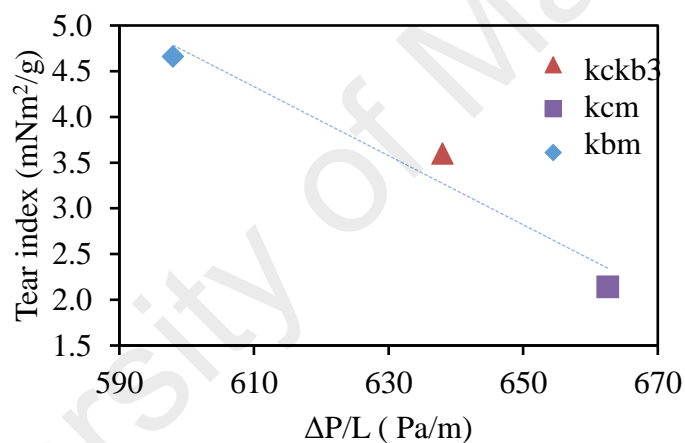


Figure 4. 38 Tear index as a function of pressure drop for Kenaf core mechanical (kcm), Kenaf bast mechanical (kbm) and blend of kcm and kbm (kckb3).

The trend remains similar for burst index versus pressure drop for kckb3, kcm and kbm **Figure 4. 39** with tear index and fiber length. With the increase of Burst index pressure drop of pulp fiber suspensions decreases

Figure 4. 40 illustrates decrease of pressure drop with the enhancement of Tensile index. The Tensile strength of the fibers corresponded the tear strength, whereby the Tensile values decreased with increase of fiber length that is kbm, kckb3 followed by kcm.

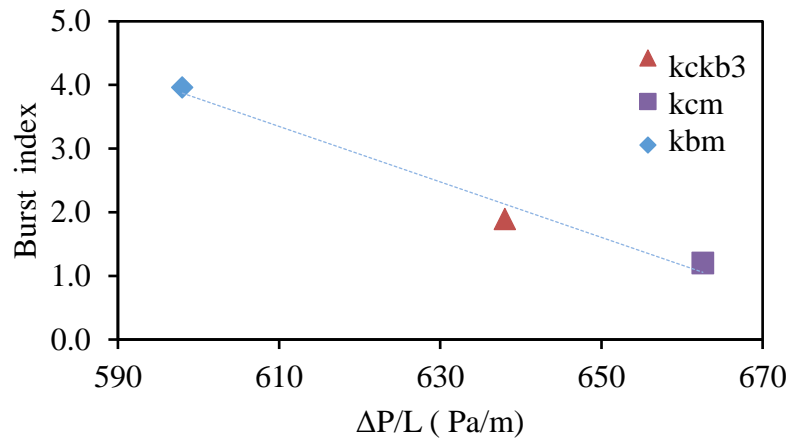


Figure 4.39 Burst index as a function of pressure drop for Kenaf core mechanical (kcm), Kenaf bast mechanical (kbm) and blend of kcm and kbm (kckb3).

Figure 4.41 represents paper folding endurance as a function of pressure drop of suspensions of the kenaf core mechanical, kenaf bast mechanical and blend of these fibers kckb3. The folding endurance increases with the decrease of pressure drop a similar trend with Tear index, Burst index and Tensile index.

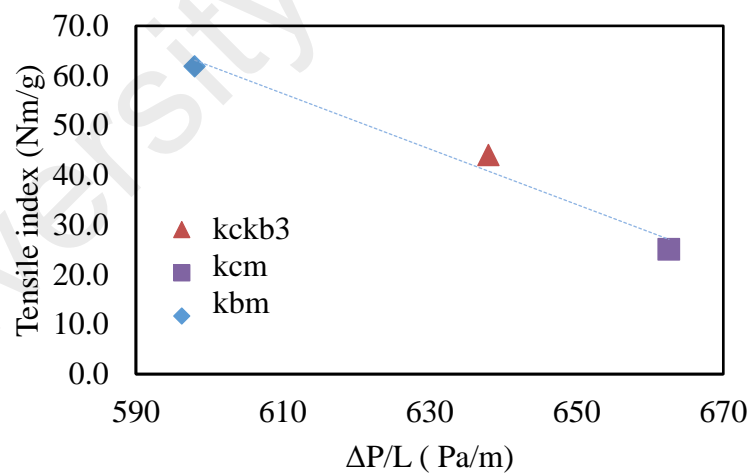


Figure 4.40 Tensile index as a function of pressure drop for Kenaf core mechanical (kcm), Kenaf bast mechanical (kbm) and blend of kcm and kbm (kckb3).

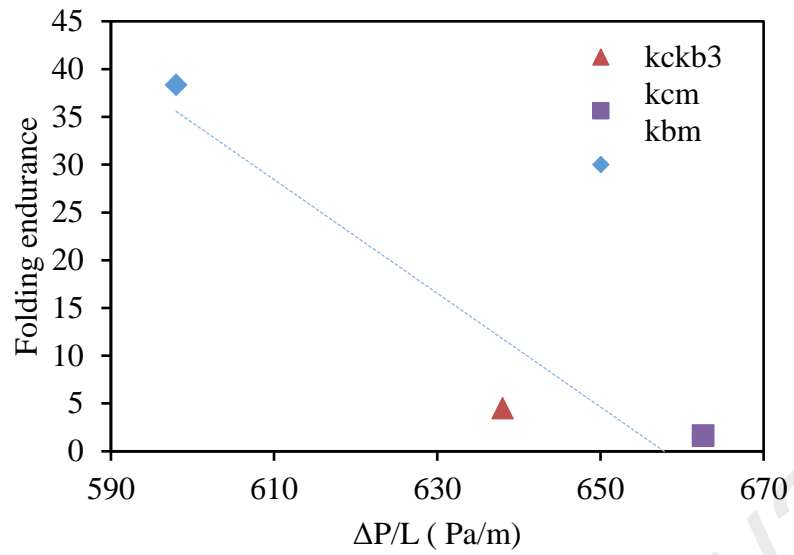


Figure 4. 41 Folding endurance as a function of pressure drop for Kenaf core mechanical (kcm), Kenaf bast mechanical (kbm) and blend of kcm and kbm (kckb3).

University of Malaysia

4.2 Nanofluids and Step Flow study

4.2.1 Preparation of Nanofluid

4.2.1.1 Preparation of Aluminum oxide and Silicon dioxide nanofluids

Dry aluminum oxide and Silicon dioxide (Al_2O_3 Nano powder with particle size ~ 50 nm and SiO_2 Nano powder with particle size ~ 50 nm), acquired from sigma aldrich, and distilled water was used to prepare the nanofluids by two step method. Both nanofluids were characterized by zeta potential and transmission electron microscope (TEM). To break down the large agglomerates, ultrasonication was applied for 60 min to get homogenous distribution of nanoparticles. During the preparation of Al_2O_3 -water and SiO_2 -water nanofluids, the main concern is to get homogenous and uniform suspension of nanoparticles by dispersing the agglomerated nanoparticles. The agglomerated nanoparticles are settled with time leading to poor suspension stability. So, the amount of nanoparticles should be carefully selected. To determine the suitable amount of dispersant and concentration effect, four weight concentrations (0.025%, 0.05%, 0.075% and 0.1%) of each sample were prepared. The method is extensively used in synthesizing nanofluids by mixing base fluids with commercially available Nano powders obtained from different mechanical, physical and chemical routes (e.g., milling, grinding, and sol-gel and vapor phase methods). Frequent use of ultrasonication or stirring decreases particle agglomeration (Chung et al., 2009). Agglomeration is a major issue in synthesizing nanofluids (X.-Q. Wang & Mujumdar, 2008). The two-step method is the most economical method for large-scale production of nanofluids because Nano powder synthesis techniques have already been scaled up to industrial production levels (Ponmani et al., 2014). Nanoparticles tend to aggregate because of high surface area and activity. Researchers suggest (Eastman et al., 2001) that the two-step method is more suitable for preparing nanofluids with oxide nanoparticles than those with metallic nanoparticles. The two step method is recognized as the most economical process for

producing nanofluids (Mukherjee & Paria, 2013).

4.2.1.2 Synthesis of MWCNT-Aspartic Acids

To functionalize multi walled carbon nanotubes (MWCNTs) with the aspartic acid, MWCNTs are first functionalized with carboxyl groups. For synthesizing oxidized MWCNTs, raw MWCNTs (Diameter: 20-30 nm, L= 5-10 micrometer, Shen Zhen company, Purity: 95%) are mixed with a mixture of H₂SO₄/HNO₃ acids in volume ratio of 1:1 for 24 h at 60°C. Using a polytetrafluoroethylene (PTFE) membrane, the resulting black mixture is filtered and at the same time rinsed with the deionized water. Then, 1gr oxidized MWCNT, 1gr aspartic acid, 200mL DMF and 10mL toluene are poured in a vessel and was ultra-sonicated for 2 hours and placed on a magnetic stirrer for 12 hours. ZrCl₄ (5% mol) is employed as a catalyst to increase the reaction rate (Allen et al., 2012). Finally, to remove unreacted aspartic acid and other impurities, the suspension is filtered using the PTFE membrane and rinsed with deionized water and Tetrahydrofuran (THF). The sample obtained is placed in the oven for 48h at 50 °C.

4.2.2 Characterization of Aluminum oxide and Silicon dioxide nanofluids

It is important to characterize the nanofluids for heat transfer enhancement. The first steps are to quantify the composition, size and loading of the nanoparticles and identify impurities in the nanofluids. Tools utilized to characterize nanofluids for this study include neutron transmission electron microscopy (TEM) imaging and zeta potential.

4.2.2.1 Alumina-water nanofluid

The agglomeration of nanoparticles results in not only settlement and clogging but also the decrement of thermal conductivity of nanofluids. So, stability analysis is importance in context to its application. Sedimentation, centrifugation, spectral analysis and zeta potential analysis are the four basic methods for evaluating stability of nanofluids. The stability of nanofluids can be also detected by the electron and optical

microscopes. Optical spectroscopy uses the interaction of light with matter as a function of wavelength or energy to obtain information about the material. Optical spectroscopy is attractive for materials characterization because it is fast, nondestructive and of high resolution. TEM is reckoned as the most important tool to determine the size distribution and the morphology of the synthesized nanoparticles. It uses electron beam to create the image of samples. **Figure 4. 42** illustrate, the TEM images of 0.1 wt.% of Al₂O₃-water nanofluid. As shown in the TEM images (**Figure 4. 42** a and b), the alumina nanoparticles are spherical in shape. However, the figures (**Figure 4. 42** c and d) depict that the sample with 0.1wt.% dispersant have the very minor agglomeration and they reached better suspension. **Figure 4. 42** presents TEM images after 1 hr sonication. The sample is generally a much better dispersion. It can be seen clearly that all particles are of same in size and their size is below 50nm. From **Figure 4. 42**,. it is also observed that the nanoparticles are spheres and have a broad size distribution. Another important aspect of the TEM is the ability to measure particle material content via the transmitted beam spectrum. This allows a distinction between large Al₂O₃ particles, debris or other impurities, and may show whether the Al₂O₃ particles are scouring and collecting surface material. **Figure 4. 42** shows that the majority is Al₂O₃, indicating good purity of the sample and giving confidence in the above method of synthesis. For this study to get higher thermal conductivity no any surfactant was used.

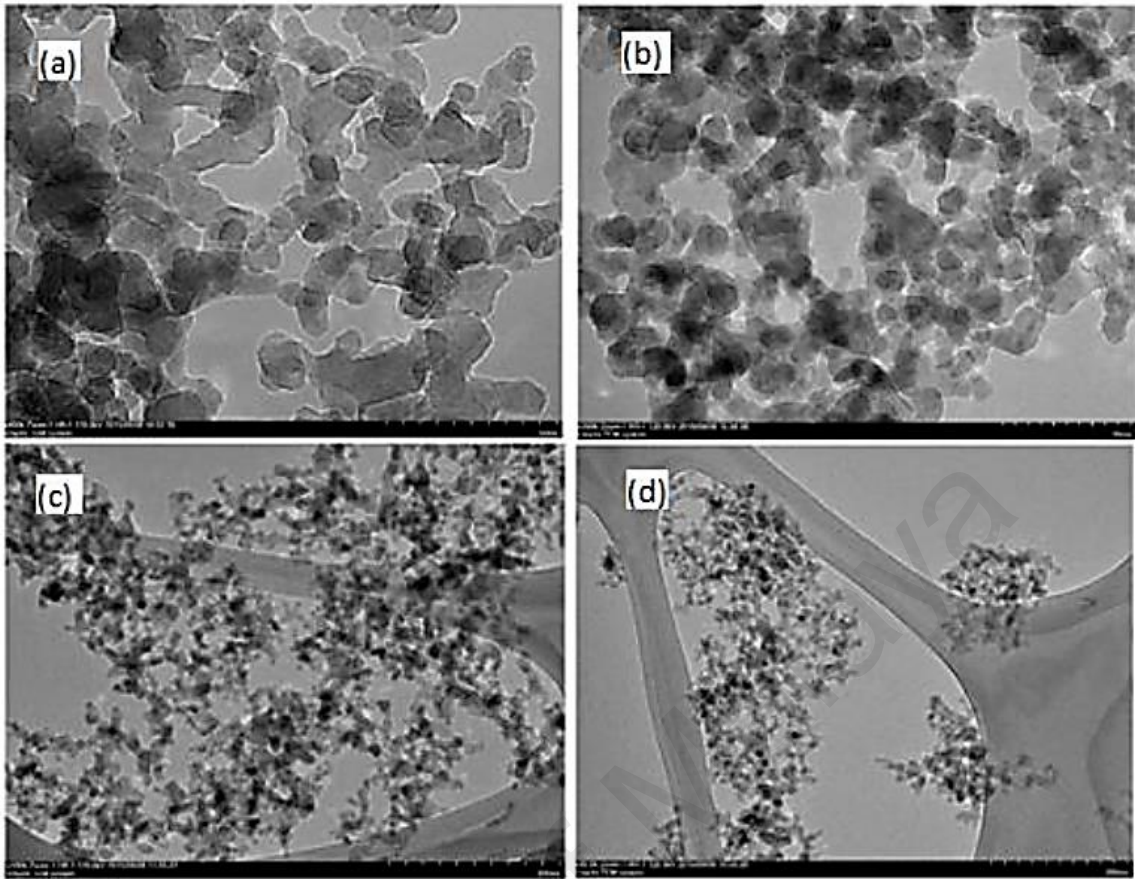


Figure 4. 42 TEM images of Al_2O_3 -water nanofluid at weight concentration of 0.1%.

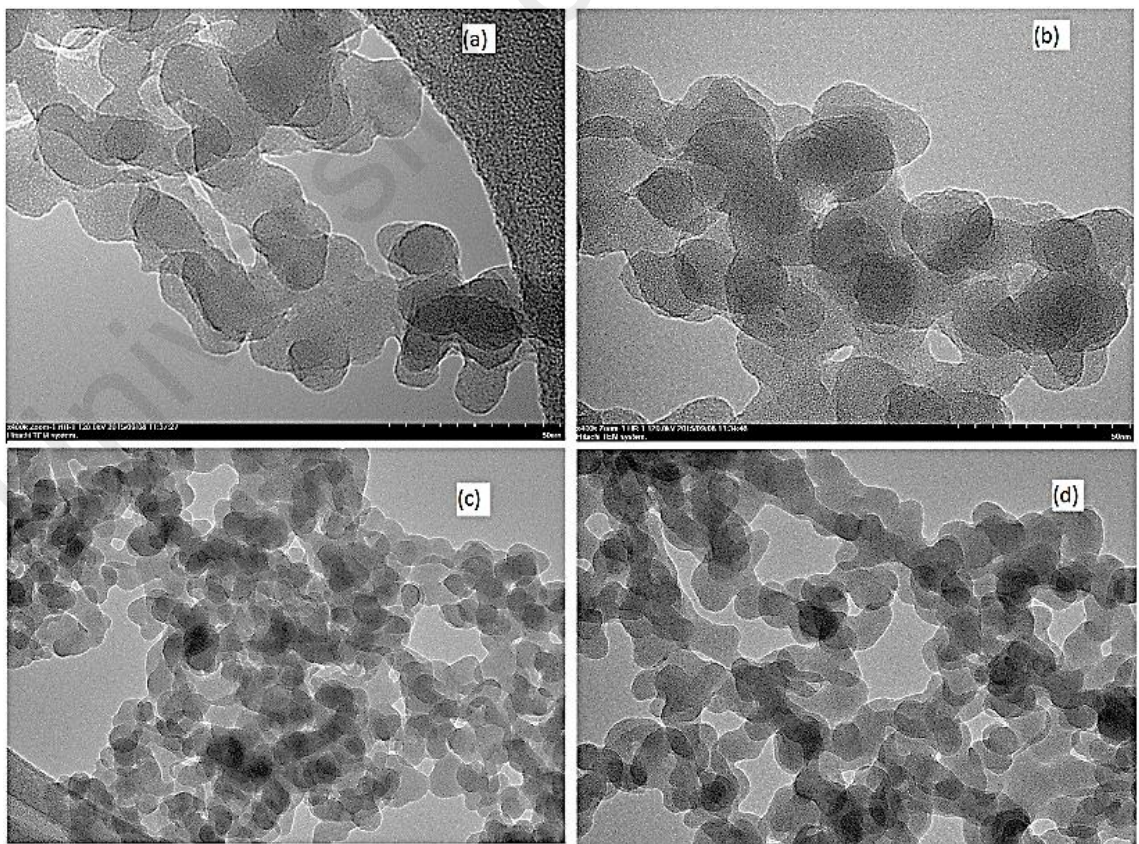


Figure 4. 43 TEM images of SiO_2 -water nanofluid at weight concentration of 0.1%.

4.2.2.2 Silicon dioxide-water nanofluid

Figure 4. 43 represent, the TEM images of 0.1 wt.% concentration of SiO₂-water nanofluid. As shown in the TEM images (**Figure 4. 43** a and b), the silica nanoparticles are circular in shape. However, the figures (**Figure 4. 43** c and d) portray that the sample with 0.1wt.% concentration have very minor agglomeration and they reached better suspension. It can be see clearly that all particles are of same in size and their size is below 50nm. **Figure 4. 43** presents TEM images after 1 hr sonication. The sample is generally a much better dispersion. In the TEM images, it is observed that the nanoparticles are spheres and have a broad size distribution. To achieve the higher thermal conductivity no any surfactant was used for this study. Another important aspect of the TEM is the ability to measure particle material content via the transmitted beam spectrum. This allows a distinction between large SiO₂ and Al₂O₃ particles, debris or other impurities, and may show whether the SiO₂ and Al₂O₃ particles are scouring and collecting surface material. **Figure 4. 42** and **Figure 4. 43** shows that most SiO₂ and Al₂O₃ indicating good purity of the sample and giving confidence in the present method of synthesis.

4.2.3 Functionalization Analysis

To study the functional groups, the characteristics of MWNT samples were determined by Fourier transform infrared spectroscopy (FTIR), thermogravimetric analysis (TGA) and Raman spectroscopy. **Figure 4. 44** shows the FTIR spectra of MWNT-COOH and MWNT-Asp. Contrary to the pristine MWNT, MWNT-Asp clearly indicated the cues of different functional groups. The extended list of peaks and their allocated groups are shown in **Table 4. 5**. It can be observed that the carboxyl groups on MWNT-COOH were of some peaks that were considerably sharper than the peaks of other groups. It is assumed that these sharp peaks were developed by the oxidation step by nitric acid or from the Asp groups that were loaded on the surfaces of the MWNT.

The N–H groups of the functionalized samples could demonstrate that amidation reactions happened between the amino groups of Asp and the carboxyl groups on the surfaces of the MWNT.

Table 4. 5 Fourier transform infrared interpretation of the pristine and functionalized MWNT

Type of functionalized MWNT	Peak(cm^{-1})	Assignments
MWNT-COOH	3400-3470	O–H stretch vibration
	1706	C=O stretching vibration of carboxylic group
	1534	C=C stretching vibration
	1052	C–O stretching vibration
MWNT-Asp	3000-3500	O–H & N–H stretching vibration of primary amine / Symmetrical –NH stretching vibration (Amide bond)
	2827 and 2712	C–H stretching vibration
	1728	–C=O stretching vibration (amide bond)
	1593	C=C stretching vibration
	1432	–NH bending vibration of primary amine
	1150	C–N stretching vibration
	1082	C–O stretching vibration

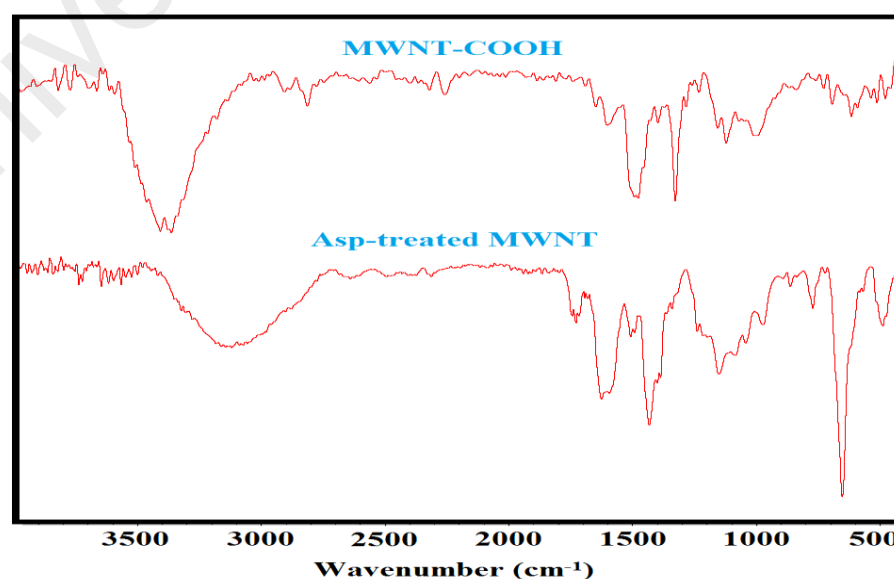


Figure 4. 44 FTIR Spectra of pristine MWNT and Asp-treated MWNT.

Raman spectroscopy indicates necessary information in order to estimate the covalent functionalization of the MWNT and has been regarded as the main characterization method for examining functionalization (A Amiri et al., 2011). This method can establish a great sensitivity to the disordered band on the structure depending on the optical skin depth (A Amiri et al., 2011; Sveningsson et al., 2001). The Raman spectra of the pristine MWNT and MWNT-Asp is presented in **Figure 4. 45** indicating the D and G bands at 1343 and 1576 cm^{-1} , respectively. The G band at 1576 cm^{-1} is related to the motion in opposite direction of two nigh carbon atoms of graphitic sheet. The respective pattern can denote the presence of the crystalline graphitic carbon in MWNT. On the other hand, the D band around 1343 cm^{-1} is associated to the amorphous carbon, Raman spectroscopy indicates necessary information in order to estimate the covalent functionalization of the MWNT and has been regarded as the main characterization method for examining functionalization (A Amiri et al., 2011). This method can establish a great sensitivity to the disordered band on the structure depending on the optical skin depth (A Amiri et al., 2011; Sveningsson et al., 2001). The Raman spectra of the pristine MWNT and MWNT-Asp is presented in **Figure 4. 45**

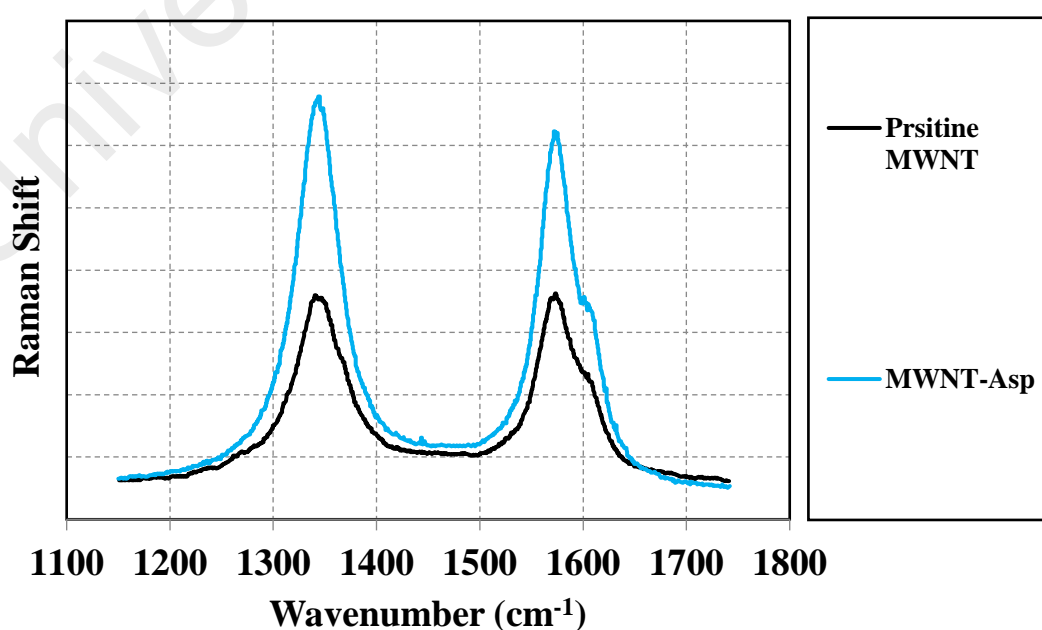


Figure 4. 45 Raman Spectra of pristine MWNT and Asp-treated MWNT.

indicating the D and G bands at 1343 and 1576 cm^{-1} , respectively. The G band at 1576 cm^{-1} is related to the motion in opposite direction of two nigh carbon atoms of graphitic sheet. The respective pattern can denote the presence of the

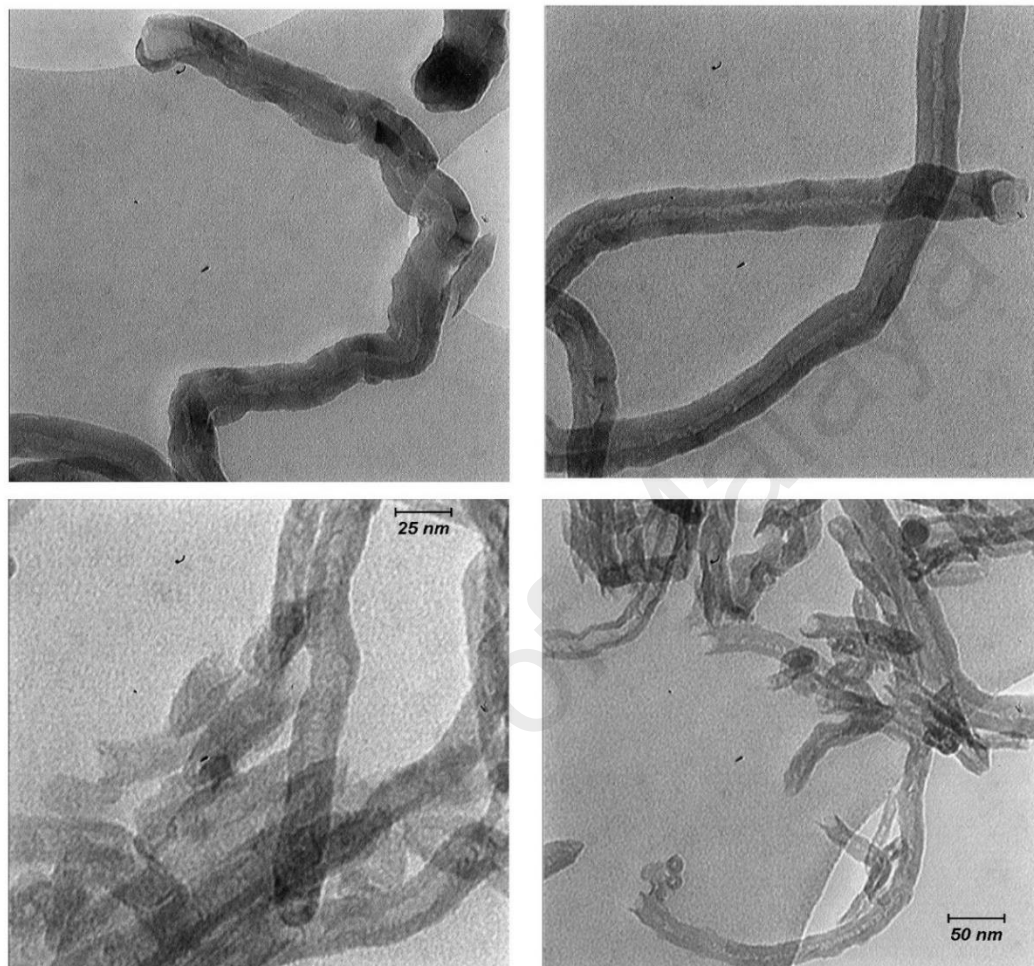


Figure 4. 47 TEM images of MWNT-Asp

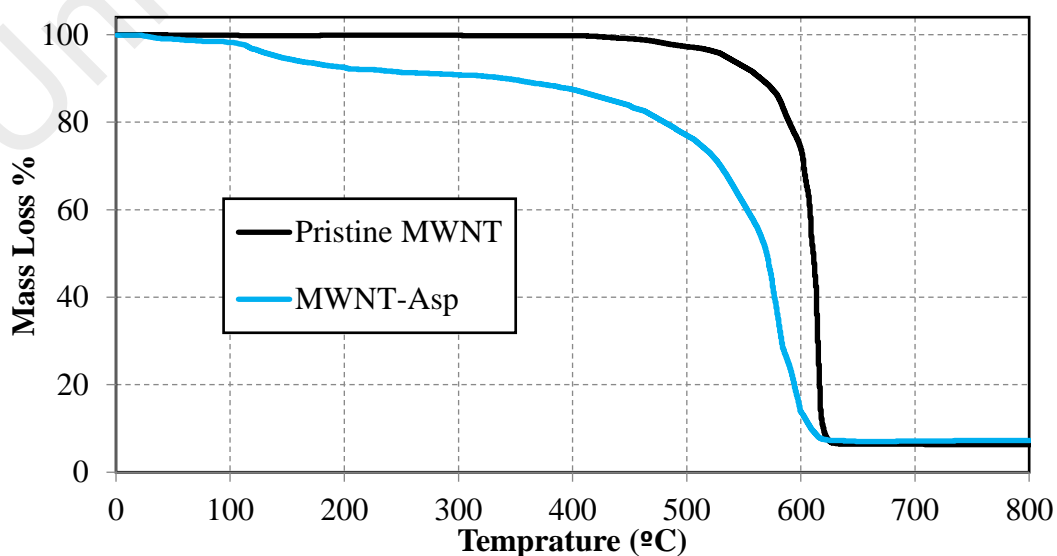


Figure 4. 46 TGA curves of pristine MWNT and Asp-treated MWNT

crystalline graphitic carbon in MWNT. On the other hand, the D band around 1343 cm^{-1} is associated to the amorphous carbon, which occurred by adding functional groups to the backbone. The intensity ratios of D and G bands (ID/G) can be employed for assessing the amount of amorphous carbon relative to graphitic carbon (A Amiri et al., 2011). It can be observed in **Figure 4. 45** that the ID/G ratio of MWNT-Asp are more than pristine MWNT, because of the increase in the structure defects, indicating effective functionalization of the MWNT with target groups. Here, the remarkable fact is that the higher the ID/G value, the higher extent of covalent amidation will be.

Figure 4. 47 indicates the TEM images of the MWNT-Asp. After functionalization, some of the nanotubes lost their caps. So, opening end of MWNT was ascribed to the acid treatment part, demonstrating that nitric acid may decrease the length and open end-caps of MWNT (Ahmad Amiri et al., 2012).

Also, TGA curve of the pristine MWNT and MWNT-Asp are indicated in **Figure 4. 46**. While no weight loss is observed in the curve of pristine MWNT, a sharp weight loss is obvious in the temperature range of 100-250 $^{\circ}\text{C}$ for the MWNT-Asp. The surface morphology of the MWNT-Asp was investigated by TEM for more evidence.

4.2.4 Stability

4.2.4.1 Alumina-water nanofluid

The stable homogeneous Al_2O_3 nanofluids were prepared for this study without using any surfactant. Absorbance as a function of wavelength plotted for Al_2O_3 -water nanofluid at weight concentration of 0.1% to measure the amount of the specific particle within the binary system, as illustrated **Figure 4. 48** (a). **Figure 4. 48** (b) illustrates the absorbance intensity as a function of wavelength for the Al_2O_3 -water measured at specific time for the duration of 31 days. It showed significant dispersibility of Al_2O_3 in aqueous media. The measurement was carried out at the range of wavelength for Al_2O_3 -water nanofluid to trace the deviation in the intensity which can be used to describe the

suspension stability at the constant weight concentration of Al₂O₃-water nanofluid.

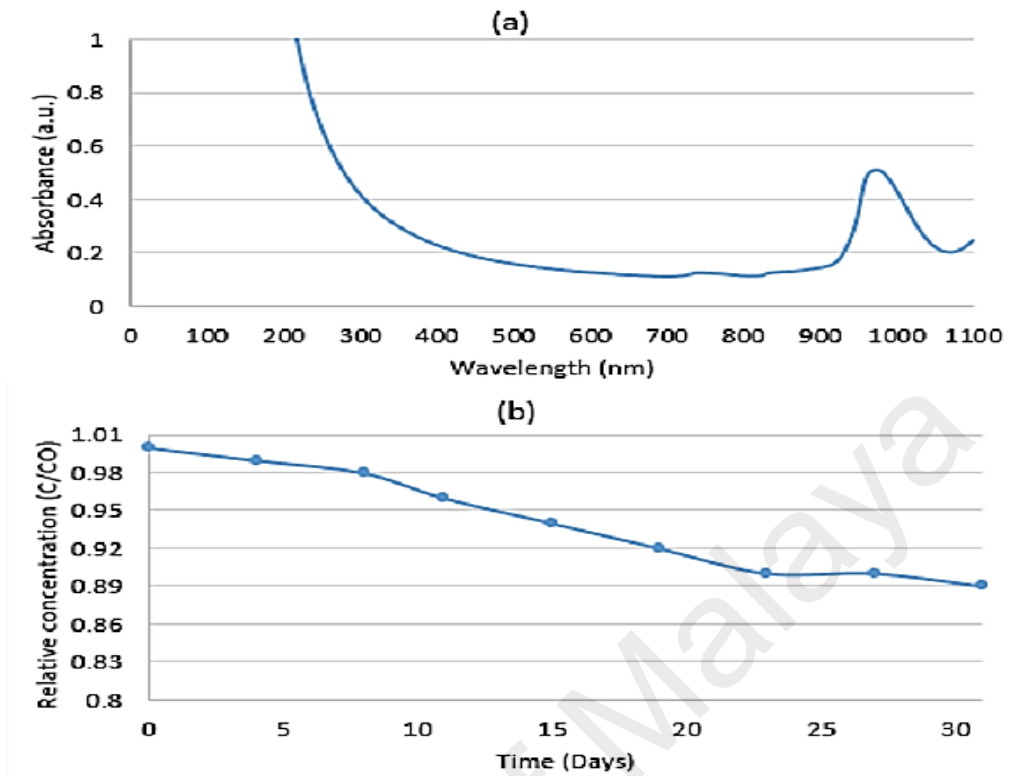


Figure 4.48 (a) Absorbance as a function of wavelength for Al₂O₃-water nanofluid at weight concentration of 0.1% and (b) Colloidal Stability of Al₂O₃-water nanofluid.

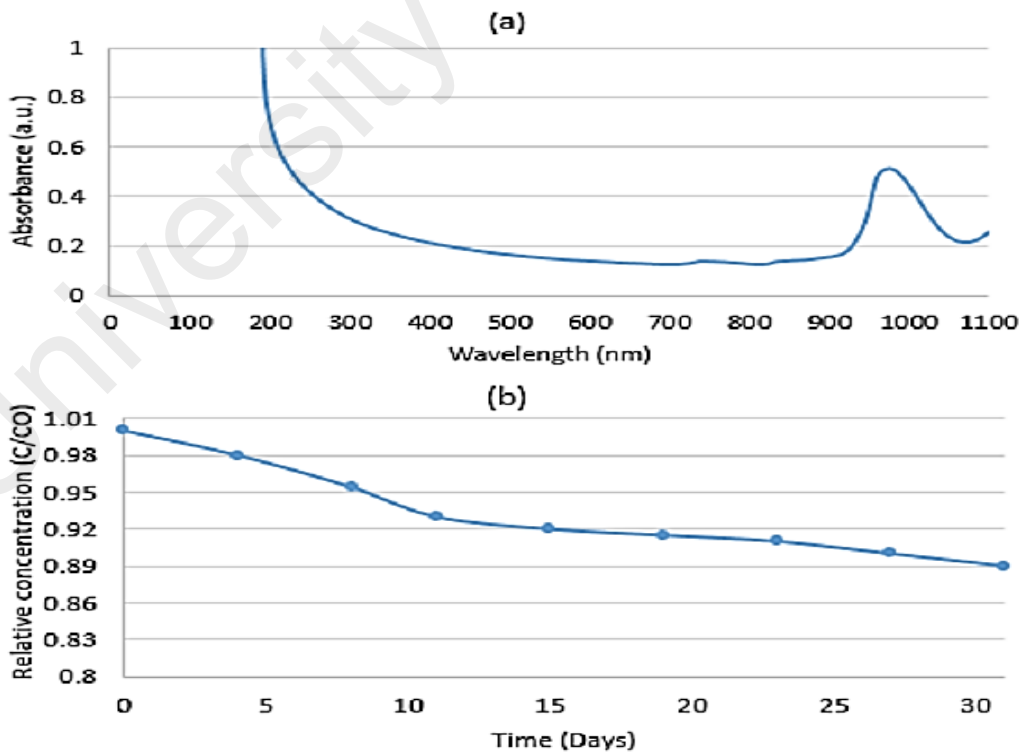


Figure 4.49 (a) Absorbance as a function of wavelength for SiO₂-water nanofluid at weight concentration of 0.1% and (b) Colloidal Stability of Silica-water nanofluid.

The colloidal mixture shows a downward trend of relative concentration as the time progresses, indicating that the level of particle concentration and thus the stability lessened. Also, the relative concentration (absorbance intensity) including Al_2O_3 -water shows the less sedimentation.

4.2.4.2 Silica-water nanofluid

Stable homogeneous SiO_2 -Water nanofluid were prepared for this study without addition of surfactant. Absorbance as a function of wavelength plotted for SiO_2 -water nanofluid at weight concentration of 0.1% to measure the amount of the specific particle within the binary system, as illustrated **Figure 4. 49** (a). **Figure 4. 49** (b) illustrates the absorbance intensity as a function of wavelength for the SiO_2 -Water measured at specific time for the duration of 31 days. It showed significant dispersibility of SiO_2 in aqueous media. The measurement was carried out at the range of wavelength for Silica-water nanofluid to trace the deviation in the intensity which can be used to describe the suspension stability at the constant weight concentration of SiO_2 -Water nanofluid. The colloidal mixture show a downward trend of relative concentration as the time progresses, indicating that the level of particle concentration and thus the stability lessened. Also, the relative concentration (absorbance intensity) including SiO_2 -Water shows the less sedimentation.

Table 4. 6 demonstrates the particle size distributions and zeta potential for Al_2O_3 -water and SiO_2 -water nanofluids. Al_2O_3 -water measurements showed less aggregation and coagulation at highest weight concentration of 0.1 wt.%. The particle size distribution for Al_2O_3 nanofluids show a gradual increase in the overall hydrodynamic size, which causes the formation of small aggregation that authenticates the UV-vis results. Besides, SiO_2 -water nanofluid showing good dispersibility and coagulation at weight concentration of 0.1 wt.%. Per the stabilization theory, the electrostatic repulsions between the particles increase if zeta potential has a high

absolute value which then leads to a good stability of the suspensions. Particles with a high surface charges lead less agglomeration, since contact is opposed. Zeta potential is one of the common procedures for characterization of dispersion stability of the colloids and provides a measure of the magnitude and sign of the effective surface charge associated with the double layer around the colloid particle. The measurement of the zeta potential has carried out the electrophoretic behavior and additional details to understand the dispersion behavior of metal oxides in water. **Table 4. 6** also shows the zeta-potential and the polydispersity index (PDI) for Al₂O₃ and SiO₂. The zeta-potential and polydispersity index (PDI) are commonly utilized as an index of the magnitude of electrostatic interaction between colloidal particles and thus can be considered as a measure of the colloidal stability of the solution. As per **Table 4. 6**, zeta potential must be as large as possible (positively or negatively) to make a common repulsive force between the particles. It is noted that after one hour sonication of Al₂O₃-water nanofluid showing high amount of positive charges and is around +50 mV over a period of 7 days. The zeta potential measurements of SiO₂-water nanofluid indicating sufficient stability over a period of 7 days at 25°C. The zeta-potential gradually showing some fluctuations over a period of 7 days, despite remaining mostly stable with time. The nanofluids which has a measured zeta-potential above +30 mV or below -30 mV are having good stability (Vandsburger, 2009). It implies that the force of electrostatic repulsion between metal oxides is sufficient to get over the attraction force between particles.

Table 4. 6 Zeta potential, particle size distribution, polydispersity Index (PDI and mobility of oxides nanofluids.

Sample	Duration (day)	Particle size distribution (nm) _{avg}	Polydispersity index (PDI)	Zeta Potential (mV)	Mobility (μmcm/Vs)
Al ₂ O ₃	7	138.9	0.196	50.4	3.94
SiO ₂	7	208.3	0.280	-35.6	-2.781

4.2.5 Thermo-physical properties

4.2.5.1 Viscosity

Viscosity of nanofluids is one of the most important parameter, which determines the quality of the heat transfer fluid. Like simple fluids, temperature is the most important parameter on viscosity of nanofluids. A good understanding of the rheological properties and flow behavior of nanofluids is necessary before nanofluids can be commercialized for the heat transfer applications. The factors influencing the viscosity include, concentration, size of nanoparticles, temperature, and shear rate, etc. Thus, more investigations should be carried out on the viscosity of nanofluids. As expected, distilled water exhibits a Newtonian behavior within the range of shear rate. The viscosity value of distilled water was 1.034, which close to theoretical values at 20°C. The relative deviation is less than 2.5%. This is of the same order of magnitude as the experimental uncertainty. In general, the viscosity plots show close resemblance to the DW water measurement with negligibly small increase in magnitude at increasing nanoparticle concentration. To determine the rheological behaviors of MWNT-Asp-water nanofluid, the viscosity of the aqueous MWNT-Asp was measured at the temperature range of 20 to 50°C and the results are presented in **Table 4. 7**. It is noted that water based MWNT-asp nanofluids at low concentrations showing slightly lower viscosity values than that of the higher concentration. It shows that loading of the MWNT-asp nanoparticles increase the friction and flowing resistance of fluids which ultimately causes increase of viscosity. While by rising the temperature, the nanoparticles are motivated more and create a higher space for them. This is expected due to the weakening of the inter-particle and inter-molecular adhesion forces. Following the trend of water, the samples of MWNT-Asp nanofluid also exhibit the shear thinning property. The cause of this non-Newtonian shear thinning can be explained generally as follows.

At low shear rates, as the spindle rotates in the fluid, the structure of the fluid molecule changes temporarily and gradually aligns themselves in the direction of increasing shear and produce less resistance and hence a reduction in viscosity. When the shear rate is high enough the maximum amount of shear ordering possible is attained, the aggregates are broken down to smaller size decreasing the friction and hence the viscosity (Rashin & Hemalatha, 2013). If the shear rate is further increased it will not make any alteration to the viscosity. Due to small size and large surface area of nanoparticle there is possibility for structuring at low shear rates and a deformation and restructuring at high shear rates. Hence, nanofluid also follows the same trend. It is observed that at all the temperatures the shear thinning property is more pronounced at higher concentrations. This points out that at low concentrations the nature of base fluid plays a major role in shear thinning, but at higher concentrations there is significant contribution from the interaction between nanoparticle and fluid.

Table 4. 7 Viscosity of different nanofluids in the various temperatures (mPa.s)

	20°C	40°C	60°C	80°C
Water	1.002	0.699	0.483	0.354
MWNT-Asp 0.05 wt.%	1.190	0.815	0.565	0.440
MWNT-Asp 0.1 wt.%	1.258	0.870	0.605	0.464

To determine the rheological behaviors of Al₂O₃-water and SiO₂-water nanofluids, the viscosity of the Al₂O₃-water and SiO₂-water nanofluid versus shear rate was measured at the temperature range of 20 to 50°C and the results are presented in **Figure 4. 51** and **Figure 4. 50**. In **Figure 4. 51** and **Figure 4. 50**, viscosities of Al₂O₃-water and SiO₂-water nanofluids without any surfactants are plotted as a function of

concentrations and temperature. The results showed that shear thinning occurred at the 0.025wt% to 0.1wt%. The degree of shear thinning increases as the solid

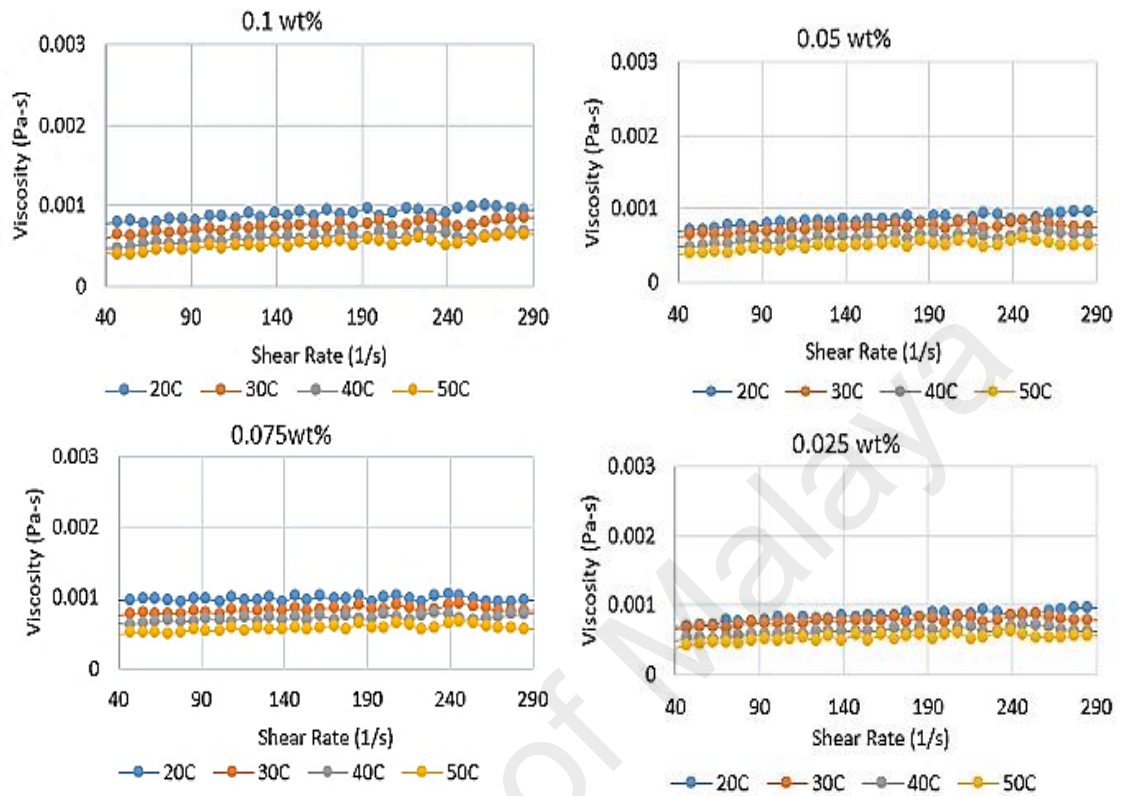


Figure 4. 51 Viscosity as a function of shear rate for Alumina-water nanofluid at different concentration and temperature.

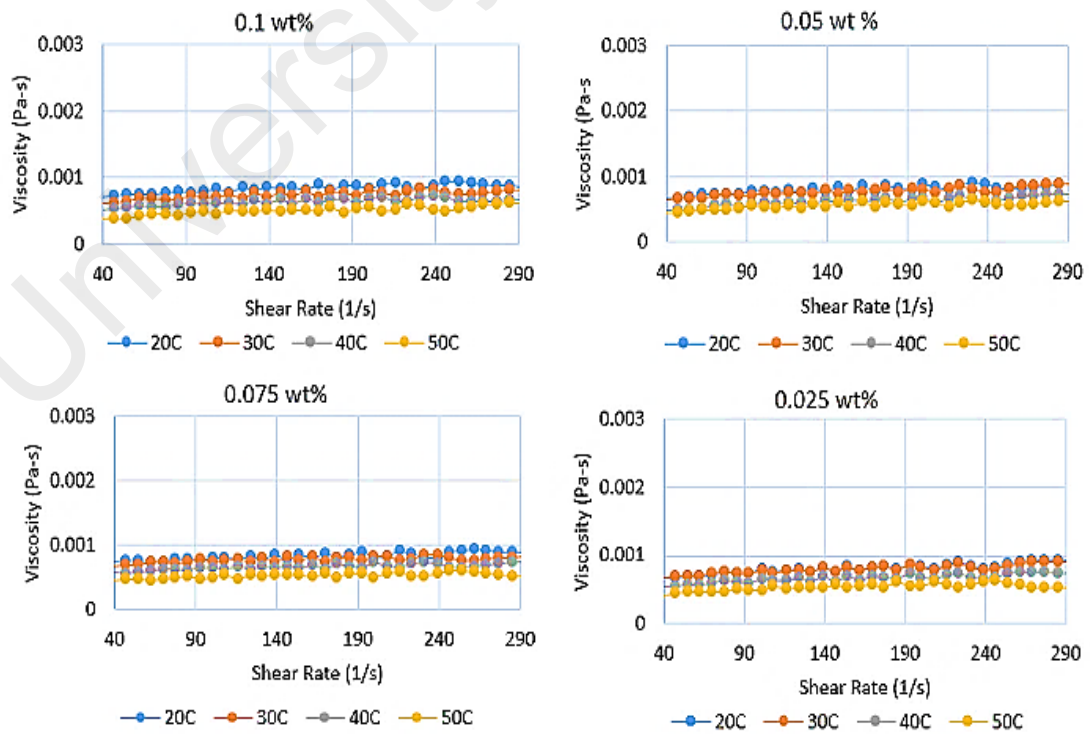


Figure 4. 50 Viscosity as a function of shear rate for Silica-water nanofluid at different concentration and temperature.

content in colloid increases. It was also noticed that the viscosities of nanofluids were getting close to the solvent viscosity at high shear rates. The results indicate that the prepared nanofluids are suitable to use at elevated temperatures. Since, by increasing the temperature, thermal movement of molecules and Brownian motion intensifies, and intra-molecular interactions become weakened. In addition, rheological test on nanofluids revealed that the higher concentration will increase the viscosity; however, other investigated parameters such as temperature and size have a significant influence on the viscosity of nanofluids. In addition, a rheometer consists of outer (chamber) cylinder, and inner (spindle) cylinder and the nanofluid is located between them. As the spindle rotates in the nanofluid, the molecular structure of the Nano-particles changes temporarily and slowly aligns themselves in the direction of increasing shear. A Newtonian fluid has the same viscosity when stronger or weaker forces (shear rate) are applied.

The measured experimental viscosity results revealed that the prepared nanofluids are suitable to use at elevated temperatures; however, other investigated parameters such as temperature and concentration have important influence on viscosity behavior.

4.2.5.2 Thermal conductivity

Thermal conductivity of all the nanofluids at all concentrations were measured over the range of temperature using KD2 pro thermal conductivity meter (Decagon Devices, Inc., Pullman, WA, USA) which is based on transient hot wire method. Different weight concentrations were considered and the variation of thermal conductivity with concentration and temperature were studied.

Thermal conductivity of Al₂O₃-Water and SiO₂-Water nanofluids at all concentrations were measured at the temperature range from 25°C to 50°C by using KD2 pro thermal conductivity meter. Four different weight concentrations (0.025%,

0.05%, 0.075% and 0.1%) were considered and the variation of thermal conductivity with concentration and temperature has been studied. To avoid sharp increase of effective viscosity, both nanofluids were considered at low concentrations. **Figure 4. 52** (a and b) shows the thermal conductivity plot of Al₂O₃-water and SiO₂-water nanofluids

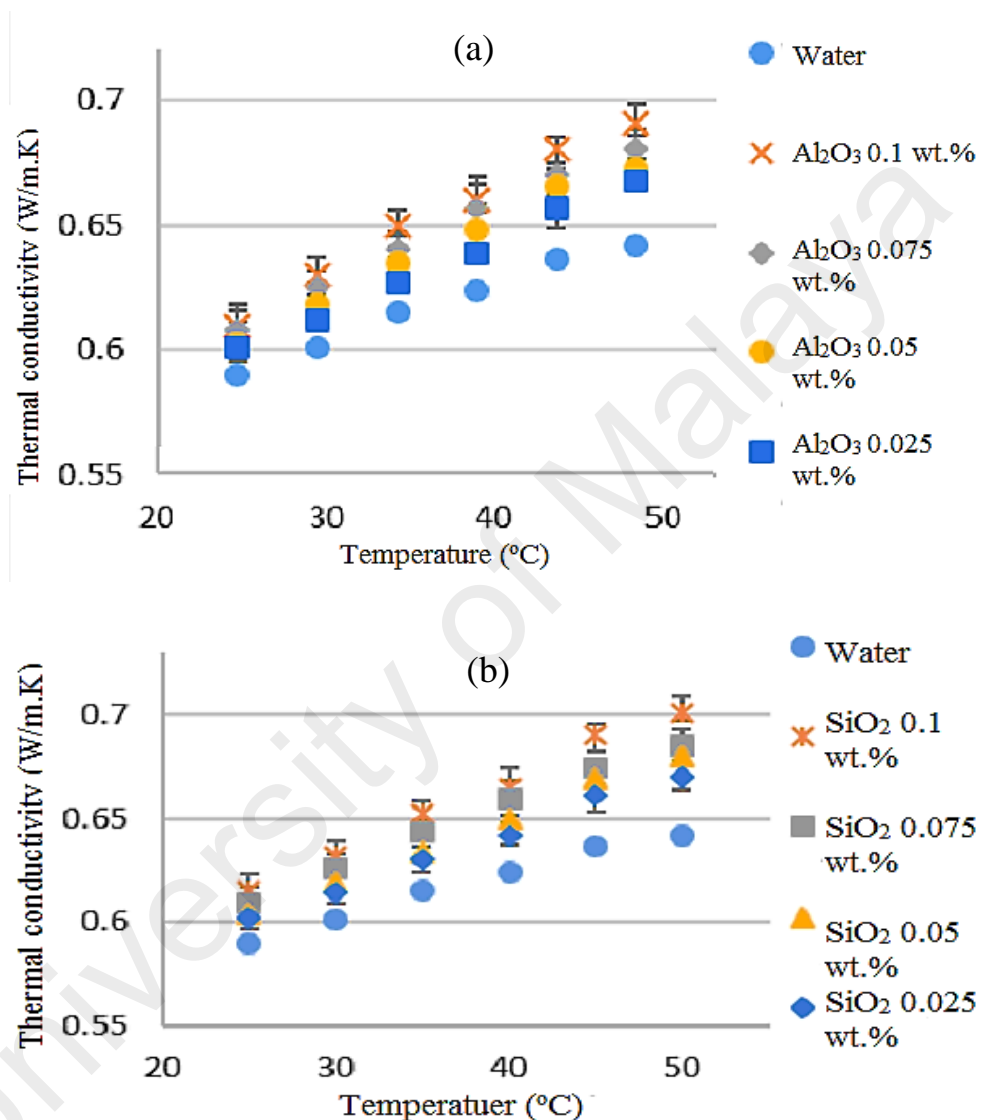


Figure 4. 52 Thermal conductivity as a function of concentration and temperature (a) Al₂O₃-water nanofluid, and (b) SiO₂-water nanofluid

as a function of temperature and concentration. It is noted from **Figure 4. 52** (a and b), the thermal conductivity enhancement increases non-linearly with nanoparticles concentration for both types of nanofluids. The maximum enhancement for Al₂O₃-water and SiO₂-water were found up to 7.4% and 9%, respectively compared to the base fluids. Upon comparison between alumina Al₂O₃-water and SiO₂-water nanofluids, the

SiO₂-water nanofluid showed superiority in performance. The increase in thermal conductivity with temperature is more sensible in SiO₂. Thermal conductivity trend of both nanofluids showing increase of the thermal conductivity with the increase of concentration. Thus, it confirms that the temperature plays a key role in increasing the thermal conductivity of nanofluids.

Thermal conductivity of MWNT-Asp-water nanofluid is presented in **Table 4. 8** for different weight concentration over the range of temperature 20°C to 50°C. Results shows the behavior of thermal conductivity of MWNT-Asp-water nanofluid. The data showing that the temperature and concentration play a key role in enhancement of thermal conductivity. The main mechanism for thermal conductivity enhancement with increase of temperature is attributed to the Brownian motion of the nanoparticles suspended in the water (base-fluid) (Aravind et al., 2011)

Table 4. 8 Thermal conductivity (W/m.K) of MWNT-Asp-water nanofluid at different concentrations and temperatures.

	20°C	30°C	40°C	50°C
Water	0.595	0.616	0.629	0.639
MWNT-Asp 0.025 wt. %	0.598	0.625	0.642	0.658
MWNT-Asp 0.05 wt. %	0.609	0.636	0.660	0.688
MWNT-Asp 0.075 wt. %	0.625	0.662	0.695	0.729
MWNT-Asp 0.1 wt. %	0.658	0.695	0.730	0.770

Table 4. 9 to

Table 4. 11 the results of Specific heat and Density of MWNT-Asp-water, Al₂O₃-water and SiO₂-water nanofluids with different concentrations. All the data were measured at constant bulk temperature of 30°C. Results shows the behavior of density of nanofluids. The data show that the temperature has also influence on density of nanofluids. Density of all nanofluids is higher than the base fluid (water) and with

increase of temperature, density of nanofluid is decreasing. Further if nanoparticle weight concentration increases from 0.025 wt.% to 0.1wt.%, the density increases. A heat flux type differential calorimeter was (TA DSC Q20) used to measure the specific heat capacity of nanofluids. DSC, is a thermal analysis technique that measure material's heat capacity (C_p) changing with temperature. A sample of known mass is heated or cooled and the changes in its heat capacity are tracked as changes in the heat flow. The term differential scanning calorimeter refers to both the techniques of measuring calorimetric data while scanning as well, which is a specific instrument design. The technique can be carried out with other types of instruments. Range of DSC is (-50 to 350°C).

Table 4. 9 Density and Specific heat capacity of the MWNT-Asp-water at the bulk temperature of 30°C.

MWNT-Asp Concentrations (Wt.%)	Density (kg/m ³)	Specific heat (J/kg.K)
0.1	1003.517	
0.075	1002.884	
0.05	1002.251	
0.025	1001.616	

Table 4. 10 Density and Specific heat capacity of the Al₂O₃-water at the bulk temperature of 30°C.

Al ₂ O ₃ Concentrations (Wt.%)	Density (kg/m ³)	Specific heat (J/kg.K)
0.1	1072.747	3039.524
0.075	1052.473	3261.876
0.05	1032.95	3519.326
0.025	1014.139	3820.899

Table 4. 11 Density and Specific heat capacity of the SiO₂-water at the bulk temperature of 30°C.

SiO ₂ Concentrations (Wt.%)	Density (kg/m ³)	Specific heat (J/kg.K)
0.1	1057.886	2796.342
0.075	1041.705	3048.497
0.05	1026.011	3350.635
0.025	1010.783	3719.252

4.2.6 Heat transfer to nanofluid flow in a Backward-facing step

For the first time, experimental investigation of heat transfer over a backward facing step using Al₂O₃-water, SiO₂-water and MWNT-Asp-water nanofluids is presented for the turbulent flow regime. Heat transfer over a backward-facing step is investigated experimentally in the present study for different Reynolds numbers and weight concentrations of nanofluids.

4.2.6.1 Alumina-water nanofluid

The effect of concentration of Al₂O₃-water nanofluids on the Nusselt number at a range of Reynolds number 4000 - 16000 has been studied and the results are presented in **Figure 4. 53**.

Distribution of the measured local Nusselt number (Nu_x) in the range of Reynolds number 4000—16000 for different weight concentrations (0.025, 0.05, 0.075 and 0.1 wt.%) of nanoparticles have compared with the distilled water data in **Figure 4. 53**. The local Nusselt number (Nu_x) peaked at the X/D range of 4 to 6 before starting to decrease gradually. The results in **Figure 4. 53** revealed that the prepared water-based Al₂O₃-water nanofluids have higher Nu_x than that of pure water. Furthermore, an increase in the concentration of Al₂O₃ nanoparticles led to an enhancement in Nu_x . The

region where the Nu_x values are increasing up to the maximum peak is the recirculation zone and the zone where the Nu_x have peaked is the reattachment zone and consequently, the decrease of Nu_x after the maximum peak up to almost straight line is the zone where fluids become fully-developed.

For an appropriate evaluation of heat transfer, the average heat transfer coefficient of Al_2O_3 -water nanofluid was compared with water (h_c) data at different weight concentrations (0.025, 0.05, 0.075 and 0.1 wt.%) over a range of Reynolds number, as shown in **Figure 4. 54** (a). The average heat transfer coefficient increases with the increase of weight concentrations and Reynolds number. At the weight

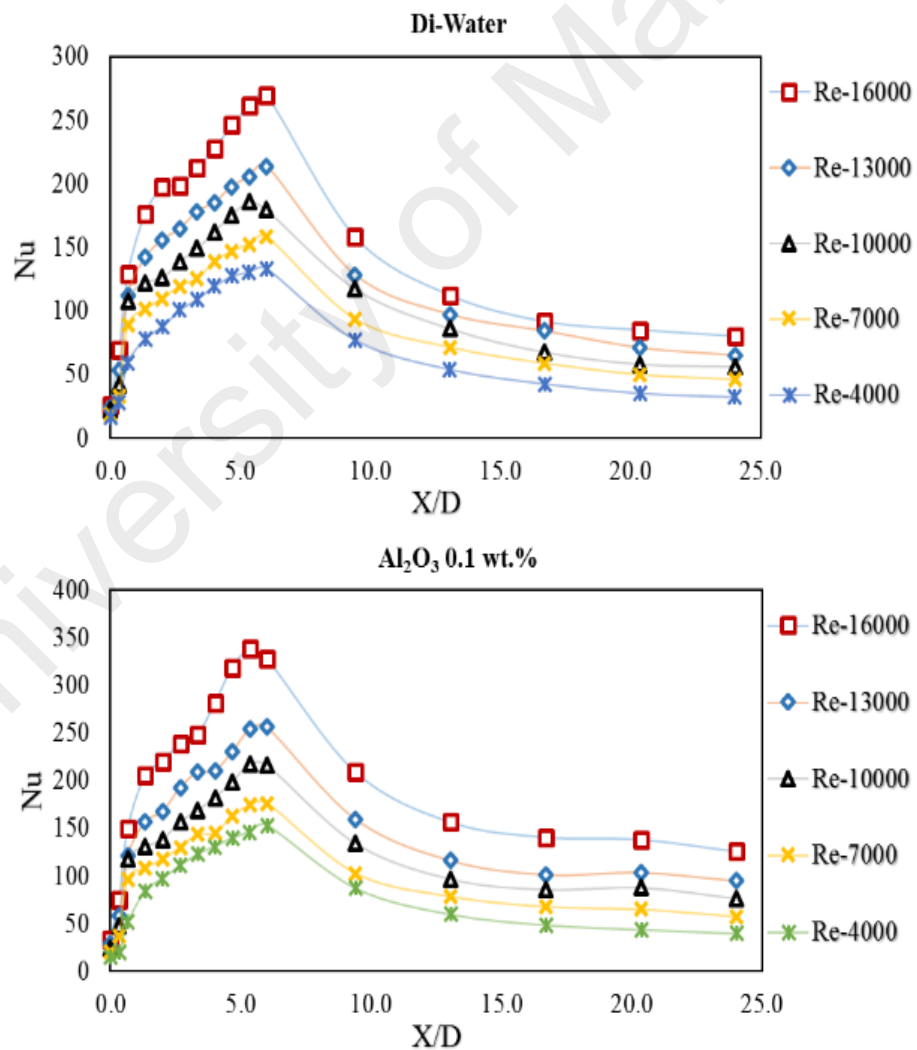
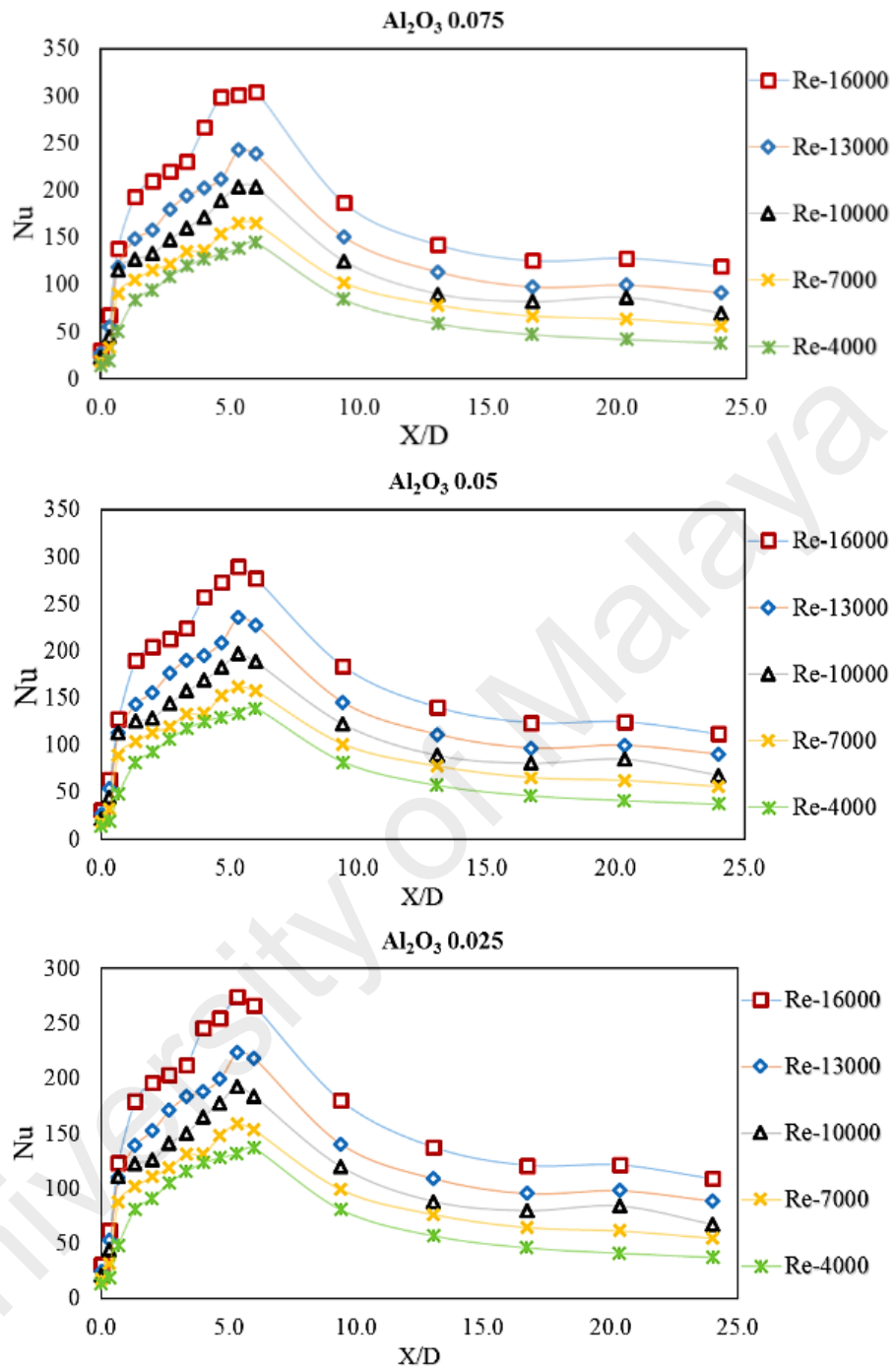


Figure 4. 53 Experimental Nusselt number of distilled water and Al_2O_3 -water nanofluids at different weight concentrations of 0.025%, 0.05%, 0.075% and 0.1% for different Reynolds numbers

Figure 4. 53 Continued.



concentration of 0.1 wt.% and Reynolds number 16,000, the highest average heat transfer coefficient $4855 \text{ W/m}^2\cdot\text{K}$ was achieved.

Figure 4. 54 (b) presents heat transfer enhancement percentage of four different weight concentrations (0.025, 0.05, 0.075, and 0.1%) and five Reynolds numbers (4000, 7000, 10000, 13000, 16000) at a constant DC power supply of 600 W. The average heat transfer coefficient increases with the increase of concentrations and Reynolds number.

Results revealed that with the increase of Reynolds number from 4000 to 16,000, the average (percent) heat transfer coefficient enhancement (η) increased from 9.6 to 26.3 % at weight concentration of 0.1%; from 5.9 to 16.7% at weight concentration of 0.075%; from 3.3 to 11.5% at weight concentration of 0.05% and from 2.1 to 7% at weight concentration of 0.025%. Heat transfer enhancement in the presence of nanoparticles increases linearly with the increase of concentration and Reynolds number.

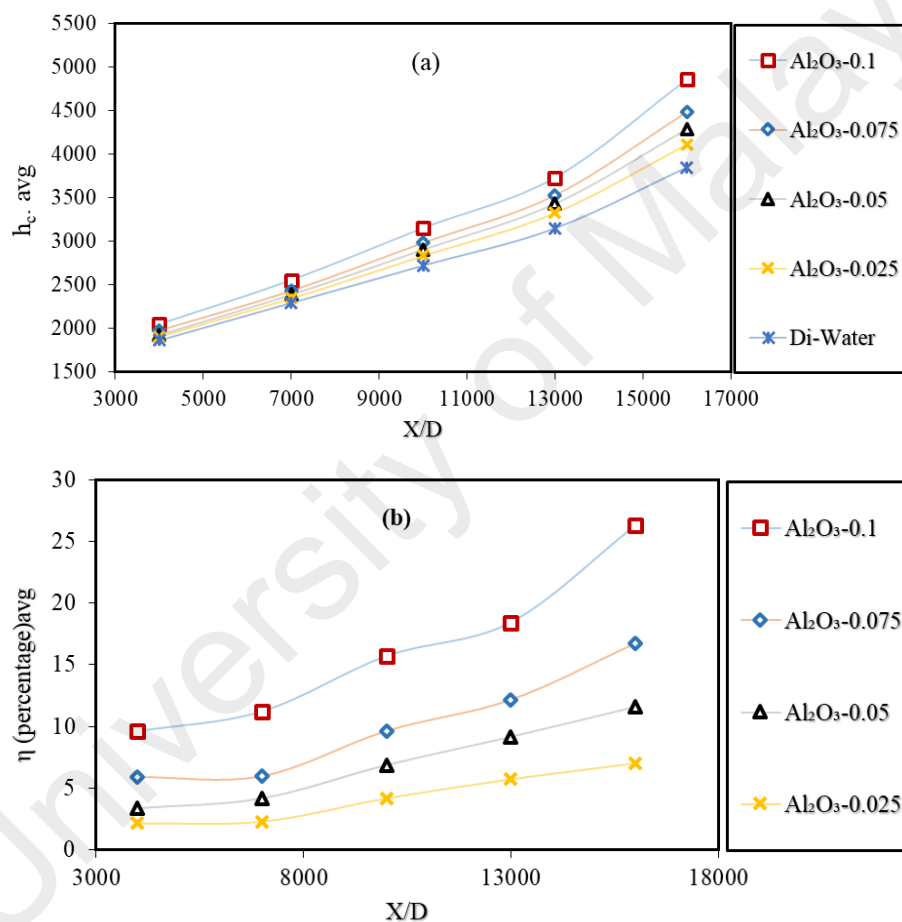


Figure 4.54 (a) Average heat transfer coefficient of distilled water and Alumina-water nanofluids over a backward-facing step and (b) Average (percent) heat transfer coefficient enhancement versus Reynolds number at different weight concentrations.

Heat transfer enhancement with the increase of nanoparticles concentration in nanofluid has occurred due to the enhancement of the rate of energy exchange at laminar sub-layer as eddies formation increases with the increase of nanoparticles concentration. A Sh Kherbeet et al. (2012) has reported that the enhancement of heat

transfer is due to increase in energy exchange rates by random and irregular movements of particles as concentration increases. While, many researchers have reported that the heat transfer enhancement is due to the increase of thermal conductivity of fluid from the addition of nanoparticles to the fluid (Ahmad Amiri et al., 2017; S. Choi et al., 2001; Hosseini et al., 2017; S. Lee et al., 1999; Masuda et al., 1993; Sadri, Hosseini, et al., 2017; Sadri, Zangeneh Kamali, et al., 2017). In contrast A. Sh Kherbeet et al. (2012) reported that the heat transfer enhancement is due to increase in viscosity with an increase of nanoparticles concentration. Viscosity gradient and a non-uniform shear rate source the particle migration which leads to higher heat transfer coefficient as numerically showed by some researchers (Wen & Ding, 2005). On the other hand, Aravind et al. (2011) qualitatively studied and explained the cause of heat transfer enhancement which could be achieved by either decreasing thermal boundary layer thickness or increasing thermal conductivity.

Previously researchers have reported enhancement of heat transfer due to the increase of nanofluid concentration but still, the mechanism of heat transfer enhancement with the nanofluid concentration has not been clearly understood.

Figure 4. 55 presents heat transfer coefficient (h_c) versus x/d over a range of Reynolds number (Re) for water and Al_2O_3 -water nanofluid at different weight concentration for the Re number of 16000, 10000, and 4000. The results reveal that the maximum h_c increase with the increase of Re number and concentration of nanoparticles in the fluid, which satisfies the findings of other researchers (A Sh Kherbeet et al., 2012). The highest h_c were obtained at the higher Re of 16000 and weight concentration of 0.1%, similar results were obtained by the previous researcher for a study of heat transfer in backward-facing step (Ahmad Amiri et al., 2016)

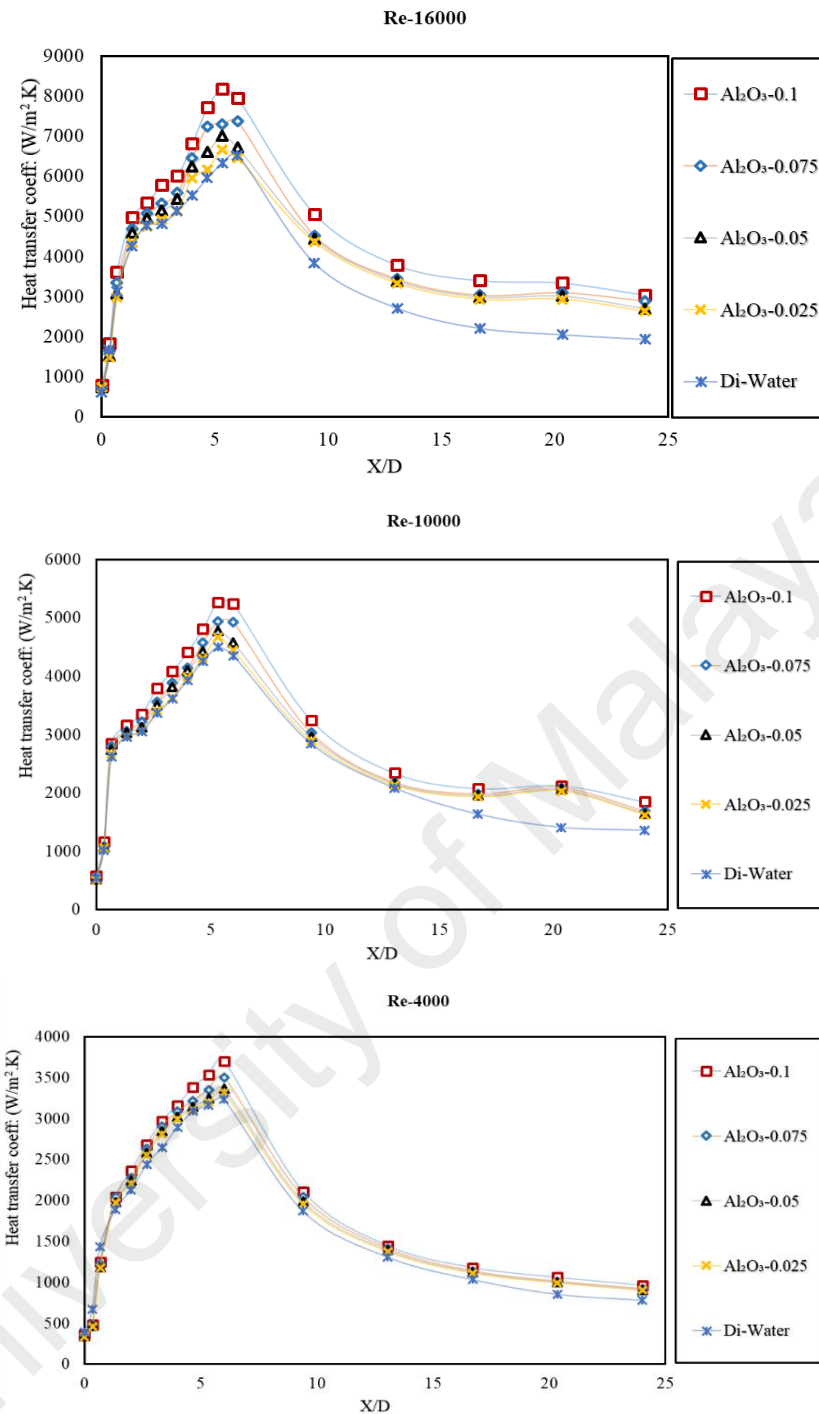


Figure 4. 55 The effect of Reynolds numbers and weight concentrations of Al_2O_3 -water nanofluids on the local heat transfer coefficient at different axial ratios.

Performance index (ϵ) that is the ratio of the heat transfer rate to the pressure drop, has been measured for the evaluation of the economic performance of the working fluids. Recently many researchers reported that the heat transfer performance improves with the addition of solid nanoparticles but along with heat transfer improvement it also sources additional undesirable pressure drop. Consequently, the performance index is

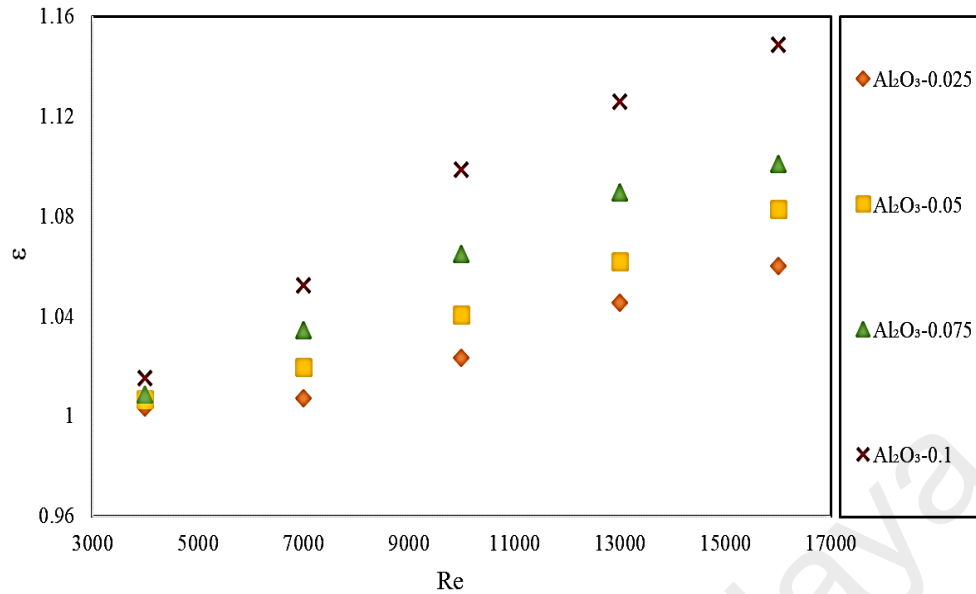


Figure 4. 56 Performance index (ϵ) for the backward-facing step in the presence of distilled water and Al_2O_3 -water nanofluids with different weight concentration

reported to assay both heat transfer and pressure drop. The deviations of the average performance index for Al_2O_3 -water nanofluids are presented at different weight concentrations and Reynolds numbers in **Figure 4. 56**. It is observed that the performance index of alumina-water nanofluid at all weight concentrations are higher than unity, that showing the effectiveness of the Al_2O_3 -water nanofluids for being used over the backward-facing step. Furthermore, it is observed that with the increase of weight concentration of solid alumina nanoparticles in nanofluids, the performance index also increases as per expectation. The figure also shows that the good performance index curve is achieved at a weight concentration of 0.1% at different Re numbers, followed by a gradual decrease of the performance index with a decrease of Re and weight concentration.

Friction loss data in these experimental investigations are presented in the form of pressure drop as a function of Reynolds number. The data are presented in **Figure 4. 57** for water and Al_2O_3 -water nanofluids at four different concentrations (0.025, 0.05, 0.075 and 0.1 wt.%) at the Reynolds number range from 4000 to 16000.

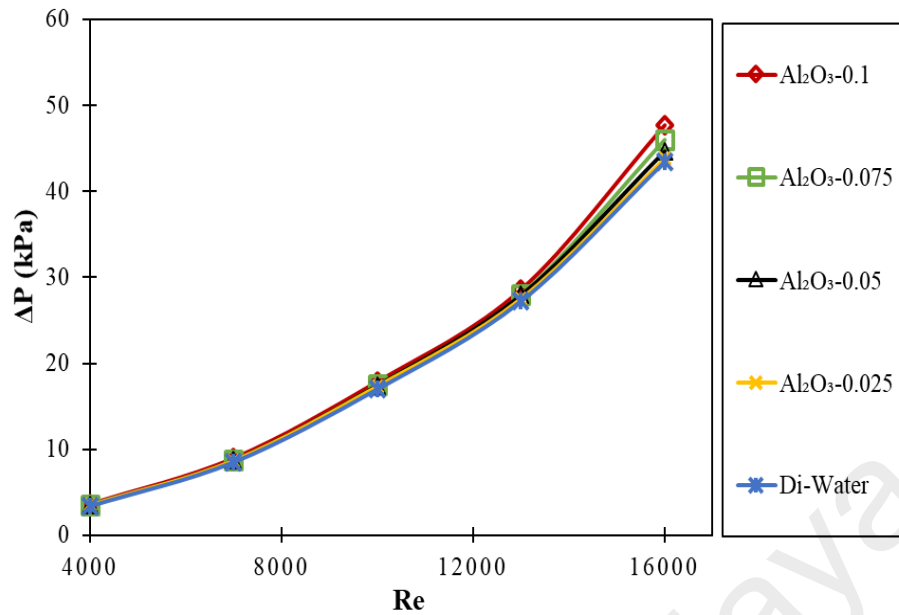


Figure 4. 57 Experimental Pressure drop of distilled water and Al₂O₃-water nanofluids at weight concentrations of 0.025%, 0.05%, 0.075% and 0.1% for different Re number.

Figure 4. 57 shows the pressure drop enhances with the increase of Reynolds number and the highest pressure drop data point is observed at a higher weight concentration (0.1 wt.%) of Al₂O₃-water nanofluid and at the higher Reynolds number of 16000. Similarly, the lowest pressure peak is observed at the lower concentration (0.025 wt.%) of Al₂O₃-water nanofluid and at the lower Reynolds number of 4000. Although the difference in pressure drops are not significant in peaks of different concentrations of Al₂O₃-water nanofluids. The increase of pressure drop is due to increase of friction owing to increase of turbulence with the enhanced Reynolds number. Further, in **Figure 4. 57** the addition of nanoparticles increases the viscosity of base fluid slightly due to which a little difference between the different curves at varying concentrations are observed.

4.2.6.2 Silica-water nanofluid

The effect of concentration of SiO₂-water nanofluids on the Nusselt number at a range of Reynolds number 4000 - 16000 had studied and the results are presented in **Figure 4. 58**.

Distribution of the measured local Nusselt number (Nu_x) in the range of Reynolds number 4000—16000 for different weight concentrations (0.05 and 0.1 wt.%) of nanoparticles have compared with the distilled water data in **Figure 4. 58**. The local Nusselt number (Nu_x) peaked at the X/D range of 4 to 6 before starting to decrease gradually.

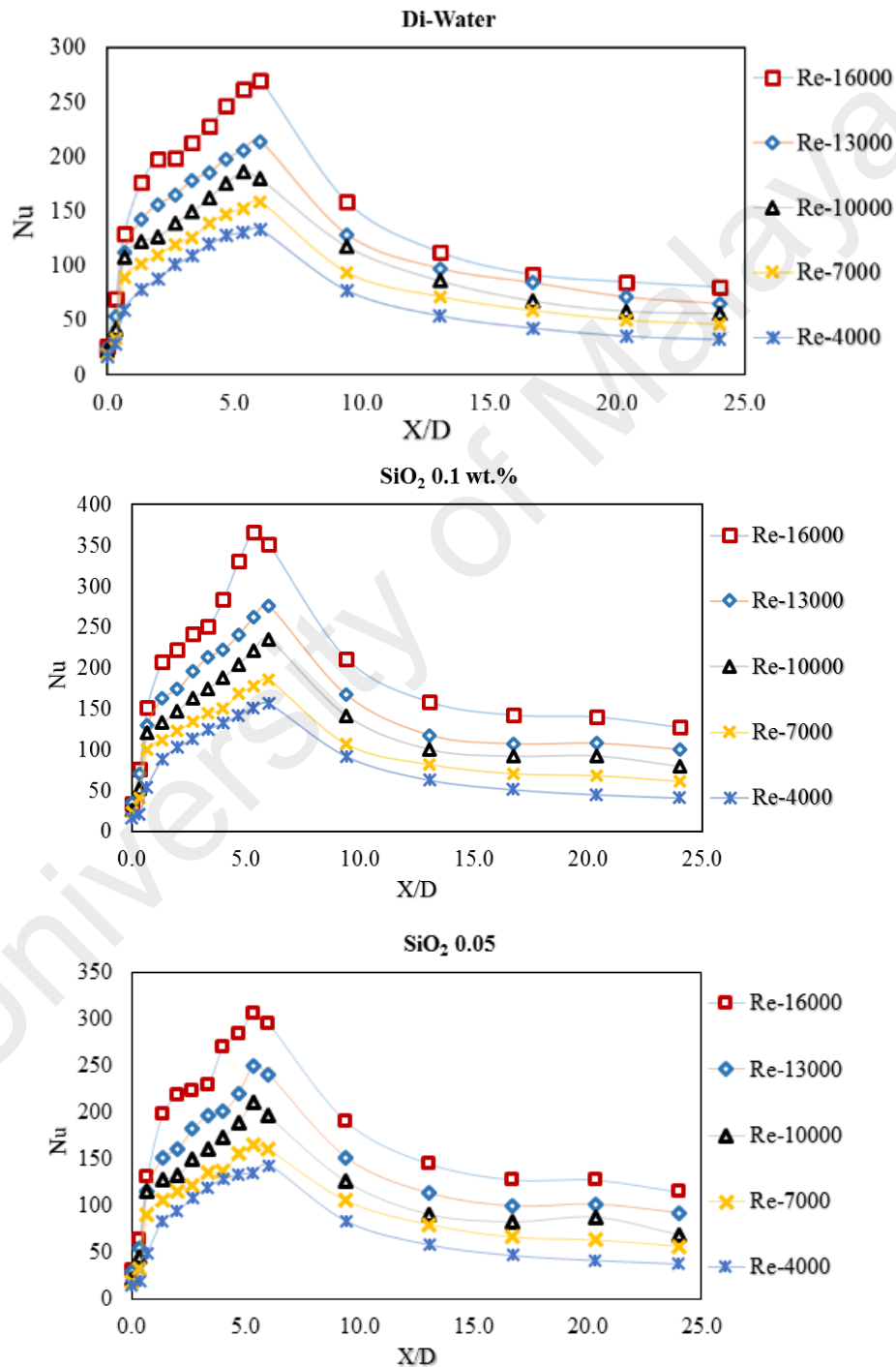


Figure 4. 58 Experimental Nusselt number of distilled water and SiO₂-water nanofluids at different weight concentrations of 0.05% and 0.1% for different Reynolds numbers

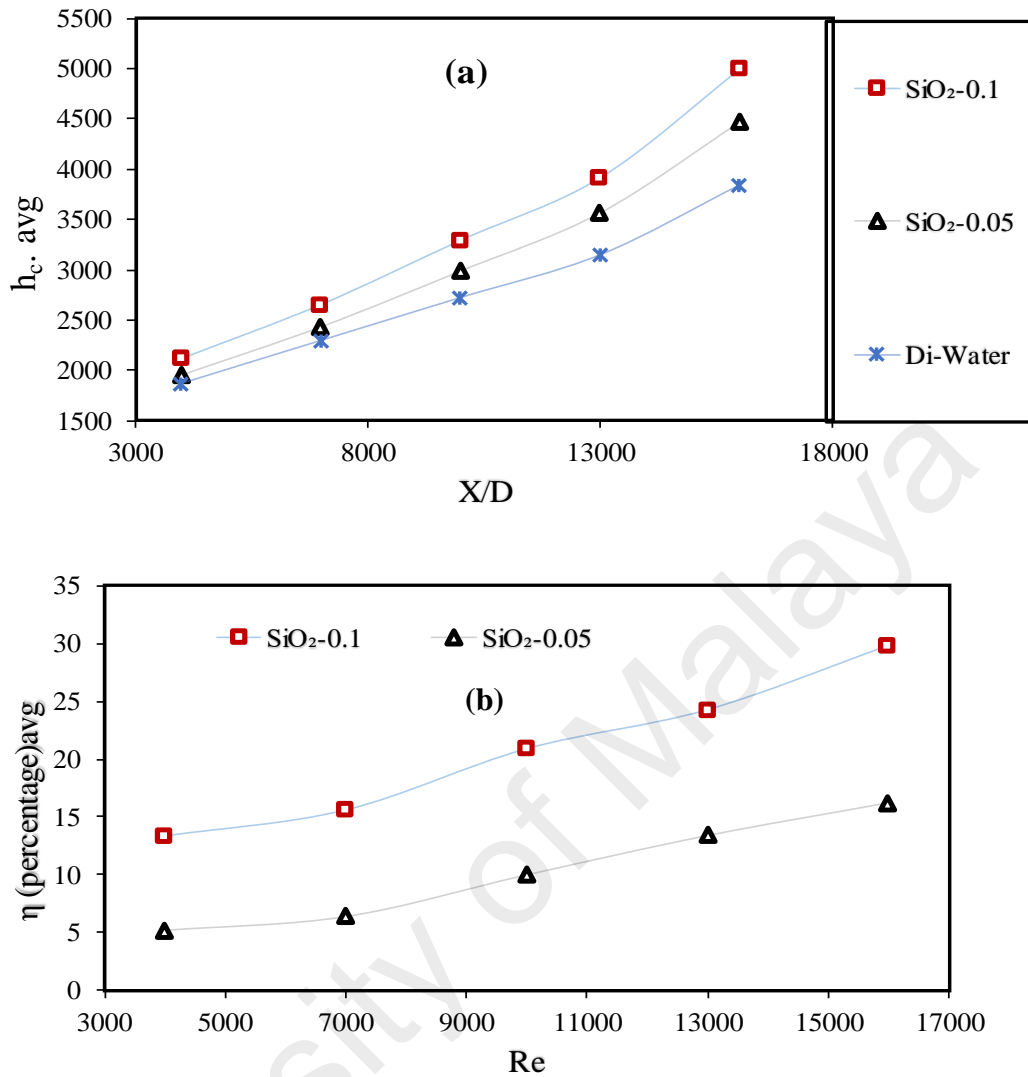


Figure 4. 59 (a) Average heat transfer coefficient of distilled water and SiO₂-water nanofluids over a backward-facing step and (b) Average (percent) heat transfer coefficient enhancement versus Reynolds number at different weight concentrations

The results in Figure 4. 58 revealed that the prepared water-based SiO₂-water nanofluids have higher Nu_x than that of pure water. Furthermore, an increase in the concentration of Silica nanoparticles led to an enhancement in Nu_x .

For an appropriate evaluation of heat transfer, the average heat transfer coefficient of SiO₂-water nanofluid was compared with water (h_c) data at different weight concentrations (0.05 and 0.1 wt.%) over a range of Reynolds number, as shown in **Figure 4. 59 (a)**. The average heat transfer coefficient increases with the increase of weight concentrations and Reynolds number. At the weight concentration of 0.1 wt.%

and Reynolds number 16,000, the highest average heat transfer coefficient 4994 $W/m^2.K$ was achieved.

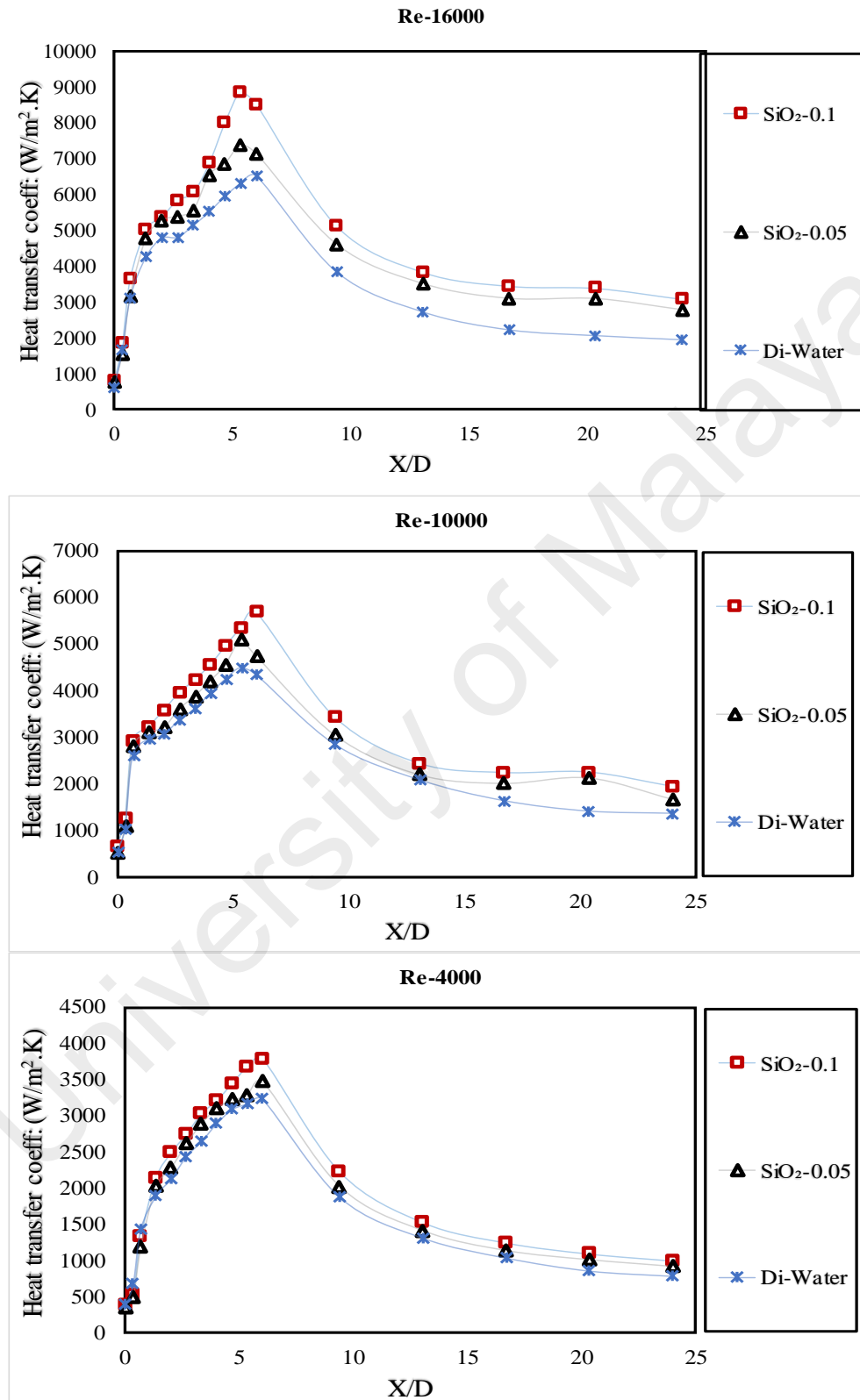


Figure 4. 60 The effect of Reynolds numbers and weight concentrations of SiO₂-water nanofluids on the local heat transfer coefficient at different axial ratios.

Figure 4. 59 (b) presents the heat transfer enhancement percentage at four different weight concentrations (0.025, 0.05, 0.075, and 0.1%) and at five Reynolds numbers (4000, 7000, 10000, 13000, 16000) at a constant DC power supply of 600 W. The average heat transfer coefficient increases with the increase of concentrations and Reynolds number. Results revealed that with the increase of Reynolds number from 4000 to 16,000, the average (percent) heat transfer coefficient enhancement (η) increased from 13.3 to 29.9 % at weight concentration of 0.1% and from 5.2 to 16.3% at weight concentration of 0.05%. Heat transfer enhancement in the presence of SiO₂-water nanofluid enhances linearly with the increase of concentration and Reynolds number.

Figure 4. 60 presents heat transfer coefficient (h_c) versus X/D over a range of Reynolds number (Re) for water and SiO₂-water nanofluid at different weight concentrations for the Re number of 16000, 10000, and 4000. The results reveal that the maximum h_c increase with the increase of Re number and concentration of nanoparticles in the fluid, satisfies the findings of other researchers (A Sh Kherbeet et al., 2012). The highest h_c were obtained at the higher Re of 16000 and weight concentration of 0.1%, similar results were obtained in case of study of heat transfer of SiO₂-water nanofluid in section 4.2.6.1.

Friction loss data in these experimental investigations are presented in the form of pressure drop as a function of Reynolds number. The data are presented in **Figure 4. 61** shows the pressure drop enhances with the increase of Reynolds number and the highest pressure drop data point is observed at a higher weight concentration (0.1 wt.%) of SiO₂-water nanofluid and at the higher Reynolds number of 16000. Similarly, the lowest pressure peak is observed at the lower concentration (0.05 wt.%) of SiO₂-water nanofluid and at the lower Reynolds number of 4000. Although the difference in pressure drops are not significant in peaks of different concentrations of SiO₂-water

nanofluids. The increase of pressure drop is due to increase of friction owing to increase of turbulence with the enhanced Reynolds number.

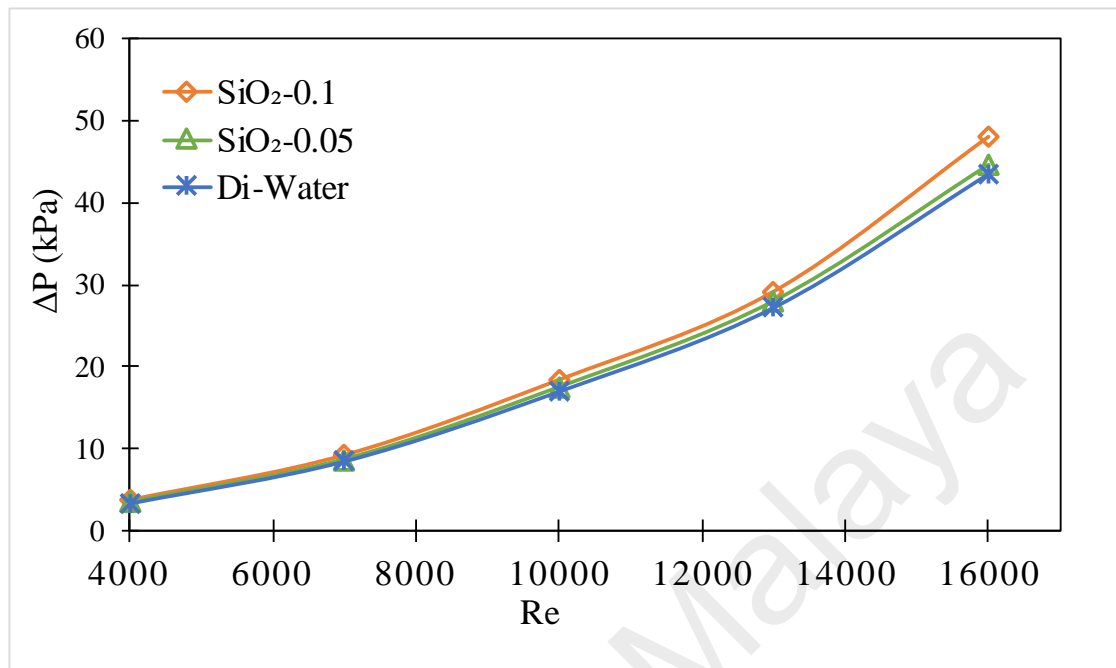


Figure 4. 61 Experimental Pressure drop of distilled water and SiO₂-water nanofluids at weight concentrations of 0.05% and 0.1% for different Re number.

4.2.6.3 MWNT-asp-water nanofluid

The effect of concentration of MWNT-asp-water nanofluids on the Nusselt number at a range of Reynolds number 4000 - 16000 had studied and the results are presented in **Figure 4. 62**.

Distribution of the measured local Nusselt number (Nu_x) in the range of Reynolds number 4000—16000 for different weight concentrations (0.05 and 0.1 wt.%) of MWNT-asp nanoparticles have compared with the distilled water data in **Figure 4. 62**. The local Nusselt number (Nu_x) peaked at the X/D range of 4 to 6 before starting to decrease gradually. The results in **Figure 4. 62** revealed that the prepared water-based MWNT-asp-water nanofluids have higher Nu_x than that of pure water. Furthermore, an increase in the concentration of MWNT-asp nanoparticles led to an enhancement in Nu_x .

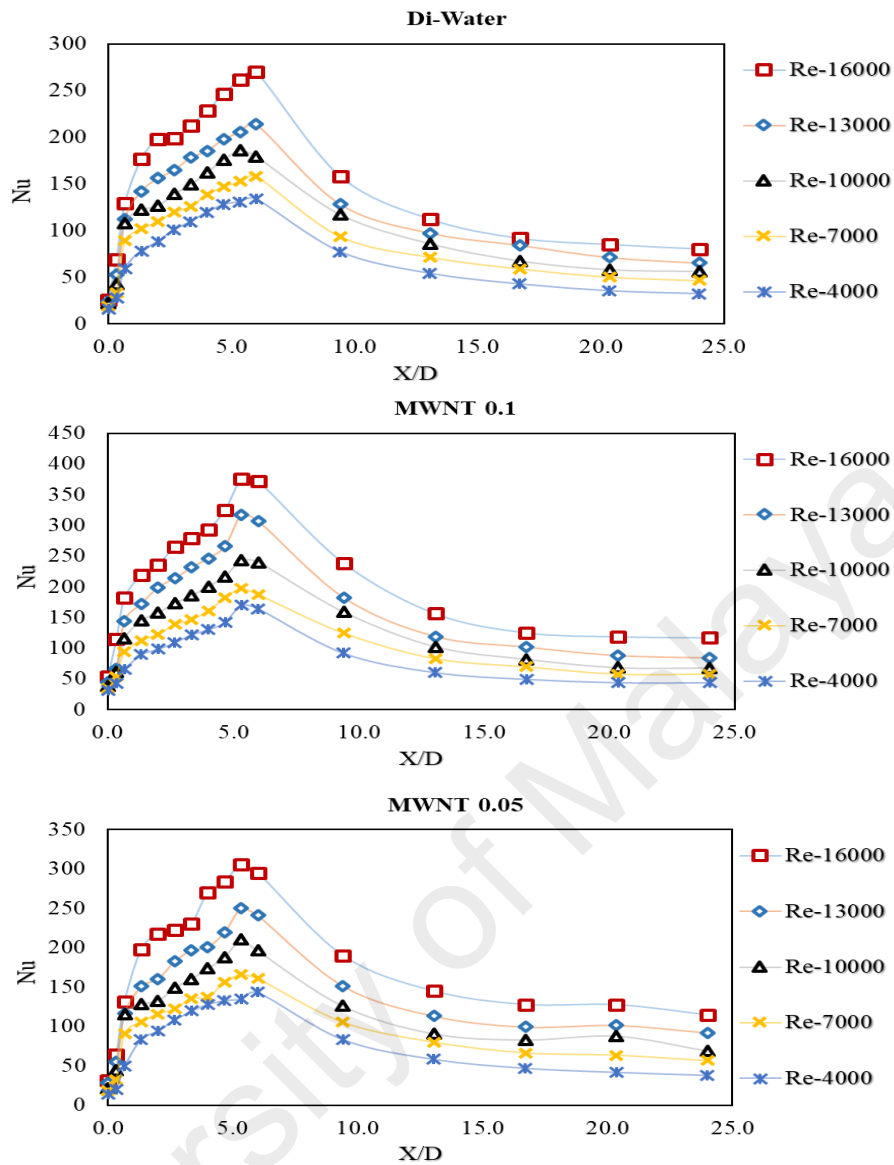


Figure 4. 62 Experimental Nusselt number of distilled water and MWNT-water nanofluids at different weight concentrations of 0.05% and 0.1% and at different Reynolds numbers

For an appropriate evaluation of heat transfer, the average heat transfer coefficient of MWNT-asp-water nanofluid was compared with water (h_c) data at different weight concentrations (0.05 and 0.1 wt.%) over a range of Reynolds number, as shown in **Figure 4. 63** (a). The average heat transfer coefficient increases with the increase of weight concentrations and Reynolds number. At the weight concentration of 0.1 wt.% and Reynolds number 16,000, the highest average heat transfer coefficient $5251 \text{ W/m}^2\cdot\text{K}$ was achieved.

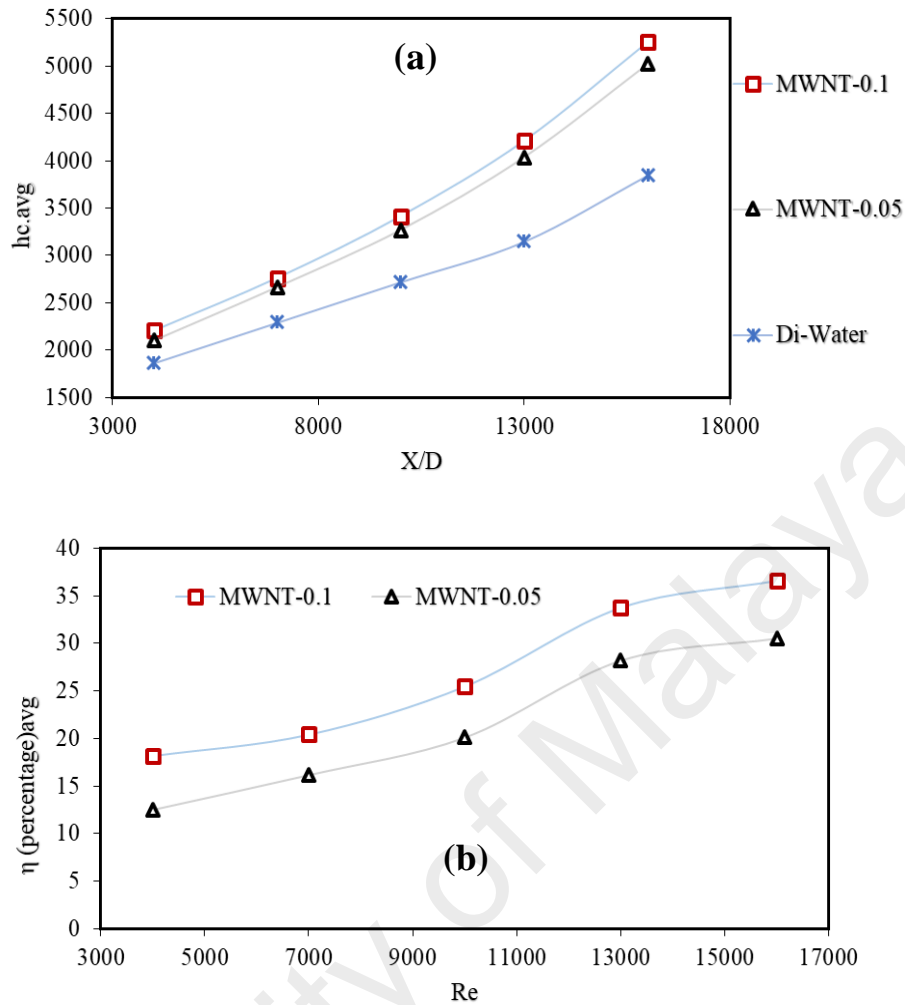


Figure 4. 63 (a) Average heat transfer coefficient of distilled water and MWNT-Asp--water nanofluids over a backward-facing step and (b) Average (percent) heat transfer coefficient enhancement versus Reynolds number at different weight concentrations

Figure 4. 63 (b) presents the heat transfer enhancement percentage of four different weight concentrations (0.05 and 0.1%) and five Reynolds numbers (4000, 7000, 10000, 13000, 16000) at a constant DC power supply of 600 W. The average heat transfer coefficient increases with the increase of concentrations and Reynolds number. Results revealed that with the increase of Reynolds number from 4000 to 16,000, the average (percent) heat transfer coefficient enhancement (η) increased from 18.2 to 36.6 % at weight concentration of 0.1% and from 12.5 to 30.5 % at weight concentration of 0.05%. Heat transfer enhancement in the presence of water-based MWNT-asp nanofluid enhances linearly with the increase of concentration and Reynolds number.

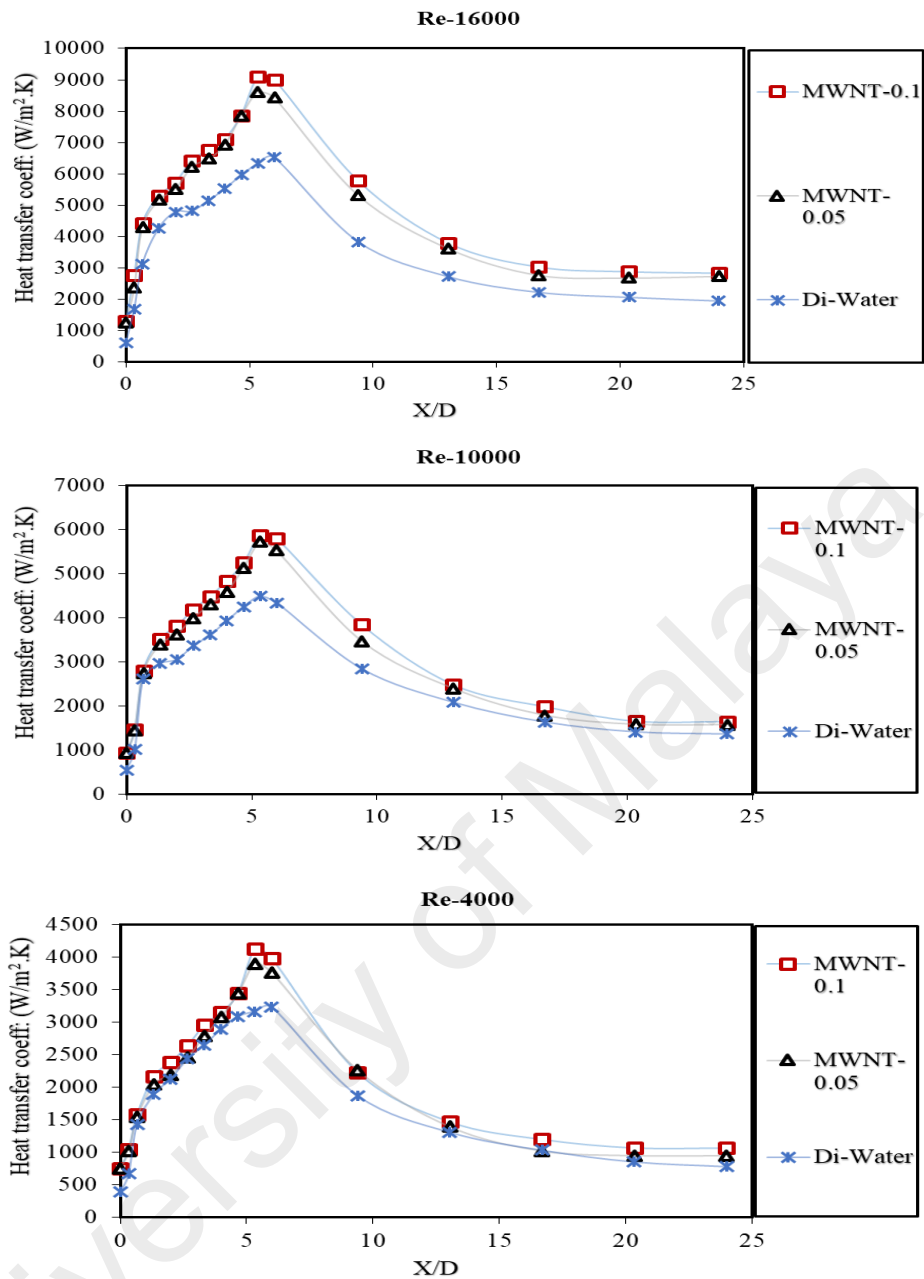


Figure 4. 64 The effect of Reynolds numbers and weight concentrations of MWNT-Asp-water nanofluids on the local heat transfer coefficient at different axial ratios.

Figure 4. 64 presents heat transfer coefficient (h_c) versus x/d over a range of Reynolds number (Re) for water and MWNT-asp-water nanofluid at different weight concentrations for the Re number of 16000, 10000, and 4000. The results reveal that the maximum h_c increases with the increase of Re number and concentration of the nanoparticles in the fluid. The highest h_c were obtained at the higher Re of 16000 and weight concentration of 0.1%, similar results were obtained in case of study of heat transfer of MWNT-asp-water nanofluid in section 4.2.6.1.

Friction loss data in these experimental investigations are presented in the form of pressure drop as a function of Reynolds number. The data are presented in **Figure 4.65** for water and MWNT-asp-water nanofluids at two different concentrations (0.05 and 0.1 wt.%) and at the Reynolds number range from 4000 to 16000.

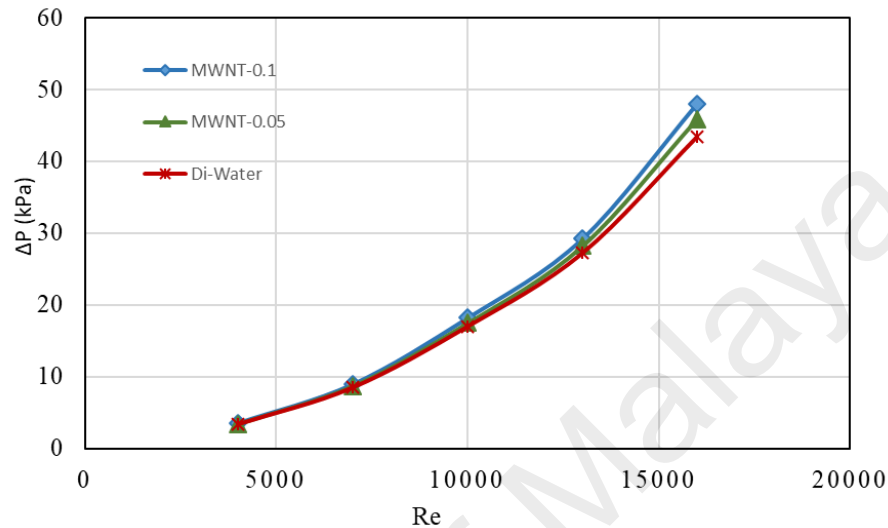


Figure 4.65 Experimental Pressure drop of distilled water and MWNT-Asp-water nanofluids at weight concentrations of 0.05% and 0.1% for different Re number.

Figure 4.65 shows the pressure drop enhances with the increase of Reynolds number and the highest pressure drop data point is observed at a higher weight concentration (0.1 wt.%) of MWNT-asp-water nanofluid and at the higher Reynolds number of 16000. Similarly, the lowest pressure peak is observed at the lower concentration (0.05 wt.%) of MWNT-asp-water nanofluid and at the lower Reynolds number of 4000. Although the difference in pressure drops are not significant in peaks of different concentrations of MWNT-asp-water nanofluids. The increase of pressure drop is due to the increase of friction owing to the increase of turbulence with the enhanced Reynolds number.

CHAPTER 5: CONCLUSION AND FURTHER WORKS

5.1 Conclusion

The aim of this research work was to investigate heat transfer and frictional pressure drop of non-wood fiber suspensions in closed conduit flow and nanofluid flow in backward-facing step. The following conclusions could be drawn from the obtained experimental results.

Fiber concentration and velocities are the key variables influencing both the h_c and pressure drop of fiber suspensions flow in pipeline. Heat transfer and friction loss of fiber suspensions reduce with the increase of concentration of the suspensions. Chemical processing of fiber enhances fiber flexibility and uniformity of fiber surfaces than that of mechanically processed fibers. Chemical processing and bleaching enhances fiber flexibility which reduces heat transfer and drag loss. At a low fiber concentration (0.2 wt.%), the flowing non-wood fiber suspensions in a pipeline show heat transfer enhancement.

h_c values for the same species of fibers at concentration of 0.6 wt.% and 1.6 m/s correlated well with fiber length, lumen and width, where h_c decreases with the increase in fiber length and fiber flexibility. An approximate linear relationship between h_c values and fiber/paper properties (from a specific non-wood fiber species) represents the possibility of prediction of the specific fiber and paper properties by monitoring heat transfer data.

The minimum drag ratio occurs at different flow velocities depending on pulp samples. The drag ratio slightly increases with velocity after the minimum drag ratio point in case of long fibers. Enhancement of long fibers percentage in blended (short-kenaf core, long-kenaf bast) suspensions, retard heat transfer coefficient.

The water-based nanofluids at a low concentration dissipate heat at a higher rate than that of water. Heat transfer rate rises highly, at a loading of only 0.1 wt.%

nanoparticles in distilled water. An increase of Reynolds number and the concentration of nanoparticles led to an increase of heat transfer rate. The pressure drop variation increases with the increase of Reynolds number and nanoparticles concentration, where the changes are insignificant in the present range of investigation.

5.2 Suggestion for further works

The research works presented in this thesis have new insights into the flow behavior of non-wood pulp fibers suspensions in pipe flow. Based on the present findings the following recommendations for future works could be made:

- 1- Study of the flow behavior of non-wood fibers suspensions in very low velocities to investigate plug flow.
- 2- Study on the flow behavior of other types of natural fibers, a mixture of wood and non-wood can be proposed to extend the research avenues. Meanwhile, investigation of other measurable fiber and paper properties could be conducted to correlate with heat transfer and pressure loss characteristics of fiber suspensions.
- 3- Study on the effect of other preferable types of additive materials e.g. Nano fibrillated cellulose on pressure loss behavior of pulp suspensions can be an area of interest.
- 4- Study on the effect of flow passage expansion ratio on heat transfer coefficient.
- 5- Comparative study of forward and backward facing steps on heat transfer and frictional losses using different nanofluids.
- 6- Study of different metals effect on heat transfer to nanofluids in step flow

References

- Abbott, D., & Kline, S. (1962). Experimental investigation of subsonic turbulent flow over single and double backward facing steps. *Journal of basic engineering*, 84(3), 317-325.
- Abe, K., Kondoh, T., & Nagano, Y. (1994). A new turbulence model for predicting fluid flow and heat transfer in separating and reattaching flows—I. Flow field calculations. *International Journal of Heat and Mass Transfer*, 37(1), 139-151.
- Abe, K., Kondoh, T., & Nagano, Y. (1995). A new turbulence model for predicting fluid flow and heat transfer in separating and reattaching flows—II. Thermal field calculations. *International Journal of Heat and Mass Transfer*, 38(8), 1467-1481.
- Abu-Mulaweh, H. (2003). A review of research on laminar mixed convection flow over backward-and forward-facing steps. *International Journal of Thermal Sciences*, 42(9), 897-909.
- Abu-Mulaweh, H. I. (2005). Turbulent mixed convection flow over a forward-facing step—the effect of step heights. *International Journal of Thermal Sciences*, 44(2), 155-162.
- Abu-Nada, E. (2008). Application of nanofluids for heat transfer enhancement of separated flows encountered in a backward facing step. *International Journal of Heat and Fluid Flow*, 29(1), 242-249.
- Al-aswadi, A. A., Mohammed, H. A., Shuaib, N. H., & Campo, A. (2010). Laminar forced convection flow over a backward facing step using nanofluids. *International Communications in Heat and Mass Transfer*, 37(8), 950-957.
- Alemasov, V., Glebov, G., & Kozlov, A. (1989). Thermo-anemometric methods for studying flows with separation. *Kazan'Branch of the USSR Academy of Sciences, Kazan*, 178.
- Allen, C. L., Chhatwal, A. R., & Williams, J. M. (2012). Direct amide formation from unactivated carboxylic acids and amines. *Chemical Communications*, 48(5), 666-668.
- Amiri, A., Arzani, H. K., Kazi, S., Chew, B., & Badarudin, A. (2016). Backward-facing step heat transfer of the turbulent regime for functionalized graphene nanoplatelets based water–ethylene glycol nanofluids. *International Journal of Heat and Mass Transfer*, 97, 538-546.
- Amiri, A., Maghrebi, M., Baniadam, M., & Heris, S. Z. (2011). One-pot, efficient functionalization of multi-walled carbon nanotubes with diamines by microwave method. *Applied Surface Science*, 257(23), 10261-10266.
- Amiri, A., Shanbedi, M., Eshghi, H., Heris, S. Z., & Baniadam, M. (2012). Highly dispersed multiwalled carbon nanotubes decorated with Ag nanoparticles in water and experimental investigation of the thermophysical properties. *The Journal of Physical Chemistry C*, 116(5), 3369-3375.
- Amiri, A., Shanbedi, M., Rafieerad, A. R., Rashidi, M. M., Zaharinie, T., Zubir, M. N. M., . . . Chew, B. T. (2017). Functionalization and exfoliation of graphite into mono layer graphene for improved heat dissipation. *Journal of the Taiwan Institute of Chemical Engineers*, 71, 480-493.
- Aravind, S. J., Baskar, P., Baby, T. T., Sabareesh, R. K., Das, S., & Ramaprabhu, S. (2011). Investigation of structural stability, dispersion, viscosity, and conductive heat transfer properties of functionalized carbon nanotube based nanofluids. *The Journal of Physical Chemistry C*, 115(34), 16737-16744.
- Armaly, B. F., Li, A., & Nie, J. (2003). Measurements in three-dimensional laminar separated flow. *International Journal of Heat and Mass Transfer*, 46(19), 3573-3582.

- Ashori, A. (2006). Nonwood fibers—A potential source of raw material in papermaking. *Polymer-Plastics Technology and Engineering*, 45(10), 1133-1136.
- Avancha, R. V., & Pletcher, R. H. (2002). Large eddy simulation of the turbulent flow past a backward-facing step with heat transfer and property variations. *International Journal of Heat and Fluid Flow*, 23(5), 601-614.
- Barbosa-Saldaña, J. G., & Anand, N. (2007). Flow over a three-dimensional horizontal forward-facing step. *Numerical Heat Transfer, Part A: Applications*, 53(1), 1-17.
- Beck, M. P., Yuan, Y., Warriar, P., & Teja, A. S. (2009). The effect of particle size on the thermal conductivity of alumina nanofluids. *Journal of Nanoparticle Research*, 11(5), 1129-1136.
- Beck, M. P., Yuan, Y., Warriar, P., & Teja, A. S. (2010). The thermal conductivity of aqueous nanofluids containing ceria nanoparticles: AIP.
- Bhattacharya, P., Saha, S., Yadav, A., Phelan, P., & Prasher, R. (2004). Brownian dynamics simulation to determine the effective thermal conductivity of nanofluids. *Journal of Applied Physics*, 95(11), 6492-6494.
- Bhogare, R. A., & Kothawale, B. (2013). A review on applications and challenges of nanofluids as coolant in automobile radiator. *International journal of scientific and research publications*, 3(8), 435-441.
- Bianco, V., Manca, O., & Nardini, S. (2014). Performance analysis of turbulent convection heat transfer of Al₂O₃ water-nanofluid in circular tubes at constant wall temperature. *Energy*, 77, 403-413.
- Biermann, C. J. (1996). *Handbook of Pulping and Papermaking*: Elsevier Science.
- Blasius, H. (1908). Grenzschichten in Flüssigkeiten mit kleiner Reibung. 2. *angew. Math.*
- Boelter, L., Young, G., & Iversen, H. (1948). An Investigation of Aircraft Heaters XXVII: Distribution of Heat-transfer Rate in the Entrance Section of a Circular Tube.
- Boughamoura, A., Belmabrouk, H., & Nasrallah, S. B. (2003). Numerical study of a piston-driven laminar flow and heat transfer in a pipe with a sudden expansion. *International Journal of Thermal Sciences*, 42(6), 591-604.
- Charani, P. R., Dehghani-Firouzabadi, M., Afra, E., & Shakeri, A. (2013). Rheological characterization of high concentrated MFC gel from kenaf unbleached pulp. *Cellulose*, 20(2), 727-740.
- Chen, H., Ding, Y., He, Y., & Tan, C. (2007). Rheological behaviour of ethylene glycol based titania nanofluids. *Chemical Physics Letters*, 444(4), 333-337.
- Chen, H., Witharana, S., Jin, Y., Kim, C., & Ding, Y. (2009). Predicting thermal conductivity of liquid suspensions of nanoparticles (nanofluids) based on rheology. *Particuology*, 7(2), 151-157.
- Chen, Y., Nie, J., Armaly, B., & Hsieh, H.-T. (2006). Turbulent separated convection flow adjacent to backward-facing step—effects of step height. *International Journal of Heat and Mass Transfer*, 49(19), 3670-3680.
- Choi, C., Yoo, H., & Oh, J. (2008). Preparation and heat transfer properties of nanoparticle-in-transformer oil dispersions as advanced energy-efficient coolants. *Current Applied Physics*, 8(6), 710-712.
- Choi, S., Zhang, Z., Yu, W., Lockwood, F., & Grulke, E. (2001). Anomalous thermal conductivity enhancement in nanotube suspensions. *Applied physics letters*, 79(14), 2252-2254.
- Chon, C. H., Kihm, K. D., Lee, S. P., & Choi, S. U. (2005). Empirical correlation finding the role of temperature and particle size for nanofluid (Al₂O₃) thermal conductivity enhancement. *Applied physics letters*, 87(15), 153107.

- Chung, S. J., Leonard, J. P., Nettleship, I., Lee, J.-K., Soong, Y., Martello, D. V., & Chyu, M. K. (2009). Characterization of ZnO nanoparticle suspension in water: Effectiveness of ultrasonic dispersion. *Powder technology*, 194(1), 75-80.
- Colebrook, C. F., BLENCH, T., CHATLEY, H., ESSEX, E., FINNIECOME, J., LACEY, G., . . . MACDONALD, G. (1939). CORRESPONDENCE. TURBULENT FLOW IN PIPES, WITH PARTICULAR REFERENCE TO THE TRANSITION REGION BETWEEN THE SMOOTH AND ROUGH PIPE LAWS.(INCLUDES PLATES). *Journal of the Institution of Civil engineers*, 12(8), 393-422.
- Cui, H., & Grace, J. R. (2007). Flow of pulp fibre suspension and slurries: A review. *International Journal of Multiphase Flow*, 33(9), 921-934.
- Daily, J. W., & Bugliarello, G. (1958). *The effects of fibers on velocity distribution, turbulence and flow resistance of dilute suspensions*: Hydrodynamics Laboratory, Department of Civil and Sanitary Engineering, Massachusetts Institute of Technology.
- Das, S. K., Putra, N., & Roetzel, W. (2003). Pool boiling characteristics of nano-fluids. *International Journal of Heat and Mass Transfer*, 46(5), 851-862.
- Das, S. K., Putra, N., Thiesen, P., & Roetzel, W. (2003). Temperature dependence of thermal conductivity enhancement for nanofluids. *Journal of heat transfer*, 125(4), 567-574.
- Derakhshandeh, B., Kerekes, R., Hatzikiriakos, S., & Bennington, C. (2011). Rheology of pulp fibre suspensions: A critical review. *Chemical Engineering Science*, 66(15), 3460-3470.
- Ding, Y., & Wen, D. (2005). Particle migration in a flow of nanoparticle suspensions. *Powder technology*, 149(2), 84-92.
- Dittus, F., & Boelter, L. (1930). University of California publications on engineering. *University of California publications in Engineering*, 2, 371.
- Duangthongsuk, W., & Wongwises, S. (2009). Heat transfer enhancement and pressure drop characteristics of TiO₂-water nanofluid in a double-tube counter flow heat exchanger. *International Journal of Heat and Mass Transfer*, 52(7), 2059-2067.
- Duangthongsuk, W., & Wongwises, S. (2010). An experimental study on the heat transfer performance and pressure drop of TiO₂-water nanofluids flowing under a turbulent flow regime. *International Journal of Heat and Mass Transfer*, 53(1), 334-344.
- Duffy, G., Kazi, M., & Chen, X. (2002). *Pressure drop measurement—a new way to monitor wood pulp quality*. Paper presented at the Proceedings of the 56th Annual Appita Conference, Rotorua, New Zealand.
- Duffy, G., Kazi, S., & Chen, X. (2000). *New Way to Monitor Wood Pulp Fibre Quality Using Heat Transfer Coefficient*. Paper presented at the Proceedings of the 54th Annual Appita Conference, Melbourne, Australia, Apr.
- Duffy, G., Kazi, S., & Chen, X. (2011). Heat transfer and pressure drop characteristics of suspensions of synthetic and wood pulp fibres in annular flow. *Applied Thermal Engineering*, 31(14), 2971-2980.
- Duffy, G., & Titchener, A. (1975). Disruptive shear stress of pulp networks. *Svensk papperstidning*.
- Duffy, G. G. (1972). A study of the flow properties of New Zealand wood pulp suspensions.
- Duffy, G. G., Kazi, S. N., & Chen, X. (2000). Heat transfer to fibre suspensions in annular flow. *Chemeca 2000: Opportunities and Challenges for the Resource and Processing Industries*, 457.

- Duffy, G. G., Longdill, G., & Lee, P. (1978). High-consistency flow of pulp suspensions in pipes. *Tappi [Technical Association of the Pulp and Paper Industry](USA)*.
- Duffy, G. G., Titchener, A., Lee, P., & Moller, K. (1976). Mechanisms of flow of pulp suspensions in pipes. *APPITA Aust Pulp Pap Ind Tech Assoc*.
- Durst, F., Melling, A., & Whitelaw, J. (1974). Low Reynolds number flow over a plane symmetric sudden expansion. *Journal of Fluid Mechanics*, 64(01), 111-128.
- Dutt, D., Upadhyay, J., Singh, B., & Tyagi, C. (2009). Studies on Hibiscus cannabinus and Hibiscus sabdariffa as an alternative pulp blend for softwood: An optimization of kraft delignification process. *Industrial crops and products*, 29(1), 16-26.
- Eastman, J. A., Choi, S., Li, S., Yu, W., & Thompson, L. (2001). Anomalously increased effective thermal conductivities of ethylene glycol-based nanofluids containing copper nanoparticles. *Applied physics letters*, 78(6), 718-720.
- Eastman, J. A., Phillpot, S., Choi, S., & Keblinski, P. (2004). Thermal transport in nanofluids 1. *Annu. Rev. Mater. Res.*, 34, 219-246.
- Ede, A., Hislop, C., & Morris, R. (1956). Effect on the local heat-transfer coefficient in a pipe of an abrupt disturbance of the fluid flow: abrupt convergence and divergence of diameter ratio 2/1. *Proceedings of the Institution of Mechanical Engineers*, 170(1), 1113-1130.
- Evans, W., Fish, J., & Keblinski, P. (2006). Role of Brownian motion hydrodynamics on nanofluid thermal conductivity. *Applied physics letters*, 88(9), 093116.
- Fällman, M. C. (2009). Turbulence measurements in fiber suspension flows: experimental methods and results.
- Fendler, J. H. (2001). Colloid chemical approach to nanotechnology. *Korean Journal of Chemical Engineering*, 18(1), 1-13.
- Filetti, E., & Kays, W. M. (1967). Heat transfer in separated, reattached, and redevelopment regions behind a double step at entrance to a flat duct. *Journal of heat transfer*, 89(2), 163-167.
- Forgacs, O. (1957). *The hydrodynamic behaviour of paper-making fibres*.
- Gharehkhani, S., Yarmand, H., Goodarzi, M. S., Shirazi, S. F. S., Amiri, A., Zubir, M. N. M., . . . Wongwises, S. (2017). Experimental investigation on rheological, momentum and heat transfer characteristics of flowing fiber crop suspensions. *International Communications in Heat and Mass Transfer*, 80, 60-69.
- Gnielinski, V. (1975). New equations for heat and mass transfer in the turbulent flow in pipes and channels. *NASA STI/recon technical report A*, 75, 22028.
- Goharzadeh, A., & Rodgers, P. (2009). Experimental measurement of laminar axisymmetric flow through confined annular geometries with sudden inward expansion. *Journal of Fluids Engineering*, 131(12), 124501.
- Goldstein, R. J., Eriksen, V., Olson, R., & Eckert, E. (1970). Laminar separation, reattachment, and transition of the flow over a downstream-facing step. *Journal of Basic Engineering*, 92(4), 732-739.
- Goto, S., Nagazono, H., & Kato, H. (1986). The flow behavior of fiber suspensions in Newtonian fluids and polymer solutions. *Rheologica acta*, 25(3), 246-256.
- Guo, Z.-Y., Li, D.-Y., & Liang, X.-G. (1996). Thermal effect on the recirculation zone in sudden-expansion gas flows. *International Journal of Heat and Mass Transfer*, 39(13), 2619-2624.
- Hagen, K. D. (1999). *Heat transfer with applications*: Prentice Hall.
- Haghighi, E., Nikkam, N., Saleemi, M., Behi, M., Mirmohammadi, S. A., Poth, H., . . . Palm, B. (2013). Shelf stability of nanofluids and its effect on thermal conductivity and viscosity. *Measurement Science and Technology*, 24(10), 105301.

- Hamilton, R., & Crosser, O. (1962). Thermal conductivity of heterogeneous two-component systems. *Industrial & Engineering chemistry fundamentals*, 1(3), 187-191.
- Han, J. S., & Rowell, J. S. (1997). *Chemical composition of fibers*: Lewis Publishers.
- Hassan, N. H. M., Muhammed, S., & Rushdan, I. (2014). Properties of Gigantochloa scortechinii paper enhancement by beating revolution. *Journal of Tropical Resources and Sustainable Science*, 2, 59-67.
- He, Q., Tong, M., & Liu, Y. (2007). Measurement of specific heat of TiO₂-BaCl₂-H₂O nano-fluids with DSC. *Refrigeration & Air-Conditioning*, 7(4), 19-22.
- Higgins, B., & Wahren, D. (1982). Optimum consistency for pumping pulp. *Tappi*, 65(3), 131-133.
- Hosseini, M., Sadri, R., Kazi, S. N., Bagheri, S., Zubir, N., Bee Teng, C., & Zaharinie, T. (2017). Experimental Study on Heat Transfer and Thermo-Physical Properties of Covalently Functionalized Carbon Nanotubes Nanofluids in an Annular Heat Exchanger: A Green and Novel Synthesis. *Energy & Fuels*.
- Hua, X., Tanguy, P. A., Li, R., & Van Wagner, J. S. (1996). Effect of basestock formation on paper coating. *Tappi journal*, 79(5), 112-116.
- Hubbe, M. A. (2007). Flocculation and redispersion of cellulosic fiber suspensions: A review of effects of hydrodynamic shear and polyelectrolytes. *BioResources*, 2(2), 296-331.
- James P, C. (1981). *Pulp and Paper: Chemistry and Chemical Technology* (C. James P Ed. Vol. 3).
- Jäsberg, A. (2007). *Flow behaviour of fibre suspensions in straight pipes: new experimental techniques and multiphase modeling*: University of Jyväskylä.
- Jia-Fei, Z., Zhong-Yang, L., Ming-Jiang, N., & Ke-Fa, C. (2009). Dependence of nanofluid viscosity on particle size and pH value. *Chinese Physics Letters*, 26(6), 066202.
- Kaldor, A., Karlgren, C., & Verwest, H. (1990). Kenaf-a fast growing fiber source for papermaking. *Tappi journal*, 73(11), 205-208.
- Kanna, P. R., & Das, M. K. (2006). Heat transfer study of two-dimensional laminar incompressible wall jet over backward-facing step. *Numerical Heat Transfer, Part A: Applications*, 50(2), 165-187.
- Kazi, M. S. N. (2001). *Heat Transfer to Fibre Suspensions: Studies in Fibre Characterisation and Fouling Mitigation*.
- Kazi, M. S. N., Duffy, G. G., & Chen, X. D. (1999). Heat transfer in the drag reducing regime of wood pulp fibre suspensions. *Chemical Engineering Journal*, 73(3), 247-253.
- Kazi, S., Duffy, G., & Chen, X. (2012). Validation of heat transfer data for fibre suspensions in coaxial pipe heat exchangers. *Experimental Thermal and Fluid Science*, 38, 210-222.
- Kazi, S., Duffy, G., & Chen, X. (2014a). Study of the effect of entrance length on heat transfer to fibre suspensions in annular flow heat exchangers. *International Journal of Heat and Mass Transfer*, 78, 548-556.
- Kazi, S., Duffy, G., & Chen, X. (2014b). Validation of heat transfer and friction loss data for fibre suspensions in a circular and a coaxial pipe heat exchanger. *International Journal of Thermal Sciences*, 79, 146-160.
- Kazi, S., Duffy, G., & Chen, X. (2015). Heat transfer coefficient of flowing wood pulp fibre suspensions to monitor fibre and paper quality. *Applied Thermal Engineering*, 78, 172-184.
- Kebllinski, P., Phillpot, S., Choi, S., & Eastman, J. (2002). Mechanisms of heat flow in suspensions of nano-sized particles (nanofluids). *International Journal of Heat and Mass Transfer*, 45(4), 855-863.

- Kerekes, R., & Schell, C. (1992). Characterization of fibre flocculation regimes by a crowding factor. *Journal of pulp and paper science*, 18(1), J32-J38.
- Kerekes, R., Soszynski, R., & Doo, T. (1985). *The flocculation of pulp fibres*. Paper presented at the Papermaking Raw Materials: Their Interaction with the Production Process and Their Effect on Paper Properties-Transactions of the Eighth Fundamental Research Symposium held at Oxford: September 1985.
- Kherbeet, A. S., Mohammed, H., Munisamy, K. M., & Salman, B. (2014). Combined convection nanofluid flow and heat transfer over microscale forward-facing step. *International Journal of Nanoparticles*, 7(1), 1-25.
- Kherbeet, A. S., Mohammed, H., & Salman, B. (2012). The effect of nanofluids flow on mixed convection heat transfer over microscale backward-facing step. *International Journal of Heat and Mass Transfer*, 55(21), 5870-5881.
- Kherbeet, A. S., Mohammed, H., Salman, B., Ahmed, H. E., Alawi, O. A., & Rashidi, M. (2015). Experimental study of nanofluid flow and heat transfer over microscale backward-and forward-facing steps. *Experimental Thermal and Fluid Science*, 65, 13-21.
- Kherbeet, A. S., Mohammed, H. A., Munisamy, K. M., & Salman, B. H. (2014). The effect of step height of microscale backward-facing step on mixed convection nanofluid flow and heat transfer characteristics. *International Journal of Heat and Mass Transfer*, 68, 554-566.
- Kherbeet, A. S., Mohammed, H. A., & Salman, B. H. (2012). The effect of nanofluids flow on mixed convection heat transfer over microscale backward-facing step. *International Journal of Heat and Mass Transfer*, 55(21-22), 5870-5881.
- Kitano, T., & Kataoka, T. (1981). The rheology of suspensions of vinylon fibers in polymer liquids. I. Suspensions in silicone oil. *Rheologica Acta*, 20(4), 390-402.
- Kitoh, A., Sugawara, K., Yoshikawa, H., & Ota, T. (2007). Expansion ratio effects on three-dimensional separated flow and heat transfer around backward-facing steps. *Journal of heat transfer*, 129(9), 1141-1155.
- Kole, M., & Dey, T. (2010). Viscosity of alumina nanoparticles dispersed in car engine coolant. *Experimental Thermal and Fluid Science*, 34(6), 677-683.
- Korteoja, M., Lukkarinen, A., Kaski, K., & Niskanen, K. (1997). Computational study of formation effects on paper strength. *Journal of pulp and paper science*, 23(1), J18-J22.
- Korteoja, M., Salminen, L., Niskanen, K., & Alava, M. (1998). Statistical variation of paper strength. *Journal of pulp and paper science*, 24(1), 1-7.
- Kwak, K., & Kim, C. (2005). Viscosity and thermal conductivity of copper oxide nanofluid dispersed in ethylene glycol. *Korea-Australia Rheology Journal*, 17(2), 35-40.
- Labbé, O., Sagaut, P., & Montreuil, E. (2002). Large-eddy simulation of heat transfer over a backward-facing step. *Numerical Heat Transfer: Part A: Applications*, 42(1-2), 73-90.
- Lee, D. (2007). Thermophysical properties of interfacial layer in nanofluids. *Langmuir*, 23(11), 6011-6018.
- Lee, D. H., Lee, J. S., Park, H. J., & Kim, M. K. (2011). Experimental and numerical study of heat transfer downstream of an axisymmetric abrupt expansion and in a cavity of a circular tube. *Journal of Mechanical Science and Technology*, 25(2), 395-401.
- Lee, J.-H., Hwang, K. S., Jang, S. P., Lee, B. H., Kim, J. H., Choi, S. U., & Choi, C. J. (2008). Effective viscosities and thermal conductivities of aqueous nanofluids containing low volume concentrations of Al₂O₃ nanoparticles. *International Journal of Heat and Mass Transfer*, 51(11), 2651-2656.

- Lee, S., Choi, S.-S., Li, S., and, & Eastman, J. (1999). Measuring thermal conductivity of fluids containing oxide nanoparticles. *Journal of heat transfer*, 121(2), 280-289.
- Li, C., & Peterson, G. (2007). Mixing effect on the enhancement of the effective thermal conductivity of nanoparticle suspensions (nanofluids). *International Journal of Heat and Mass Transfer*, 50(23), 4668-4677.
- Li, J., Li, Z., & Wang, B. (2002). Experimental viscosity measurements for copper oxide nanoparticle suspensions. *Tsinghua Science and Technology*, 7(2), 198-201.
- Li, S., & Eastman, J. (1999). Measuring thermal conductivity of fluids containing oxide nanoparticles. *J. Heat Transf*, 121(2), 280-289.
- Lima, R., Andrade, C., & Zapparoli, E. (2008). Numerical study of three recirculation zones in the unilateral sudden expansion flow. *International Communications in Heat and Mass Transfer*, 35(9), 1053-1060.
- Macagno, E. O., & Hung, T.-K. (1967). Computational and experimental study of a captive annular eddy. *Journal of Fluid Mechanics*, 28(1), 43-64.
- MacKenzie, J., Martinez, D. M., & Olson, J. A. (2014). A quantitative analysis of turbulent drag reduction in a hydrocyclone. *The Canadian Journal of Chemical Engineering*, 92(8), 1432-1443.
- Maiga, S. E. B., Palm, S. J., Nguyen, C. T., Roy, G., & Galanis, N. (2005). Heat transfer enhancement by using nanofluids in forced convection flows. *International Journal of Heat and Fluid Flow*, 26(4), 530-546.
- Main, N. M., Talib, R. A., Ibrahim, R., Rahman, R. A., & Mohamed, A. Z. (2015). Linerboard Made from Soda-Antraquinone (Soda-AQ) Treated Coconut Coir Fiber and Effect of Pulp Beating. *BioResources*, 10(4), 6975-6992.
- Martinelli, R. C. (1947). Heat transfer to molten metals. *Trans. ASME*, 69(8), 947-959.
- Martinez, D., Kiiskinen, H., Ahlman, A.-K., & Kerekes, R. (2003). On the mobility of flowing papermaking suspensions and its relationship to formation. *Journal of pulp and paper science*, 29(10), 341-347.
- Masuda, H., Ebata, A., & Teramae, K. (1993). Alteration of thermal conductivity and viscosity of liquid by dispersing ultra-fine particles. Dispersion of Al₂O₃, SiO₂ and TiO₂ ultra-fine particles.
- Mehrez, Z., Bouterra, M., El Cafsi, A., Belghith, A., & Le Quere, P. (2009). The influence of the periodic disturbance on the local heat transfer in separated and reattached flow. *Heat and mass transfer*, 46(1), 107-112.
- Mewis, J., & Metzner, A. (1974). The rheological properties of suspensions of fibres in Newtonian fluids subjected to extensional deformations. *Journal of Fluid Mechanics*, 62(03), 593-600.
- Middis, J., Muller-Steinhagen, H., & Duffy, G. (1994). Heat transfer and frictional pressure drop characteristics of model nylon fibre suspensions. *Appita*, 47(2), 154-158.
- Moayed, A. R. (1999). Characterization of Fibre Suspension Flows at Papermaking Consistencies.
- Mohammed, H., Al-Aswadi, A., Shuaib, N., & Saidur, R. (2011). Convective heat transfer and fluid flow study over a step using nanofluids: a review. *Renewable and Sustainable Energy Reviews*, 15(6), 2921-2939.
- Mohammed, H., Al-aswadi, A., Abu-Mulaweh, H., & Shuaib, N. (2011). Influence of nanofluids on mixed convective heat transfer over a horizontal backward-facing step. *Heat Transfer—Asian Research*, 40(4), 287-307.
- Mossello, A. A., Harun, J., Shamsi, S. R. F., Resalati, H., Tahir, P. M., Ibrahim, R., & Mohmamed, A. Z. (2010). A review of literatures related to kenaf as a alternative for pulpwoods. *Agricultural Journal*, 5(3), 131-138.

- Mukherjee, S., & Paria, S. (2013). Preparation and stability of nanofluids-A Review. *IOSR Journal of Mechanical and civil engineering*, 9(2), 63-69.
- Murugesan, C., & Sivan, S. (2010). Limits for thermal conductivity of nanofluids. *Thermal Science*, 14(1), 65-71.
- Nag, D., & Datta, A. (2007). On the eddy characteristics of laminar axisymmetric flows through confined annular geometries with inward expansion. *Proceedings of the Institution of Mechanical Engineers, Part C: Journal of Mechanical Engineering Science*, 221(2), 213-226.
- Nawab, M., & Mason, S. (1958). Viscosity of dilute suspensions of thread-like particles. *The Journal of Physical Chemistry*, 62(10), 1248-1253.
- Nguyen, C., Desgranges, F., Roy, G., Galanis, N., Maré, T., Boucher, S., & Mintsa, H. A. (2007). Temperature and particle-size dependent viscosity data for water-based nanofluids—hysteresis phenomenon. *International Journal of Heat and Fluid Flow*, 28(6), 1492-1506.
- Nie, J., & Armaly, B. F. (2002). Three-dimensional convective flow adjacent to backward-facing step-effects of step height. *International Journal of Heat and Mass Transfer*, 45(12), 2431-2438.
- Nikuradse, J., Forsch. (1932). *Arb. Ing. Wes*, 356.
- Ogbonnaya, C., Roy-Macauley, H., Nwalozie, M., & Annerose, D. (1997). Physical and histochemical properties of kenaf (*Hibiscus cannabinus* L.) grown under water deficit on a sandy soil. *Industrial crops and products*, 7(1), 9-18.
- Ota, T., Yanaoka, H., Shibuya, K., Nakajima, M., & Yoshikawa, H. (2000). Numerical analysis of separated flow and heat transfer in an enlarged channel. *Nihon Kikai Gakkai Ronbunshu, B Hen/Transactions of the Japan Society of Mechanical Engineers, Part B*, 66(648), 2109-2116.
- Özerinç, S., Kakaç, S., & Yazıcıoğlu, A. G. (2010). Enhanced thermal conductivity of nanofluids: a state-of-the-art review. *Microfluidics and Nanofluidics*, 8(2), 145-170.
- Öztop, H. F. (2006). Turbulence forced convection heat transfer over double forward facing step flow. *International Communications in Heat and Mass Transfer*, 33(4), 508-517.
- Oztop, H. F., Mushatet, K. S., & Yılmaz, İ. (2012). Analysis of turbulent flow and heat transfer over a double forward facing step with obstacles. *International Communications in Heat and Mass Transfer*, 39(9), 1395-1403.
- Paavilainen, L. (1990). Importance of particle size-fibre length and fines-for the characterization of softwood kraft pulp. *Paperi ja puu*, 72(5), 516-526.
- Paavilainen, L. (1993). Conformability, flexibility and collapsibility of sulphate pulp fibres. *Paperi ja puu*, 75(9-10), 689-702.
- Park, S.-K., & Ota, T. (2010). An experimental approach to turbulent heat transfer using a symmetric expanded plane channel. *Journal of mechanical science and technology*, 24(4), 857-863.
- Patel, H. E., Das, S. K., Sundararajan, T., Sreekumaran Nair, A., George, B., & Pradeep, T. (2003). Thermal conductivities of naked and monolayer protected metal nanoparticle based nanofluids: Manifestation of anomalous enhancement and chemical effects. *Applied physics letters*, 83(14), 2931-2933.
- Petukhov, B. (1970). Heat transfer and friction in turbulent pipe flow with variable physical properties. *Advances in heat transfer*, 6, 503-564.
- Philip, J., & Shima, P. (2012). Thermal properties of nanofluids. *Advances in colloid and interface science*, 183, 30-45.
- Pinho, F., Oliveira, P., & Miranda, J. (2003). Pressure losses in the laminar flow of shear-thinning power-law fluids across a sudden axisymmetric expansion. *International Journal of Heat and Fluid Flow*, 24(5), 747-761.

- Ponmani, S., William, J. K. M., Samuel, R., Nagarajan, R., & Sangwai, J. S. (2014). Formation and characterization of thermal and electrical properties of CuO and ZnO nanofluids in xanthan gum. *Colloids and Surfaces A: Physicochemical and Engineering Aspects*, 443, 37-43.
- Prasher, R., Bhattacharya, P., & Phelan, P. E. (2005). Thermal conductivity of nanoscale colloidal solutions (nanofluids). *Physical review letters*, 94(2), 025901.
- Prasher, R., Song, D., Wang, J., & Phelan, P. (2006). Measurements of nanofluid viscosity and its implications for thermal applications. *Applied physics letters*, 89(13), 133108.
- Putra, N., Thiesen, P., & Roetzel, W. (2003). Temperature dependence of thermal conductivity enhancement for nanofluids. *J Heat Transf*, 125, 567-574.
- Ramires, M. L., Nieto de Castro, C. A., Nagasaka, Y., Nagashima, A., Assael, M. J., & Wakeham, W. A. (1995). Standard reference data for the thermal conductivity of water. *Journal of Physical and Chemical Reference Data*, 24(3), 1377-1381.
- Rashin, M. N., & Hemalatha, J. (2013). Synthesis and viscosity studies of novel ecofriendly ZnO-coconut oil nanofluid. *Experimental Thermal and Fluid Science*, 51, 312-318.
- Rojas, O. J., & Hubbe, M. A. (2005). The dispersion science of papermaking. *Journal of dispersion science and technology*, 25(6), 713-732.
- Sadri, R., Hosseini, M., Kazi, S. N., Bagheri, S., Zubir, N., Ahmadi, G., . . . Zaharinie, T. (2017). A novel, eco-friendly technique for covalent functionalization of graphene nanoplatelets and the potential of their nanofluids for heat transfer applications. *Chemical Physics Letters*, 675, 92-97.
- Sadri, R., Zangeneh Kamali, K., Hosseini, M., Zubir, N., Kazi, S. N., Ahmadi, G., . . . Golsheikh, A. M. (2017). Experimental study on thermo-physical and rheological properties of stable and green reduced graphene oxide nanofluids: Hydrothermal assisted technique. *Journal of dispersion science and technology*, 38(9), 1302-1310.
- Safaei, M., Togun, H., Vafai, K., Kazi, S., & Badarudin, A. (2014). Investigation of heat transfer enhancement in a forward-facing contracting channel using FMWCNT nanofluids. *Numerical Heat Transfer, Part A: Applications*, 66(12), 1321-1340.
- Saikia, C., Goswami, T., & Ali, F. (1997). Evaluation of pulp and paper making characteristics of certain fast growing plants. *Wood Science and Technology*, 31(6), 467-475.
- Sajadi, A., & Kazemi, M. (2011). Investigation of turbulent convective heat transfer and pressure drop of TiO₂/water nanofluid in circular tube. *International Communications in Heat and Mass Transfer*, 38(10), 1474-1478.
- Sakuraba, K., Fukazawa, K., & Sano, M. (2004). Control of turbulent channel flow over a backward-facing step by suction or injection. *Heat Transfer—Asian Research*, 33(8), 490-504.
- Saldana, J., Anand, N., & Sarin, V. (2005). Numerical simulation of mixed convective flow over a three-dimensional horizontal backward facing step. *Journal of heat transfer*, 127(9), 1027-1036.
- Santosh Christopher, D., Kanna, P. R., Madhusudhana, G., Venkumar, P., & Mohammed, H. (2012). Numerical investigation of heat transfer from a two-dimensional sudden expansion flow using nanofluids. *Numerical Heat Transfer, Part A: Applications*, 61(7), 527-546.
- Sarkar, J. (2011). A critical review on convective heat transfer correlations of nanofluids. *Renewable and Sustainable Energy Reviews*, 15(6), 3271-3277.
- Seban, R. (2012). Heat transfer to separated and reattached subsonic turbulent flows obtained downstream of a surface step. *Journal of the Aerospace Sciences*.

- Selimefendigil, F., & Öztop, H. F. (2013). Numerical analysis of laminar pulsating flow at a backward facing step with an upper wall mounted adiabatic thin fin. *Computers & Fluids*, 88, 93-107.
- Sharma, R. (1980). Drag reduction by fibers. *The Canadian Journal of Chemical Engineering*, 58(6), 3-13.
- Sitprasert, C., Dechaumphai, P., & Juntasaro, V. (2009). A thermal conductivity model for nanofluids including effect of the temperature-dependent interfacial layer. *Journal of Nanoparticle Research*, 11(6), 1465-1476.
- Sixta, H. (2006). *Handbook of pulp*: Wiley-vch.
- Sjöström, E. (1993). *Wood chemistry: fundamentals and applications*: Gulf Professional Publishing.
- Smook, G. A. (1992). *Handbook for pulp & paper technologists*: Tappi.
- Solangi, K., Kazi, S., Luhur, M., Badarudin, A., Amiri, A., Sadri, R., . . . Teng, K. (2015). A comprehensive review of thermo-physical properties and convective heat transfer to nanofluids. *Energy*, 89, 1065-1086.
- Soong, C., & Hsueh, W. (1993). Mixed convection in a suddenly-expanded channel with effects of cold fluid injection. *International Journal of Heat and Mass Transfer*, 36(6), 1477-1484.
- Stüer, H., Gyr, A., & Kinzelbach, W. (1999). Laminar separation on a forward facing step. *European Journal of Mechanics-B/Fluids*, 18(4), 675-692.
- Sugawara, K., YOSHIKAWA, H., & OTA, T. (2004). LES of Three-Dimensional Separated Flow and Heat Transfer in a Symmetric Expansion Plane Channel. *Thermal science and engineering*, 12(4), 11-12.
- Sugawara, K., Yoshikawa, H., & Ota, T. (2005). LES of turbulent separated flow and heat transfer in a symmetric expansion plane channel. *Journal of fluids engineering*, 127(5), 865-871.
- Sundar, L. S., Naik, M., Sharma, K., Singh, M., & Reddy, T. C. S. (2012). Experimental investigation of forced convection heat transfer and friction factor in a tube with Fe₃O₄ magnetic nanofluid. *Experimental Thermal and Fluid Science*, 37, 65-71.
- Sveningsson, M., Morjan, R.-E., Nerushev, O. A., Sato, Y., Bäckström, J., Campbell, E. E., & Rohmund, F. (2001). Raman spectroscopy and field-emission properties of CVD-grown carbon-nanotube films. *Applied Physics A*, 73(4), 409-418.
- Tantra, R., Schulze, P., & Quincey, P. (2010). Effect of nanoparticle concentration on zeta-potential measurement results and reproducibility. *Particuology*, 8(3), 279-285.
- TAPPI, T. (2002). 205 om-88. Forming handsheets for physical tests of pulp. *TAPPI test methods*. Atlanta: TAPPI.
- TAPPI, T. (2006). Folding endurance of paper (MIT tester). *T 511 om-02*.
- Teng, T.-P., Hung, Y.-H., Jwo, C.-S., Chen, C.-C., & Jeng, L.-Y. (2011). Pressure drop of TiO₂ nanofluid in circular pipes. *Particuology*, 9(5), 486-491.
- Terekhov, V., & Bogatko, T. (2008). Effect of boundary layer thickness before the flow separation on aerodynamic characteristics and heat transfer behind an abrupt expansion in a round tube. *Thermophysics and Aeromechanics*, 15(1), 91-97.
- Terekhov, V., & Pakhomov, M. (2009). Predictions of turbulent flow and heat transfer in gas-droplets flow downstream of a sudden pipe expansion. *International Journal of Heat and Mass Transfer*, 52(21), 4711-4721.
- Terekhov, V., Yarygina, N., & Zhdanov, R. (2003). Some features of a turbulent separated flow and heat transfer behind a step and a rib. 2. heat transfer in a separated flow. *Journal of applied mechanics and technical physics*, 44(4), 522-531.

- Thalen, N., & Wahren, D. (1964). Shear modulus and ultimate shear strength of some paper pulp fibre networks. *Sven. Papperstidn*, 67(7), 259-264.
- Thiruvengadam, M., Armaly, B. F., & Drallmeier, J. (2009). Three dimensional mixed convection in plane symmetric-sudden expansion: Symmetric flow regime. *International Journal of Heat and Mass Transfer*, 52(3), 899-907.
- Tillman, P., & Hill, J. M. (2007). Determination of nanolayer thickness for a nanofluid. *International Communications in Heat and Mass Transfer*, 34(4), 399-407.
- Togun, H., Safaei, M. R., Sadri, R., Kazi, S. N., Badarudin, A., Hooman, K., & Sadeghinezhad, E. (2014). Numerical simulation of laminar to turbulent nanofluid flow and heat transfer over a backward-facing step. *Applied Mathematics and Computation*, 239, 153-170.
- Tsou, F., Chen, S.-J., & Aung, W. (1991). Starting Flow and Heat Transfer Downstream of a Backward-Facing. *Journal of heat transfer*, 113, 583.
- Uruba, V., Jonáš, P., & Mazur, O. (2007). Control of a channel-flow behind a backward-facing step by suction/blowing. *International Journal of Heat and Fluid Flow*, 28(4), 665-672.
- Vajjha, R. S., Das, D. K., & Kulkarni, D. P. (2010). Development of new correlations for convective heat transfer and friction factor in turbulent regime for nanofluids. *International Journal of Heat and Mass Transfer*, 53(21), 4607-4618.
- Vandsburger, L. (2009). Synthesis and covalent surface modification of carbon nanotubes for preparation of stabilized nanofluid suspensions.
- Velazquez, A., Arias, J., & Mendez, B. (2008). Laminar heat transfer enhancement downstream of a backward facing step by using a pulsating flow. *International Journal of Heat and Mass Transfer*, 51(7), 2075-2089.
- Ververis, C., Georghiou, K., Christodoulakis, N., Santas, P., & Santas, R. (2004). Fiber dimensions, lignin and cellulose content of various plant materials and their suitability for paper production. *Industrial crops and products*, 19(3), 245-254.
- Villar, J., Revilla, E., Gómez, N., Carbajo, J., & Simón, J. (2009). Improving the use of kenaf for kraft pulping by using mixtures of bast and core fibers. *Industrial crops and products*, 29(2), 301-307.
- Von Karman, T. (1930). Mechanische Ähnlichkeit und Turbulenz, nach Ges. Wiss. *Göttingen. Math. Physik. Klasse*, 5, 58-76.
- Wahren, D. (1964). *On three-dimensional fibre networks*.
- Wang, B.-X., Zhou, L.-P., & Peng, X.-F. (2003). A fractal model for predicting the effective thermal conductivity of liquid with suspension of nanoparticles. *International Journal of Heat and Mass Transfer*, 46(14), 2665-2672.
- Wang, B.-X., Zhou, L.-P., & Peng, X.-F. (2006). Surface and size effects on the specific heat capacity of nanoparticles. *International Journal of Thermophysics*, 27(1), 139-151.
- Wang, X.-Q., & Mujumdar, A. S. (2008). A review on nanofluids-part II: experiments and applications. *Brazilian Journal of Chemical Engineering*, 25(4), 631-648.
- Wen, D., & Ding, Y. (2005). Effect of particle migration on heat transfer in suspensions of nanoparticles flowing through minichannels. *Microfluidics and Nanofluidics*, 1(2), 183-189.
- Witharana, S., Palabiyik, I., Musina, Z., & Ding, Y. (2013). Stability of glycol nanofluids—the theory and experiment. *Powder technology*, 239, 72-77.
- Xie, H.-q., Wang, J.-c., Xi, T.-g., & Liu, Y. (2002). Thermal conductivity of suspensions containing nanosized SiC particles. *International Journal of Thermophysics*, 23(2), 571-580.

- Xie, H., Fujii, M., & Zhang, X. (2005). Effect of interfacial nanolayer on the effective thermal conductivity of nanoparticle-fluid mixture. *International Journal of Heat and Mass Transfer*, 48(14), 2926-2932.
- Xue, L., Keblinski, P., Phillpot, S., Choi, S.-S., & Eastman, J. (2004). Effect of liquid layering at the liquid–solid interface on thermal transport. *International Journal of Heat and Mass Transfer*, 47(19), 4277-4284.
- Yang, J.-T., & Tsai, C.-H. (1996). High temperature heat transfer of separated flow over a sudden-expansion with base mass injection. *International Journal of Heat and Mass Transfer*, 39(11), 2293-2301.
- Yoshikawa, H., Ishikawa, K., & Ota, T. (2004). *Numerical Simulation of Three-dimensional Separated Flow and Heat Transfer in an Enlarged Rectangular Channel*. Paper presented at the NATIONAL HEAT TRANSFER SYMPOSIUM OF JAPAN.
- Yoshikawa, H., Yoshikawa, M., & Ota, T. (2002). *Numerical Simulation of Heat Transfer in Unsteady Separated and Reattached Flow Around a Symmetric Sudden Expansion Channel*. Paper presented at the NATIONAL HEAT TRANSFER SYMPOSIUM OF JAPAN.
- Youssef, M. S., Aly, A. A., & Zeidan, E.-S. B. (2012). Computing the pressure drop of nanofluid turbulent flows in a pipe using an artificial neural network model.
- Yu, C.-J., Richter, A., Datta, A., Durbin, M., & Dutta, P. (1999). Observation of molecular layering in thin liquid films using X-ray reflectivity. *Physical Review Letters*, 82(11), 2326.
- Yu, W., & Choi, S. (2003). The role of interfacial layers in the enhanced thermal conductivity of nanofluids: a renovated Maxwell model. *Journal of Nanoparticle Research*, 5(1-2), 167-171.
- Zhou, L.-P., Wang, B.-X., Peng, X.-F., Du, X.-Z., & Yang, Y.-P. (2010). On the specific heat capacity of CuO nanofluid. *Advances in mechanical engineering*, 2, 172085.
- Zhou, S., & Ni, R. (2008). Measurement of the specific heat capacity of water-based Al₂O₃ nanofluid. *Applied physics letters*, 92(9), 093123.
- Zhu, H., Jia, Z., Chen, Y., Weadock, N., Wan, J., Vaaland, O., . . . Hu, L. (2013). Tin anode for sodium-ion batteries using natural wood fiber as a mechanical buffer and electrolyte reservoir. *Nano letters*, 13(7), 3093-3100.

List of Publications

1. **Syed Muzamil Ahmed***, Ghulamullah Khan, S.N Kazi, M Dahari, Mohd Nashrul Mohd Zubir, Pervaiz Ahmad, R Ibrahim, M. Hassan. "Effect of various refining processes for Kenaf Bast non-wood pulp fibers suspensions on heat transfer coefficient in circular pipe heat exchanger" (Submitted to Journal of 'Heat and Mass Transfer', Status Under revision)
2. **Syed Muzamil Ahmed***, Salim Newaz Kazi*, Ghulamullah Khan, Mahidzal Dahari, Mohd Nashrul Mohd Zubir, Pervaiz Ahmad, Elham Montazer "Experimental investigation on momentum and drag reduction of flowing Malaysian crop suspensions in closed conduit" (Presented on 5th-6th April in International Technical Postgraduate Conference, Organized by Faculty of Engineering University of Malaya and Published in IOP Conference Series: Materials Science and Engineering)
3. **Syed Muzamil Ahmed***, S.N Kazi*, M Dahari, Mohd Nashrul Mohd Zubir, Ghulamullah Khan, R Ibrahim, Pervaiz Ahmad. "Study of heat transfer and friction loss of kenaf core non-wood fiber suspensions in closed conduit flow" (Submitted to Journal of 'Applied Thermal Engineering', Status Under review)
4. **Syed Muzamil Ahmed***, Ahmad Amiri, Kazi Newaz, Mahidzal Dahari, Nashrul Zubir, Ghulamullah Khan, Pervaiz Ahmad "Experimental study of forced convective heat transfer to nanofluid flow in backward-facing step - Effect of Concentration and Reynolds number" (Submitted to Journal of 'International Communications in Heat and Mass Transfer', initial submission January 2017, Status Under review)
5. **Syed Muzamil Ahmed***, Salim Newaz Kazi*, Ghulamullah Khan, Mahidzal Dahari, Mohd Nashrul Mohd Zubir, Pervaiz Ahmad, Rushdan Ibrahim, Mohd Sayuti Ab Karim "Experimental investigation on drag reduction of flowing crop suspensions in circular pipe heat exchanger" (Submitted to Journal of 'International Journal of Multiphase Flow', initial submission March 2017, Status under review)